The Skeletal Environment and Comorbid Hyperglycemia Influence *Staphylococcus aureus* Virulence During Osteomyelitis

By

Casey Butrico

Dissertation

Submitted to the Faculty of the

Graduate School of Vanderbilt University

in partial fulfillment of the requirements

for the degree of

DOCTOR OF PHILOSOPHY

in

Microbiology and Immunology

May 12, 2023

Nashville, Tennessee

Approved:

Mariana Byndloss, D.V.M., Ph.D.

Henrique Serezani, Ph.D.

Eric Skaar, Ph.D., M.P.H.

Jeffrey Spraggins, Ph.D.

James Cassat, M.D., Ph.D.

ACKNOWLEDGEMENTS

I would like to thank the Vanderbilt Pathology, Microbiology, and Immunology (PMI) department for giving me opportunities to grow, lead, and explore uncharted territory during my time at Vanderbilt University. I am particularly grateful for the PMI department Graduate Student Association (GSA), the Chemical Biology of Infectious Diseases (CBID) Training Grant, and the Vanderbilt Institute for Infection, Immunology, and Inflammation (VI4) Science Communication Internship. Thank you to Dr. Eric Skaar, Dr. Natalie Silmon de Monerri, Dr. Raphael Silmon, and Dr. Annaliesa Anderson for organizing an opportunity for me to work at Pfizer in the Bacterial Vaccines and Technology group. I would also like to acknowledge Karisa Calvitti for introducing me to various forms of science communication through VI4 and Liz Roelofsz for assisting with all things GSA-related. The leadership roles I was afforded and the internships I completed during graduate school shaped my desire to pursue a career in science communication and gave me the skills necessary to do so.

I would like to acknowledge my PI, Jim Cassat for his guidance and support the past five years. I have gained skills in formulating hypotheses, designing experiments, presenting, and writing because of your mentorship. I grew in my ability to communicate science and learned how to both listen and lead as a member of your team. Thank you for your patience, support, and feedback.

Thank you to my committee members, Dr. Mariana Byndloss, Dr. Henrique Serezani, Dr. Eric Skaar, and Dr. Jeffrey Spraggins, for your advice and insight. I would also like to acknowledge Dr. Erin Green in the Skaar laboratory for her generous experimental guidance conducting transposon sequencing. I am honored to have such a respected group of scientists who supported me throughout my Ph.D., and I am grateful for your time. Your expertise and guidance were instrumental for my success.

I would like to acknowledge the contributions of the Cassat laboratory members for my scientific and personal growth. There is no one I was able to relate to more during my time at Vanderbilt University than you all. Thank you for celebrating with me, offering countless hours of encouragement, and providing troubleshooting and experimental advice. Words cannot describe how lucky I feel to have worked with such an inspiring group of peers and role models. I am particularly grateful for Dr. Aimee Potter for her willingness to teach me all that she knew about bacterial metabolism and microbiology experimental techniques. I must also thank my personal editor, scientific confidant, and fellow laboratory weekend-worrier, Jenna Petronglo. I truly could not have survived graduate school without your help, humor, and above all, friendship. I would like to acknowledge Dr. Caleb Ford and Dr. Kara Eichelberger for their mentorship, positive attitudes, and overall contagious love for science. Dr. Niki Putnam, Dr. Thomas Spoonmore, Dr. Christopher Peek, Dr. Juan Barraza, Dr. Brittney Gimza, Clara Si, and Christopher Good – thank you all for your generous feedback and friendship in the Cassat laboratory. Finally, thank you to Jacob Curry and the other fantastic Cassat Laboratory Research Assistants over the years for keeping us all on track. You are all amazing, and I cannot wait to see what the future has in store for each of you.

Thank you to my scientific mentors at Gettysburg College and Janssen for nurturing my love of science. Dr. Jennifer Powell, thank you for introducing me to the field of microbiology and for encouraging me to pursue an internship opportunity at Janssen. Dr. Nicolas Dracopoli and Dr. Daneen Schaeffer, thank you for exposing me to the world of pharmaceutical research. I am grateful for your willingness to mentor me from the ground up.

I am thankful for my amazing friends, who live both near and far, who have provided me countless opportunities to laugh, explore, and grow outside of the laboratory. Caity and Jim Hughes, Sophia and Brian Cruse, Ellyn Thomas, Ryan Youngerman, and Rob Dold – you all make Nashville home. I am also thankful for my best friends that I formed in a single college

dormitory who are now scattered around the country: Kathryn Rankin, Casey Beck, Priiti Sahu, Samantha Sterbenz, and Emily Foley. Your calls are always a welcome break from science. I am so grateful for our girls' trips and memories over the past 11 years.

I have the most incredible, supportive family who were steadfast in their encouragement during my Ph.D. Thank you to William Hatfield, my partner, for unconditionally believing in me. It is because of your confidence that I am pursuing a career I am truly passionate about. You make me feel like I can achieve anything. Thank you to my brothers, Christopher and Mark Butrico, for your contagious positivity and forever optimistic point of views. Finally, I would like to thank my parents, Kelly and William Butrico. Having you both a phone call away to celebrate milestones and provide encouragement during the lows of graduate school drove me to finish my Ph.D. Your genuine curiosity about infectious disease and scientific research methodology were constant reminders of the importance of my work and science communication. I'm incredibly grateful for all that you do for me and would be nowhere without your unwavering support. I love you all.

TABLE OF CONTENTS

LIST OF FIGURES

Figure

LIST OF TABLES

Table

A portion of the following section (*Chapter I, Introduction and Background*) was originally published in *Toxins* (2020).

Butrico CE, Cassat JE. 2020. Quorum sensing and toxin production in *Staphylococcus aureus* osteomyelitis: pathogenesis and paradox. *Toxins*. 12 (516).

doi: 10.3390/toxins12080516

CHAPTER I. INTRODUCTION AND BACKGROUND

Introduction

Staphylococcus aureus is a human pathogen capable of infecting nearly every organ of the human body. Metabolic flexibility combined with a large virulence repertoire enables *S. aureus* to survive in multiple tissues including the skin, lungs, heart, liver, kidneys, and bone.[1–4] The prevalence of antibiotic-resistant strains of *S. aureus* contribute to the significant global healthcare burden.[5] Individuals with comorbid conditions, such as diabetes, are at a greater risk for contracting *S. aureus* infections due to changes in immune cell function, metabolite abundance, and tissue homeostasis.[6–9] In addition to emerging antibiotic resistance, increasing rates of diabetes diagnoses in the United States rationalizes continued study of *S. aureus* and staphylococcal diseases.[10,11]

Inflammation of bone in response to an invading pathogen, or infectious osteomyelitis, can occur via spread of hematogenous or contiguous infection, surgeries and interventions, or traumatic injury.[5,12] *S. aureus* is the most common etiological agent of osteomyelitis, and treatment often requires extensive courses of antibiotics.[5,12] Despite high antibiotic bioavailability in the bone, the formation of biofilms and abscesses limit efficacy of antibiotics.[13,14] Antibiotic resistance and/or tolerance and subsequent treatment failure can necessitate surgical debridement to physically remove the infected and chronically inflamed tissue.[12] The identification of metabolism pathways critical for *S. aureus* survival could inform more targeted therapeutic development to enhance osteomyelitis patient outcomes. Furthermore, the discovery of important *S. aureus* virulence mechanisms that promote bacterial growth during comorbid hyperglycemia could reveal targeted strategies for infection prevention and treatment in individuals with diabetes.

In this thesis, we examine the hypothesis that *S. aureus* uses nutrient transporters and metabolic genes to facilitate bacterial survival during osteomyelitis. We also hypothesized that virulence factors involved in *S. aureus* response to inflammation are important for bacterial survival during osteomyelitis in a hyperglycemic host. In Chapter I, we highlight background on staphylococcal pathogenesis, murine models of hyperglycemia, the influence of hyperglycemia on bone and tissue homeostasis, and *S. aureus* adaptation during infection. Chapter II characterizes the role of a putative amino acid permease necessary for *S. aureus* survival and dissemination. In Chapter III, we use a murine model of hyperglycemia to identify how the comorbid condition influences *S. aureus* burdens and dissemination during osteomyelitis. Furthermore, Chapter III reveals a virulence factor that contributes to *S. aureus* survival in osteomyelitis infection during hyperglycemia. Lastly, Chapter IV outlines future directions to 1) further understand the context in which nutrient transporters contribute to *S. aureus* survival *in vivo* and 2) elucidate the mechanism by which *S. aureus* pathogenesis is altered in osteomyelitis during hyperglycemia.

Osteomyelitis as a model for invasive *S. aureus* infection

S. aureus osteomyelitis is a paradigm for invasive infection and is imperative to study due to the severe complications and treatment difficulties associated with this disease.[5] Infection complications unique to osteomyelitis include increased bone destruction and enhanced risk for the development of bone fractures.[15] The combination of bone damage and a disruption of vasculature during infection leads to poor antibiotic penetration.[4,14] *S. aureus* can also form biofilms and multicellular abscess communities, which further complicate antibiotic delivery.[4] Thus, treatment of osteomyelitis often necessitates long courses of antibiotics.[16] Even with appropriate treatment, recurrence rates remain as high as 20%.[16] In many cases, surgical debridement to physically remove the necrotic and infected bone tissue becomes

necessary.[17] The study of human disease and the development of animal models are both important for understanding the pathogenesis of *S. aureus* osteomyelitis.[3,18–20]

S. aureus can infect bone through traumatic injury or spread from other infectious foci.[12] While osteomyelitis infections most frequently manifest in children from hematogenous spread of bacteria colonizing the skin or nares, contiguous spread from trauma or surgery is more common in adults.[12,21] The ability of *S. aureus* to induce significant bone damage is dependent upon the ability of the bacteria to express toxins.[22] *S. aureus* toxins, such as phenol soluble modulins (PSMs), also mediate bone destruction and influence the homeostatic balance of bone forming osteoblasts and bone resorbing osteoclasts.[3] In bone, *S. aureus* can reside in different microenvironments including on necrotic bone fragments (known as sequestra), within bone marrow abscesses, under the periosteum of intact bone, or within the canalicular system of cortical bone.[22–24] Regardless of the precise niche within skeletal tissues, *S. aureus* often exists within microcolonies where the bacteria can adapt and respond to resource fluctuations, innate immune responses, and bacterial density.[25–27] In Chapter II of this thesis, we use a post-traumatic model of osteomyelitis to identify the role of a putative nutrient transporter in promoting *S. aureus* survival. In Chapter III, we induce osteomyelitis in mice with hyperglycemia to understand how *S. aureus* adapts to the altered nutrient microenvironment in bone in the presence of a common metabolic comorbidity.

Hyperglycemia and infection

Hyperglycemia, or elevated blood glucose concentration, can occur in response to endocrine disorders, medications, acute phases of illness, insulin resistance, and/or genetic predisposition.[28] In humans, hyperglycemia is characterized by blood glucose greater than 125 mg/dl while fasting.[28] The incidence of chronic hyperglycemia has increased dramatically over the last two decades in the United States, with the most recent data suggesting that 37.3 million

people are currently living with diabetes mellitus.[29] Hyperglycemia can broadly manifest as type 1 or type 2 diabetes, although other subtypes also exist, such as gestational, neonatal, medication-induced, and latent autoimmune diabetes in adults (LADA).[28,30,31] Approximately ten percent of all patients with diabetes have type 1 diabetes, while around 90 percent of patients have type 2.[32] Type 1 diabetes occurs in response to insulin deficiency due to autoreactive T cells that destroy insulin-producing beta cells.[31] This type of diabetes is a multifactorial disease with genetic, environmental, and epigenetic factors all influencing the onset of the condition.[31] Type 2 diabetes is characterized by adequate insulin production paired with the inability of cells to effectively respond to insulin, also known as insulin resistance.[10] While genetic factors also contribute to type 2 diabetes onset, lifestyle factors known to increase risk include poor diet, sedentary time, short sleep duration, and stress.[33] Although type 1 and 2 diabetes result in distinct changes in physiology, both types of diabetes render individuals 4.4 times more likely to develop an infection.[34] Multiple murine models were developed to study distinct aspects of physiology associated with chronic hyperglycemia, and each model should be considered to best address how hyperglycemia influences infection outcomes.

Murine models are used to study diabetes.

To study the influence of hyperglycemia that more resemble type 1 diabetes, murine models were developed to recapitulate the inability to produce insulin (**Table 1**).[35] Chemical induction of type 1 diabetes is useful for studying the metabolic implications of hyperglycemia and can be achieved with treatment of streptozotocin (STZ) or alloxan.[35,36] STZ and alloxan have similar structures to glucose and are therefore imported by Glut-2 transporters in beta cells in fasted animals.[35,36] Once internalized, STZ causes alkylation of DNA, poly(adenosine phosphate-ribose) polymerase (PARP) activation, and nicotinamide adenine dinucleotide (NAD^+) depletion.[37,38] NAD^+ is an important redox agent during Adenosine 5'-triphosphate

(ATP) synthesis, and depletion of NAD^+ therefore results in decreased ATP production.[37] Reduction in available ATP leads to beta cell death and a lack of insulin production.[37] STZ can be administered intraperitoneally (I.P.) in a single high dose (100 – 200 mg/kg) or in a lower dose (40 mg/kg) over the course of five days.[39,40] Female mice are more resistant to STZ, likely due to a protective role of estrogen in promoting the degradation of misfolded proinsulin.[41,42] Therefore, male mice are typically used in this model. Alloxan is a redox-cycling compound that generates superoxide and hydrogen peroxide once internalized in beta cells.[38] Alloxan is typically administered I.P. in mice ranges from 50 – 200 mg/kg.[38] A disadvantage of both chemically induced models of type 1 diabetes is that the compounds can have toxic effects to other tissues. [35,36] Alloxan has a particularly narrow dose range that will induce diabetes without toxicity to the kidneys and other organs.[38] A transgenic mouse model that contains a rat insulin promoter fused to the diphtheria toxin receptor coding sequence (RIP-DTR) can also be used for selective beta cell ablation.[43] Administration of diphtheria toxin to these mice results in a rapid and near-complete depletion of beta cells, although this compound is also toxic to humans and requires caution while handeling.[43]

The autoimmune response to beta cells that occurs during type 1 diabetes is modeled with non-obese diabetic (NOD) mice, an autoimmune murine model.[44] This model was discovered in an inbred strain of mice with over ten genetic mutations that lead to insulin autoantibody production and spontaneous T cell-mediated beta cell destruction.[35,45] Beta cell destruction typically begins around 3-4 weeks of age.[35] A pre-diabetes state manifests until diabetes occurs around 10-14 weeks, although the age of onset can vary.[35] The frequency with which NOD mice develop diabetes is also variable, with 60-90% of females and 10-30% of males developing hyperglycemia.[44,46] Limitations of the NOD model include the variability of the age of onset of hyperglycemia as well as the absence of important antigen presenting

capacity in macrophages.[35,45,47] Therefore, this model is less favorable for assessing the influence of hyperglycemia on infection.

Less frequently used models of type 1 diabetes include the Akita genetic mouse model and virus-induced type 1 diabetes. [48] The Akita murine model contains a mutation in the insulin-2 gene that prevents proper insulin processing.[48] The accumulation of unfolded insulin results in endoplasmic reticulum (ER) stress and severe diabetes by 3-4 weeks of age.[48] This model presents with systemic complications, including polyuria and hyperinsulinemia and leads to premature death around 12 weeks.[49] The Akita murine model is useful for studying vascular, renal, and neurological complications associated with diabetes, due to its early and severe onset.[50,51] However, Akita mice are not suitable for infection studies with long durations or additional morbid stress. Akita mice also exhibit decreased bone mass, impaired fracture healing, and weaker bone structure, which pose an additional variable in osteomyelitis studies.[52] Viruses are also used to induce beta cell destruction, such as coxsackie B virus and encephalomyocarditis virus.[53–55] A transgenic virus model that uses lymphocytic choriomeningitis virus antigen expressed on beta cells has been described, although this model was developed in rats.[56] Virus-induced diabetes models are complicated by the inconsistent replication rate of viruses and the timing of the viral infection.[56]

Type 2 diabetes is characterized by insulin resistance, which is primarily modeled with a high fat diet or a genetic model to induce obesity (**Table 2**).[35] High fat chow (58% fat) is substituted for normal chow (11% fat) to induce weight gain in a high fat diet model.[57] Changes in animal weight are observed within a week of altered chow consumption.[58] The weight gain is associated with insulin resistance and impaired glucose tolerance, which recapitulates a mechanism by which humans develop type 2 diabetes.[58] Genetic models of type 2 diabetes include monogenic mice with defective leptin signaling, a pathway responsible for feelings of satiation. The $Lep^{ob/ob}$ mouse model was discovered in an outbred colony of mice due to a

mutation in the leptin gene itself.[59] $Lep^{ob/ob}$ mice exhibit hyperinsulinemia early in life, with hyperglycemia developing by 3-5 months.[60] Limitations of this model include that the homozygous mice are sterile and cannot be bred, transient hyperglycemia occurs and can rebound due to a lack of complete beta cell failure, and mice exhibit other phenotypically abnormal traits such as decreased physical activity and changes in temperature regulation.[35] Similarly, the $Lepr^{db/db}$ murine model has recessive mutations in the leptin receptor.[61] These mice develop hyperinsulinemia early in life, with hyperglycemia onset occurring around 4-8 weeks.[62] A limitation of $Lepr^{db/db}$ mice is that they develop ketoacidosis after a few months of life, resulting in a short lifespan.[63] Examples of polygenic murine models of type 2 diabetes include the New Zealand Obese (NZO), TALLYHO/Jng, and KK mouse models. The NZO model was discovered in an inbred strain of mice and is characterized by decreased expression of the *glut2*, loss of serine/threonine-protein kinase (AKT) activity, and decreased beta cell integrity.[64] The TALLYHO/Jng strain of mice was developed by inbreeding and selecting mice that demonstrated characteristics of type 2 diabetes.[65] TALLYHO/Jng mice become moderately obese, although only males develop hyperglycemia around 10-14 weeks of age.[66] The KK mouse model has similar characteristic but also exhibits signs of nephropathy, making this model useful for diabetic nephropathy studies.[67] Polygenic models of type 2 diabetes more accurately recapitulate the multifactorial nature of type 2 diabetes onset but do not provide negative control mice for experimentation.

Taken together, there are many murine models of diabetes, and the mechanism by which the mice develop hyperglycemia and subsequent changes in physiology should be considered when selecting a model for experimental analysis.[68] In Chapter III, we use STZ to model the metabolic condition of hyperglycemia in male mice to measure changes in infection dynamics during osteomyelitis.

Table 1. Murine models of type 1 diabetes[35,68]

Murine model	Description	Limitations
Streptozotocin	Chemical-induced beta cell death that results in hypoinsulinemia and hyperglycemia	Off-target cytotoxicity; variable effects inducing hyperglycemia; females are less susceptible
Alloxan	Chemical-induced blockade of glucose sensor glucokinase in beta cells	Narrow dose range; high level of ketoacidosis; males more susceptible
RIP-DTR	Rat insulin promoter fused to the diphtheria toxin receptor coding sequence that results in beta cell death upon treatment with diphtheria toxin[43]	Diphtheria toxin is toxic to humans
Non-obese diabetic mouse	Polygenic model identified in inbred colony; autoimmune response to pancreatic islets	Macrophages major histocompatibility complex (MHC) class II molecule-deficient; lack of control over age of diabetes onset; females more susceptible
Akita mouse	Monogenic model with *ins2* gene mutation that results in incorrect folding of insulin, leading to beta cell toxicity	Lack of control over age of diabetes onset; development of diabetic nephropathy[69]; males develop more severe hyperglycemia
Virus-induced	Selective destruction of beta cells or stimulation of auto-reactive T cells (virus-dependent)	Inability to control viral titer and infection of other cells

Table 2. Murine models of type 2 diabetes[35,68]

Murine model	Description	Limitations
High fat diet	Altered chow diet with 58% fat content	Sustained feeding required for full onset of type 2 diabetes symptoms; variety of metabolic effects in addition to hyperglycemia
$Lep^{ob/ob}$ $Lep^{db/db}$, and $Lepr^{ob/ob}$ mice	Murine strains with mutations in leptin gene or leptin gene receptor, preventing feelings of satiation and increasing food consumption	Develop ketoacidosis; limited lifespan[62,63]
New Zealand Obese mouse	Polygenic model; decreased expression of *glut2* gene as well as other genetic abnormalities	Highest levels of adiposity, hypercholesterolemia, and hypertension[70]
TALLYHO/Jng mouse	Polygenic model with thousands of genetic mutations that lead to greater beta cell mass and characteristic type 2 diabetes phenotypes[71]	Diabetes onset does not occur until 10-14 weeks; only males develop glucose intolerance[72]
KK mouse	Polygenic model	Development of diabetic nephropathy

Hyperglycemia results in more severe *S. aureus* infections in murine models of infection.

The influence of hyperglycemia on *S. aureus* infection severity has been studied in hind paw, skin, sepsis, and implant-associated infections.[73-75] Prior work identified increased *S. aureus* burdens and larger lesions in the skin of STZ-treated hyperglycemic mice compared to vehicle-treated control mice at multiple days post-infection.[73,74] In a hind paw model of infection in NOD mice, *S. aureus* burdens were also elevated in hyperglycemic mice compared to NOD euglycemic infections.[75] To study implant-associated infection, Farnsworth et al. induced hyperglycemia with a high fat diet as well as STZ treatment and observed greater *S. aureus* burdens within the bone of diabetic mice compared to control infections.[6] However, the influence of STZ-induced hyperglycemia on post-traumatic osteomyelitis infection outcome was previously unknown and is addressed in Chapter III of this work.

Hyperglycemia from type 1 diabetes influences immune cell function.

Innate immune cells are responsible for rapidly responding to pathogen associated molecular patterns (PAMPs) and cytokine gradients to neutralize invading bacteria during infection. As summarized by Cheng, et al., neutrophils are critical immune cells involved in the formation of staphylococcal abscesses through their recruitment to the infectious site and subsequent formation of zones of necrotic and healthy cells.[27,76] Prior studies have highlighted a role of interleukin-1 beta (IL-1ß) and lipid mediator leukotriene B_4 (LTB_4) in neutrophil-mediated contributions to abscess formation.[77,78] Macrophages are myeloid-derived phagocytic cells that also associate with abscesses, generally encircling the periphery.[79] Macrophages contribute to the containment of *S. aureus* through phagocytosis and recruitment of additional immune cells.[80] Coordinated innate immune response to invading pathogens is required for containment and subsequent clearance of the infectious bacteria.

Murine models of hyperglycemia that resemble type 1 diabetes have revealed changes in innate immune responses during *S. aureus* infection compared to infection in euglycemic

mice.[73-75,81-85] Brandt et al. identified that STZ-treated hyperglycemic mice contain excess LTB_4, which limits neutrophil chemotaxis and reactive oxygen species (ROS) production, increases macrophage MyD88 signaling, and subsequently elevates IL-1ß production.[73,81] Furthermore, bacterial burdens in the skin were greater in STZ-treated hyperglycemic mice but could be controlled with a pharmacological antagonist or genetic deletion of the receptor for LTB_4.[73] Phagocytes consume less glucose and have diminished respiratory burst capacity in skin infection during STZ-induced hyperglycemia, as well as *in vitro* when derived from NOD mice.[74,75] NOD mice also exhibit decreased neutrophil clearance and prolonged tumor necrosis factor alpha (TNFα) production during intraperitoneal (I.P.) infection with *S. aureus*.[82] These findings suggest that infection resolution may occur more slowly or less efficiently in a hyperglycemic host compared to a euglycemic host. Inhibited wound healing and increased tissue damage are also exacerbated during hyperglycemia by increased rates of neutrophil extracellular trap (NET) formation, observed in cells isolated from STZ-treated mice.[83] Other immune cell populations, including dendritic cells and T cells, also exhibit altered ability to sense and respond to *S. aureus* during hyperglycemia.[73,84,85] In conclusion, multiple studies support a dysregulation of immune cell function during hyperglycemia in murine models of type 1 diabetes, which contribute to exacerbated infection severity.

Many human and *in vitro* studies of the influence of hyperglycemia on the immune response to invading *S. aureus* are consistent with *in vivo* discoveries using murine models.[86-89] For example, multiple groups observed that neutrophils cultured *in vitro* in the presence of high glucose exhibit decreased respiratory burst and phagocytosis capacity.[86–89] Neutrophils isolated from the blood of patients with diabetes also phagocytose *S. aureus* to a lesser extent than neutrophils from healthy controls.[89] While research has been conducted to further our understanding of how hyperglycemia influences innate immune cell function *in vitro* and in murine models of skin, sepsis, and implant-associated infection, little is known about how

immune alterations influence infection outcome and bacterial fitness in osteomyelitis.[73,78,90] Chapter III of this work identifies *S. aureus* genes that contribute to bacterial survival in osteomyelitis in altered physiological conditions during comorbid hyperglycemia.

Physiological changes associated with chronic hyperglycemia.

Chronic hyperglycemia has broad physiological implications on tissue homeostasis and organ health due to the influence of high glucose concentrations on inflammatory processes (**Fig. 1**). Vascular disease, neuropathy, and ketoacidosis complicate management of diabetes and increase risk of infection.[91–94] Altered glucose metabolism by host cells results in overproduction of ROS and formation of advanced glycation end products (AGE), which activate additional proinflammatory pathways.[91–94] AGE production also recruits macrophages, which causes plaque formation and can lead to atherosclerosis.[94] Impeded blood flow prevents proper immune cell recruitment to the site of infection, inhibits wound healing, and complicates antibiotic delivery.[95] Diabetic ketoacidosis (DKA) further disrupts vascular function and influences pH homeostasis in blood and tissues.[95] DKA stems from a compensatory production of counterregulatory hormones during insulin deficiency.[96] Cells perform ketogenesis, or lipidolysis of free fatty acids, as a source of energy in the absence of insulin.[92] The breakdown of lipids produces ketone bodies, such as 3-beta-hydroxybutyrate, acetone, and acetoacetate.[92] Ketoacids are associated with hyperinflammation and augmented production of pro-inflammatory cytokines, such as TNFα and IL-1ß.[97] Neuropathy manifests during chronic hyperglycemia due to the multifactorial presentation of inflammation, AGE formation, and oxidative stress.[98] This loss of nervous system response impedes sweat gland function, keratinizes skin, and impairs sensations, which all increase the risk of developing infection.[98,99] To study the multifactorial and systemic changes in physiology induced by hyperglycemia on *S. aureus* fitness, we use a murine model of hyperglycemia in Chapter III of this work.

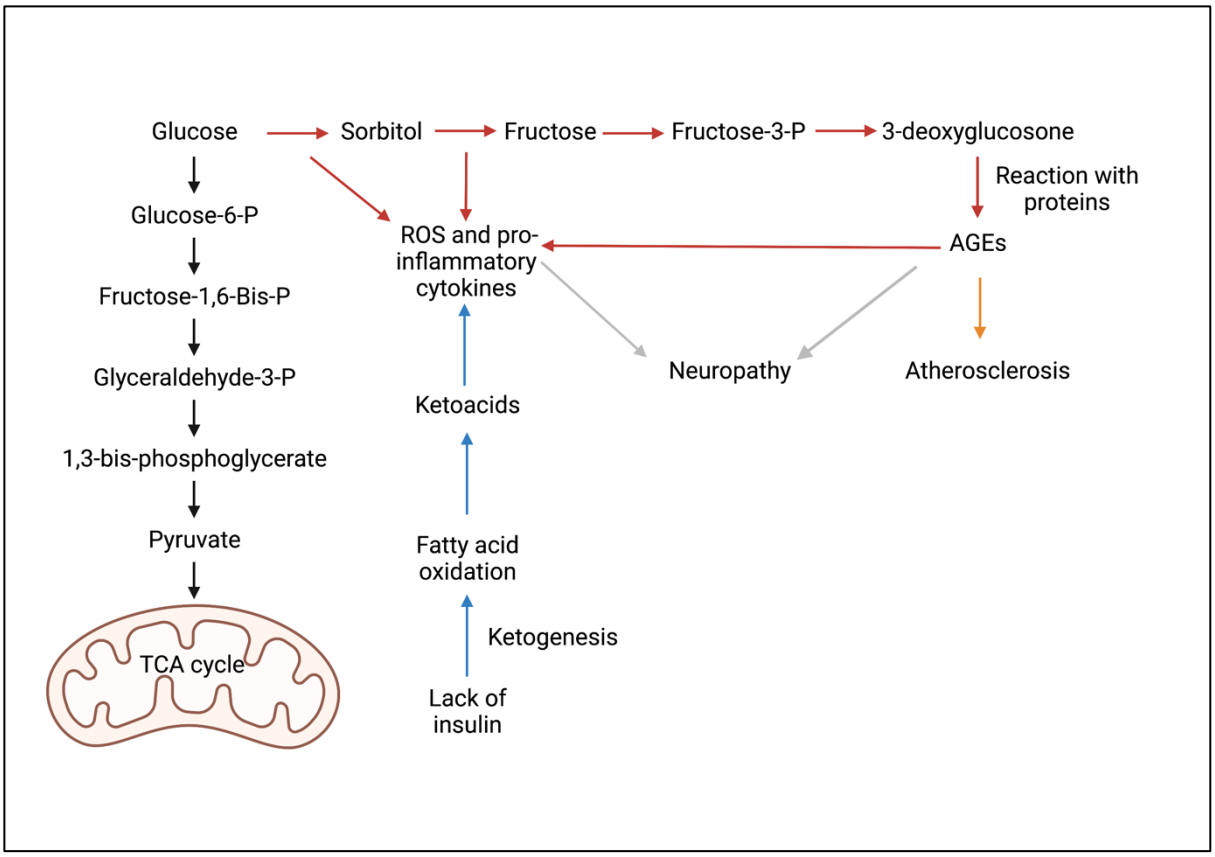

Figure 1. Hyperglycemia alters tissue and organ homeostasis. In the presence of abundant glucose and insulin, cells perform glycolysis by breaking down glucose to pyruvate (black) and subsequently running the TCA cycle for ATP production. In the presence of abundant glucose and a deficiency of insulin, alternative glucose metabolism (red), results in formation of advanced glycation end products (AGEs) and formation of reactive oxygen species (ROS). AGEs recruit macrophages, which block vascular function and lead to atherosclerosis (orange). The combined production of ROS and AGEs also leads to neuropathy (gray). Lack of insulin alters hormonal homeostasis and activates ketogenesis, or the oxidation of fatty acids to ketoacids (blue). Ketogenesis further produces pro-inflammatory cytokines, ROS, and acidifies the blood. Figure created with BioRender.

Hyperglycemia impacts bone homeostasis.

In addition to the risk of developing neuropathy, vascular issues, and ketoacidosis, patients with chronic hyperglycemia experience decreased bone mineral density and greater incidence of bone fractures.[100] Rat models of diabetes have supported that hyperglycemia results in reduction of bone mineral density and greater micro-architecture damage.[101,102] Furthermore, a study by Motyl and McCabe reported that bone volume and osteocalcin (an osteoblast-secreted factor that increases bone matrix mineralization) expression are significantly lower in STZ-treated hyperglycemic mice compared to control mice 19 days after a low dose course of STZ treatment was initiated.[103] However, the sample size in this study was small and the biological difference modest, thus warranting further investigation. In a rat model of type 1 diabetes, the animals exhibited augmented alveolar (dental) bone loss after four weeks, compared to healthy controls.[104] STZ-induced hyperglycemia decreases alkaline phosphatase (ALP), osteocalcin, and hydroxyproline, which are all markers of bone building osteoblast activity.[105] Simultaneously, tartrate-resistant acid phosphatase (TRAP) and cathepsin K, markers of bone resorbing osteoclasts, increase during hyperglycemia.[105,106] Overall, the data suggest that hyperglycemia increases bone resorption, decreases bone formation, and leads to greater risk of fracture formation. However, the influence of hyperglycemia on bone homeostasis during osteomyelitis were previously uncharacterized. In Chapter III, we address how hyperglycemia alters infection-induced bone loss during *S. aureus* osteomyelitis.

***S. aureus* virulence factors are important during infection in a hyperglycemic host.**

The contribution of individual *S. aureus* virulence genes have been assessed during hyperglycemic infection.[107-109] For example, one study used NOD mice to reveal a contribution of the glucose-responsive catabolite control protein A gene, CcpA, for *S. aureus* survival during hyperglycemia.[107] To more comprehensively assess changes in host and bacterial gene

transcription during skin infection in a murine model of STZ-induced hyperglycemia, Jacquet at al. used a dual RNA sequencing approach.[108] Through this study, 513 *S. aureus* genes were identified as differentially expressed in hyperglycemic infection compared to euglycemic infection, 340 of which were upregulated.[108] Of the upregulated genes, there was an enrichment for genes involved in the tricarboxylic acid (TCA) cycle and glycolysis as well as genes involved in translational machinery and stress response.[108] Furthermore, correlative studies have revealed small sets of *S. aureus* virulence genes associated with worse infection outcomes and more severe disease in diabetes patients.[109] However, few additional studies have comprehensively investigated how changes in *S. aureus* virulence contribute to worse infection outcomes during hyperglycemia. Specifically, *S. aureus* virulence genes that contribute to osteomyelitis infection severity during hyperglycemia were previously unknown. This outstanding research question is addressed in work in Chapter III.

Staphylococcus aureus virulence and metabolic adaptation

The capability of *S. aureus* to grow in a multitude of host tissues suggests the bacteria can sense and respond to heterogeneous host immune responses and local nutrient availability.[1-4] *S. aureus* responds to immune and nutrient stress in part by secreting virulence factors, including enzymes that degrade host tissues, cytolytic toxins that target host cells, and molecules that incapacitate immune defenses.[110] Importantly, the production of bacterial virulence factors has tradeoffs, including an increased energy requirement and the potential to incite host immune defenses and increase inflammation.[111,112] Accordingly, *S. aureus* senses a combination of bacterial- and host-derived environmental cues to regulate the production of virulence factors that are essential for full *S. aureus* pathogenicity during osteomyelitis.[113]

***S. aureus* regulates virulence and metabolism in response to environmental cues.**

S. aureus is capable of sensing and responding to multiple environmental stimuli.[1,22] For example, the accessory gene regulator (Agr) system is a key mediator of bacterial responses to *S. aureus* density and regulates the production of many *S. aureus* virulence factors to promote bacterial survival and dissemination.[22] Although not the focus of this thesis, Agr serves as a relevant example of how *S. aureus* two component systems and metabolite-responsive transcription factors crosstalk to regulate metabolism and virulence gene expression (**Fig. 2**).[1] Due to the crosstalk between Agr and other signal regulators, *S. aureus* virulence factor production is influenced by amino acid abundance, carbon source availability, bacterial quorum, and oxygen abundance.

The *S. aureus* genome encodes multiple metabolite-responsive transcription factors including CodY, a highly conserved regulatory protein that functions as a transcription factor during stationary phase in Gram-positive pathogens.[114,115] CodY senses met branched-chain amino acids and GTP to regulate both central metabolism and virulence gene expression.[114,115] CodY directly regulates numerous genes involved in amino acid biosynthesis, nutrient transport, and virulence.[115] CodY also indirectly regulates other virulence genes via repression of the *agr* locus.[116] Several adherence-related genes are activated directly by CodY, including fibronectin-binding protein A (*fnbA*) and staphylococcal protein A (*spa*).[115] Other virulence genes that are influenced by the Agr system are regulated indirectly by CodY, such as coagulase (*coa*).[115] Thus, CodY increases expression of virulence genes associated with *S. aureus* adherence via inhibition of RNAIII transcription as well as directly by promoting virulence gene transcription. In Chapter II, we identify a gene (*pheP*) that is important for *S. aureus* survival during osteomyelitis and encodes a putative nutrient transporter regulated by CodY. The regulation of this gene by CodY illuminates a potential metabolic and virulence state of *S. aureus* that potentiates *pheP* expression.

A second well-conserved bacterial catabolite-responsive transcription factor is catabolite control protein A (CcpA), which is responsible for controlling expression of select metabolism and virulence genes in the presence of glucose.[117] Deletion of *ccpA* in *S. aureus* leads to down-regulation of RNAIII, thereby resulting in altered transcription patterns of alpha-hemolysin (*hla*) and *spa*.[117] The influence of CcpA on virulence factor production provides another crucial link between host metabolic state and *S. aureus* pathogenesis. This interaction also suggests that glucose concentration within the bacterial niche or organ tissue could drastically alter the virulence profile of *S. aureus*, which we investigate further in Chapter III of this work. Due to the availability of glucose in bone and characterized bacterial glycolytic metabolism during osteomyelitis, CcpA likely influences the ability of *S. aureus* to infect bone, but this remains to be tested.

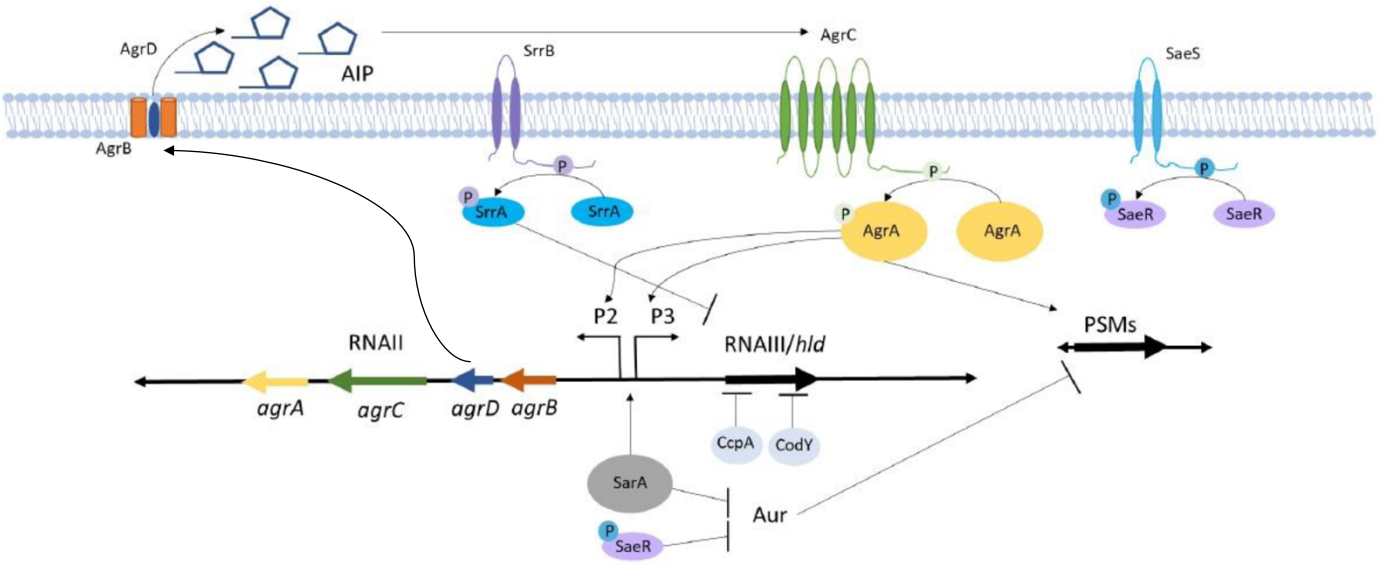

Figure 2. Accessory gene regulator (Agr) is regulated by auto-inducing signals and crosstalk with other two-component systems. Quorum-mediated Agr signaling is influenced by regulatory proteins, staphylococcal accessory regulator A (SarA), carbon catabolite control protein A (CcpA), and CodY. Agr signaling is also altered by two-component systems, such as staphylococcal respiratory response AB (SrrAB) and *Staphylococcus aureus* exoprotein expression response regulator (SaeRS), which are responsive to oxygen (SrrAB) and nutrient availability (SaeRS), as well as host immune stress. AgrB facilitates the formation of extracellular AIP from the AgrD precursor. Agr signaling occurs through AIP-mediated signal transduction at a threshold concentration that activates AgrC phosphotransferase activity to phosphorylate AgrA. AgrA activates the transcription of RNAIII via P3 to regulate virulence factors implicated in *S. aureus* acute osteomyelitis. AgrA binding to P2 results in transcription of RNAII, leading to additional *agrA*, *agrC*, *agrD*, and *agrB* mRNA. Phosphorylated AgrA also enhances the transcription of phenol-soluble modulins (PSMs) directly. SarA and SaeR indirectly augment PSM production via inhibition of the protease Aureolysin (Aur).

***S. aureus* genes facilitate survival in high glucose concentrations.**

The presence of glucose results in CcpA-mediated preferential use of glycolysis over other pathways such as the TCA cycle, pentose phosphate pathway, and gluconeogenesis.[26] Glycolysis is a critical pathway that enables *S. aureus* survival in bone, despite the highly glycolytic metabolism of resident bone cells.[26,118,119] Sustained glucose use by *S. aureus* results in carbon overflow metabolism, producing acetate as a byproduct.[120] *S. aureus* has a number of genes that contribute to sustained fitness in acidifying conditions.[121] The alpha-acetolactate synthase/decarboxylase (AlsSD) pathway is used by *S. aureus* during carbon overflow metabolism to produce a neutral byproduct, acetoin, as opposed to acidic lactate or acetate.[122] The urease enzyme (UreB) catalyzes the hydrolysis of urea to ammonia, which is further ionized to water and ammonium.[123] The production of ammonium effectively consumes a proton, thereby increasing the pH.[123] Additionally, the arginine deiminase pathway (ADI) catabolizes arginine to produce ammonia and increase the pH.[124] Acid production results in formation of ROS and increases the requirement for superoxide dismutase (SOD) activity.[125] *S. aureus* contains two SODs, superoxide dismutase A (SodA) and superoxide dismutase M (SodM), that are critical for *S. aureus* survival in the presence of superoxide during distinct phases of growth.[126] SodA functions to detoxify ROS during exponential phase, while SodM has a greater role during stationary phase.[126] The role of SodA in *S. aureus* survival during hyperglycemic osteomyelitis was previously unknown and is detailed in Chapter III of this work. Despite the repertoire of mechanisms to combat acidic environmental stress, after multiple days of growth in high glucose concentrations, acidic byproduct accumulation effectively lowers the pH, thereby limiting *S. aureus* survival.[120,123]

Taken together, *S. aureus* contains multiple transcriptional regulators and stress-response pathways that control bacterial metabolism and virulence in response to amino acid and carbohydrate abundance. Prior work identified changes in *S. aureus* gene transcription

during skin infection in the presence of increased circulating glucose concentration.[108] However, few studies have examined the mechanisms by which bacterial fitness changes during invasive osteomyelitis in a hyperglycemic host. In Chapter III of this thesis, we investigate how increased blood glucose concentration influences which genes facilitate *S. aureus* survival and virulence during invasive infection.

Transposon sequencing is a powerful tool to discern genes involved in *S. aureus* fitness.

In Chapters II and III, we sought to identify genes that facilitate *S. aureus* survival *in vivo* in various host conditions. Transposon sequencing (TnSeq) has been used to determine bacterial genes required for survival *in vivo* in different infection models and *in vitro* in various conditions.[127–131] TnSeq is a sensitive and high throughput tool that involves generating a highly saturated transposon mutant library, subjecting the transposon mutant library to a selective event, and conducting parallel sequencing analyses to identify the fitness of *S. aureus* mutants.[132] Previous work in our laboratory harnessed the power of TnSeq to identify central metabolism and hypoxic response genes important for *S. aureus* survival during osteomyelitis infection.[2,26] Further analysis of the central metabolism pathways essential for *S. aureus* survival revealed competitive inhibition of a nutrient transporter that resulted in the need for intracellular catabolism of amino acids.[26] This study supported the use of TnSeq to identify critical metabolism pathways and nutrient transporters that promote *S. aureus* growth *in vivo* during osteomyelitis. In both Chapters II and III, we harness the power of TnSeq to identify genes that contribute to *S. aureus* virulence or survival during osteomyelitis infection. Specifically, Chapter II reveals the importance of a putative amino acid permease, PheP, for *S. aureus* survival *in vivo* during osteomyelitis and disseminated infection. In Chapter III, we use TnSeq to identify genes involved in *S. aureus* stress response during osteomyelitis in hyperglycemic mice. We reveal the importance of UreB and SodA, two enzymes with known roles in *S. aureus* virulence during glucose-induced stress.

Conclusions

This dissertation describes our contribution to the study of *S. aureus* metabolism and virulence genes that influence bacterial survival during invasive infection. We examined the genetic components of *S. aureus* survival in euglycemic infection and identified an uncharacterized amino acid permease that is critical for staphylococcal virulence during osteomyelitis and disseminated infection. Furthermore, we used a model of hyperglycemia with comorbid osteomyelitis infection to identify changes in bone homeostasis and bacterial burdens compared to euglycemic infection. Using this murine model of hyperglycemia, we were able to identify genes involved in *S. aureus* virulence that were particularly important for bacterial survival during this metabolic comorbidity.

CHAPTER II. PUTATIVE NUTRIENT TRANSPORTER IDENTIFIED AS ESSENTIAL FOR *STAPHYLOCOCCUS AUREUS* PATHOGENESIS

Introduction

The mechanisms by which *S. aureus* adapts to altered nutrients and host-derived stressors *in vivo* are incompletely understood. However, the recent expansion of tools to distinguish changes in bacterial fitness, including transposon sequencing (TnSeq) and BioLog Phenotype MicroArray plates, provide high-throughput methods to identify growth limitations and genetic determinants of *S. aureus* fitness. The previous TnSeq experiment in our laboratory identified *pheP* (SAUSA300_1231), a putative amino acid permease gene, as essential for *S. aureus* survival during osteomyelitis.[2] A prior publication revealed that PheP contributes to *S. aureus* survival under glucose-limited and microaerobic conditions.[133] The observed growth defect of a *pheP* mutant under microaerobic conditions was rescued with addition of phenylalanine.[133] Interestingly, *S. aureus* is not auxotrophic for phenylalanine.[134] However, a prior study revealed that in the absence of glucose and in conditions with limited oxygen availability, biosynthesis of phenylalanine may be inadequate to support *S. aureus* growth.[133] Nutrient transporters can be promiscuous in the amino acids that they transport, varying based on abundance of nutrients and other stressors, as observed with the aspartate/glutamate transporter, GltT.[26] Thus, we hypothesized that the role of PheP *in vivo* during *S. aureus* osteomyelitis may vary from the *in vitro* cultured conditions previously described.

Amino acid sequence analysis of the *pheP* gene revealed 12 regions of hydrophobicity indicative of membrane spanning domains, interrupted by hydrophilic regions. The PheP sequence has the greatest homology with acid-polyamine-organocation superfamily transport proteins.[135] *S. aureus* PheP exhibits the greatest protein sequence identity with other hypothetical amino acid family proteins encoded by the *Staphylococcus epidermidis* and

Staphylococcus massiliensis species. The greatest homology (75%) with a characterized transporter was identified in *S. piscifermentans* and encodes a gamma-aminobutyrate (GABA) permease. A GABA permease in multiple *Bacillus* species also contains a high degree of sequence homology (47.8%). Finally, Lactobacillus species contain lysine-specific permeases with ~50% homology to the PheP protein sequence. The homology analysis revealed notable amino acid sequence similarities of PheP with lysine and GABA transferases, which may suggest that *S. aureus* PheP is also capable of transporting either substrate.

In the following chapter, we identify the importance of *pheP* for *S. aureus* survival during both osteomyelitis and disseminated infection. We comprehensively analyzed the growth of a *pheP* mutant strain under various metabolic and inhibitor stresses with BioLog plates and identified the importance of *pheP* for *S. aureus* survival in the presence of GABA shunt intermediates supplied as an alternative carbon source. This chapter also reveals *S. aureus* processes that do not require *pheP* and frames future directions for identifying the underlying physiology behind the importance of this gene *in vivo*. Furthermore, in this chapter we summarize other central metabolism, nutrient transporter, and virulence-related genes that were identified with TnSeq but were not essential for *S. aureus* growth *in vivo* during osteomyelitis.

Results

PheP is essential for *S. aureus* survival during osteomyelitis infection.

Tnseq identified the *pheP* gene as essential for *S. aureus* survival during osteomyelitis.[2] To validate the role of *S. aureus* PheP *in vivo*, we assessed the colony forming unit (CFU) burdens of a WT *attC*::empty (WT^{attC}), *pheP*::Tn *attC*::empty ($pheP^{attC}$), and *pheP*::Tn *attC*::*pheP* ($pheP^{attC::pheP}$) strain of *S. aureus* in osteomyelitis mono-infections. We established infection by inoculating mice with $1x10^6$ CFU of USA300 lineage strain AH1263 WT^{attC}, $pheP^{attC}$, and $pheP^{attC::pheP}$ using a post-traumatic model of osteomyelitis, in which bacteria are

inoculated directly into a cortical defect in the mid-femur.[2,3] Over the course of the infection, mice were monitored for changes in weight. Mice infected with *pheP*^{attC} *S. aureus* had significantly less weight loss each day post-infection compared to mice infected with WT^{attC} (**Fig. 3A**). Additionally, *S. aureus* burdens were lower in femurs of mice infected with *pheP*^{attC} compared to WT^{attC} at day 4 post-infection (**Fig. 3B**). However, there were no differences in CFU recovered from the kidneys, heart, or liver of animals infected with *pheP*^{attC} and WT^{attC} (**Fig. 3C-E**). These data confirm the importance of PheP in promoting *S. aureus* osteomyelitis at day 4 post-infection and validate the ability to complement *pheP*^{attC} *in vivo*.

To further assess the role of *S. aureus* PheP *in vivo*, we quantified the CFU burdens of WT^{attC}, *pheP*^{attC}, and *pheP*$^{attC::pheP}$ *S. aureus* in osteomyelitis at day 14 post-infection, a time point that models a chronic infection in mice. We established infection by inoculating mice with 1x10^6 CFU of WT^{attC}, *pheP*^{attC}, and *pheP*$^{attC::pheP}$. Over the course of the infection, mice were monitored for changes in weight. Mice infected with *pheP*^{attC} *S. aureus* had significantly less weight loss days 4 through 11 compared to mice infected with WT^{attC} (**Fig. 4A**). *pheP*$^{attC::pheP}$ infected mice had greater percent starting weights than WT^{attC} on days 7 through 9, which could be indicative of incomplete complementation *in cis* (**Fig. 4A**). *S. aureus* burdens were significantly lower in femurs of mice infected with *pheP*^{attC} compared to WT^{attC} at day 14 post-infection (**Fig. 4B**). Collectively, these data confirm the importance of PheP in promoting *S. aureus* osteomyelitis at day 14 post-infection.

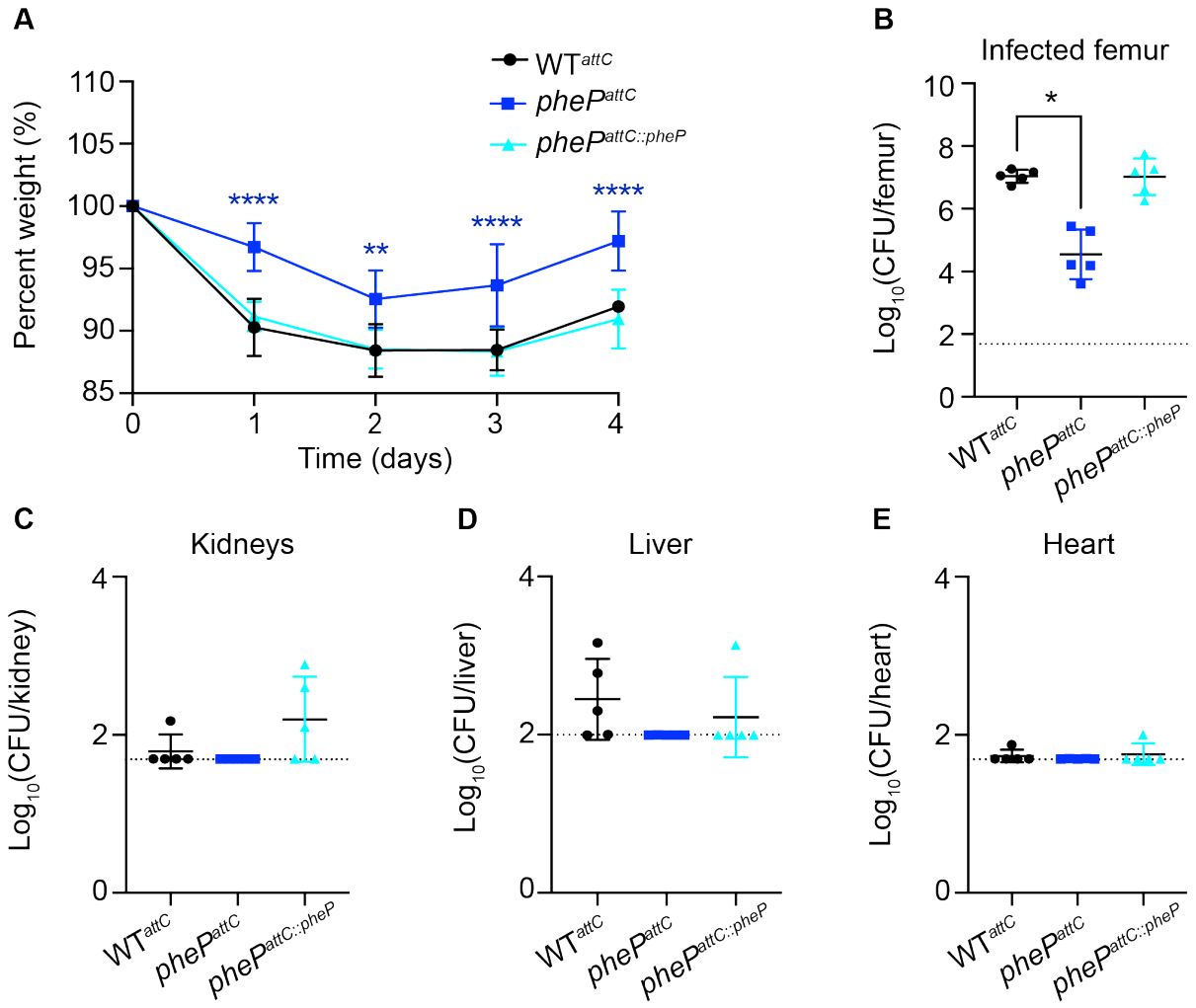

Figure 3. PheP is important for *S. aureus* survival at day 4 in osteomyelitis infection. Eight-week old female mice were infected with 1x10^6 CFU of WT *attC*::empty (WT^{attC}), *pheP*::Tn *attC*::empty (*pheP*^{attC}), and *pheP*::Tn *attC*::*pheP* (*pheP*$^{attC::pheP}$) *S. aureus* via intraosseous injection. (A) Weights were recorded every 24 hrs and normalized to the starting weight of each animal on the day of infection (percent weight). Mice were sacrificed at day 4 post-infection, and the colony forming units (CFU) of bacteria were enumerated in the (B) infected femur, (C) kidneys, (D) liver, and heart. N = 5 mice per group. Dotted lines indicate limit of detection. Horizontal lines indicate mean, and error bars represent SD. Significance determined with two-way ANOVA and Dunnett's multiple comparisons test (A) and Kruskal-Wallis test (B-E). *p<0.05, **p<0.01, ****p<0.0001. All comparisons made relative to WT^{attC}.

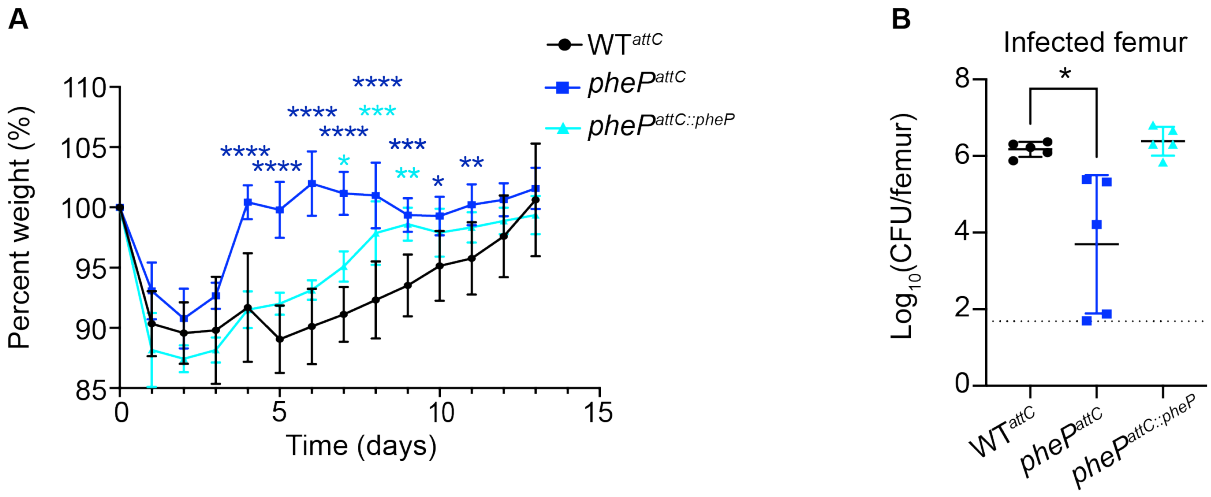

Figure 4. PheP is important for *S. aureus* survival at day 14 in osteomyelitis infection. Eight-week old female mice were infected with 1x10^6 CFU of WT *attC*::empty (WT^{attC}), *pheP*::Tn *attC*::empty (*pheP*^{attC}), and *pheP*::Tn *attC*::*pheP* (*pheP*$^{attC::pheP}$) *S. aureus* via intraosseous injection. (A) Weights were recorded every 24 hrs and normalized to the starting weight of each animal on the day of infection (percent weight). (B) Mice were sacrificed at day 14 post-infection, and the bacterial burden (CFU) was enumerated in the infected femur. N = 5 mice per group. Dotted lines indicate limit of detection. Horizontal lines indicate mean, and error bars represent SD. Significance determined with two-way ANOVA and Dunnett's multiple comparisons test (A) and Kruskal-Wallis test (B). *p<0.05, **p<0.01, ***p<0.001, ****p<0.0001. All comparisons made relative to WT^{attC}.

PheP is essential for *S. aureus* survival during disseminated infection.

PheP is critical for *S. aureus* survival *in vivo* during osteomyelitis infection. To assess whether PheP is also important for *S. aureus* survival in other tissues and with a different inoculation route, we assessed the CFU burdens of WT and *pheP* mutant *S. aureus* in intravenous infection. We inoculated mice by injection into the retroorbital venous plexus with $1x10^7$ CFU of WT and *pheP*::Tn (*pheP*) S. *aureus* to establish infection. Over the course of the infection, mice were monitored for changes in weight. Mice infected with *pheP* mutant *S. aureus* had significantly less weight loss each day post-infection compared to mice infected with WT (**Fig. 5A**). *S. aureus* burdens were lower in the kidneys, heart, and liver of mice infected with a *pheP* mutant compared to WT at day 4 post-infection (**Fig. 5B-D**). The inability of a *pheP* mutant to survive and disseminate during intravenous infection can be rescued by complementation *in cis* (**Fig. 6**). These data confirm the importance of PheP in promoting *S. aureus* disseminated infection at day 4 post-infection and are consistent with a recent publication that highlighted the importance of PheP for *S. aureus* survival in multiple infection models.[136]

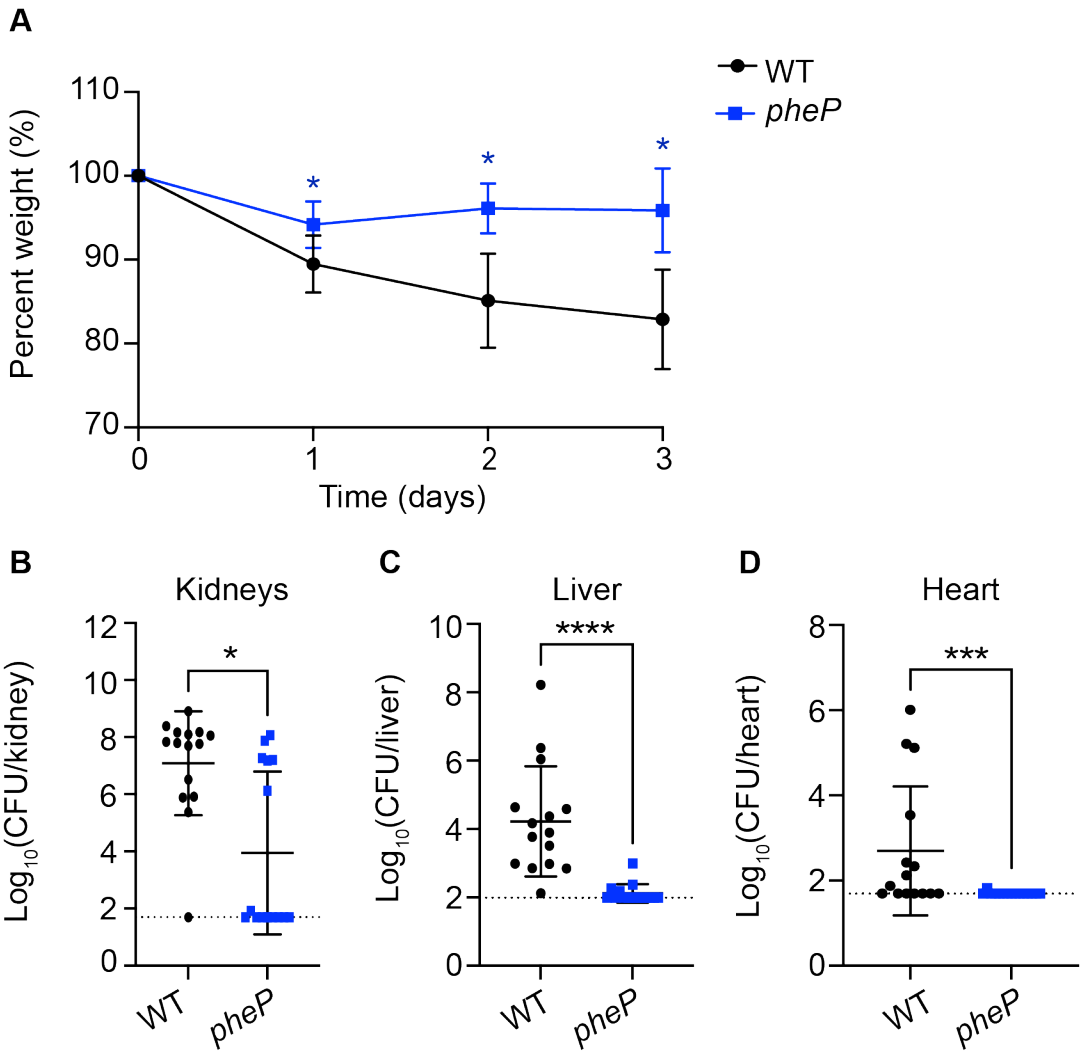

Figure 5. *S. aureus* requires PheP for survival during intravenous infection. Eight-week old female mice were infected with 1x10^7 CFU of WT and *pheP*::Tn (*pheP*) *S. aureus* via retro-orbital injection. (A) Weights were recorded every 24 hrs and normalized to the starting weight of each animal the on day of infection (percent weight). Mice were sacrificed at day 4 post-infection, and the bacterial burden (CFU) was enumerated in the (B) kidneys, (C) liver, and (D) heart. N = 15 mice per group. Dotted lines indicate limit of detection. Horizontal lines indicate mean, and error bars represent SD. Significance determined with multiple unpaired t-tests corrected for multiple comparisons (A) and Mann Whitney test (B-D). *p<0.05, ***p<0.001, ****p<0.0001.

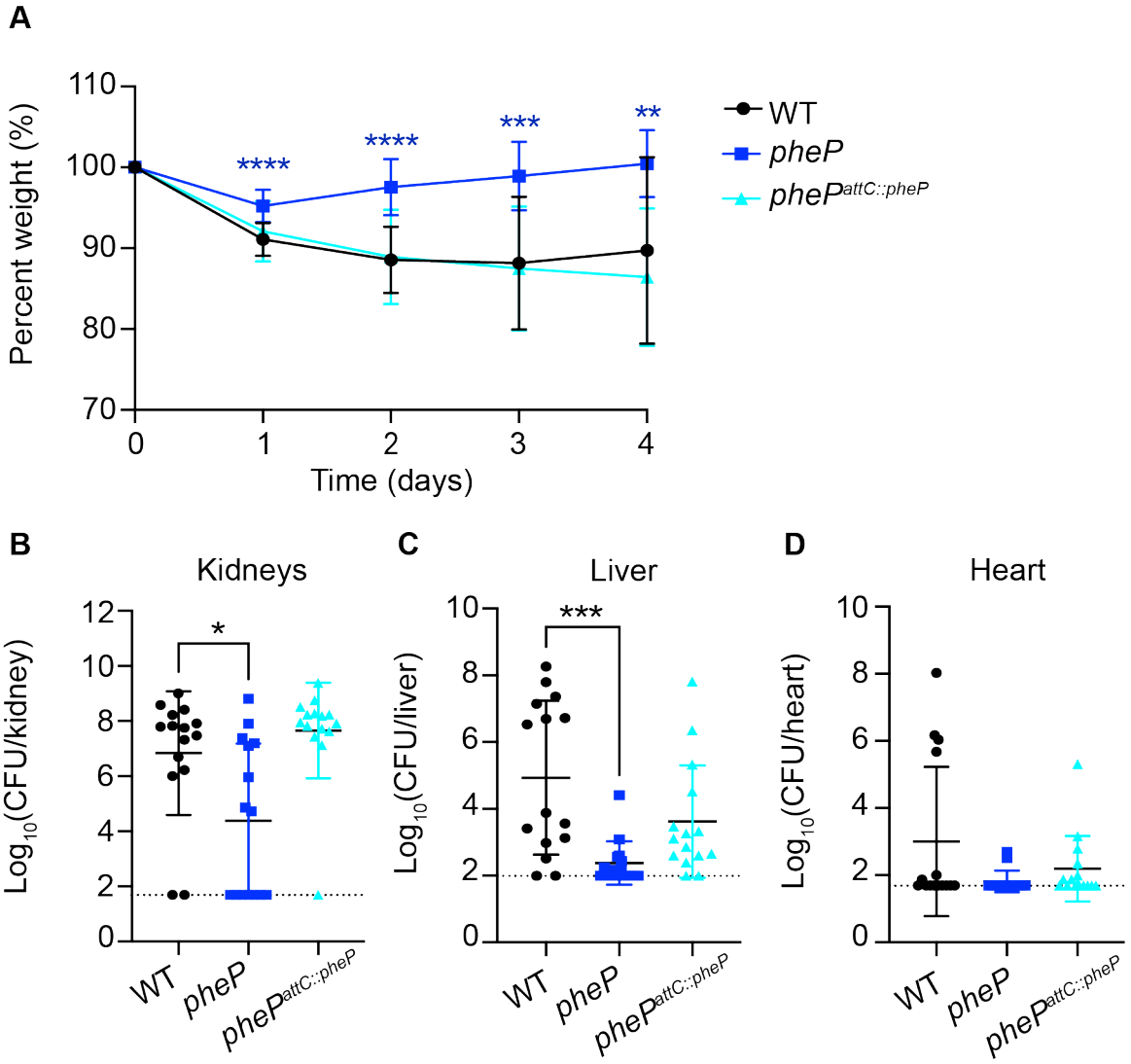

Figure 6. Complementation of *pheP* mutant rescues *S. aureus* growth during intravenous infection. Eight-week old female mice were infected with 1x10^7 CFU of WT, *pheP*::Tn (*pheP*), and *pheP*::Tn *attC*::*pheP* (*pheP*$^{attC::pheP}$) *S. aureus* via retro-orbital injection. (A) Weights were recorded every 24 hrs and normalized to the starting weight of each animal on the day of infection (percent weight). Mice were sacrificed at day 4 post-infection, and the bacterial burden (CFU) was enumerated in the (B) kidneys, (C) liver, and (D) heart. N = 15 mice per group. Dotted lines indicate limit of detection. Horizontal lines indicate mean, and error bars represent SD. Significance determined with two-way ANOVA and Dunnett's multiple comparisons test (A) and Kruskal-Wallis test (B-D). *p<0.05, **p<0.01, ***p<0.001, ****p<0.0001. All comparisons made relative to WT.

pheP* mutant exhibits altered growth kinetics *in vitro* compared to WT *S. aureus.

Mutation of *pheP* renders *S. aureus* unable to survive in osteomyelitis and disseminated infection. However, a *pheP*::Tn mutant can survive in nutrient rich brain heart infusion broth (BHI) and Tryptic Soy Broth (TSB) to the same extent as WT (**Fig. 7A**). To compare the growth of WT and *pheP*::Tn in minimal media, we grew WT and *pheP*::Tn *S. aureus* in chemically defined media (CDMG), as previously described.[137] *pheP*::Tn had a greater lag phase compared to WT, and there were no differences in growth between the WT and *pheP*::Tn complemented strain (**Fig. 7B**). These data demonstrate that the *pheP* mutant strain is unable to grow as well as WT in defined media, although the source of the growth limitation is unclear. To identify specific conditions in which a *pheP*::Tn mutant is unable survive *in vitro* compared to WT *S. aureus*, we grew both strains in Phenotype MicroArray plates 1-10 (Biolog) and measured the change in OD590 hourly for 12 hrs and at 24 hrs (data from 8 and 24 hrs included in **Appendix A**). Biolog Phenotype MicroArray plates allow for quantitative measurement of thousands of cellular phenotypes in the presence of various metabolites, chemicals, and antimicrobial molecules.[138–140] In particular, plates 1 and 2 (PM1 and PM2) allow for identification of compounds that can be utilized by bacteria to grow in the absence of preferred carbon sources. At 8 and 24 hrs, *pheP*::Tn had > 25% decreased growth compared to WT in compounds in PM1 and PM2 associated with the GABA shunt metabolic pathway (**Fig. 8** and **Appendix A**). There were no differences between WT and *pheP*::Tn growth in PM1 and PM2 in the presence of phenylalanine as the alternative carbon source (**Appendix A**). These data are consistent with predicted PheP function based on amino acid sequence homology with lysine, proline, and GABA transporters in other species. To further assess the ability of a *pheP* mutant to transport and use glutamate, proline, and arginine, we grew WT and *pheP*::Tn *S. aureus* in CDMG with and without glutamate, proline, and arginine. As observed in **Fig. 7B**, the *pheP* mutant had a defect in growth in complete CDMG, as measured by changes in OD600 over 24 hrs (**Fig. 9A**).

In the absence of glutamate, *pheP*::Tn retained a significant lag phase compared to WT (**Fig. 9B**). In the absence of arginine and proline, both WT and the *pheP*::Tn were unable to survive (**Fig. 9C and D**). To further assess the ability of PheP to transport proline, we grew WT and the *pheP* mutant in the presence of a toxic proline analog, Azetidine-2-carboxylic acid (Aze). While the *pheP* mutant retained a growth defect in CDMG compared to WT regardless of the presence of Aze, WT and *pheP*::Tn both grew in the presence of the toxic analog (**Fig. 10**). Thus far, studies to elucidate the substrate transported by PheP are inconclusive. Future studies are required to assess additional toxic analogs as well as media without structurally similar amino acids to ensure the toxic analogs are the only exogenous source.

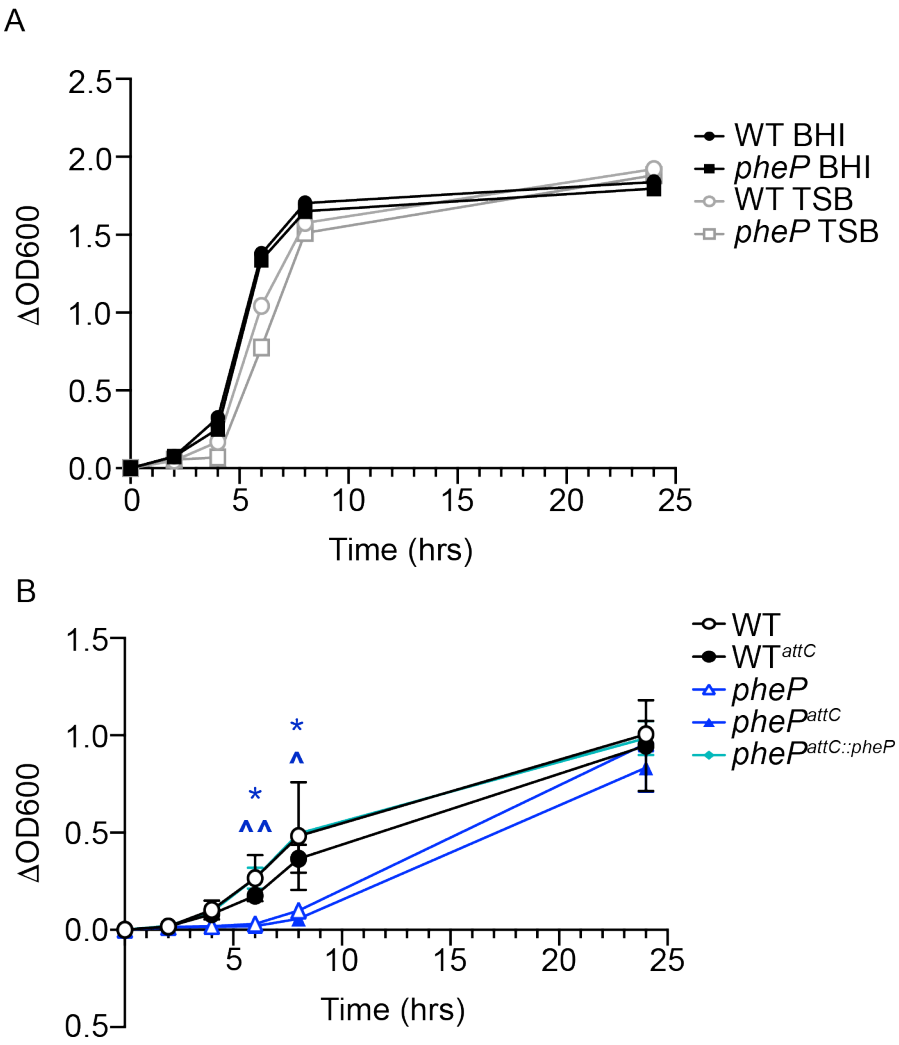

Figure 7. *S. aureus pheP* mutant has a defect in growth in chemically defined media. (A) WT and *pheP*::Tn (*pheP*) *S. aureus* strains were grown in BHI and TSB, and (B) WT, WT *attC*::empty (WT^{attC}), *pheP*::Tn (*pheP*), *pheP*::Tn *attC*::empty (*pheP*^{attC}), and *pheP*::Tn *attC*::*pheP* (*pheP*$^{attC::pheP}$) *S. aureus* strains were grown in chemically defined media with glucose (CDMG). 200 µL of each culture was grown in plates aerobically shaking at 37°C. OD600 was quantified at 0, 2, 4, 6, 8, and 24 hrs and normalized to time 0 hr. N = 3 technical replicates (A), and n = 3 technical and n = 3 biological replicates (B). Line represents mean, and error bars represent standard deviation. Error bars not visible are too small to see under symbols (A). Significance determined with two-way ANOVA and Dunnett's multiple comparisons test. *p<0.05 *pheP*, ^p<0.05 *pheP*^{attC}, ^^p<0.01 *pheP*^{attC} all in comparison to WT^{attC}.

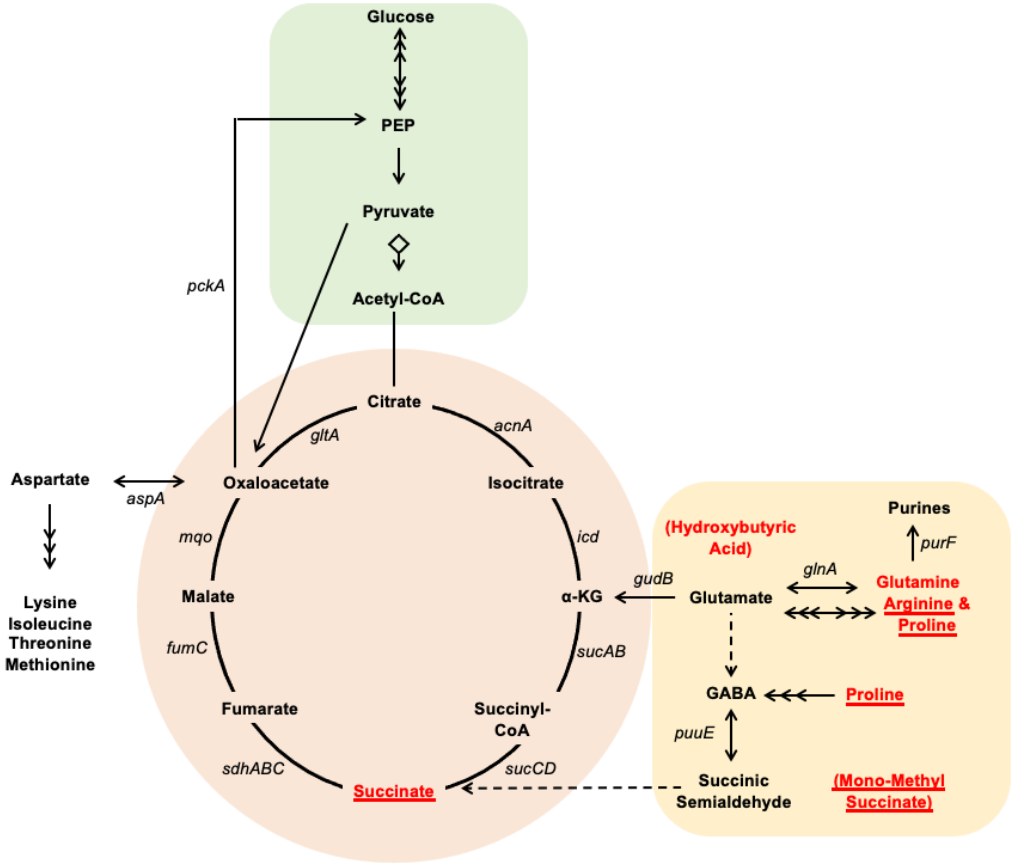

Figure 8. Biolog assay reveals *pheP* mutant is unable to grow as well as WT *S. aureus* with GABA shunt intermediates. Central metabolism schematic includes abbreviated glycolysis/gluconeogenesis (green box), tricarboxylic acid cycle (salmon circle), and gamma aminobutyric acid (GABA) shut pathway (yellow box). Triple arrows indicate multiple steps, and dashed arrows indicate unconfirmed pathways in *S. aureus*. WT and *pheP*::Tn *S. aureus* strains were each grown in Biolog Phenotype MicroArray assays with Carbon Source PM1 and PM2 MicroPlate. OD590 was read every 60 min for 12 hrs and at 24 hrs. Red metabolites signify >25% decreased *pheP*::Tn growth compared to WT at 8 hours, and red underlines indicate >25% decreased *pheP*::Tn growth compared to WT at 12 hours. Assays were supplemented with the given metabolites as alternative carbon sources.

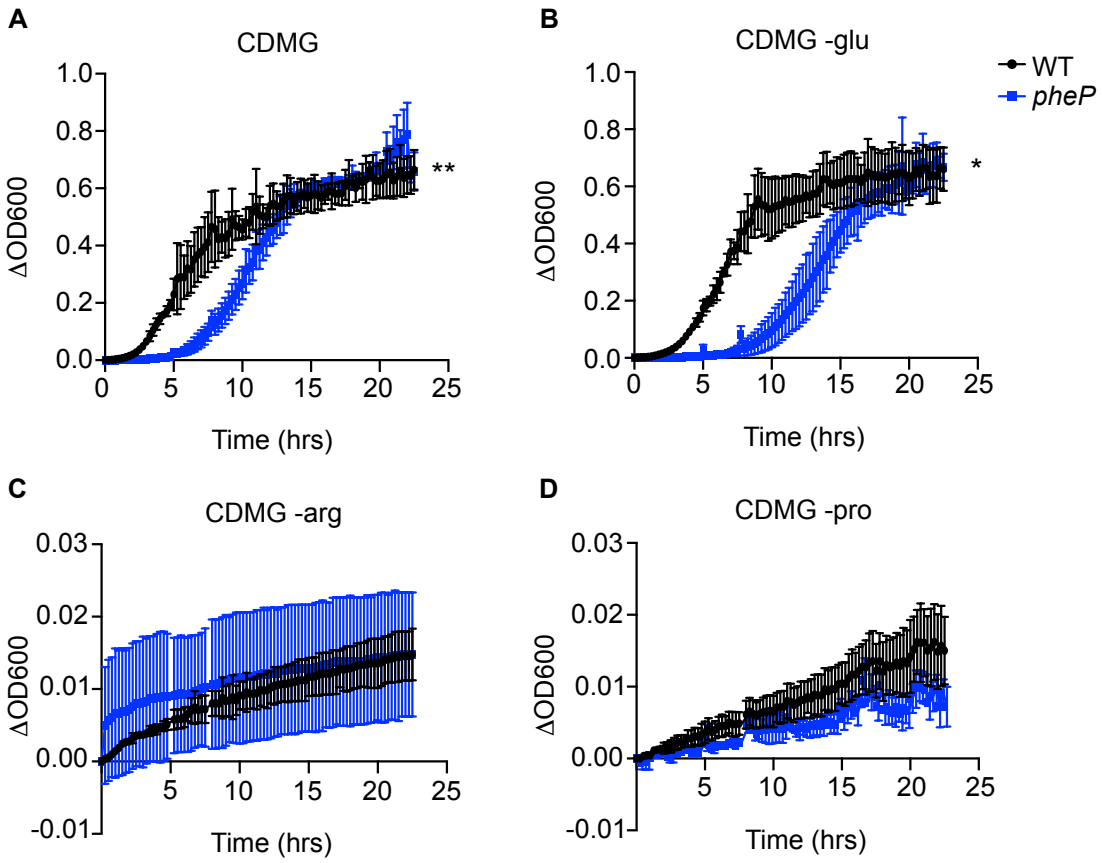

Figure 9. WT and *pheP* mutant *S. aureus* grow similarly in the absence of amino acids involved in the GABA shunt pathway. WT and *pheP*::Tn (*pheP*) *S. aureus* strains were grown in chemically defined media with and without select amino acids in 96 well plates grown aerobically shaking at 37°C. OD600 was quantified at every 15 min for 24 hrs and normalized to OD600 at 0 hr. N = 3 technical replicates, and n = 3 biological replicate. Lines represent mean, and error bars represent standard deviation. Significance determined with two-way ANOVA. *p<0.05, **p<0.01.

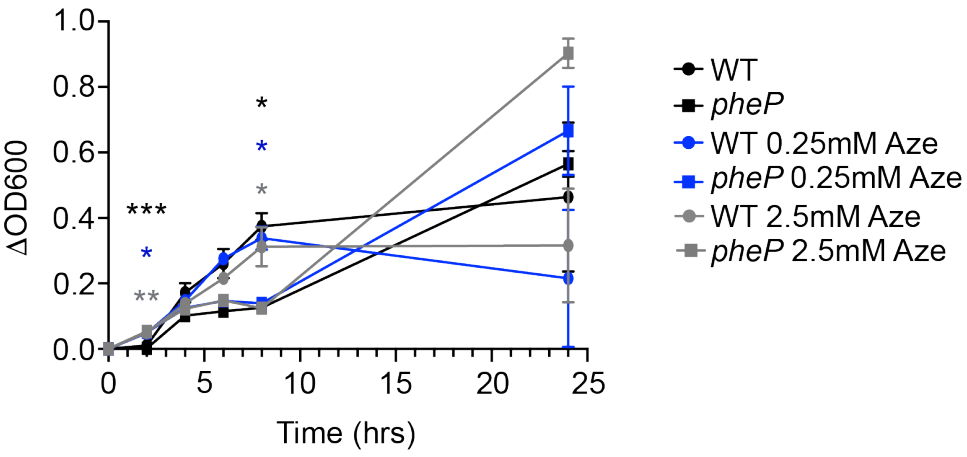

Figure 10. Mutation of *pheP* does not confer a growth advantage for *S. aureus* in the presence of toxic proline. WT and *pheP*::Tn (*pheP*) *S. aureus* strains were grown in chemically defined media in 200 µL in plates aerobically shaking at 37°C with toxic proline analog Azetidine-2-carboxylic acid (Aze). OD600 was quantified at 0, 2, 4, 6, 8, and 24 hrs and normalized to OD600 at 0 hr. N = 3 technical replicates, and n = 3 biological replicates. Lines represent mean, and error bars represent standard deviation. Significance determined with two-way ANOVA. All comparisons made to WT unsupplemented media and all significant differences are with *pheP* compared to WT with respective media condition color. *p<0.05, **p<0.01, ***p<0.001.

Mutation of genes involved in pathways with potential redundancy to PheP function do not alter *pheP* mutant viability.

Based on homology with other transporters, we identified known nutrient transporters and metabolic pathways that could have redundant functions with PheP to assess compensatory functions between genes. We created a *pheP* marked knockout strain (*pheP*::kan) and transduced in transposon mutants in genes encoding transporters that import proline and glycine (*opuD*), lysine (*lysA*), proline (*putP*), and glutamate (*gltS*). We also made a triple mutant strain with *pheP*::kan, SAUSA300_1225::Tn, and SAUSA300_1286::Tn (*lysC*) due to the relationship between aspartate and lysine metabolism. Specifically, aspartate is used *in vivo* for purine synthesis and can be metabolized to lysine.[26] Finally, the *pheP* gene contains a CodY consensus sequence upstream of the gene. We hypothesized that in the presence of branched chain amino acids, CodY negatively regulates the expression of *pheP*. To alleviate repression of the *pheP* gene, we created a *codY* mutant strain and as a control used a *codY*::Tn *pheP*::kan double mutant. For this experiment, we grew WT and the single, double, and triple mutants under oxygenated and microaerobic conditions in unbuffered RPMI for 24 hrs. Unbuffered media was used to allow for pH fluctuation within the cultures, as proline, glutamate, and lysine import can offer protective roles for *S. aureus* in low pH.[121] The absence of a functional *pheP* gene alone or in combination with other metabolic genes did not influence the growth of *S. aureus* in unbuffered RPMI at 24 hrs (**Fig. 11**).

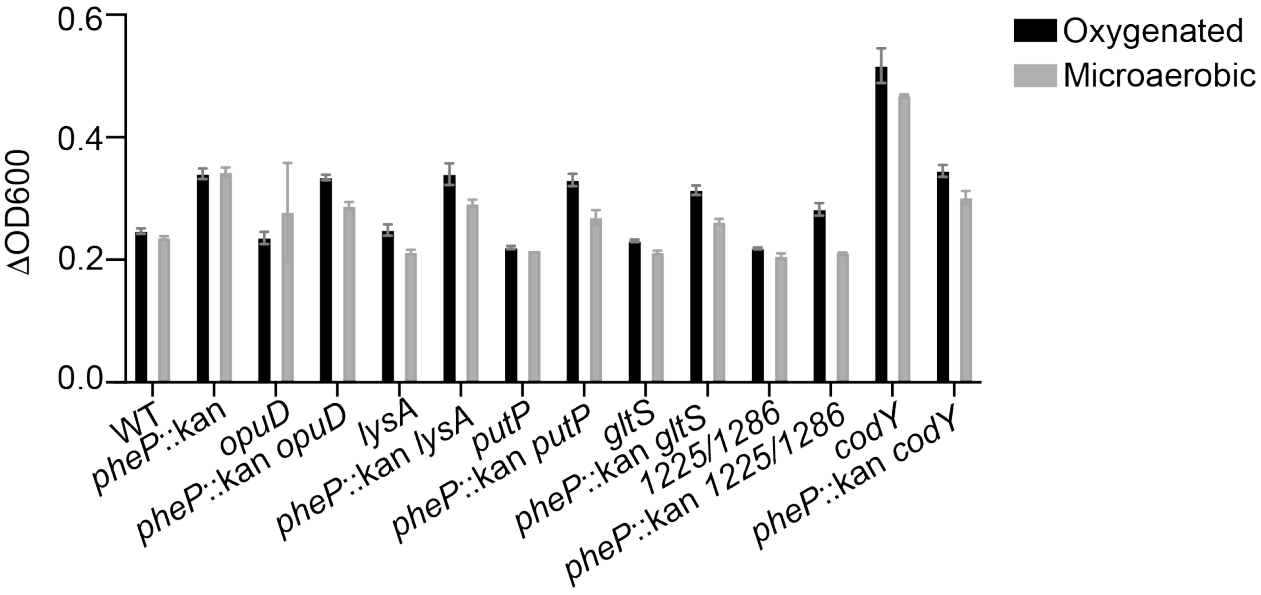

Figure 11. Mutation of genes involved in processes with potential redundancy with PheP does not alter growth. WT, *pheP*::kan, *opuD*::Tn (*opuD*), *pheP*::kan *opuD*, *lysA*::Tn (*lysA*), *pheP*::kan *lysA*, *putP*::Tn (*putP*), *pheP*::kan *putP*, *gltS*::Tn (*gltS*), *pheP*::kan *gltS*, SAUSA300_1225::Tn SAUSA300_1286::Tn (1225/1286), *pheP*::kan 1225/1286, *codY*::Tn (*codY*), and *pheP*::kan *codY S. aureus* strains were grown in 10 mL unbuffered RPMI in flasks aerobically (oxygenated) or under microaerobic conditions shaking at 37°C. OD600 was quantified at 24 hrs and normalized to OD600 at time 0 hrs. N = 3 technical replicates. Bars represent mean, and error bars represent standard deviation. Significance determined with one-way ANOVAs comparing strains within oxygenated and microaerobic conditions. All comparisons made relative to WT within a given condition.

***pheP* mutant supernatant is as toxic as WT supernatant to bone marrow macrophages.**

In addition to exploring the substrate that PheP transports to facilitate *S. aureus* survival in intravenous and osteomyelitis infection, we sought to understand the mechanism by which PheP contributes to bacterial fitness. Due to the intricate link between metabolism and virulence, we hypothesized that PheP imports or exports a metabolite that influences *S. aureus* virulence, thus increasing bacterial fitness *in vivo*. To test the effects of secreted factors produced from WT and *pheP* mutant *S. aureus*, we harvested bacterial supernatant from both strains grown in RPMI with casamino acids for 15 hrs. We concentrated the supernatant and applied them in different volumes to bone marrow derived macrophages (BMMs). We measured the viability of the BMMs exposed to *S. aureus* supernatant for 3 and 24 hrs using CellTiter Glo and found no differences in survival between the cells exposed to *pheP*::Tn and WT supernatant (**Fig. 12**). These data suggest that the secreted factors produced by WT and *pheP* mutant *S. aureus* do not differ in cytotoxicity toward host cells when the strains are grown *ex vivo* in nutrient rich media.

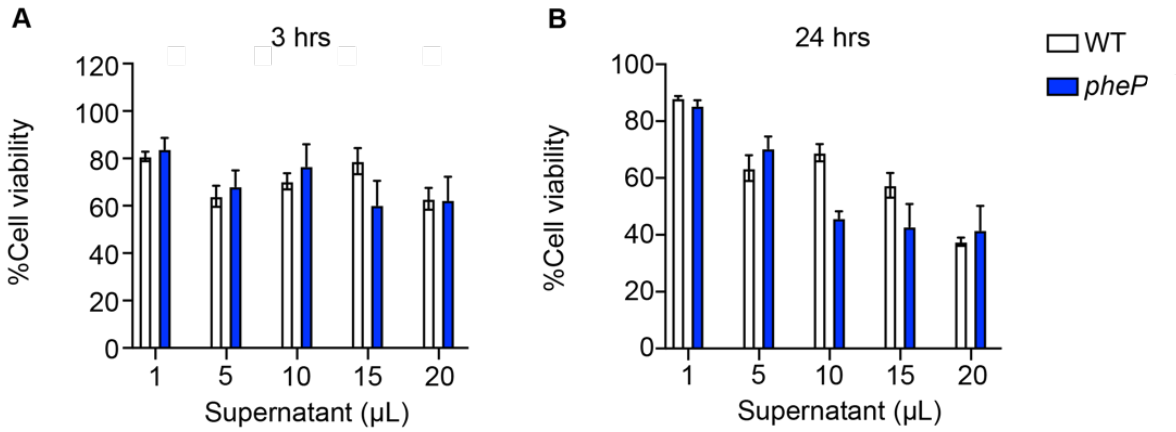

Figure 12. Bone marrow macrophage cytotoxicity is similar in the presence of WT and *pheP* mutant supernatant. WT and *pheP*::Tn (*pheP*) *S. aureus* supernatants were prepared by inoculating 3 colonies into RPMI and 1% casamino acids and growing aerobically for 15 hrs. Supernatant was concentrated via centrifugation. Bone marrow was isolated from eight- to twelve-week old mice and differentiated in CMG14-12 supernatant as a source of M-CSF. Cells were seeded into 96 well plates and supernatants were added in various volumes. Cell viability was assessed at (A) 3 hrs and (B) 24 hrs. N = 3 technical replicates per group. Results are expressed as percent of RPMI control. Bars represent mean, and error bars represent standard deviation. Significance determined with multiple unpaired t-tests corrected for multiple comparisons. All comparisons made relative to WT within a given condition.

PheP is not required for *S. aureus* intracellular survival or biofilm formation.

S. aureus can form multicellular bacterial communities within immune cells to promote bacterial survival and persistence. Invasion of host cells can protect *S. aureus* from innate immune defenses and promote dissemination.[14] Due to the decreased dissemination of *pheP* compared to WT observed during intravenous infection (**Fig. 5 and 6**), we hypothesized that PheP contributes to *S. aureus* survival within host cells. To test this hypothesis, we performed gentamicin protection assays with various multiplicities of infection (MOIs) of WT and *pheP* mutant *S. aureus*. The *pheP* mutant strain of *S. aureus* was internalized to the same extent as WT at 1.5 hrs post-infection (**Fig. 13A**). Additionally, both strains survived within the BMMs to similar extents at 24 hrs (**Fig. 13B**). These findings suggest PheP is not essential for *S. aureus* intracellular fitness *in vitro*.

Extracellular biofilm formation is another mechanism by which *S. aureus* forms tolerant cell populations with various metabolic and virulence subpopulations.[14] To measure changes in biofilm formation between WT and *pheP*::kan, we used crystal violet staining to quantify the amount of adherent biomass after 24 hrs of static bacterial culture. Both strains formed biofilm to similar levels (**Fig. 14**), suggesting PheP is not critical for biofilm formation *ex vivo*.

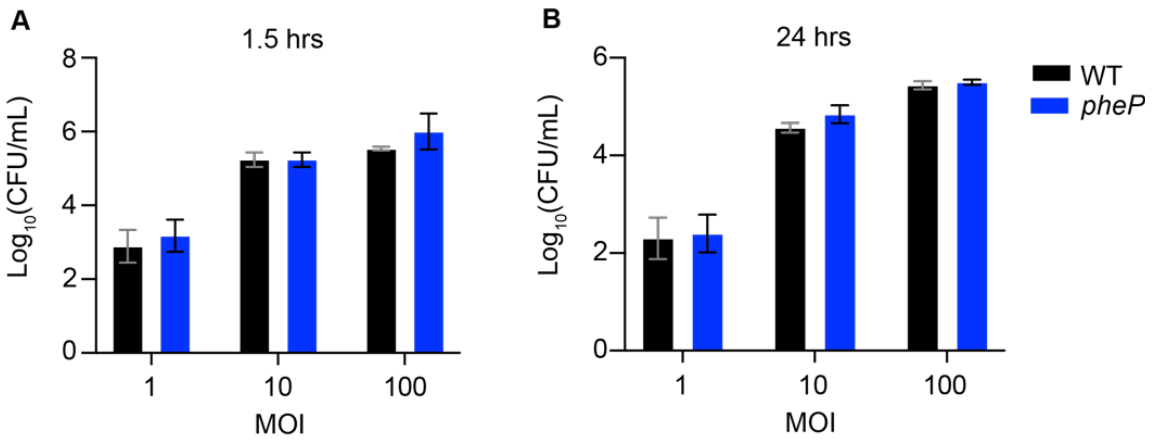

Figure 13. WT and *pheP* mutant *S. aureus* survive intracellularly in bone marrow macrophages. Bone marrow was harvested from nine-week old female mice and cells were differentiated in CMG14-12 supernatant as a source of M-CSF. WT and *pheP*::Tn (*pheP*) were added to bone marrow macrophages at MOIs of 1, 10, and 100 and allowed to internalize. Gentamicin was added to media to kill extracellular bacteria. Cells were lysed and intracellular CFU were enumerated at (A) 1.5 hr and (B) 24 hrs. N = 3 technical replicates per group. Bars indicate mean, and error bars represent SD. Significance determined with multiple unpaired t-tests corrected for multiple comparisons. All comparisons made to WT within a given condition.

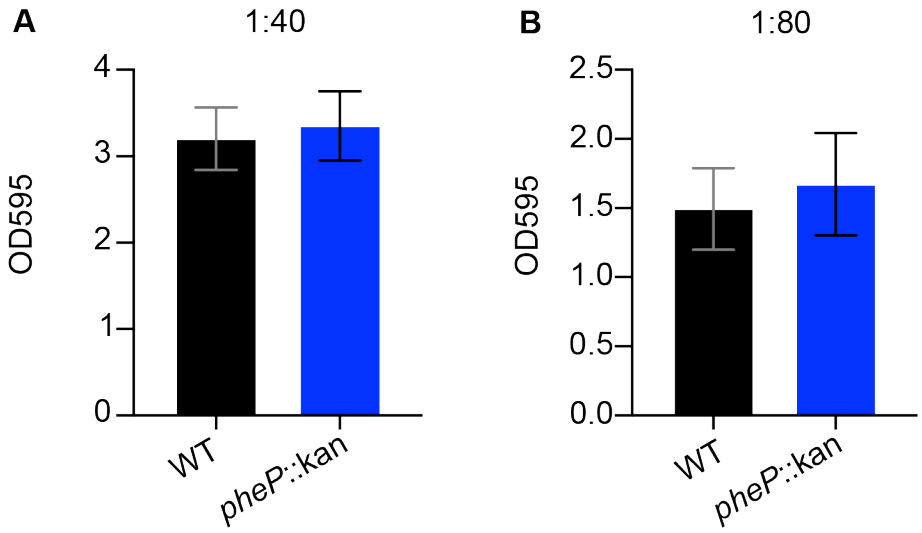

Figure 14. *pheP* mutant *S. aureus* forms biofilms similarly to WT *S. aureus.* WT and *pheP*::kan *S. aureus* strains were grown in TSB static at 37°C in human plasma coated 96 well plates for 24 hrs. Non-adherent cells were removed, and wells were washed prior to fixation with methanol. Adherent biomass was stained with crystal violet, eluted in methanol, and measured with OD590. Eluted dye was diluted (A) 1:40 and (B) 1:80. N = 3 technical replicates. Bars indicate mean, and error bars indicate SD. Significance determined with Student's t-test.

Validation of osteomyelitis TnSeq hits using mono-infections.

In addition to *pheP*, many other genes were identified as essential for *S. aureus* survival during osteomyelitis infection with TnSeq.[2] We prioritized studying genes with known or predicted roles in virulence or metabolism. The genes *empbp* and *nuc* encode a secretory extracellular matrix and plasma binding protein and a thermonuclease, respectively and were identified as essential for *S. aureus* survival. Empbp is important for *S. aureus* aggregation and abscess formation, and Nuc facilitates biofilm dispersal and dissemination.[27,141–143] To test the role of Empbp and Nuc *in vivo* during osteomyelitis, we conducted mono-infections by inoculating mice with $1x10^6$ CFU of WT, *empbp*::Tn, and *nuc*::Tn *S. aureus* strains. Over the course of the infection, mice were monitored for changes in weight. Mice infected with *nuc*::Tn *S. aureus* had significantly less weight loss at 3, 4, 5, and 9 days post-infection compared to mice infected with WT (**Fig. 15A**). However, *empbp*::Tn and *nuc*::Tn infected murine femurs contained the same burden of *S. aureus* compared to WT at day 14 post-infection (**Fig. 15B**). Additional studies with more time points and lower inocula may reveal differences in viability of the *empbp* and *nuc* mutants compared to WT.

Other genes identified in the transposon screen as essential for *S. aureus* survival during osteomyelitis included metabolism and stress-response genes. SAUSA300_1697 encodes a putative dipeptidase, PepV; SAUSA300_0988 encodes a potassium uptake protein, KtrA; SAUSA300_1924 encodes a holin; SAUSA300_0432 encodes a putative sodium-dependent transporter; and SAUSA300_1002 encodes a spermidine/putrescine transporter, PotD.[136,144–147] To test the role of each of these genes *in vivo* during osteomyelitis, we conducted mono-infections by inoculating mice with $1x10^6$ CFU of WT, SAUSA300_1697::Tn, SAUSA300_0988::Tn, SAUSA300_1924::Tn, SAUSA300_0432::Tn, and SAUSA300_1002::Tn mutant *S. aureus* strains. The mice infected with the mutants each had the same CFU at day 14 post-infection compared to WT (**Fig. 16**). These studies suggest that

mutating each of these genes alone does not influence the ability of *S. aureus* to survive *in vivo* during osteomyelitis at day 14 under the conditions tested.

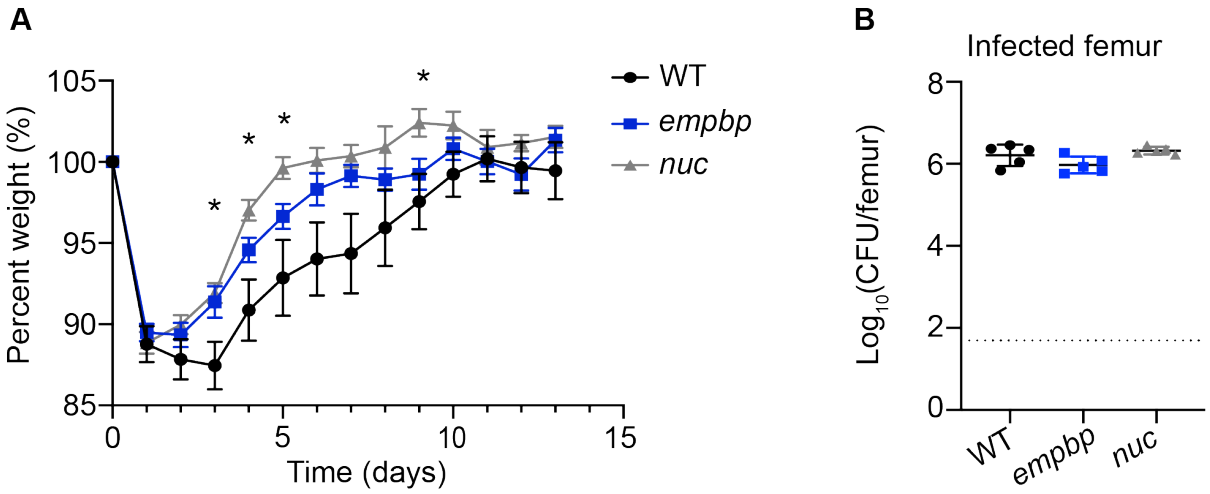

Figure 15. Empbp and Nuc are not important for *S. aureus* survival during osteomyelitis. Eight-week old female mice were infected with 1x10^6 CFU of WT, *empbp*::Tn (*empbp*), and *nuc*::Tn (*nuc*) *S. aureus* via intraosseous injection. (A) Weights were recorded every 24 hrs and normalized to the starting weight of each animal on the day of infection (percent weight). (B) Mice were sacrificed at day 14 post-infection, and the bacterial burden (CFU) was enumerated from each infected femur. N = 5 mice per group. Dotted lines indicate limit of detection. Lines indicate mean, and error bars represent SD. Significance determined with two-way ANOVA and Dunnett's multiple comparisons test (A) and one-way ANOVA (B). *p<0.05 *nuc*::Tn relative to WT. All comparisons made relative to WT.

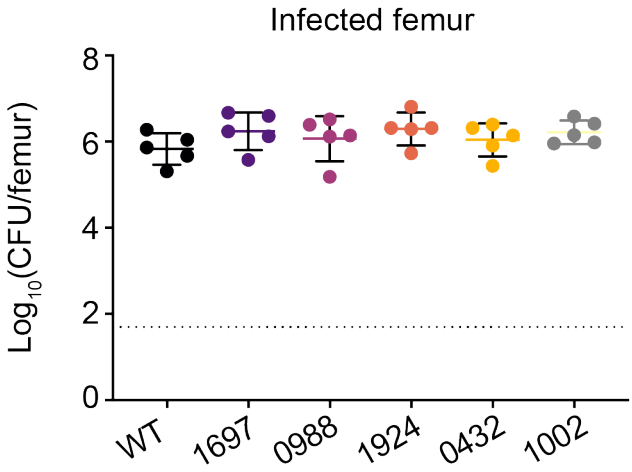

Figure 16. Certain genes identified as important for *S. aureus* survival *in vivo* with TnSeq are not important for survival during mono-infections. Eight-week old female mice were infected with $1x10^6$ CFU of WT, SAUSA300_1697::Tn, SAUSA300_0988::Tn, SAUSA300_1924::Tn, SAUSA300_0432::Tn, and SAUSA300_1002::Tn *S. aureus* via intraosseous injection. Mice were sacrificed at day 14 post-infection, and the bacterial burden (CFU) was enumerated in each infected femur. N = 5 mice per group. Dotted lines indicate limit of detection. Horizontal lines indicate mean, and error bars represent SD. Significance determined with one-way ANOVA corrected for multiple comparisons. All comparisons made relative to WT.

Table 3. Primers used for the creation of *S. aureus* strains

Primer name	Primer sequence fwd	Primer sequencing rev
CB70	ATCGAGAATTCGAGAAC CGAACCCATGCA	ATCGAAGATCTTCTCCCATCTATTT AAATATACC
CB71	ATCGAAGATCTATAAATT CTCATACGGCAGATG	ATCGAGGTACCTGATATTTGAATA AGATATCTTGTG
CB137	CTGACGAATTCAGCTGCA TTAATGAATCGGC	ATCGTGGTACCAAGCATTTTCAGGT ATAGGTG
CB122	ATGAGATCT CTAAGCTAGGGGTTTCAA AATCG	ATGAGATCTGGCGCTAGGTACTAA AACAATTC
CB44	TAATACATATTATAATTT AACC	AAAGATATTAAAGTATATCTG

Discussion

S. aureus has a diverse set of metabolic and nutrient acquisition strategies that enable the bacterium to thrive in nearly every organ of the human body. Prior work in our laboratory identified the importance of glycolysis and aspartate biosynthesis pathways for *S. aureus* survival *in vivo* during osteomyelitis.[26] Various transporters and two component systems were also identified as important in an *in vivo* osteomyelitis TnSeq study.[2] *pheP*, a gene encoding a putative amino acid transporter, was among the genes that were critical for *S. aureus* survival during osteomyelitis infection. We further validated the importance of PheP for *S. aureus* survival and dissemination during osteomyelitis as well as during intravenous infection. However, the mechanism by which PheP functions has yet to be uncovered.

A prior publication revealed that PheP contributes to *S. aureus* survival under glucose-limited and microaerobic conditions.[133] During aerobic growth, the *S. aureus pheP* mutant strain can survive to the same extent of WT, suggesting a possible respiration-linked transport of phenylalanine.[133] The observed growth defect of a *pheP* mutant under microaerobic conditions was rescued with addition of phenylalanine.[133] Interestingly, *S. aureus* is not auxotrophic for phenylalanine.[134] However, a prior study revealed that in the absence of glucose and in conditions with limited oxygen availability, biosynthesis of phenylalanine may be inadequate to support *S. aureus* growth.[133] Limitations presented by the prior work include that the decreased survival of the *pheP* mutant in the absence of glucose was unexplained and was not rescued by addition of exogenous phenylalanine. Additionally, nutrient transporters can be promiscuous in the amino acids that they transport, varying based on abundance of nutrients and other stressors, as observed with the aspartate/glutamate transporter, GltT.[26] Therefore, we sought to identify the context in which PheP is used by *S. aureus* for survival during osteomyelitis and disseminated infection.

Amino acid sequence analysis of the *pheP* gene revealed 12 regions of hydrophobicity indicative of membrane spanning domains, interrupted by hydrophilic regions. The PheP sequence has the greatest homology with acid-polyamine-organocation superfamily transport proteins.[135] The homology analysis revealed notable amino acid sequence similarities of PheP with lysine and GABA transferases, which may suggest that *S. aureus* PheP is capable of transporting either substrate.

In **Figure 9**, we show that a *pheP* mutant does indeed have reduced growth in the presence of GABA shunt intermediates supplied as the carbon source compared to WT *S. aureus* using Biolog Phenotype Microarray analysis. GABA is an amino acid that has been implicated in immune responses as well as bacterial virulence.[148-150] Specifically, one publication identified a decrease in GABA receptor expression on macrophages in mice during bacterial infection.[148] Stimulation with a GABA receptor agonist increased macrophage responsiveness and promoted bacterial clearance. [148] *S. aureus* infection models support an increase in GABA accumulation in tissues during infection, although the implications for the bacteria are unclear.[148] *Pseudomonas* species bacterial cytotoxicity toward host cells was also found to increase in the presence of GABA.[149,150] We therefore hypothesized that PheP transports a derivative of GABA as a virulence strategy to evade the immune response or as a means of increasing cytotoxicity of host cells. However, there were no notable differences between WT and the *pheP* mutant *S. aureus* growth in CDMG without amino acids associated with the GABA shunt pathway or in the presence of a toxic proline analog. An important future direction includes testing the ability of WT and *pheP* mutant *S. aureus* to survive in nutrient-rich and nutrient-limited conditions in the presence of GABA.

Due to the role of GABA in macrophage response to bacterial infection, we investigated the influence of *pheP* mutant supernatant and live bacteria on BMM and *S. aureus* survival compared to WT. We discovered that the *pheP* mutant strain had similar cytotoxicity toward

BMMs compared to WT *S. aureus*. Furthermore, we observed similar intracellular survival between WT and *pheP* mutant in BMMs. Collectively, these findings suggest that PheP may be important for importing an amino acid associated within the GABA shunt pathway, although the amino acid and context for its transport remains unclear.

The ability of *S. aureus* to import GABA is unclear, although many other amino acids closely associated with the structure and metabolism of GABA have well characterized transporters. *S. aureus* has three known proline transporters, OpuD, PutP, and ProP. PutP is a high affinity proline transporter, while OpuD and ProP are low affinity transporters.[151] Proline is transported by *S. aureus* for the purposes of protein synthesis but is not used an alternative carbon source in known contions.[152] Glutamate is primarily transported into *S. aureus* via GltS and can be used as an alternative carbon source in the absence of glucose.[152,153]

PheP also has a high level of sequence identity with lysine transporters in other species. *S. aureus* is not auxotrophic for lysine and contains enzymes to synthesize lysine from aspartate.[26] The gene encoding the enzyme to catalyze the last step of this process is *lysA*, which generates L-lysine from meso-2,6-diaminoheptanedioate.[26] Furthermore, SAUSA300_1225 and SAUSA300_1286 (*lysC*) encode the two aspartate isoforms necessary for lysine biosynthesis.[26] Lysine has a critical role in energy metabolism and quorum sensing in staphylococcal species.[154,155] However, mutating *pheP* in the presence of a *lysA* mutation or SAUSA300_1225 and *lysC* mutations does not appear to affect the growth of *S. aureus* in media *in vitro*. Collectively, these studies did not reveal any redundancy between PheP and other putative transporters or biosynthetic pathways under the conditions assessed.

To further evaluate the conditions in which PheP is used by *S. aureus* for survival, we evaluated the upstream promoter region of the *pheP* gene for transcriptional regulator binding sites. *S. aureus* possesses numerous response regulators that sense the abundance of metabolites and carbon sources and regulate genes involved in both metabolism and virulence,

as described in Chapter I. One such regulator is CodY, a highly conserved regulatory that functions as a transcription factor during *S. aureus* stationary phase.[114,115] CodY senses branched chain amino acids and GTP to regulate genes by binding to conserved binding recognition sites upstream of metabolism and virulence genes.[114,115] The *pheP* gene contains a CodY binding sequence and, therefore, may be repressed in the presence of branched chain amino acid abundance. To alleviate amino acid driven repression of *pheP*, we created a *codY* mutant. Future studies using toxic amino acid derivatives and nutrient limiting conditions may reveal differences in viability of a *codY* mutant strain of *S. aureus* compared to a *pheP*::kan *codY*::Tn double mutant.

In addition to *pheP*, other genes were identified as essential for *S. aureus* survival in the transposon sequencing screen.[2] We selected genes with known or predicted roles in virulence or metabolism to further study their role in *S. aureus* survival *in vivo*. The genes *empbp* and *nuc* encode a secretory extracellular matrix/plasma binding protein and thermonuclease, respectively. Empbp is important for *S. aureus* aggregation and abscess formation, while Nuc facilitates biofilm dispersal and dissemination.[27,141–143] Mutation of either *empbp* or *nuc* did not result in decreased *S. aureus* survival during osteomyelitis. However, the weight differences observed between groups of mice infected with different WT and *nuc* mutant strains at days 3-5 post-infection suggest that the *nuc* mutant strain may in fact be resulting in less severe infection compared to WT *S. aureus*. Additional studies with more time points and lower inocula are required to further assess the ability of *empbp* and *nuc* mutants to survive *in vivo* during osteomyelitis compared to WT.

Other genes that encode metabolic transporters were also identified in the transposon screen as essential for *S. aureus* survival during osteomyelitis.[2] A hypothetical gene, *pepV,* is predicted to encode a dipeptidase with diverse substrate specificity that could participate in a variety of metabolic processes.[145] Few studies have investigated the role of PepV in *S. aureus*

virulence. Uncovering the mechanism of PepV could reveal key metabolic processes involved in *S. aureus* survival during invasive infection. PotD was also studied due to its putative role in transporting spermidine/putrescine. Spermidine and spermine are the preferred substrates for transport by the Pot system, although the physiological relevance of importing these polyamines is unclear.[156] Polyamines have pleiotropic functions in and confer benefits for survival in many organisms due to their ability to scavenge ROS, act as a chemical chaperone, and contribute to acid stress response.[157]

Two ion transporters were identified in the TnSeq screen and were further studied due to their potential role in *S. aureus* fitness during osmotic stress.[2] KtrA is the regulator of the Ktr system, which is comprised on KtrA as well as two ion-conducting proteins, KtrB and KtrD.[158] The Ktr system is one of two potassium transporter systems in *S. aureus* and is important for bacterial fitness *in vivo* during bacteremia.[159] This system is important in potassium-limited alkaline conditions, and mutation of *ktr* genes results in sensitivity to osmotic stress and antimicrobial peptides.[159] A second putative ion transporter system was also identified in the TnSeq analysis, SAUSA300_0432.[2] This gene has not been studied in *S. aureus* but is hypothesized to transport sodium, and further analysis could uncover important physiological processes that increase *S. aureus* fitness.

A final gene that was identified in the TnSeq screen that was further analyzed due to its potential role in *S. aureus* biofilm development was SAUSA300_1924, a putative holin.[2] Holins are membrane-associated proteins that can accumulate and cause bacterial cell lysis. During biofilm development, *S. aureus* regulates cell death to create a scaffold for cell adhesion that allows for attachment to host tissues.[141,160] While none of the mutants involved in stress-response or metabolism that were tested in this work resulted in significantly lower CFU compared to WT *in vivo* during osteomyelitis, further analysis with double mutants and other

metabolic conditions are necessary to interrogate the impact of these genes on *S. aureus* survival.

Limitations of these studies should be considered while interpreting data from Chapter II. *In vivo* survival of mutants identified with TnSeq was analyzed at days 4 (intravenous and osteomyelitis) and 14 (osteomyelitis) with a single inoculum. Additional time points and inocula are necessary to assess differences in strain survival with a lower initial burden. TnSeq has inherent limitations, including the ability of transposon mutants to survive via compensation from other transposon mutations through nutrient sharing or community interactions. Finally, growth curves with toxic amino acid analogs and various *pheP* double mutants were analyzed at limited time points and in media conditions that could obscure changes in growth due to nutrient abundance.

Taken together, the data in this chapter reveal that PheP is required for *S. aureus* survival in both osteomyelitis and intravenous infection. Biolog Phenotype MicroArray analysis identified a group of related amino acids that may be transported or catabolized by PheP in the absence of preferred carbon sources. Further analysis is required to identify the nutritional context in which PheP becomes essential for *S. aureus* growth. The results of this study highlight a putative bacterial nutrient transporter that contributes to *S. aureus* survival in multiple infection models and provide a strong rationale for continued investigation into the mechanism of PheP.

Materials and Methods

Bacterial strains and culture conditions

Unless otherwise stated, experiments were performed with *S. aureus* USA300 lineage strain AH1263, an erythromycin and tetracycline sensitive derivative of strain LAC, which served as wildtype (WT). Transposon mutants were obtained from BEI Resources and were transduced

with phi-85 from JE2 strains into the AH1263 background. *pheP*::Tn is referred to throughout this chapter as *pheP*, and other transposon mutants are similarly abbreviated. To create the *pheP*::kan marked knockout strain, 1kb regions upstream and downstream of *pheP* (SAUSA300_1231) were amplified with primers CB70 and CB71 (**Table 3**), respectively. pKOR1 was amplified with primers CB137, and kanamycin cassette was amplified with primers CB122. Upstream and downstream regions of *pheP* were ligated into pKOR1 to flank the kanamycin cassette. pKOR1 vector was transduced into chemically competent DH5α and subsequently electroporated into RN9011 for integration site specific recombination, based on published protocols.[161] Phi-85-mediated phage transduction was used to move *pheP*::kan from the RN9011 background into USA 300 lineage strain AH1263. The *pheP* complementation construct was created by amplifying *pheP* and its endogenous promoter with primers CB44. The P*pheP-pheP* sequence amplified with primers CB44 was ligated into pJC1306 and integrated into the chromosome at attachment (*attC*) sites, as previously described.[162] pJC1306 integration without DNA ligated into the vector serves as a control and is annotated at *attC*::empty (^{attC}). All bacterial cultures were grown overnight in 5 mL TSB at 37°C with shaking at 180 rpm, except as otherwise noted. 10 μg/mL erythromycin, 2 μg/mL tetracycline, or 50 μg/mL kanamycin was added to cultures with strains possessing antibiotic resistance markers.

Murine model of osteomyelitis

All animal experiments were reviewed and approved by the Institutional Animal Care and Use Committee (ACUC) at Vanderbilt University Medical Center and performed in accordance with NIH guidelines, the Animal Welfare Act, and US Federal law. Six – eight week female C57BL/6J mice were obtained from Jackson Laboratories (stock #000664) for murine experiments. Osteomyelitis was induced with $1x10^6$ CFU in 2 μl via intraosseous injection into the femurs, as previously reported.[3] Mice were weighed daily and monitored for disease

progression. At 4 or 14 days post-infection, mice were sacrificed, and the infected femur, kidneys, liver, and heart were homogenized in Cell Lytic buffer (Sigma) and plated on Tryptic Soy Agar (TSA) for CFU quantification. Limits of detection based on volume of homogenate plated were 49 CFU per femur, heart, and kidneys and 99 CFU per liver.

Model of intravenous infection

Eight-week old female mice were infected with $1x10^7$ CFU of *S. aureus* via retro-orbital injection. Mice were weighed daily and monitored for disease progression. 4 days post-infection, mice were sacrificed, and the kidneys, liver, and heart were homogenized in Cell Lytic buffer (Sigma) and plated on TSA for CFU quantification. Limits of detection based on volume of homogenate plated were 49 CFU per femur, heart, and kidneys and 99 CFU per liver.

Comparative *S. aureus* growth analysis in CDMG *in vitro* for changes in OD600

Overnight cultures of WT and mutant strains were washed in PBS and back diluted 1:1000 into chemically defined media (CDMG), as prepared previously.[26,163] Amino acids were omitted from complete CDMG where indicated. A toxic proline analog, azetidine-2-carboxylic acid (Aze) (Thermo Fisher), was added to cultures where indicated for a final concentration of 0.25 mM or 2.5 mM Aze. The cultures were plated in non-tissue culture treated flat clear-bottom 96 well plates in 200 µl volumes in triplicate. The plated cultures were grown at 37°C with fast shaking in BioTek plate reader for OD600 reads at indicated time points. Growth was reported as OD600 compared to OD600 quantified at 0 hrs.

Comparative *S. aureus* growth analysis in RPMI *in vitro* for changes in OD600

Overnight cultures of WT and mutant strains were washed in PBS and back diluted 1:1000 in 10 mL unbuffered RPMI (Sigma-Aldrich R6504) in 50 mL Erlenmeyer flasks. The cultures were grown at 37°C with shaking at 180 rpm either loosely covered with foil (aerobic) or plugged with a rubber stopper (microaerobic). At indicated time points, cultures were plated in

non-tissue culture treated flat clear-bottom 96 well plates in 200 µl volumes in triplicate and OD600 was measured with BioTek plate reader. Growth was reported as OD600 compared to OD600 quantified at 0 hrs.

Biolog assay

Phenotype MicroArray for Microbial Cells plates 1-20 (Biolog Inc., Hayward, CA) were used to compare growth of WT and *pheP*::Tn in the presence of various nutrient sources and chemical inhibitors. The plates include the following analyses: carbon sources (PM1 and PM2A), nitrogen sources (PM3B), phosphorus and sulfur sources (PM4A), nutrient supplements (PM5), peptide nitrogen sources (PM6-PM8), osmolytes (PM9), pH (PM10), and chemical/antibiotic sensitivity panels (PM11C, PM12B, PM13B, PM14A, PM15B, PM17A, PM18C, PM19, and PM20). All reagents were prepared based on manufacturer's instructions, and 200 µl were added to each well of the Biolog plates. 2 µl of PBS suspended bacteria from overnight cultures were added to each well. Plates were wrapped in parafilm and incubated at 37°C with shaking at 180 rpm. OD590 was recorded hourly for each plate 0-12 hrs and again at 24 hrs. Growth was normalized to OD590 at time 0 hrs for each well. *pheP*::Tn growth was normalized to WT to identify conditions in which *pheP*::Tn grew/survived to a lesser extent than WT.

Whole bone marrow isolation and macrophage enrichment

Bone marrow was isolated from C57BL/6J 8 to 12 week old female mice by flushing femurs with MEM-α. Cells were then centrifuged at 1500 rpm for 5 min and resuspended in ammonium-chloride-potassium buffer for 10 min to lyse red blood cells. PBS was added to deactivate lysis, and cells were centrifuged and resuspended in MEM-α with 1X Penicillin-Streptomycin and 10% FBS (complete media) to be counted. Cells were frozen in 10% dimethyl sulfoxide (DMSO) in FBS in liquid nitrogen until use. Frozen cells were thawed rapidly at 37°C and washed in MEM-α to remove DMSO. Fresh and thawed cells were seeded

at 8 million cells per 10 cm tissue culture treated dish in complete media with CMG14-12 supernatant at 1:10 vol/vol as a source of M-CSF. Cells were cultured for 4 days before plating at 50,000 cells/well in 96-well plates in complete media with CMG14-12 supernatant at 1:40 vol/vol.

Cytotoxicity assay

Concentrated bacterial supernatants were prepared as previously reported.[3] *S. aureus* single colonies (3) were inoculated in 250 mL Erlenmeyer flasks with 50 mL RPMI and 1% casamino acids (Fisher Scientific). Flasks were cultured for 15 hrs under microaerobic conditions at 37°C shaking at 180 rpm. Cultures were centrifuged at 4000 x g for 10 min to pellet bacteria. Supernatants were sterilized with a 0.22-μm filter and concentrated to a final volume of 1.5 mL with an Amicon Ultra 3-kDa nominal molecular weight column (MilliporeSigma, Burlington, MA). Supernatants were filter sterilized and single-use aliquots were prepared on ice. Various volumes of concentrated supernatants were applied to differentiated BMMs (see whole bone marrow isolation and macrophage enrichment). Cell viability was measured at various time points with CellTiter-Glo Luminescent Cell Viability assay (Promega), based on manufacturer's instructions.

Gentamicin assay

After 3 days of culture in 96 well plates (see whole bone marrow isolation and macrophage enrichment above), BMM cell culture media was switched to complete media with CMG14-12 supernatant at 1:40 vol/vol as a source of M-CSF. Two days later, cells were washed with PBS, and unsupplemented serum- and antibiotic-free MEM-α was added. After 2 hrs, *S. aureus* strains were adjusted to a concentration of $5x10^8$ CFU/mL in sterile PBS. BMMs were infected with *S. aureus* at various MOIs. Plates were centrifuged at 1000 rpm for 1 min to ensure bacteria came into contact with BMMs. Cells were incubated for 1 hr at 37°C for bacterial internalization. Media were removed and cells were washed with PBS before adding MEM-α

supplemented 100 μg/mL gentamicin and returning the plate to incubate. After 30 min, BMMs were lysed with 0.1% Triton-X to serial dilute cultures and enumerate internalized CFU for a 1.5 hr time point. For a 24 hr time point, cells were switched to MEM-α supplemented 25 μg/mL gentamicin and lysed with Triton-X 22 hrs later to serial dilute and enumerate internalized CFU.

Biofilm assay

Single donor human plasma (Innovative Research) was diluted in 0.05 M carbonate-bicarbonate buffer pH 9.6 to 20% v/v. 96-well plates were coated with plasma solution and incubated at 4°C overnight. Bacterial cultures were grown overnight and standardized to an OD600 of 0.05 in fresh TSB. Plasma solution was removed from each well and 200 μl of standardized bacterial cultures were added. Plates were incubated at 37°C for 24 hrs. Non-adherent cells were removed and wells were washed prior to fixation with methanol. Adherent biomass was stained with crystal violet and eluted in methanol. Cultures were diluted by a factor of 40 and a factor of 80 to fall within range of detection and measured with OD590.

Graphical and statistical analysis

Statistical analyses were performed with Prism 9.4.1 (GraphPad Software). Data were checked for normality prior to statistical analysis. In experiments of three or more groups analyzed over time, data were compared with 2-way ANOVA with Dunnett's multiple comparisons test. CFU were compared between three or more groups at one time point (i.e. *in vivo*) with Kruskal-Wallis test. In comparisons of two groups, mouse weight or bacterial CFU were compared over time with multiple paired t-tests. CFU burdens were compared between two groups at one time point (i.e. *in vivo*) using Mann-Whitney tests, in the case of non-gaussian data. Normally distributed values were compared between two groups at one time point with a one-way ANOVA and Dunnett's multiple comparisons test. Changes in biofilm formation between two strains were compared with a Student's t-test.

Coauthor contributions

All experiments were conceptualized and designed by Dr. James Cassat and me. Dr. Brittney Gimza assisted with constructing the *pheP*::kan marked knockout strain. Dr. James Cassat assisted with *in vivo* osteomyelitis experiments. Jenna Petronglo assisted with all *in vivo* intravenous infections. I conducted all other experiments.

A portion of the following section (*Chapter III,* Hyperglycemia increases the severity of *Staphylococcus aureus* osteomyelitis and influences bacterial genes required for survival in bone) was originally published in *Infection and Immunity* (2023).

Butrico CE, Klopfenstein N, Green ER, Johnson JR, Peck SH, Ibberson C, Serezani CH, Cassat JE. 2023. Hyperglycemia increases the severity of *Staphylococcus aureus* osteomyelitis and influences bacterial genes required for survival in bone. *Infection and Immunity*. 2023.

doi: 10.1128/iai.0059-22

CHAPTER III: HYPERGLYCEMIA INCREASES THE SEVERITY OF *STAPHYLOCOCCUS AUREUS* OSTEOMYELITIS AND INFLUENCES BACTERIAL GENES REQUIRED FOR SURVIVAL IN BONE

Introduction

Hyperglycemia, or elevated blood glucose, can result from chronic metabolic conditions as well as acute stress and reflects the inability of the body to produce or effectively use insulin. Hyperglycemia leads to a variety of physiological and immune regulatory alterations.[73,75,84,85,164,165] Dysregulated cytokine response, altered chemotaxis, and decreased function of innate immune cells contribute to a hyperinflammatory environment and influence the pathophysiology of bacterial infections.[73,81,85] Hyperglycemia also increases oxidative stress in tissues via production of reactive oxygen species (ROS), which are generated as a consequence of electron transport chain dysfunction during mitochondrial respiration and glucose metabolism.[166] The combination of reduced immune responses and hyperinflammation leads to a greater incidence of infection in individuals with hyperglycemia.[167] Musculoskeletal infections are a common manifestation of increased infection susceptibility in hyperglycemic individuals.[168] However, how hyperglycemia alters osteomyelitis pathogenesis or bacterial adaptation to the host microenvironment during musculoskeletal infection is not fully understood.

S. aureus has a remarkable ability to infect a variety of tissues, which can be attributed to its metabolic flexibility and the capacity to produce an arsenal of virulence factors.[1,3,26,169] Multiple transcriptional regulators allow *S. aureus* to modulate its virulence in response to environmental cues, such as glucose abundance.[1] However, the virulence and metabolic mechanisms by which *S. aureus* adapts to the altered host environment during osteomyelitis in hyperglycemic mice are not well understood. We hypothesized that the alterations in glucose

availability and changes in host physiology during hyperglycemia require *S. aureus* to use distinct genes to survive and induce severe disease in the context of osteomyelitis.

To investigate the requirements for *S. aureus* survival and virulence *in vivo* during hyperglycemia, we subjected mice to acute and chronic hyperglycemia and then induced osteomyelitis using a post-traumatic model. Hyperglycemic infected mice exhibited more severe infection as measured by colony forming units (CFU) of *S. aureus* and bone destruction. We used transposon sequencing (TnSeq) to identify *S. aureus* genes required for infection in hyperglycemic osteomyelitis. Based on the TnSeq analysis, we further studied the influence of superoxide dismutase A (SodA) on disease pathogenesis due to the known role of SodA in detoxifying ROS.[170] SodA was found to be important for *S. aureus* survival in hyperglycemic mice. To study the mechanistic basis of this finding, we analyzed the growth of a *sodA* mutant *in vitro* in high glucose and identified that the *sodA* mutant exhibited a growth defect in high glucose. Collectively, Chapter III reveals the influence of hyperglycemia on increased infection severity during osteomyelitis and identifies *S. aureus* genes that may contribute to increased bacterial survival in osteomyelitis during hyperglycemia.

Results

Acute hyperglycemia increases *S. aureus* burdens during osteomyelitis.

To investigate the impact of hyperglycemia on *S. aureus* virulence during osteomyelitis, we first induced hyperglycemia in male C57BL/6J wildtype (WT) mice by treating with streptozotocin (STZ).[81,171] STZ induces hyperglycemia through cytotoxic effects on insulin-producing beta cells. We then subjected STZ- or vehicle-treated mice to osteomyelitis and determined *S. aureus* burdens following infection.[3] Because the induction of hyperglycemia following STZ treatment is variable, we measured blood glucose levels in mice 10 days after STZ treatment, at the time of infection (day 0) and at the conclusion of the experiment (day 14).[172,173] In this experiment, all mice treated with STZ were hyperglycemic

(defined as blood glucose levels of > 250 mg/dl) at days 0 and 14 of infection (**Fig. 17A**). STZ-treated hyperglycemic mice and euglycemic vehicle-treated control mice were infected 10 days after the last STZ or vehicle treatment with $1x10^6$ CFU *S. aureus* USA300 lineage strain AH1263 (WT). To infect mice, we used a post-traumatic model of osteomyelitis, in which bacteria are inoculated directly into a cortical defect in the mid-femur.[2,3] Acute hyperglycemia resulted in a significant increase in *S. aureus* burdens in the infected femurs compared to euglycemic vehicle-treated animals at day 14 post-infection (**Fig. 17B**). To assess the extent to which hyperglycemia alters *S. aureus* dissemination to other tissues, we also collected the contralateral femur, kidneys, liver, and heart. While dissemination to the contralateral femur did not significantly change, dissemination to the kidneys, liver, and heart significantly increased in acute hyperglycemic animals (**Fig. 17C-F**). Similar trends were observed with a lower inoculum of *S. aureus* (**Fig. 18**), although the only organs with significantly greater CFU in the hyperglycemic mice compared to euglycemic mice in this experiment were the infected femur and kidneys (**Fig. 18B and 18C**). These data suggest that acute hyperglycemia increases *S. aureus* survival in bone as well as dissemination to other organs during osteomyelitis.

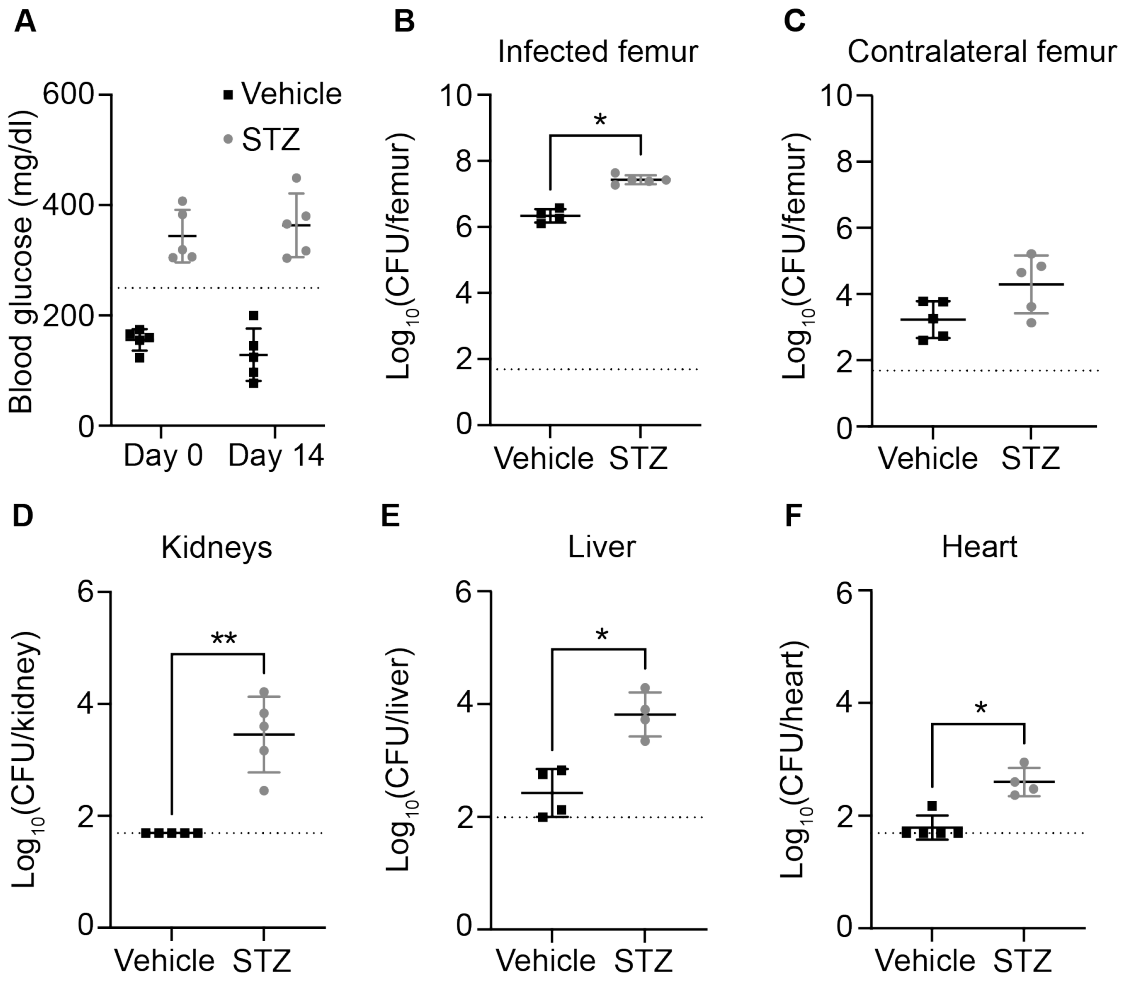

Figure 17. Acute hyperglycemia increases *S. aureus* burdens and dissemination during osteomyelitis. Eight-week old male mice were treated with sodium citrate (vehicle) or streptozotocin (STZ) intraperitoneally for 5 days. 10 days after the final injection, mice were infected with $1x10^6$ CFU of WT *S. aureus* via intraosseous injection. (A) Blood glucose concentration was quantified from a tail vein bleed immediately prior to inoculation (day 0) and the day of sacrifice (day 14). Dotted line indicates hyperglycemia threshold of 250 mg/dl. Mice were sacrificed at day 14 post-infection, and the bacterial burdens (CFU) were enumerated in (B) infected femur, (C) contralateral femur, (D) kidneys, (E) liver (n = 4 mice per group), and (F) heart (n = 4 mice in STZ-treated group). N = 5 mice per group, unless otherwise noted. Dotted lines indicate limit of detection. Horizontal lines indicate mean, and error bars represent SD. Significance determined with Mann-Whitney test (B-F). *$p<0.05$, **$p<0.01$.

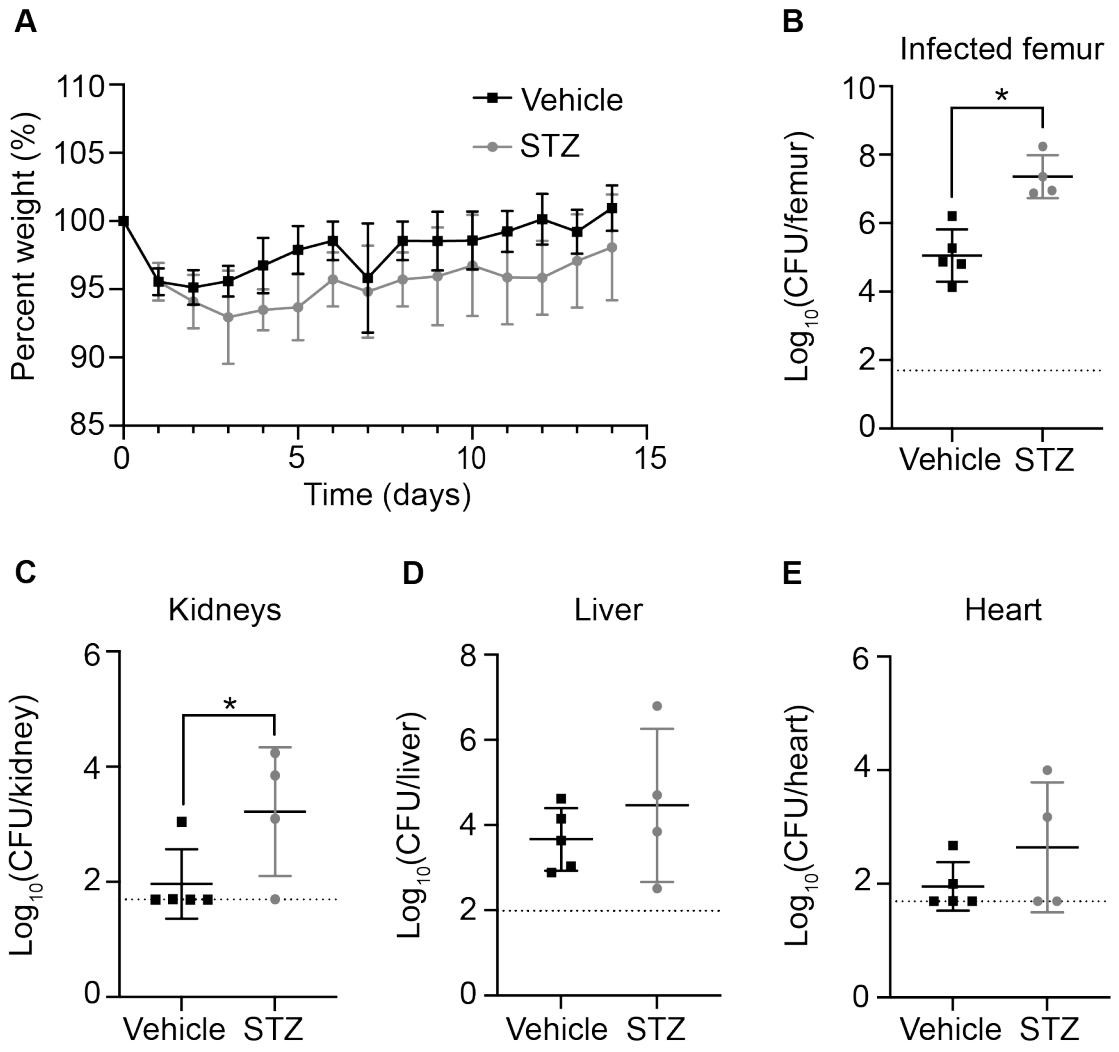

Figure 18. *S. aureus* survival during osteomyelitis increases during acute hyperglycemia with a lower inoculum. Eight-week old male mice were treated with sodium citrate (vehicle) or streptozotocin (STZ) intraperitoneally for 5 days. 10 days after the final injection, mice were infected with $1x10^5$ CFU of WT *S. aureus* via intraosseous injection. (A) Weights were recorded every 24 hrs and normalized to the starting weight of each animal on the day of infection (percent weight). Mice were sacrificed at day 14 post-infection, and the bacterial burdens (CFU) were enumerated in (B) infected femur, (C) kidneys, (D) liver, and (E) heart. N = 5 mice in vehicle-treated group, and n = 4 mice in STZ-treated group. Dotted lines indicate limit of detection. Horizontal lines indicate mean, and error bars represent SD. Significance determined with multiple paired t-tests (A) and Mann-Whitney test (B-E). *$p<0.01$.

***S. aureus* burdens increase due to hyperglycemia induced by STZ treatment.**

To confirm that changes in *S. aureus* growth and dissemination result from acute hyperglycemia induced from STZ treatment and not from off-target effects of the drug, we assessed bacterial burdens in three additional groups of mice: euglycemic vehicle-treated mice, STZ-treated mice that became hyperglycemic, and STZ-treated mice that remained euglycemic (**Fig. 19A**). We inoculated mice with $1x10^6$ CFU of *S. aureus* and measured bacterial burdens in the femur 14 days post-infection. STZ-treated hyperglycemic mice had greater *S. aureus* burdens in infected femurs compared to both euglycemic vehicle-treated and euglycemic STZ-treated mice (**Fig. 19B**). These data indicate that changes in bacterial burden in STZ-treated mice result from hyperglycemia.

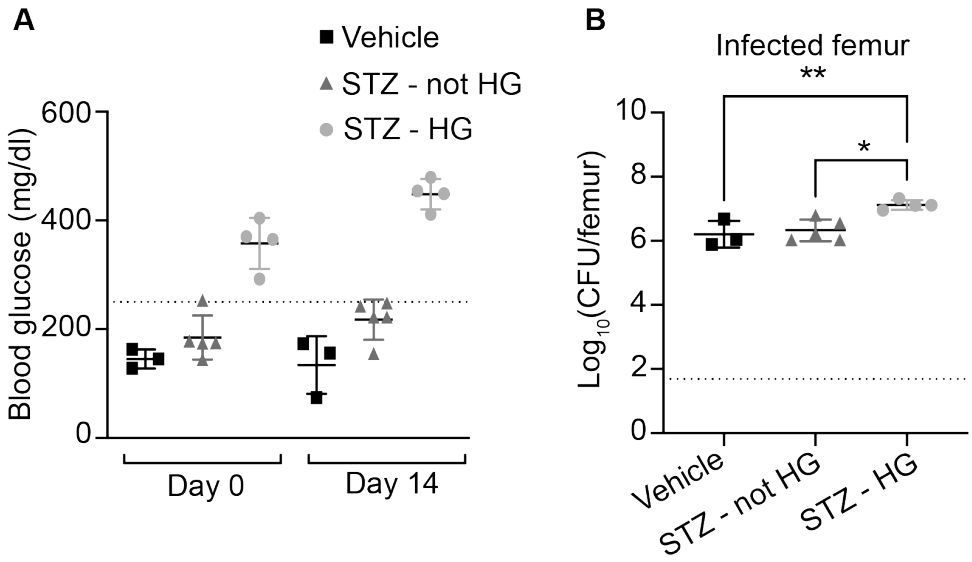

Figure 19. *S. aureus* bacterial burdens are higher in STZ-treated hyperglycemic mice compared to euglycemic STZ- or vehicle-treated mice during osteomyelitis. Eight-week old male mice were treated with sodium citrate (vehicle) or streptozotocin (STZ) intraperitoneally for 5 days. 10 days after the final injection, mice were infected with $1x10^6$ CFU of WT *S. aureus* via intraosseous injection. (A) Blood glucose concentration was quantified from the tail vein on the day of infection (day 0) and the day of sacrifice (day 14). (B) Mice were sacrificed at day 14 post-infection, and the bacterial burdens (CFU) were enumerated in infected femurs. N = 3 mice for vehicle group, n = 5 mice for STZ - not hyperglycemic (STZ - not HG) group, n = 4 mice for STZ - hyperglycemic (STZ - HG) group. Horizontal line indicates mean, and error bars indicate SD. Significance determined with one-way ANOVA and Tukey's multiple comparisons test (B). *$p<0.05$, **$p<0.01$.

Chronic hyperglycemia increases *S. aureus* burdens during osteomyelitis.

Prior studies in alternative animal models using STZ-induced hyperglycemia induced *S. aureus* infection 30 days after treatment.[73,174] To determine if a more chronic state of hyperglycemia alters the pathogenesis of staphylococcal osteomyelitis, we treated mice with STZ for 5 days and then initiated osteomyelitis 30 days after the final STZ injection. Hyperglycemia was confirmed at the start (day 0) and end (day 14) points of the infection (**Fig. 20A**). As observed with the acute model of hyperglycemia, bacterial burdens were elevated in infected femurs from hyperglycemic mice compared to euglycemic vehicle-treated mice at day 14 post-infection (**Fig. 20B**). Dissemination to contralateral femurs did not increase in infected mice 30 days after STZ treatment to induce hyperglycemia (**Fig. 20C**). However, *S. aureus* burdens in the kidneys, liver, and heart of the hyperglycemic infected mice were increased compared to euglycemic mice at day 14 post-infection (**Fig. 20D-F**). Similar trends were observed using a ten-fold lower inoculum (**Fig. 21**). Taken together, these data suggest that both acute and chronic hyperglycemia result in increased *S. aureus* bacterial burdens during osteomyelitis.

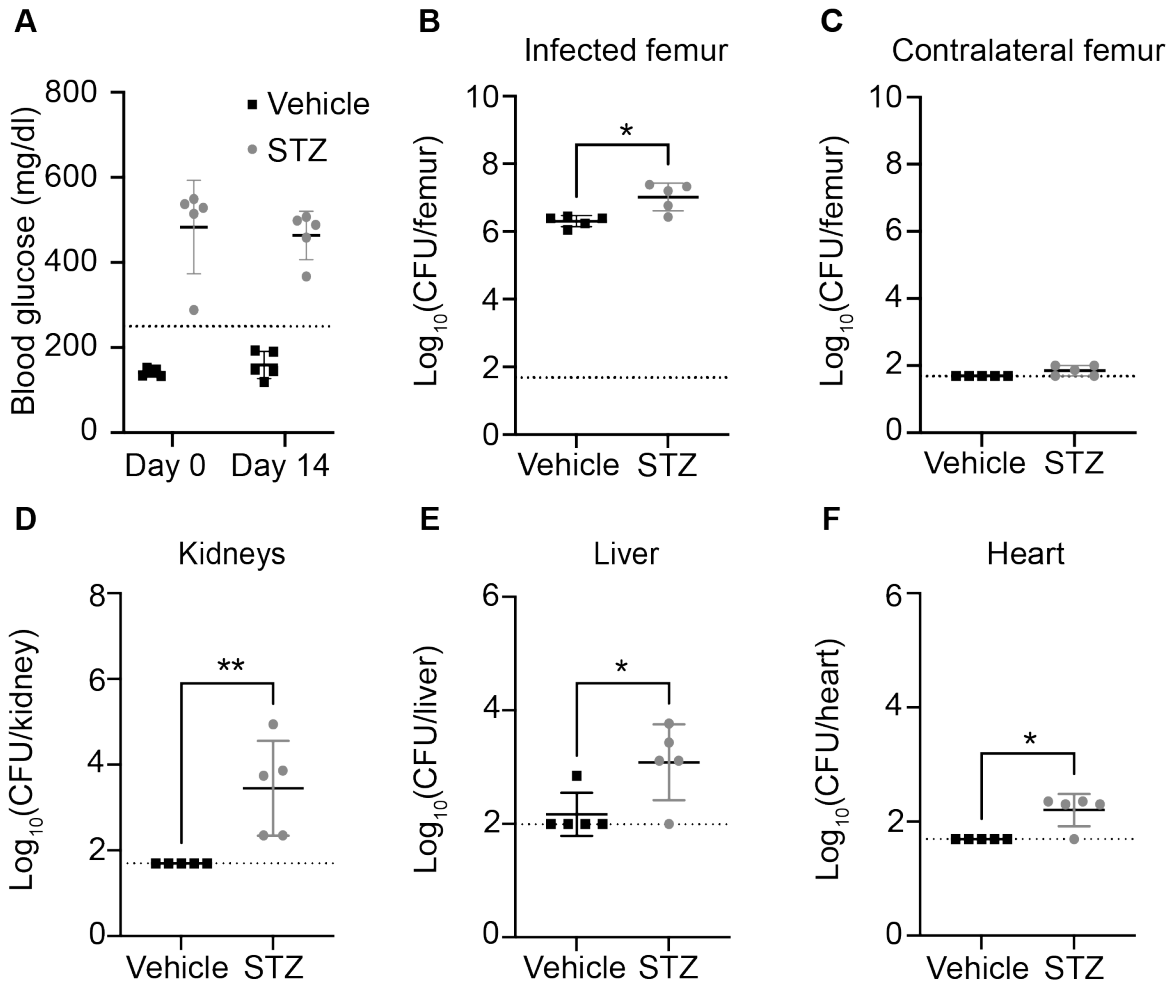

Figure 20. Chronic hyperglycemia increases *S. aureus* burdens and dissemination during osteomyelitis. Eight-week old male mice were treated with sodium citrate (vehicle) or streptozotocin (STZ) intraperitoneally for 5 days. 30 days after the final injection, mice were infected with $1x10^6$ CFU of WT *S. aureus* via intraosseous injection. (A) Blood glucose concentration was quantified from a tail vein bleed immediately prior to inoculation (day 0) and the day of sacrifice (day 14). Dotted line indicates hyperglycemia threshold of 250 mg/dl. Mice were sacrificed at day 14 post-infection, and the bacterial burdens (CFU) were enumerated in (B) infected femur, (C) contralateral femur, (D) kidneys, (E) liver, and (F) heart. N = 5 mice per group. Dotted lines indicate limit of detection. Horizontal lines indicate mean, and error bars represent SD. Significance determined with Mann-Whitney test (B-F). *$p<0.05$, **$p<0.01$.

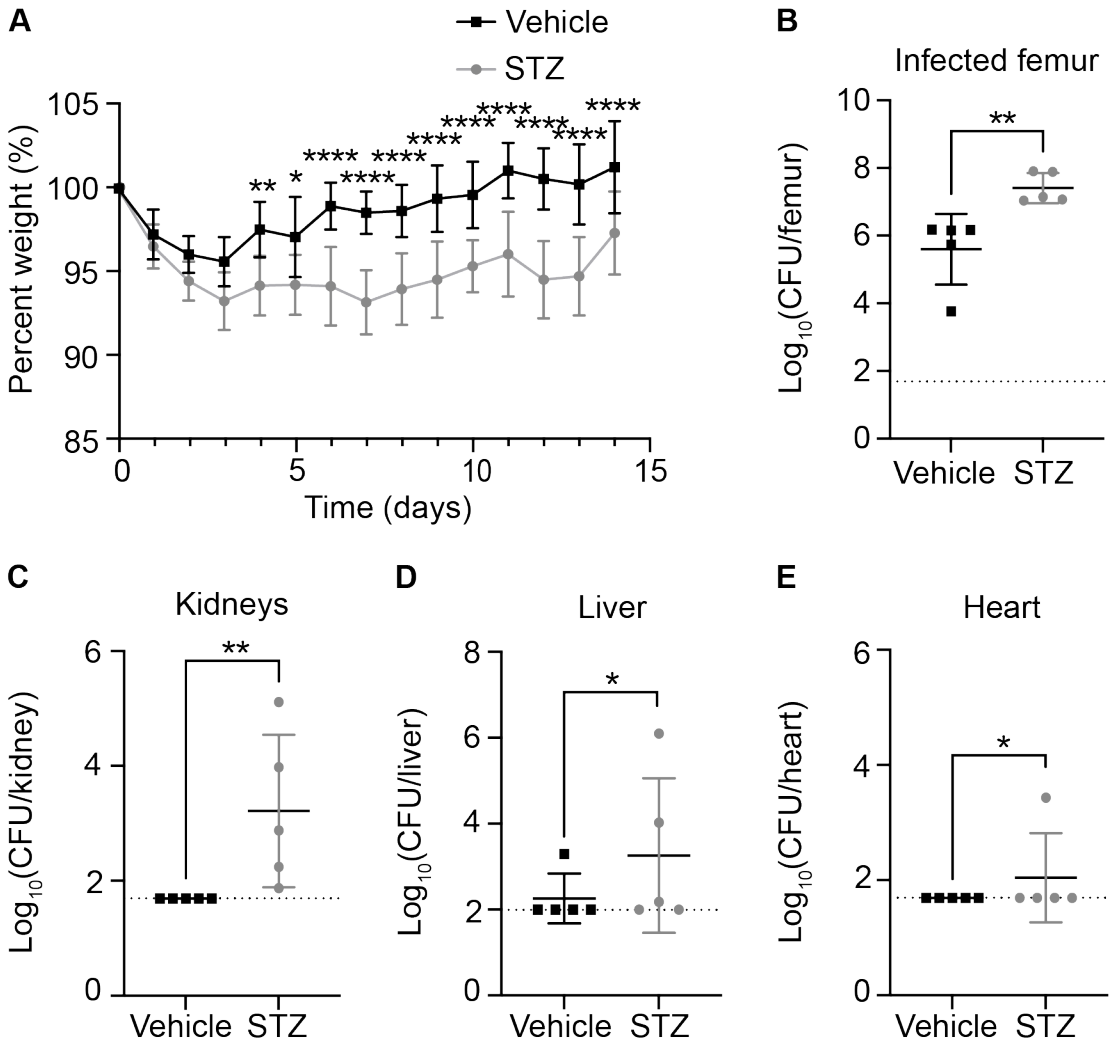

Figure 21. *S. aureus* burdens are increased in mice subjected to chronic hyperglycemia and infected with a lower inoculum. Eight-week old male mice were treated with sodium citrate (vehicle) or streptozotocin (STZ) intraperitoneally for 5 days. 30 days after the final injection, mice were infected with $1x10^5$ CFU of WT *S. aureus* via intraosseous injection. (A) Weights were recorded every 24 hrs and normalized to the starting weight of each animal on the day of infection (percent weight). Mice were sacrificed at day 14 post-infection, and the bacterial burdens (CFU) were enumerated in (B) infected femur, (C) kidneys, (D) liver, and (E) heart. N = 5 mice per group. Dotted lines indicate limit of detection. Horizontal lines indicate mean, and error bars represent SD. Significance determined with multiple paired t-tests (A) and with Mann-Whitney test (B-E). *p<0.05, **p<0.01, ****p<0.0001.

Hyperglycemia increases bone loss during *S. aureus* osteomyelitis.

To further characterize the pathogenesis of osteomyelitis during hyperglycemia, we measured bone loss following *S. aureus* infection. Significant bone damage and pathologic remodeling occur during *S. aureus* osteomyelitis in euglycemic animals.[2,3,175] Due to the increased *S. aureus* burdens observed in hyperglycemic mice compared to euglycemic mice, we hypothesized that bone destruction would increase in the setting of hyperglycemia. To first identify changes in trabecular bone due to hyperglycemia in the absence of infection, we used microcomputed tomography (μCT) to quantify changes to bone structure in STZ-treated mice that were hyperglycemic and STZ-treated mice that were not hyperglycemic. We discovered no differences in trabecular bone volume relative to total volume (%BV/TV) or trabecular number, thickness, or spacing between the femurs from STZ-treated hyperglycemic and STZ-treated non-hyperglycemic mice (**Figure 22**). To measure changes in infection-induced bone loss during hyperglycemia, STZ-treated hyperglycemic mice and vehicle-treated euglycemic mice were inoculated with $1x10^5$ CFU of *S. aureus*, due to the increased infection severity with a $1x10^6$ CFU inoculum. We used μCT to quantify changes to bone structure in the *S. aureus*-infected femurs at 14 days post-infection. The infected femurs from hyperglycemic mice had greater cortical bone loss relative to the infected femurs from euglycemic vehicle-treated mice during acute hyperglycemia (**Fig. 22A**). Similar trends in cortical bone loss were observed in infected mice with chronic hyperglycemia, although the differences were not statistically significant (**Fig. 23A**). To further characterize the impact of acute and chronic hyperglycemia on bone homeostasis, we also measured changes in the trabecular bone volume. A decrease in %BV/TV was observed in the infected femurs from hyperglycemic mice compared to infected femurs from euglycemic vehicle-treated mice (**Fig. 23B**). Because chronic hyperglycemia has been shown to alter bone volume, we normalized the %BV/TV against the uninfected contralateral femur.[176,177] Importantly, the %BV/TV in the hyperglycemic infected femurs

normalized against the %BV/TV of the contralateral femurs remained significantly lower in the hyperglycemic mice compared to the euglycemic vehicle-treated mice, suggesting the trabecular bone loss in hyperglycemic mice is related to infection and not solely a function of baseline changes in bone volume (**Fig. 23C**). Trabecular bone thickness in infected hyperglycemic animals was lower than in the infected euglycemic vehicle-treated animals, with no differences observed in trabecular spacing or number (**Fig. 23D-F**). Similar trends in trabecular bone parameters were observed in the infected femurs of mice with chronic hyperglycemia (**Fig. 24B-F**), although only the differences in %BV/TV and trabecular bone thickness were statically significant. To further characterize tissue inflammation in hyperglycemic and euglycemic mice subjected to osteomyelitis, representative histological sections of *S. aureus*-infected femurs were stained with hematoxylin and eosin (H&E) (**Fig. 25**). Representative histological sections of infected femurs from chronic hyperglycemic mice exhibited similar pathology to acute hyperglycemic infected femurs (**Fig. 26**). Notably, abscess formation is observed in acute and chronic hyperglycemic infected mice, which is a unique finding compared to the impaired abscess formation observed in skin infection during hyperglycemia.[164] Collectively, our data reveal that acute and chronic hyperglycemia contribute to greater pathologic bone destruction during *S. aureus* osteomyelitis compared to euglycemic infection. Due to the similar findings between acute and chronic hyperglycemic mice, we performed further experiments using the acute model of hyperglycemia.

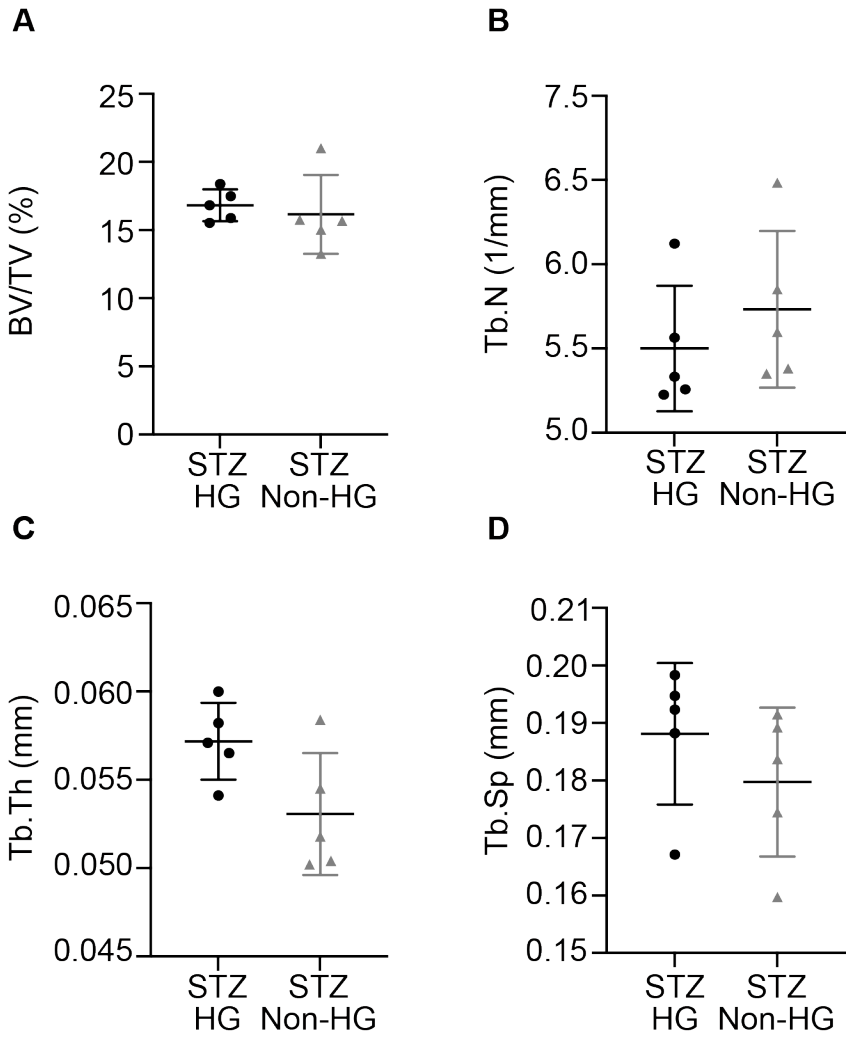

Figure 22. Similar trabecular bone volume is observed in uninfected hyperglycemic and euglycemic mice. Eight-week old male mice were treated with streptozotocin (STZ) intraperitoneally for 5 days. 10 days after, blood glucose concentration was quantified from the tail vein. Mice were split into two groups: STZ-treated hyperglycemic (STZ HG) with blood glucose > 250 mg/dl and STZ-treated not hyperglycemic (STZ Non-HG) with blood glucose < 250 mg/dl. The left femurs were isolated for microcomputed tomography. (A) Trabecular bone volume divided by total volume (%BV/TV), (C) trabecular number (Tb.N), (D) trabecular thickness (Tb.Th), and (E) trabecular spacing (Tb.Sp) were quantified from the left femurs. N = 5 mice per group. Horizontal lines indicate mean, and error bars represent SD. Significance determined with Mann-Whitney test.

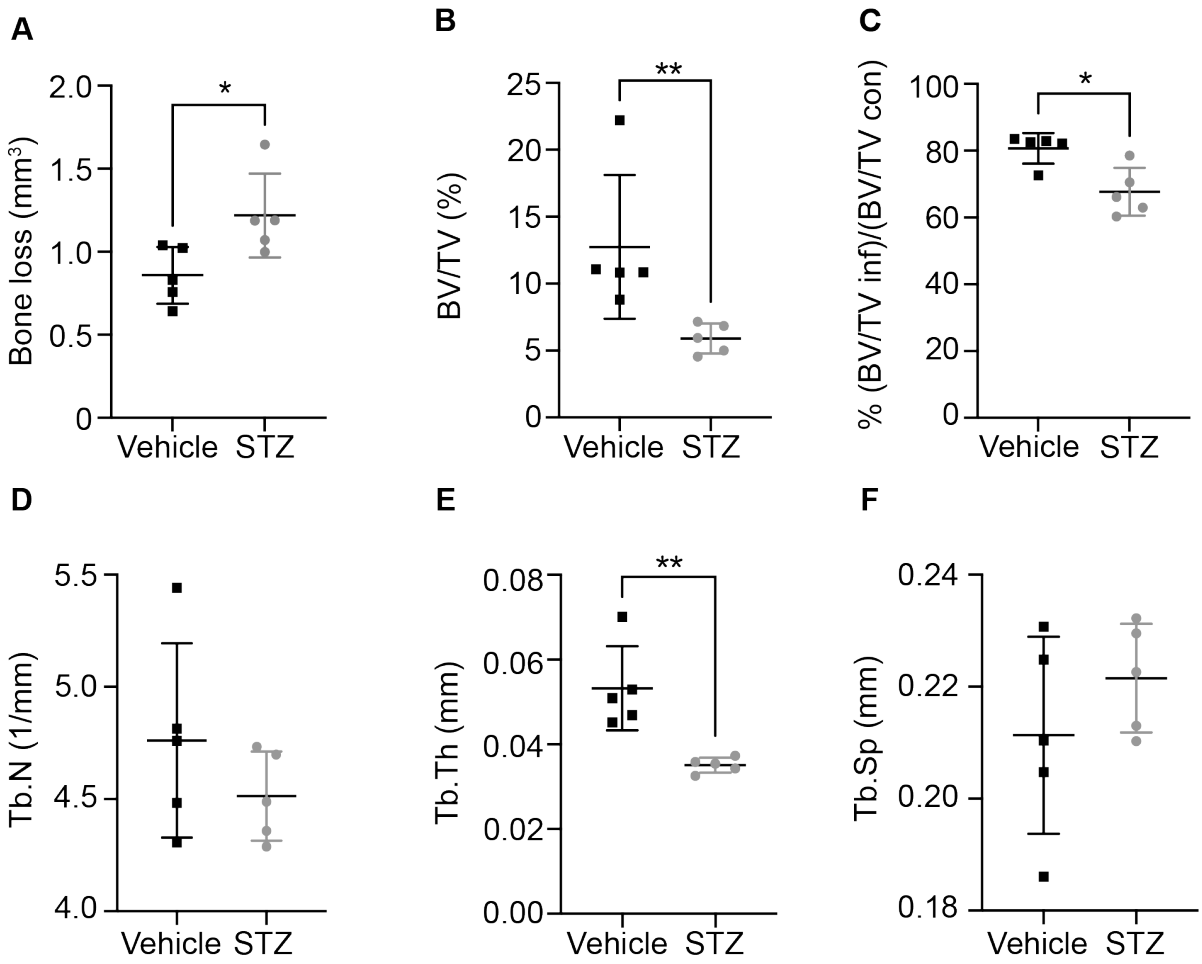

Figure 23. *S. aureus* incites greater bone destruction in acute hyperglycemic animals. Eight-week old male mice were treated with sodium citrate (vehicle) or streptozotocin (STZ) intraperitoneally for 5 days. 10 days after the final injection, mice were infected with $1x10^5$ CFU of WT *S. aureus* via intraosseous injection. At 14 days post-infection, the infected femur and contralateral femur were isolated for microcomputed tomography. (A) Cortical bone loss in infected femurs, (B) trabecular bone volume divided by total volume (%BV/TV) of infected femurs, and (C) %BV/TV of infected femurs relative to contralateral femurs were quantified. (D) Trabecular number (Tb.N), (E) trabecular thickness (Tb.Th), and (F) trabecular spacing (Tb.Sp) were quantified in infected femurs. N = 5 mice per group. Horizontal lines indicate mean, and error bars represent SD. Significance determined with Mann-Whitney test. *$p<0.05$, **$p<0.01$.

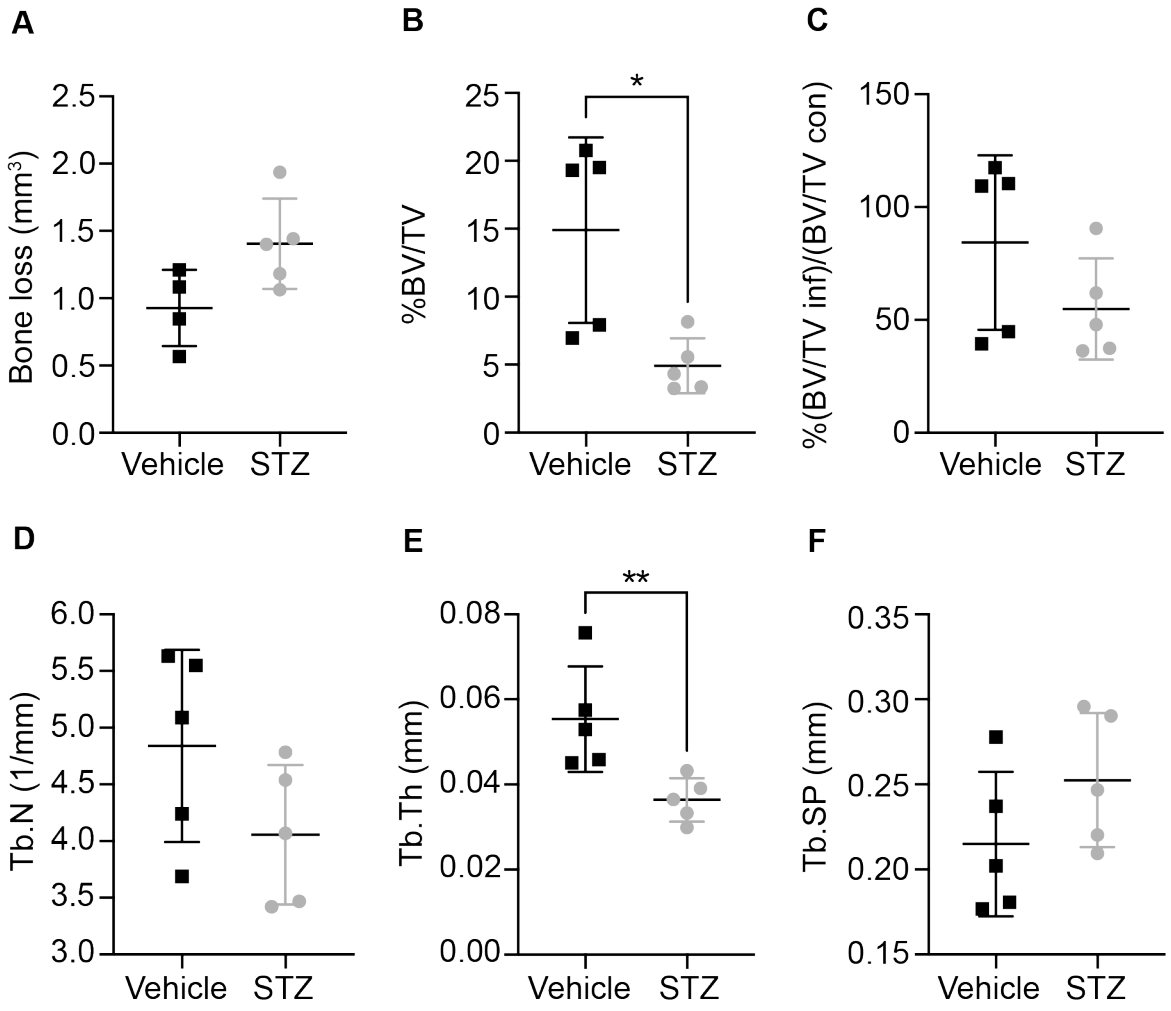
A
Bone loss (mm3)
2.5
2.0
1.5
1.0
0.5
0.0
Vehicle
STZ
B
%BV/TV
*
25
20
15
10
5
0
Vehicle
STZ
C
%(BV/TV inf)/(BV/TV con)
150
100
50
0
Vehicle
STZ
D
Tb.N (1/mm)
6.0
5.5
5.0
4.5
4.0
3.5
3.0
Vehicle
STZ
E
Tb.Th (mm)
**
0.08
0.06
0.04
0.02
0.00
Vehicle
STZ
F
Tb.SP (mm)
0.35
0.30
0.25
0.20
0.15
Vehicle
STZ

Figure 24. *S. aureus* induces bone destruction in mice subjected to chronic hyperglycemia. Eight-week old male mice were treated with sodium citrate (vehicle) or streptozotocin (STZ) intraperitoneally for 5 days. 30 days after the final injection, mice were infected with $1x10^5$ CFU of WT *S. aureus* via intraosseous injection. At 14 days post-infection, the infected and contralateral femurs were isolated and fixed in neutral buffered formalin prior to microcomputed tomography. (A) Cortical bone loss was calculated with n = 4 vehicle-treated mice and n = 5 STZ-treated mice. (B) Trabecular bone volume divided by total volume (%BV/TV) of infected femurs and (C) %BV/TV of infected femurs relative to contralateral femurs were quantified. (D) Trabecular number (Tb.N), (E) trabecular thickness (Tb.Th), and (F) trabecular spacing (Tb.Sp) were quantified in infected femurs. N = 5 mice per group unless otherwise noted. Horizontal lines indicate mean, and error bars represent SD. Significance determined with Mann-Whitney test. *$p<0.05$, **$p<0.01$.

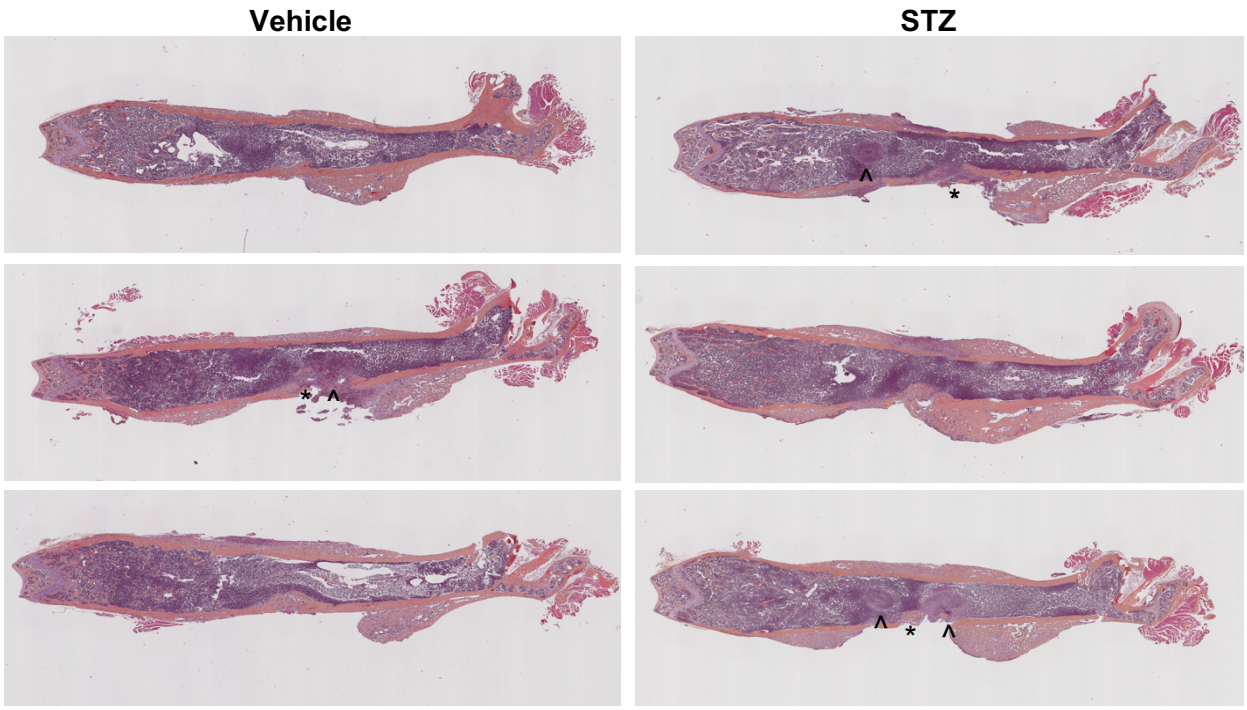

Figure 25. Histological sections of acute hyperglycemic and euglycemic infected femurs. Eight-week old male mice were treated with sodium citrate (vehicle) or streptozotocin (STZ) intraperitoneally for 5 days. 10 days after the final injection, mice were infected with $1x10^5$ CFU of WT *S. aureus* via intraosseous injection. Mice were sacrificed at day 14 post-infection, and the infected femurs were decalcified, sectioned, and stained with H&E. N = 3 mice per group. ^ = *S. aureus* abscess and * = visible cortical bone destruction.

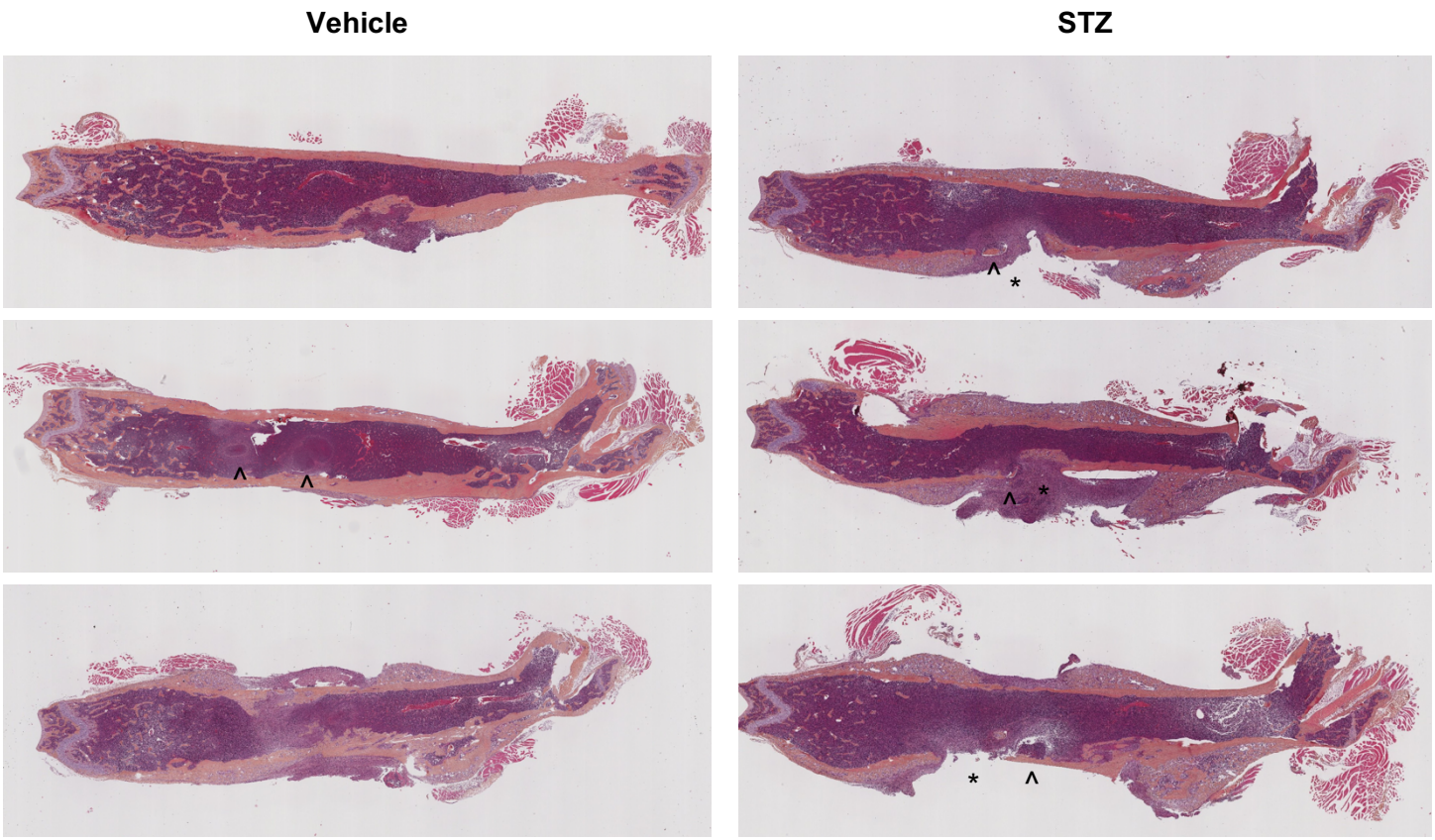

Figure 26. Histological sections of infected femurs from mice with chronic hyperglycemia or euglycemia. Eight-week old male mice were treated with sodium citrate (vehicle) or streptozotocin (STZ) intraperitoneally for 5 days. 30 days after the final injection, mice were infected with $1x10^5$ CFU of WT *S. aureus* via intraosseous injection. Mice were sacrificed at day 14 post-infection, and the infected femurs were decalcified, sectioned, and stained with H&E. N = 3 mice per group. ^ = *S. aureus* abscess and * = visible cortical bone destruction.

Genes contributing to the fitness of *S. aureus* in hyperglycemic animals.

Hyperglycemia results in increased *S. aureus* burdens within infected femurs and greater dissemination to other organs in the context of osteomyelitis. To identify genes required for staphylococcal survival in hyperglycemic tissues, we performed TnSeq in hyperglycemic and euglycemic animals with a previously characterized USA300 LAC transposon insertion library.[170] Groups of mice were treated with STZ or vehicle, and 10 days after the final treatment, mice were infected with $5x10^6$ CFU of the *S. aureus* transposon insertion library. An *in vitro* comparator consisted of growth in brain heart infusion broth (BHI) for 24 hrs to identify genes that are essential for bacterial growth in a nutrient rich condition.

TnSeq identified 71 *S. aureus* genes as essential (defined as Dval<0.01) for survival during osteomyelitis in hyperglycemic mice but not essential for growth *in vitro* or in euglycemic mice (**Fig. 27A** and **Appendix B1**). We also identified 61 *S. aureus* transposon mutants with compromised fitness (Dval>0.01 and <0.1) in hyperglycemic mice but not *in vitro* or in euglycemic mice (**Appendix B2**). Of these 132 genes, 45 encode hypothetical proteins, of which 28 genes are considered essential and 17 have compromised fitness. Of the remaining 87 genes, 61 have Kyoto Encyclopedia of Genes and Genomes (KEGG) identifiers. Of the 61 genes with KEGG identifiers, 24 are implicated in metabolic processes including glycolysis, glutamine metabolism, histidine metabolism, and purine/pyrimidine biosynthesis. Genes related directly or indirectly to glucose metabolism that were identified as either essential or compromised during osteomyelitis include and catabolite control protein A (*ccpA*, SAUSA300_1682), L-lactate dehydrogenase 1 (*ldh1,* SAUSA300_0235), dihydrolipoyl dehydrogenase (*lpdA*, SAUSA300_0996), and pyruvate ferredoxin oxidoreductase (SAUSA300_1182). Other metabolic genes identified as essential included carbamoyl phosphate synthase large subunit (*carB*, SAUSA300_1096), carbamoyl phosphate synthase

small subunit (*carA*, SAUSA300_1095), and adenine phosphoribosyltransferase (*apt*, SAUSA300_1591).

In addition to metabolic pathways identified as important for *S. aureus* growth in osteomyelitis during hyperglycemia, the remaining genes identified by TnSeq are broadly involved in bacterial stress responses. These genes can be classified by roles in DNA repair, cell signaling, gene regulation, peptidoglycan synthesis, and virulence (**Fig. 27B**). Two virulence genes identified as uniquely essential for *S. aureus* growth during osteomyelitis in hyperglycemic mice were *ureB* (SAUSA300_2239), which encodes urease B, and *sodA* (SAUSA300_1513), which encodes superoxide dismutase A. UreB is involved in maintaining pH homeostasis and is critical for *S. aureus* survival in urea-rich environments under acid stress.[123] SodA is responsible for detoxifying ROS via conversion of superoxide radicals to hydrogen peroxide.[125] Due to the hyperinflammation, acidifying conditions, presence of greater ROS concentrations during hyperglycemia, we sought to understand how UreB and SodA facilitate *S. aureus* growth in the presence of elevated glucose.

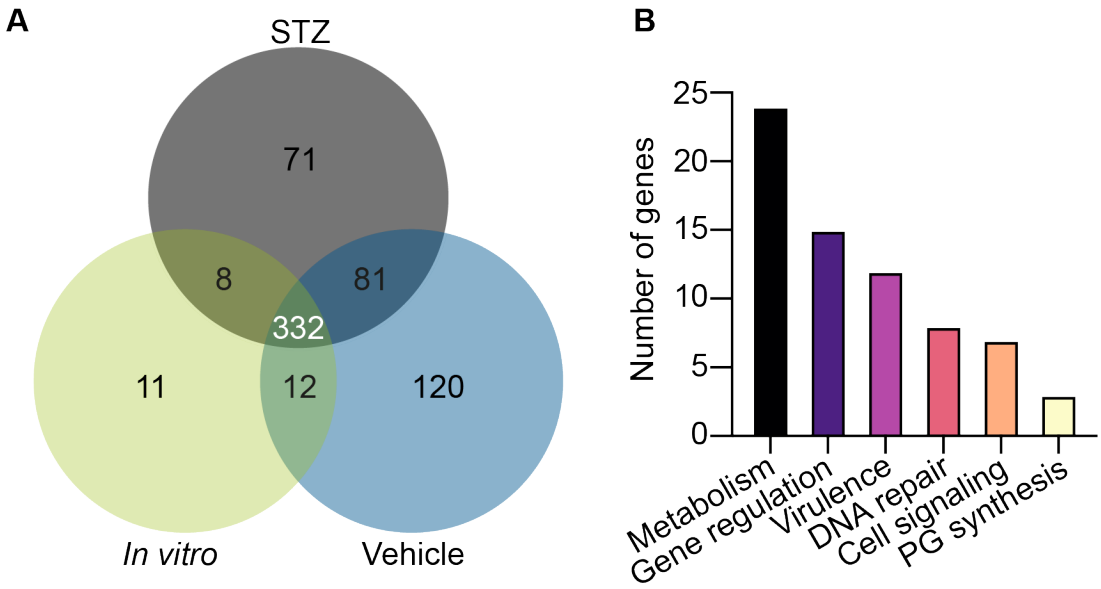

Figure 27. Transposon sequencing reveals genes essential for *S. aureus* survival during osteomyelitis in mice with hyperglycemia. Eight-week old male mice were treated with sodium citrate (vehicle) or streptozotocin (STZ) intraperitoneally for 5 days. 10 days after the final injection, mice were infected with $5x10^6$ CFU of the *S. aureus* TnSeq library via intraosseous injection. At day 4 post-infection, bacteria were recovered and Illumina Sequencing was used to identify the abundance of *S. aureus* mutants in each condition. (A) Based on Dval calculations, the number of essential genes (Dval<0.01) *in vitro* in BHI, *in vivo* in STZ-treated hyperglycemic mice, and *in vivo* in euglycemic vehicle-treated mice were enumerated. (B) The annotated genes essential for *S. aureus* survival (Dval<0.01) and the mutants with compromised fitness (Dval>0.01 and <0.1) only in the condition of osteomyelitis during hyperglycemia were organized into categories of metabolism, gene regulation, virulence, DNA repair, cell signaling, and peptidoglycan (PG) synthesis. N = 12 mice per *in vivo* group, pooled in samples of 2 for n = 6 in sequencing analysis. Data were collected during 2 independent experiments.

UreB is important for *S. aureus* survival *in vitro* in high glucose but not *in vivo* in the setting of hyperglycemia.

One consequence of *S. aureus* growth in in the presence of high glucose is the acidification of media that occurs during glucose metabolism.[178] One gene identified as important for *S. aureus* survival in osteomyelitis during hyperglycemia with TnSeq in the first experimental replicate (of two total) was *ureB*, which encodes the protein urease B. UreB is important for *S. aureus* survival *in vitro* in high glucose and functions by breaking down urea to ammonia, thereby consuming protons and raising the pH.[123] To confirm the role of *ureB* in *S. aureus* survival in elevated glucose in the absence of other host stressors, we examined the survival of WT and the *ureB* mutant strains over 5 days in tryptic soy broth (TSB, 250 mg/dl glucose) with an additional 500 mg/dl of glucose with or without 10 mM of urea by quantifying CFU every 24 hrs.[120] Both WT and the *ureB* mutant strains survived to a lesser extent in TSB with additional glucose compared to WT in TSB with additional glucose and urea (**Fig. 28**). While WT survived in TSB with glucose and urea, the *ureB* mutant had a growth defect in TSB with glucose that was not rescued with exogenous urea (**Fig. 28**). Consistent with prior studies, these findings support a role for UreB in promoting *S. aureus* survival in the presence of high glucose concentrations over the course of 5 days.[120]

Prior studies revealed that staphylococcal urease genes are transcribed during biofilm formation.[179,180] To assess the role of *ureB* in *S. aureus* biofilm formation, we grew WT and a *ureB* mutant in TSB -dextrose with various concentrations of glucose, with and without urea. After 24 hrs of static culture, WT *S. aureus* formed significantly greater biofilm in TSB -dextrose with 2 and 3 g/L of glucose with the addition of urea, compared to without urea (**Fig. 29A**). However, *ureB*::Tn did not form greater biofilm with or without urea in the presence of glucose (**Fig. 29A**). After 48 hrs, WT formed greater biofilm in the presence of 3 and 5 g/L of glucose when exogenous urea was added to the static culture (**Fig. 29B**). In comparison, in the

presence and absence of urea in various concentrations of glucose, the *ureB* mutant formed a similar amount of biofilm compared to WT in glucose without urea (**Fig. 29B**). These studies demonstrate that UreB and the addition of urea facilitate biofilm formation in the presence of glucose *in vitro*.

To further assess the role of UreB in promoting *S. aureus* survival in hyperglycemia, we infected STZ-treated hyperglycemic mice with $1x10^6$ CFU WT and *ureB* mutant *S. aureus* using the osteomyelitis model. Infected mice were monitored for changes in percent starting weight, revealing greater percent starting weights in *ureB* mutant-infected hyperglycemic mice compared to WT at days one and two post-infection (**Fig. 30A**). However, at 4 days post-infection, mice infected with the *ureB* mutant did not have differences in CFU burden within the infected femur, kidneys, heart, or liver compared to mice infected with WT *S. aureus* (**Fig. 30B-E**). Interestingly, there was also no difference in CFU recovered from mice co-infected 1:1 with WT and the *ureB* mutant at day 4 in the infected femurs (**Fig. 30B**). Collectively, these data support that UreB is important for *S. aureus* survival and biofilm formation in high glucose in the presence of urea. However, UreB is not essential for *S. aureus* survival in osteomyelitis during hyperglycemia at day 4 post-infection using an inoculum of $1x10^5$ CFU.

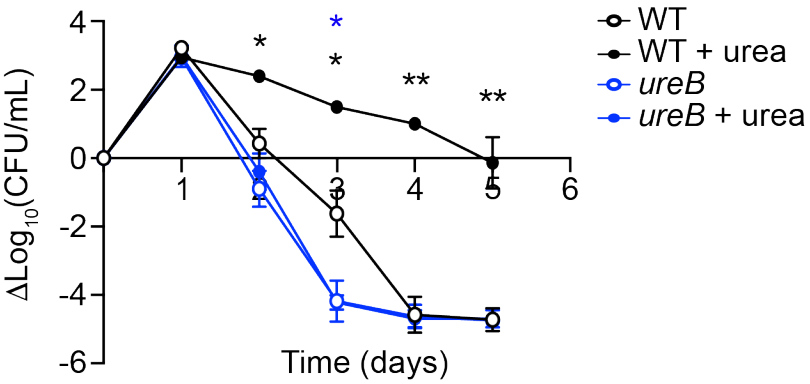

Figure 28. UreB and urea are important for *S. aureus* growth in high glucose. WT and *ureB*::Tn (*ureB*) *S. aureus* strains were grown in 10 mL TSB (containing 250 mg/dl glucose) with 500 mg/dl additional glucose and with (+ urea) and without 10 mM urea in aerobic flasks shaking at 37°C. CFU were quantified every 24 hrs over the course of 5 days and normalized to time 0 hr. N = 2 technical replicates, and n = 3 biological replicates. Line represents mean, and error bars represent standard deviation. Significance determined with two-way ANOVA and Dunnett's multiple comparisons test. *p<0.05 WT + urea, **p<0.01 WT + urea, and *p<0.05 *ureB* and *ureB* + urea. Black asterisk indicates comparison to WT + urea, and blue asterisk indicates comparison to both *ureB* in TSB and *ureB* in TSB with 500 mg/dl glucose. All comparisons made relative to WT without urea.

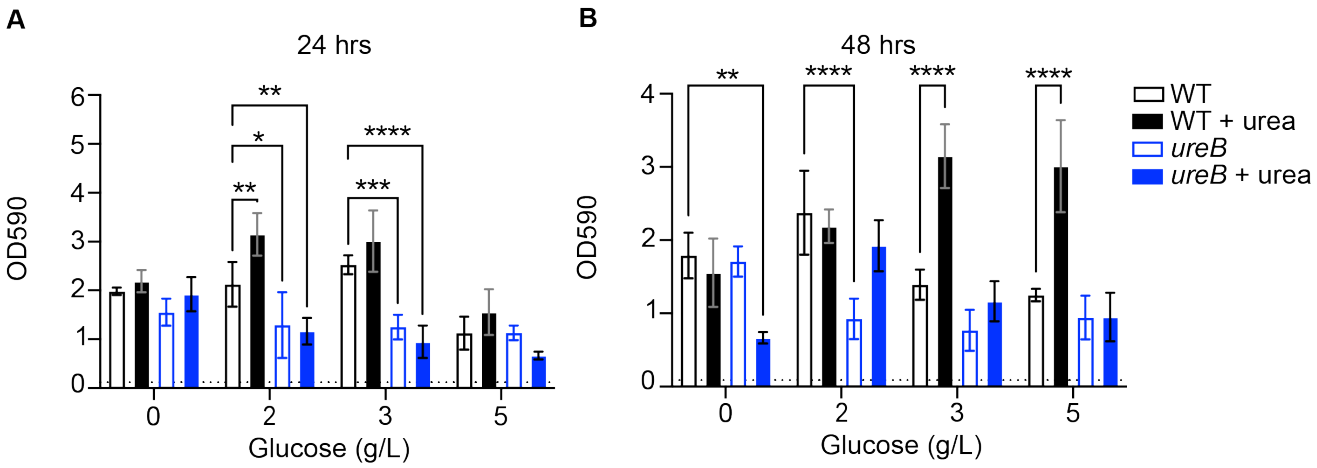

Figure 29. UreB and urea are important for *S. aureus* biofilm formation in TSB -dex with glucose. WT and *ureB*::Tn (*ureB*) *S. aureus* grown static at 37°C in TSB -dextrose with 0, 2, 3, and 5 g/L glucose with or without 10 mM urea in human plasma coated 96 well plates for (A) 24 hrs or (B) 48 hrs. Non-adherent cells were removed, and wells were washed prior to fixation with methanol. Adherent biomass was stained with crystal violet, eluted in methanol, and measured with OD590. N = 3 technical replicates per condition. Dotted lines represent average OD590 for media controls. Bars indicate mean, and error bars indicate SD. Significance determined with two-way ANOVA and Dunnett's multiple comparisons test. All comparisons were made relative to WT. *p<0.05, **p<0.01, ***p<0.001, ****p<0.0001.

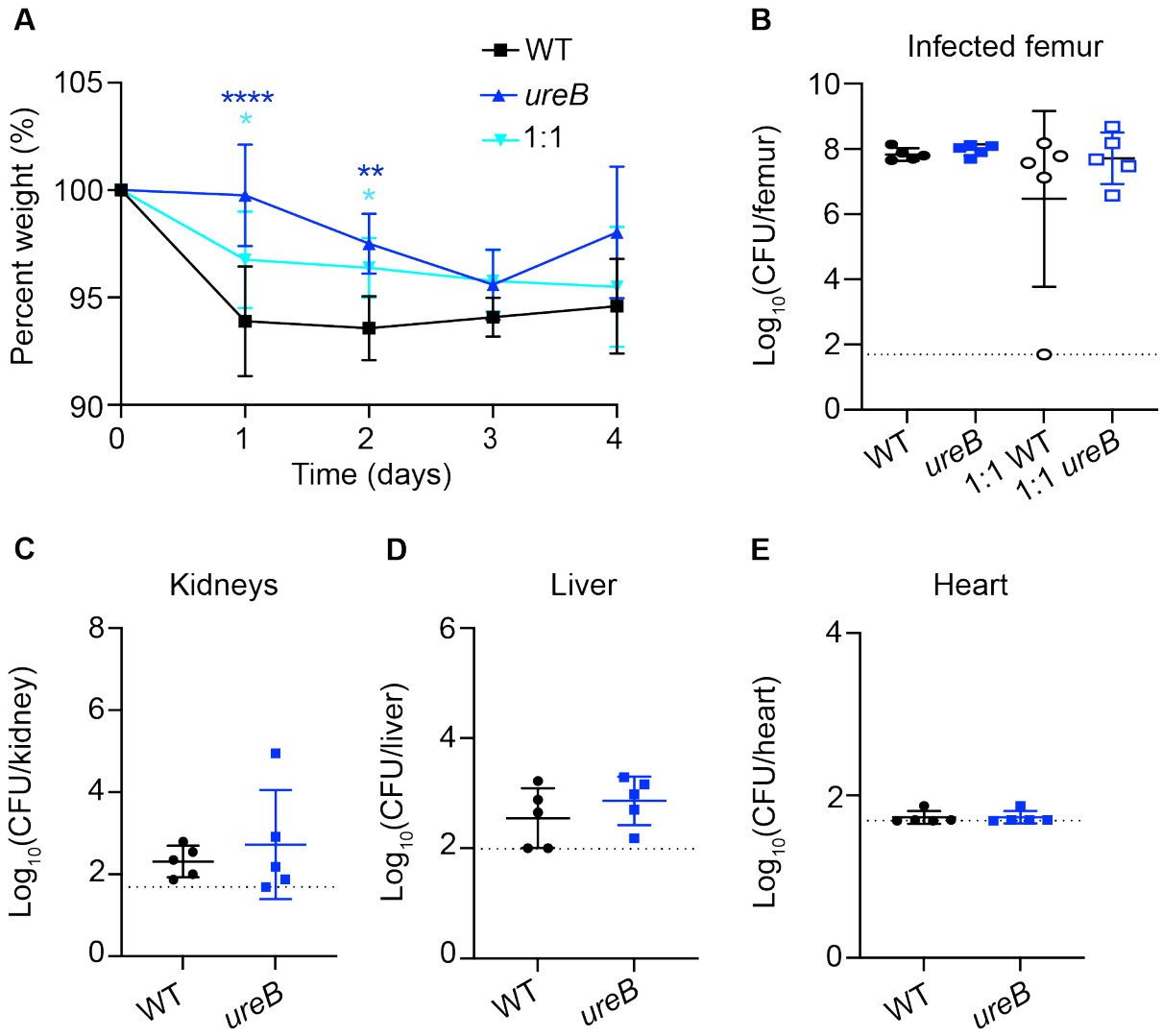
A
WT
ureB
1:1
Percent weight (%)
105
100
95
90
****
*
**
*
0
1
2
3
4
Time (days)
B
Infected femur
Log10(CFU/femur)
10
8
6
4
2
0
WT
ureB
1:1 WT
1:1 ureB
C
Kidneys
Log10(CFU/kidney)
8
6
4
2
0
WT
ureB
D
Liver
Log10(CFU/liver)
6
4
2
0
WT
ureB
E
Heart
Log10(CFU/heart)
4
2
0
WT
ureB

Figure 30. UreB is not important for *S. aureus* survival during osteomyelitis in hyperglycemic mice. Eight-week old male mice were treated with streptozotocin (STZ) intraperitoneally for 5 days. 10 days after the final injection, mice were infected with $1x10^6$ CFU of WT, *ureB*::Tn (*ureB*), and 1:1 WT:*ureB*::Tn (1:1) *S. aureus* via intraosseous injection. (A) Weights were recorded every 24 hrs and normalized to the starting weight of each animal on the day of infection (percent weight). Mice were sacrificed at day 4 post-infection, and the bacterial burden (CFU) was enumerated in the (B) infected femur, (C) kidneys, (D) liver, and (E) heart. N = 5 mice per group. Dotted lines indicate limit of detection. Horizontal lines indicate mean, and error bars represent SD. Significance determined with two-way ANOVA and Dunnett's multiple comparisons test (A), Kruskal-Wallis test (B), and Student's t-test (C-E).

Validation of TnSeq with mono-infections.

S. aureus genes identified as important for growth during hyperglycemia in the first replicate of the TnSeq experiment (of two total) included genes involved in immune cell evasion and bacterial stress response. We prioritized testing mutants with known or hypothetical roles in responding to altered physiological state associated with hyperglycemia, such as low pH and changes in neutrophil function. Superoxide dismutase A (*sodA*) and catalase (*katA*) were identified as important for *S. aureus* growth *in vivo* during hyperglycemia and have a known role in detoxifying ROS produced during inflammation.[125,181] The putative spermidine/putrescine transporter system PotABCD genes *potA* and *potB* were also identified with TnSeq as important for *S. aureus* survival during hyperglycemia. Polyamines are toxic to *S. aureus* at high concentrations but may offer a protective benefit to the bacteria in acidic pH.[121,124] Universal stress protein A2 (*uspA2*) was also identified by TnSeq as important for *S. aureus* survival during hyperglycemia and has a known role in bacterial stringent response.[182] To assess the role of each of these genes in contributing to *S. aureus* survival during hyperglycemia, we infected $1x10^5$ CFU WT, *sodA*, *potA*, *potB*, *katA*, and *uspA2* mutant *S. aureus* using an osteomyelitis model in STZ-treated hyperglycemic mice. Infected mice were monitored for changes in percent starting weight. There were no changes in percent starting weights of hyperglycemic mice infected with any mutant *S. aureus* strains compared to WT (**Fig. 31A**). At 4 days post-infection, mice infected with the mutant strains did not have differences in CFU burden within the infected femur, kidneys, heart, or liver compared to mice infected with WT *S. aureus* (**Fig. 31B-E**). Day 4 was selected for analysis due to the characteristic formation of abscesses by day 4 of infection and the fact that TnSeq sequencing was carried out at day of infection.[76] This study supports that SodA, PotA, PotB, KatA, and UspA2 are not essential for *S. aureus* survival *in vivo* during hyperglycemia with a 10^5 inoculum at day 4 post-infection, although the growth kinetics of each of these mutants requires

additional investigation. Due to the trend in lower CFU recovered from the *sodA* mutant infected mice at day 4 post-infection, we further investigated the role of SodA in *S. aureus* survival *in vitro* and modeled a more chronic infection and assessed the CFU burdens at day 14 post-infection.

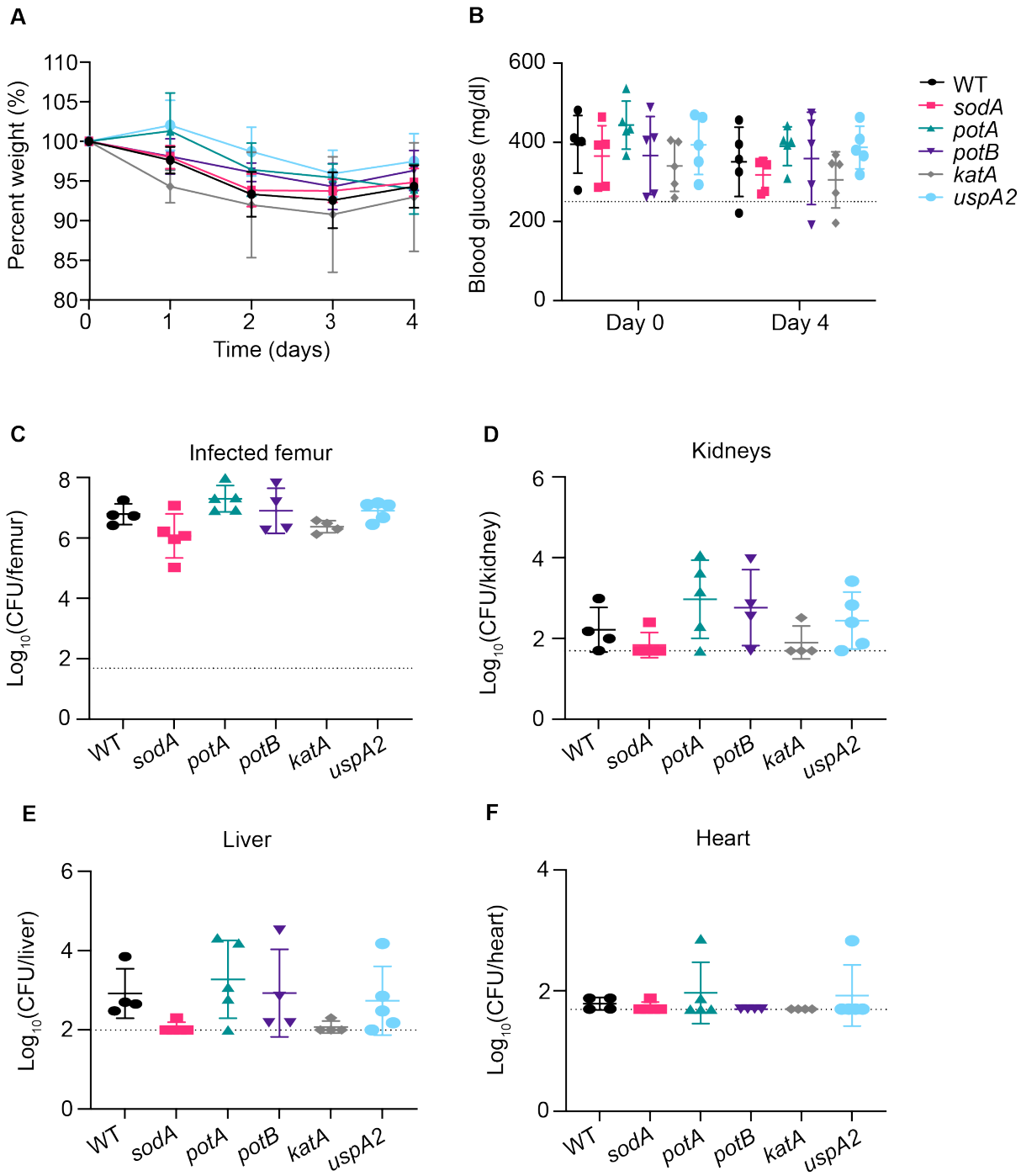
A
Percent weight (%)
110
105
100
95
90
85
80
0
1
2
3
4
Time (days)
B
Blood glucose (mg/dl)
600
400
200
0
Day 0
Day 4
WT
sodA
potA
potB
katA
uspA2
C
Infected femur
Log10(CFU/femur)
8
6
4
2
0
WT
sodA
potA
potB
katA
uspA2
D
Kidneys
Log10(CFU/kidney)
6
4
2
0
WT
sodA
potA
potB
katA
uspA2
E
Liver
Log10(CFU/liver)
6
4
2
0
WT
sodA
potA
potB
katA
uspA2
F
Heart
Log10(CFU/heart)
4
2
0
WT
sodA
potA
potB
katA
uspA2

Figure 31. Virulence and metabolism genes identified with TnSeq are not important for *S. aureus* survival in hyperglycemic mice at day 4 of osteomyelitis. Eight-week old male mice were treated with streptozotocin (STZ) intraperitoneally for 5 days. 10 days after the final injection, mice were infected with $1x10^5$ CFU of WT, *sodA*::tet (*sodA*), *potA*::Tn (*potA*), *potB*::Tn (*potB*), *katA*::Tn (*katA*), and *uspA2*::Tn (*uspA2*) *S. aureus* via intraosseous injection. (A) Weights were recorded every 24 hrs and normalized to the starting weight of each animal on the day of infection (percent weight). (B) Blood glucose concentration was quantified from the tail vein on the day of infection (day 0) and the day of sacrifice (day 4). Mice were sacrificed at day 4 post-infection, and the bacterial burden (CFU) was enumerated in the (C) infected femur, (D) kidneys, (E) liver, and (F) heart. N = 5 mice per group, prior to excluding animals below the hyperglycemic threshold. Dotted lines indicate limit of detection. Horizontal lines indicate mean, and error bars represent SD. Significance determined with two-way ANOVA and Dunnett's multiple comparisons test (A) and Kruskal-Wallis with Dunn's multiple comparisons test (C-F). All comparisons made to WT.

SodA facilitates *S. aureus* survival in high glucose *in vitro*.

While host cells produce ROS during inflammation, *S. aureus* can also produce ROS intrinsically in response to glucose metabolism that results in an electron transport chain bottleneck, catalyzing reduction of oxygen.[120] To combat ROS, the *S. aureus* genome encodes two superoxide dismutases (SODs), *sodA* and *sodM*.[125,126] The *sodA* gene was identified as essential for growth during osteomyelitis in hyperglycemic mice (Dval 0.0003), while *sodM* was not essential for growth *in vitro* (Dval 1.204), in euglycemic vehicle-treated osteomyelitis infection (Dval 1.801), or in osteomyelitis in hyperglycemic mice (Dval 0.6585). To evaluate the roles of each SOD in *S. aureus* survival in elevated glucose in the absence of other host stressors, we examined survival of WT, *sodA*::tet, and *sodM*::erm *S. aureus* strains over 5 days in TSB (250 mg/dl glucose) or in TSB with an additional 500 mg/dl of glucose by quantifying CFU every 24 hrs.[120] While WT and the *sodM* mutant survive in TSB and TSB with glucose to a similar extent over the course of 5 days, the *sodA* mutant had a growth defect in TSB with glucose compared to WT by day 2 (**Fig. 32A**). Prior studies suggest that oxygen is critical for SOD activity, which led us to hypothesize that differences in growth between WT and the SOD mutants would be minimized under conditions of limited oxygen.[125,183] In keeping with this hypothesis, WT *S. aureus* grew similarly to the *sodA* mutant strain under microaerobic conditions (**Fig. 32B**). Complementation with *sodA in cis* rescues the growth the *sodA* mutant *in vitro* when grown aerobically in TSB with glucose (**Fig. 32D**). Although *S. aureus* cultures with high glucose became more acidic over time, changes in growth between *S. aureus* strains were not explained by differences in pH (**Fig. 32C).** Furthermore, WT, *sodA* mutant, and *sodM* mutant *S. aureus* all grew similarly in TSB at a pH 4.5, 5.5, 6.5, and 7.5 over 24 hrs (**Fig. 33**). However, the *sodA* mutant has a defect in survival in acidic TSB at a pH of 4.5 at day 4 compared to WT and *sodM* mutant strains (**Fig. 34A**). *sodA* mutant survival is also significantly reduced compared to WT and *sodM* at a pH of 5.5 at days 2, 3, 4, and 5 (**Fig. 34B**). Differences

in growth were not observed between WT, *sodA* mutant, and *sodM* mutant *S. aureus* in TSB at a pH of 6.5 and 7.5 (**Fig. 34C-D**). Consistent with prior studies, these findings support a role for SodA in detoxifying intrinsically generated superoxide and may support a role for SodA in *S. aureus* survival in acidic environments.[125,184,185]

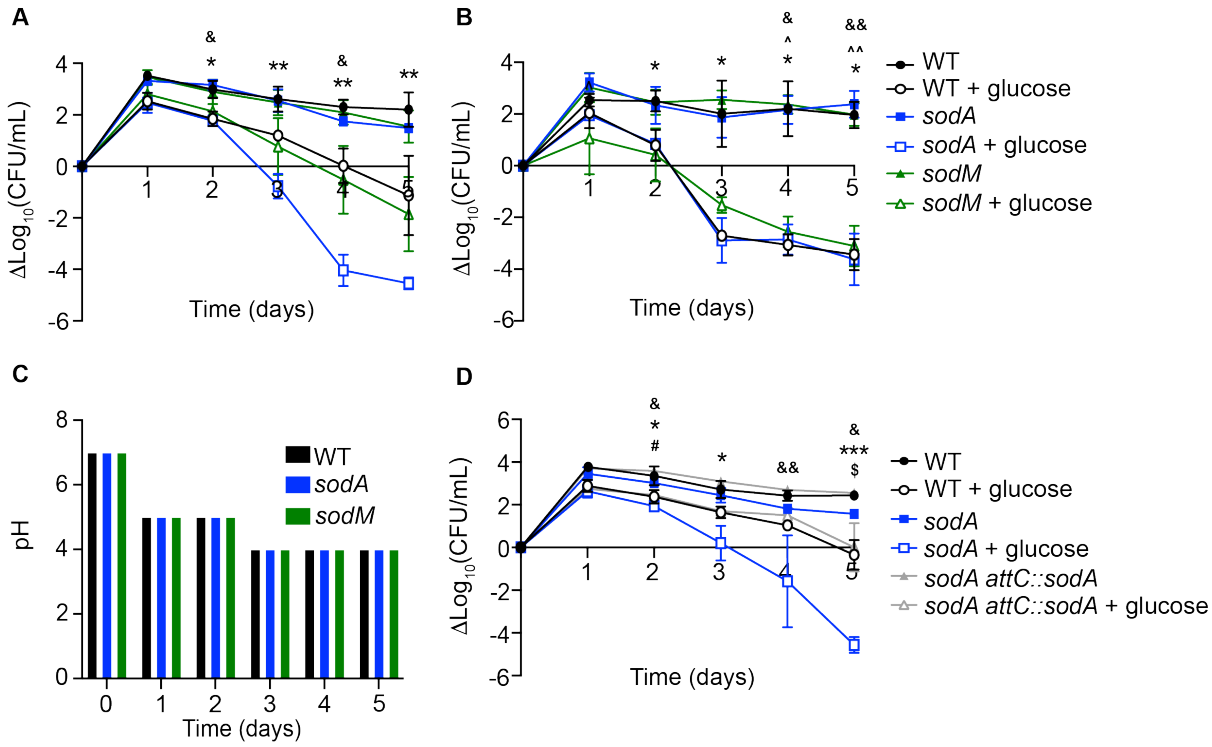

Figure 32. *S. aureus sodA* is required for survival during culture in high glucose. WT, *sodA*::tet (*sodA*), and *sodM*::erm (*sodM*) *S. aureus* strains were grown in 10 mL TSB with ("+ glucose") and without 500 mg/dl glucose in flasks covered with (A) foil (aerobic) or (B) capped (microaerobic) shaking at 37°C. CFU were quantified every 24 hrs over the course of 5 days and normalized to time 0 hr. (C) pH was measured every 24 hrs over the course of 5 days in TSB with 500 mg/dl glucose grown in aerobic microaerobic conditions. (D) WT, *sodA*::tet (*sodA*), and *sodA*::tet *attC*::*sodA* (*sodA attC::sodA*) *S. aureus* were grown in 10 mL TSB and TSB with 500 mg/dl glucose ("+ glucose") in flasks covered with foil (aerobic). N = 2 technical replicates, and n = 3 biological replicates. Line represents mean (A, B, and D). Significance determined with two-way ANOVA and Dunnett's multiple comparisons test. *p<0.05, **p<0.01, ***p<0.001 *sodA*::tet TSB + glucose; &p<0.05, &&p<0.01 WT TSB + glucose; ^p<0.05, ^^p<0.01 *sodM*::erm TSB + glucose; #p<0.01 *sodA*::tet *attC*::*sodA* TSB + glucose; $p<0.01 *sodA*::tet TSB. All comparisons made to WT in TSB.

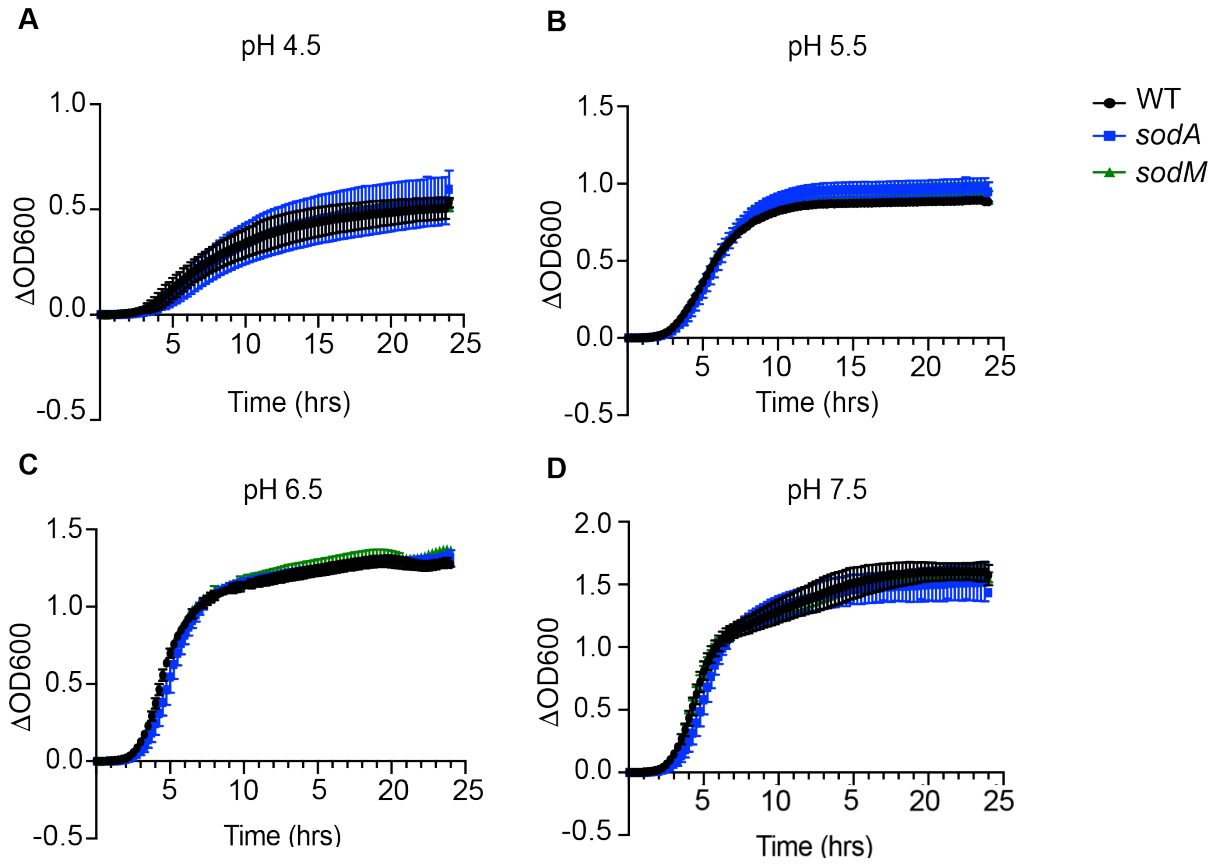

Figure 33. *S. aureus sodA* mutant does not have a growth defect in TSB at different pH values over 24 hrs. WT, *sodA*::tet (*sodA*), and *sodM*::erm (*sodM*) *S. aureus* strains were grown in TSB at (A) pH 4.5, (B) pH 5.5, (C) pH 6.5, and (D) pH 7.5 in 96 well plates aerobically shaking at 37°C. OD600 were quantified every 15 min over the course of 24 hrs and normalized to time 0 hr. N = 3 technical replicates, and n = 3 biological replicates. Line represents mean, and error bars represent standard deviation. Significance determined with two-way ANOVA. All comparisons made to WT.

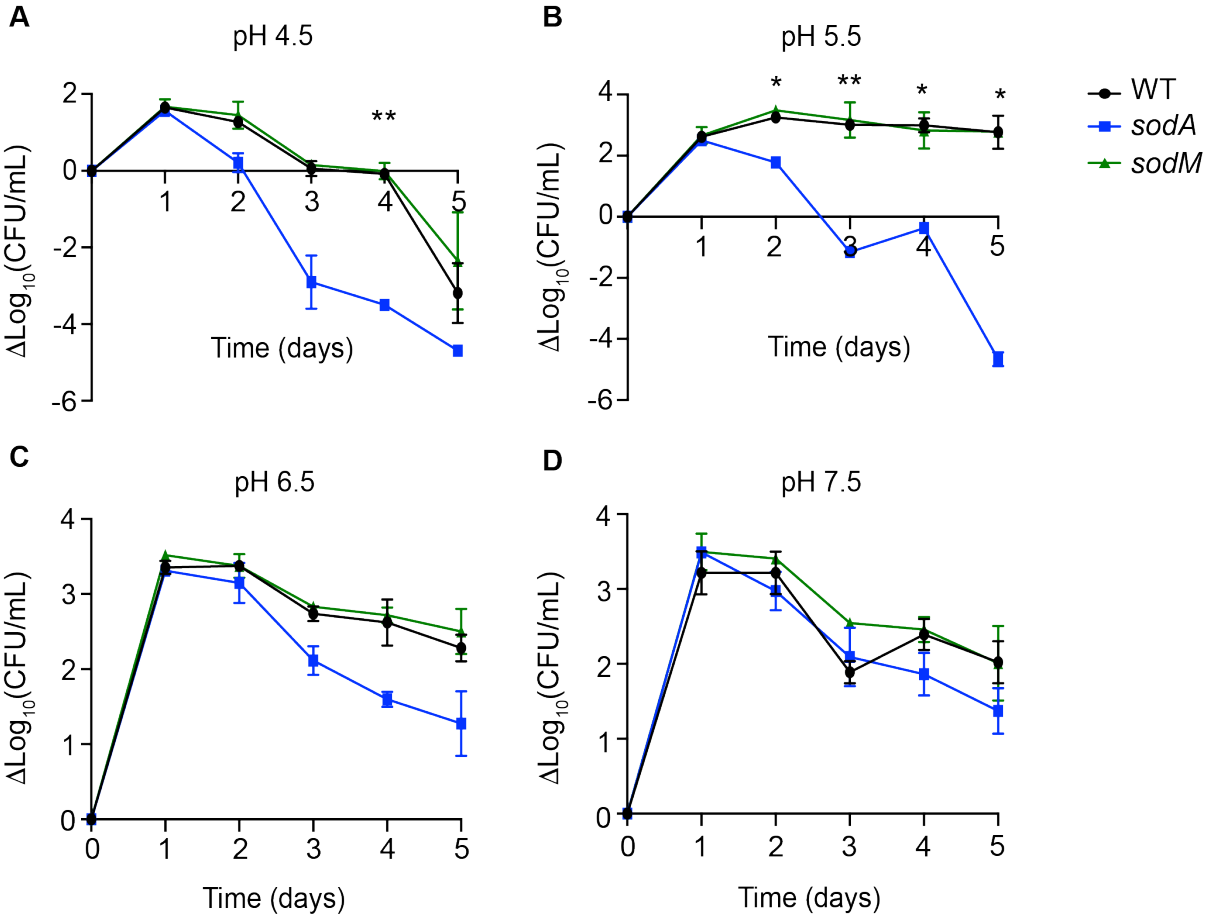

Figure 34. *S. aureus sodA* mutant has distinct growth kinetics in TSB at lower pH over 5 days. WT, *sodA*::tet (*sodA*), and *sodM*::erm (*sodM*) *S. aureus* strains were grown in 10 mL TSB at (A) pH 4.5, (B) pH 5.5, (C) pH 6.5, and (D) pH 7.5 in flasks covered with foil (aerobic) shaking at 37°C. CFU were quantified every 24 hrs over the course of 5 days and normalized to time 0 hr. N = 3 technical replicates, and n = 3 biological replicates. Line represents mean, and error bars represent standard deviation. Significance determined with two-way ANOVA and Dunnett's multiple comparisons tests. *p<0.05 *sodA*::tet, **p<0.01 *sodA*::tet. All comparisons made to WT.

SodA is not essential for *S. aureus* intracellular survival.

S. aureus can survive intracellularly in macrophages during infection, and macrophage function becomes altered during hyperglcyemia.[73,164,186] To investigate whether hyperglycemia influences SOD mutant *S. aureus* survival intracellularly, we measured changes in bacterial intracellular survival in bone marrow-derived macrophages (BMMs) derived from STZ-treated mice that became hyperglycemic and from STZ-treated mice that remained euglycemic. The BMMs were differentiated *in vitro* and were cultured in complete media or complete media supplemented with 30 mM (540 mg/dl) glucose for two days prior to adding *S. aureus* to assess the influence of high glucose exposure *in vivo* as well as high glucose exposure after differentiation. A concentration of 30 mM of glucose was selected in accordance with prior publications that highlighted changes in inflammatory properties of macrophages exposed to 30 mM glucose.[187,188] Two hours after the addition of WT, *sodA* mutant, and *sodM* mutant *S. aureus*, bacterial internalization was measured. The only significant difference in *S. aureus* internalization was an increased intracellular survival of the *sodM* mutant compared to WT at 2 hrs in the BMMs derived from hyperglycemic mice and cultured in the absence of additional glucose (**Fig. 35A**). There were no differences in *S. aureus* intracellular survival between WT and SOD mutant strains at 24 hrs, regardless of the glucose exposure or source of BMMs (**Fig. 35B**). Additional replicates and conditions with macrophage stimulation are important to further test the importance of SODs for *S. aureus* intracellular survival in conditions of high glucose.

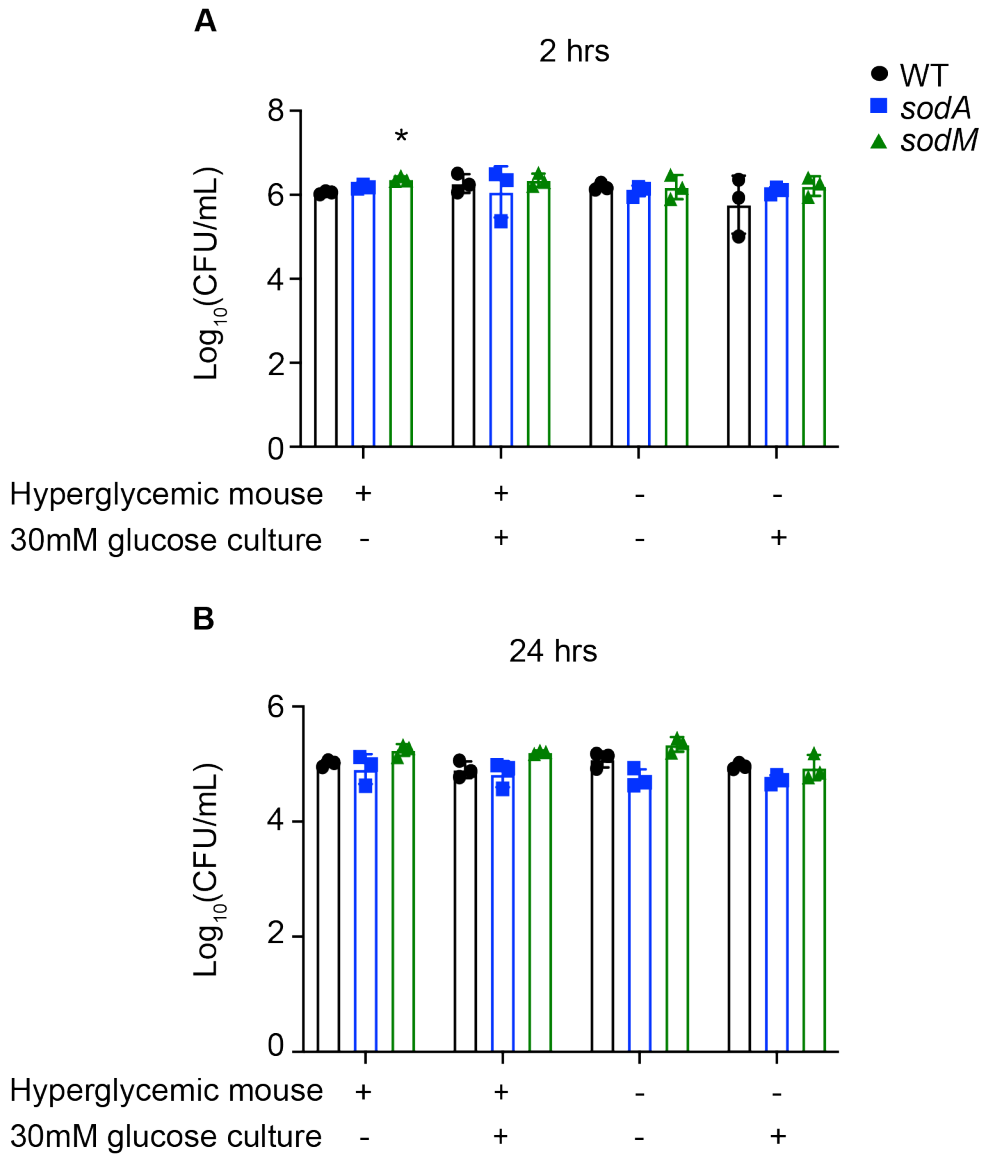
A
2 hrs
WT
sodA
sodM
Log10(CFU/mL)
8
6
4
2
0
*
Hyperglycemic mouse + + - -
30mM glucose culture - + - +
B
24 hrs
Log10(CFU/mL)
6
4
2
0
Hyperglycemic mouse + + - -
30mM glucose culture - + - +

Figure 35. *S. aureus* SODs are not important for *S. aureus* survival in bone marrow macrophages. Eight-week old male mice were treated with streptozotocin (STZ) intraperitoneally for 5 days. Four weeks following STZ treatment, at the equivalent time of a 14 day infection harvest, bone marrow was harvested from mice that became hyperglycemic (hyperglycemic mouse +) and mice that did not become hyperglycemic (hyperglycemic mouse -). Bone marrow was differentiated in CMG14-12 as a source of M-CSF. Two days prior to adding bacteria to cultures, media was changed to include an additional 30 mM glucose (30 mM glucose culture +) or maintained without additional glucose (30 mM glucose culture -). WT, *sodA*::tet (*sodA*), and *sodM*::erm (*sodM*) *S. aureus* strains were added to bone marrow macrophage cells at a MOI of 100 and allowed to internalize. Gentamicin was added to media to kill extracellular bacteria. Cells were lysed and intracellular CFU were enumerated at (A) 2 hr and (B) 24 hrs. N = 3 technical replicates per group. Bars indicate mean, and error bars represent SD. Significance determined with two-way ANOVA and Dunnett's multiple comparisons test. *$p<0.05$. All comparisons made to WT.

SodA enhances *S. aureus* survival during osteomyelitis in hyperglycemic mice.

To validate the role of *S. aureus* SODs *in vivo*, we assessed the CFU burdens of WT, *sodA*::tet, *sodM*::erm*, and sodA*::tet *sodM*::erm strains of *S. aureus* in osteomyelitis mono-infections during hyperglycemia. Following STZ treatment, we inoculated mice with $1x10^5$ CFU of each mutant strain or WT. Over the course of the infection, mice were monitored for changes in weight. Mice infected with *sodA*, *sodM*, and *sodA sodM* mutants had significantly less weight loss at multiple days post-infection compared to mice infected with WT (**Fig. 36A**). *S. aureus* burdens were lower in femurs of mice infected with *sodA* and *sodA sodM* mutants compared to WT at day 14 post-infection (**Fig. 36B**). Furthermore, the kidneys, liver, and heart from hyperglycemic mice infected with the *sodA sodM* mutant had lower *S. aureus* burdens compared to WT infected mice (**Fig. 36C-E**). Complementation of *sodA* may partially rescue the ability of *sodA*::tet *S. aureus* to disseminate similarly to WT, although the differences in bacterial burden are only statistically significant in the heart and require additional investigation (**Fig. 37D-E**). The percent starting weight of mice infected with the *sodA* complemented strain were also not statistically different than WT infected mice (**Fig. 37A**). Within the infected femurs, there were no differences between WT, *sodA*::tet, and *sodA*::tet *attC*::*sodA*, which may suggest incomplete complementation (**Fig. 37B**). Collectively, these data confirm the importance of SodA in promoting *S. aureus* osteomyelitis during hyperglycemia and validate the importance of SODs for bacterial dissemination.

To assess whether *S. aureus* SODs are essential during osteomyelitis in euglycemic mice, we inoculated vehicle-treated control mice with $1x10^5$ CFU WT, *sodA* mutant, or *sodM* mutant *S. aureus* and measured bacterial burdens in the femur 14 days post-infection. Neither group of SOD mutant infected mice showed differences in percent starting weight compared to WT, apart from *sodA*::tet infected mice having significantly greater percent starting weight at day 2 compared to WT (**Fig. 38A**). WT, *sodA* mutant, and *sodM* mutant infected animals

showed no differences in burdens in the infected femurs at day 14 post-infection (**Fig. 38B**). These data suggest that the fitness defect of the *sodA* mutant is more pronounced in hyperglycemic osteomyelitis.

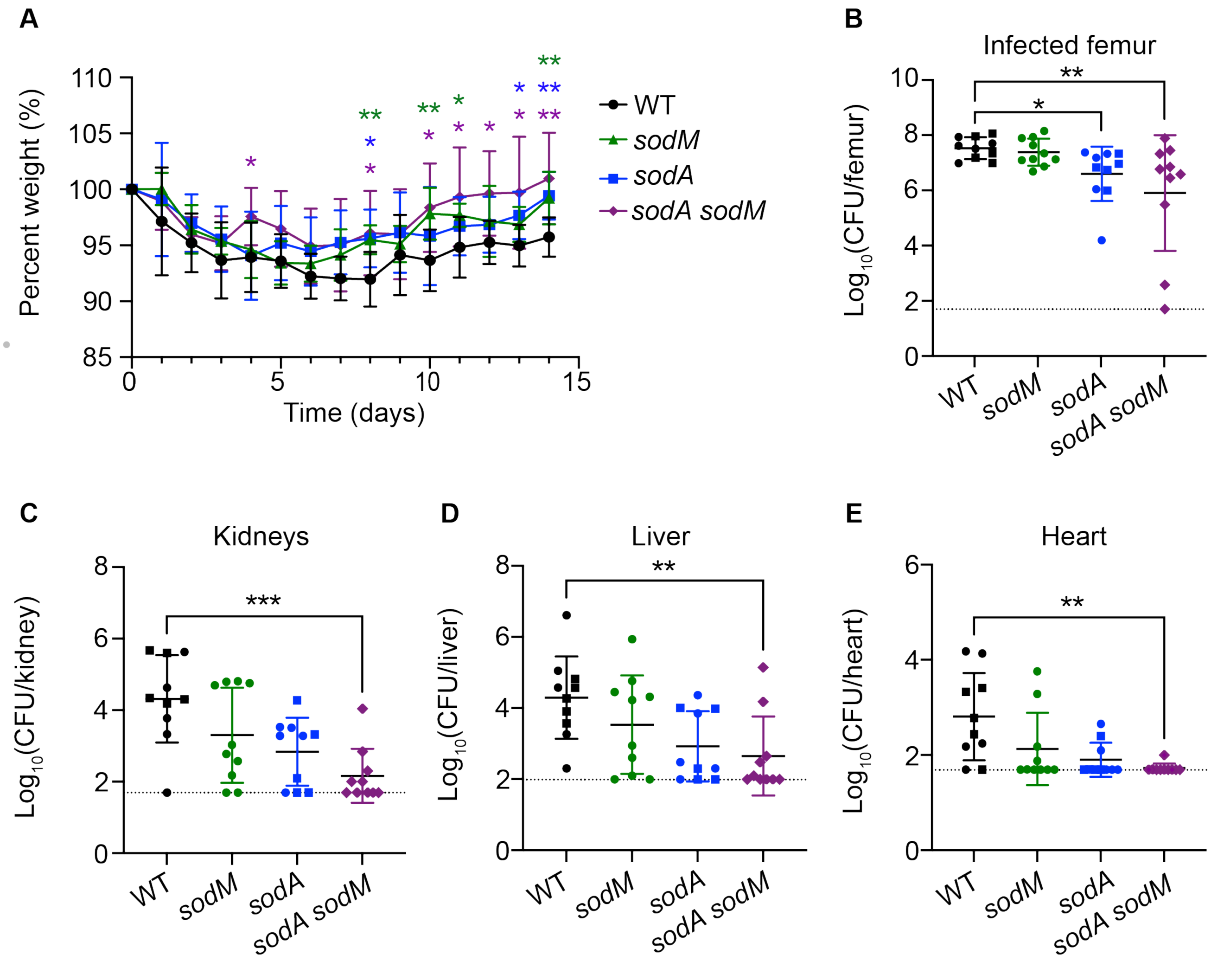
A
Percent weight (%)
Time (days)
WT
sodM
sodA
sodA sodM
B
Infected femur
Log10(CFU/femur)
C
Kidneys
Log10(CFU/kidney)
D
Liver
Log10(CFU/liver)
E
Heart
Log10(CFU/heart)
WT
sodM
sodA
sodA sodM

Figure 36. SodA is important for *S. aureus* survival during osteomyelitis in hyperglycemic mice. Eight-week old male mice were treated with streptozotocin (STZ) intraperitoneally for 5 days. 10 days after the final injection, mice were infected with $1x10^5$ CFU of WT, *sodA*::tet (*sodA*), *sodM*::erm (*sodM*), and *sodA*::tet *sodM*::erm (*sodA sodM*) *S. aureus* via intraosseous injection. (A) Weights were recorded every 24 hrs and normalized to the starting weight of each animal on the day of infection (percent weight). Mice were sacrificed at day 14 post-infection, and the bacterial burdens (CFU) were enumerated in (B) infected femur, (C) kidneys, (D) liver, and (E) heart. Different shapes indicate data collected from distinct experiments. N = 10 mice per group. Dotted lines indicate limit of detection. Horizontal lines indicate mean, and error bars represent SD. Significance determined with two-way ANOVA and Dunnett's multiple comparisons test (A) and Kruskal-Wallis with Dunn's multiple comparisons test (B-E). *$p<0.05$, **$p<0.01$, ***$p<0.001$. All comparisons made to WT.

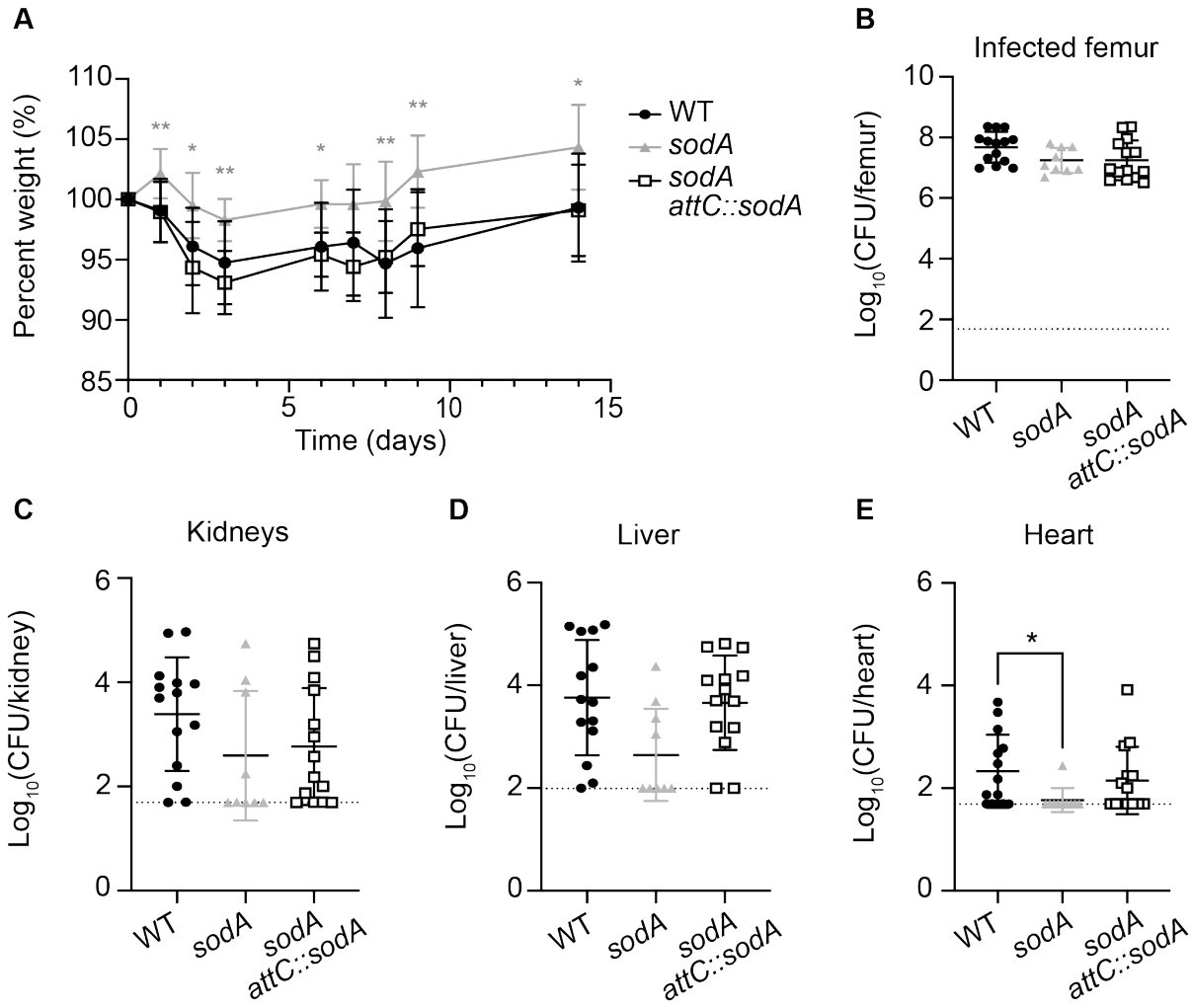
A
Percent weight (%)
Time (days)
WT
sodA
sodA attC::sodA
B
Infected femur
Log10(CFU/femur)
C
Kidneys
Log10(CFU/kidney)
D
Liver
Log10(CFU/liver)
E
Heart
Log10(CFU/heart)
WT
sodA
sodA attC::sodA

Figure 37. Complementation of *sodA* may restore *S. aureus* growth *in vivo* during osteomyelitis in hyperglycemic mice. Eight-week old male mice were treated with streptozotocin (STZ) intraperitoneally for 5 days. 10 days after the final injection, mice were infected with $1x10^5$ CFU of WT, *sodA*::tet (*sodA*), and *sodA*::tet *attC*::*sodA* (*sodA attC::sodA*) *S. aureus* via intraosseous injection. (A) Weights were recorded every 1-4 days and normalized to the starting weight of each animal on the day of infection (percent weight). Mice were sacrificed at day 14 post-infection, and the bacterial burden (CFU) was enumerated in the (B) infected femur, (C) kidneys, (D) liver, and (E) heart. N = 14 mice in WT and *sodA attC::sodA* infected groups, and n = 9 mice in *sodA* infected group. Dotted lines indicate limit of detection. Horizontal lines indicate mean, and error bars represent SD. Significance determined with two-way ANOVA and Dunnett's multiple comparisons test (A) and Kruskal-Wallis with Dunn's multiple comparisons test (B-E). *$p<0.05$, **$p<0.01$. All comparisons made to WT (A) and comparisons made between all groups (B-E).

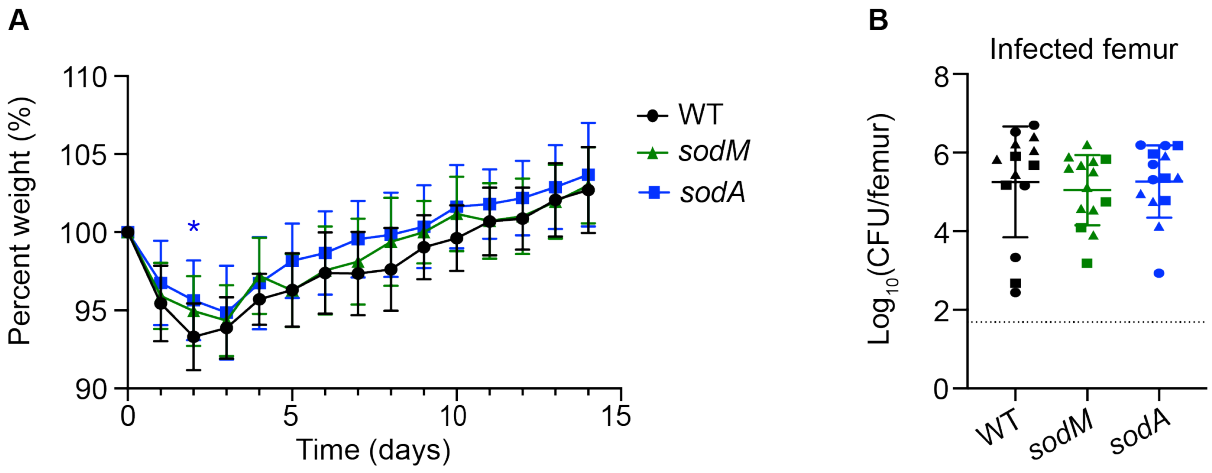

Figure 38. SodA is not necessary for *S. aureus* survival during osteomyelitis in euglycemic mice. Eight-week old male mice were treated with sodium citrate (vehicle) intraperitoneally for 5 days. 10 days after the final injection, mice were infected with $1x10^5$ CFU of WT, *sodA*::tet (*sodA*), and *sodM*::erm (*sodM*) *S. aureus* via intraosseous injection. (A) Weights were recorded every 24 hrs and normalized to the starting weight of each animal on the day of infection (percent weight). (B) Mice were sacrificed at day 14 post-infection, and the bacterial burdens (CFU) were enumerated in infected femurs. Different shapes indicate data collected from distinct experiments. N = 14 mice per group. Dotted line indicates limit of detection. Horizontal lines indicate mean, and error bars represent SD. Significance determined with two-way ANOVA and Dunnett's multiple comparisons test (A) and Kruskal-Wallis with Dunn's multiple comparisons test (B). *$p<0.05$ *sodA*::tet compared to WT. All comparisons made to WT.

Dysregulation of neutrophils increases *S. aureus* burdens during osteomyelitis.

Neutrophils have a critical role in mediating *S. aureus* clearance during infection.[189,190] Prior studies support that hyperglycemia influences neutrophil function.[83,191,192] Anti-Ly6G antibody was previously reported to deplete neutrophils, although more recent studies suggest the antibody functions by inhibiting neutrophil function.[193–195] To assess the role of functional neutrophils in infection control during osteomyelitis infection, mice were treated with IgG2a isotype control (isotype) or anti-Ly6G antibody (anti-Ly6G) over the course of the study. Isotype control treated and anti-Ly6G treated mice were infected with $1x10^6$ CFU of WT *S. aureus* via intraosseous injection. Anti-Ly6G treatment resulted in a significant increase in *S. aureus* burdens in the infected femurs compared to isotype treated mice at days 2 and 10 post-infection (**Fig. 39A**). To enumerate neutrophils in the blood at days 2, 5, 7, and 10, complete blood counts (CBCs) were measured. At day 10, there were significantly greater neutrophil counts in the anti-Ly6G treated *S. aureus* infected mice compared to isotype treated infected animals (**Fig. 39B**). These data suggest that functional neutrophils are important for control of *S. aureus* burdens in bone during osteomyelitis and that anti-Ly6G treatment may induce emergency hematopoiesis, consistent with prior studies.[194]

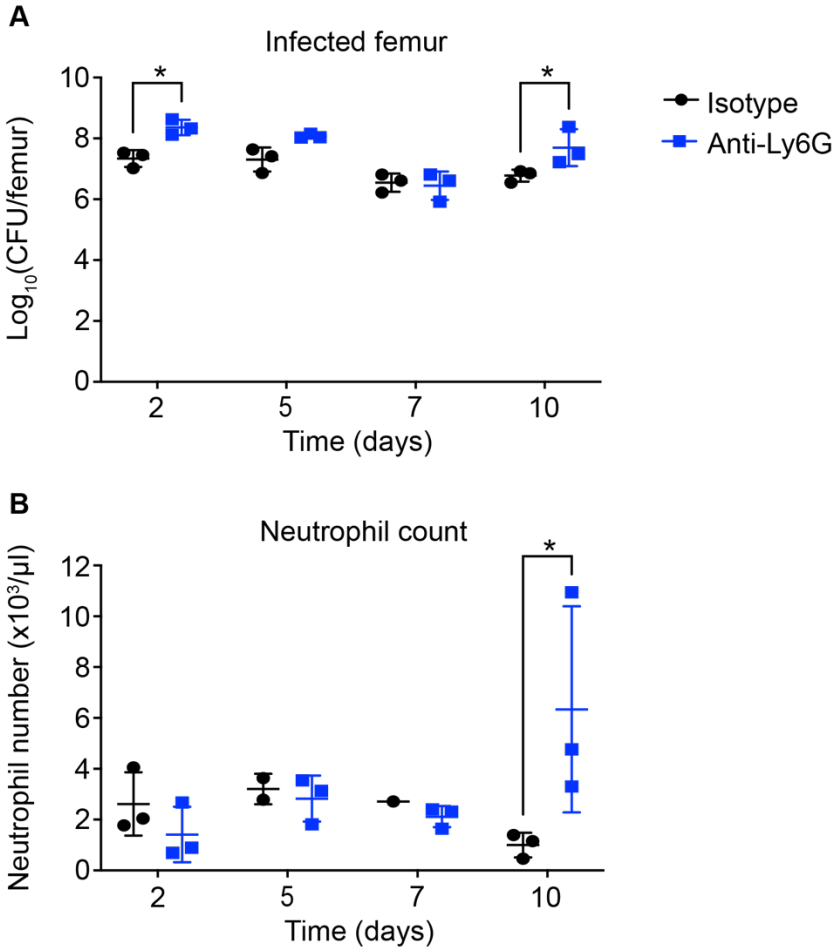

Figure 39. Treatment of mice with anti-Ly6G monoclonal antibody increases *S. aureus* burdens during osteomyelitis. Eight-week old female mice were treated with IgG2a isotype control (Isotype) or anti-Ly6G antibody (Anti-Ly6G) over the course of the study. Mice were infected with $1x10^6$ CFU of WT *S. aureus* via intraosseous injection. (A) Mice were sacrificed at days 2, 5, 7, and 10 post-infection, and the bacterial burden (CFU) was enumerated in the infected femur. (B) Neutrophils were enumerated at the time of sacrifice via complete blood count (CBC) test. N = 3 mice per group. Horizontal lines indicate mean, and error bars represent SD. Significance determined with Student's t-tests corrected for multiple comparisons. *$p<0.05$.

Dysregulation of neutrophils increases bone loss during *S. aureus* osteomyelitis.

In addition to their role in innate immune response, neutrophils also influence bone fracture healing.[196] To assess the role of functional neutrophils in bone homeostasis during osteomyelitis, mice were treated with isotype or anti-Ly6G antibody over the course of the study. Isotype control treated and anti-Ly6G treated mice were infected with $1x10^6$ CFU of WT *S. aureus* via intraosseous injection. We used μCT to quantify changes to trabecular bone structure in the *S. aureus*-infected femurs at 14 days post-infection. The infected femurs from anti-Ly6G treated mice had decreased trabecular %BV/TV relative to isotype treated infected mice (**Fig. 40A**). Trabecular bone number was less and spacing was greater in infected anti-Ly6G treated mice compared to isotype treated infected mice, with no differences observed in trabecular thickness (**Fig. 40B-D**). Collectively, our data reveal that dysregulation of neutrophils contributes to greater pathologic bone destruction during *S. aureus* osteomyelitis compared to euglycemic infection.

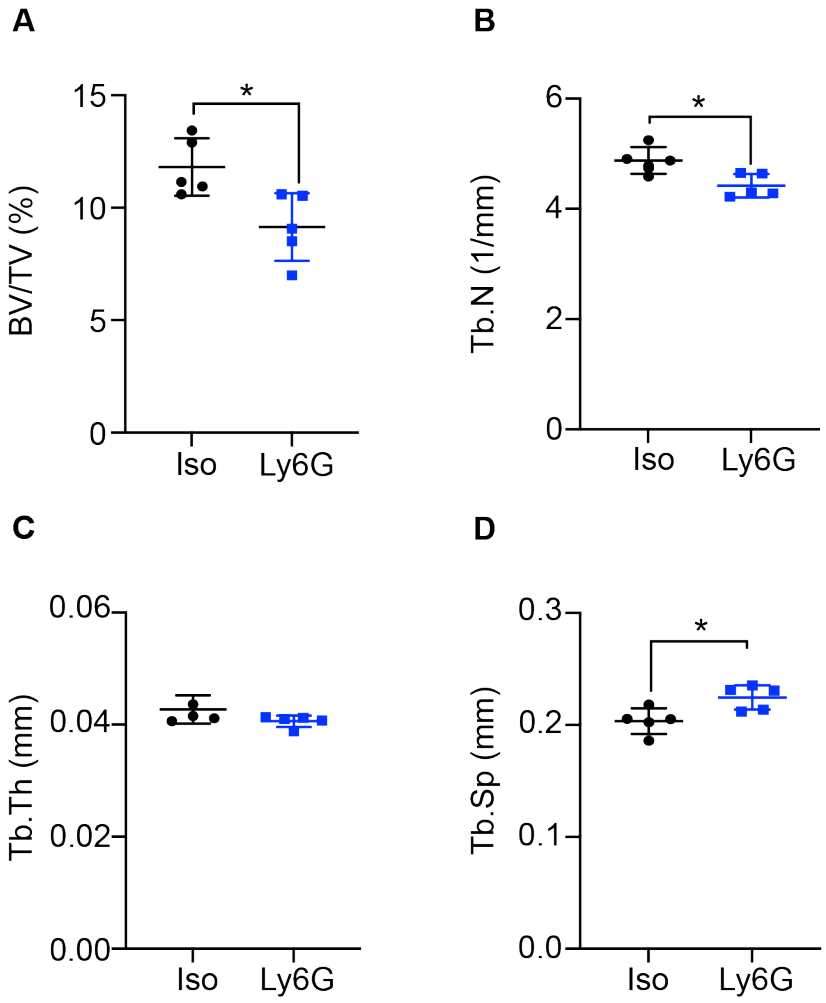

Figure 40. Modulation of neutrophils increases infection-induced bone loss during osteomyelitis. Eight-week old female mice were treated with IgG2a isotype control (Iso) or anti-Ly6G antibody (Ly6G) over the course of the study. Mice were infected with $1x10^6$ CFU of WT *S. aureus* via intraosseous injection. At 14 days post-infection, the infected femurs were isolated and fixed in neutral buffered formalin prior to microcomputed tomography. (A) Percent trabecular bone volume divided by total volume (%BV/TV), (B) trabecular number (Tb.N), (C) trabecular thickness (Tb.Th), and (D) trabecular spacing (Tb.Sp) were quantified in infected femurs. N = 5 mice per group. Horizontal lines indicate mean, and error bars represent SD. Significance determined with Mann-Whitney test. *$p<0.01$.

Discussion

Using a chemically-induced model of hyperglycemia, we discovered increased *S. aureus* burdens and significantly greater bone loss during infection in hyperglycemic mice compared to euglycemic infection in a post-traumatic osteomyelitis model. We also discovered increased dissemination of *S. aureus* to other organs in hyperglycemic mice. The gene encoding SodA was found to be critical for *S. aureus* survival during hyperglycemic infection and for *S. aureus* growth *in vitro* in the presence of high glucose. These findings are consistent with prior clinical studies that correlated poor *S. aureus* infection outcomes in hyperglycemic individuals, both with and without diabetes.[197,198] This work further reveals a *S. aureus* virulence factor that contributes to increased osteomyelitis pathogenesis during hyperglycemia and supports the hypothesis that metabolic comorbidities shape the essential *S. aureus* genes required for invasive infection.

Multiple murine *S. aureus* infection models have identified increases in infection severity in the setting of hyperglycemia, including footpad infections in STZ-induced hyperglycemic mice.[73,74,108,199] More severe infections were also observed in STZ-induced hyperglycemic mice in an implant-related orthopedic infection model, as measured by *S. aureus* burdens, bone density, and biofilm formation.[90] Models of type 2 diabetes likewise revealed increased osteomyelitis infection severity associated with hyperglycemia.[6,200,201] Elevated *S. aureus* burdens were observed in skin infection due to aberrant neutrophil chemotaxis, dysregulated abscess formation, and impaired wound healing during hyperglycemia.[78,83] Our study contributes to a greater understanding of how hyperglycemia influences *S. aureus* infection pathogenesis by revealing changes in bacterial survival during post-traumatic osteomyelitis as well as significantly greater infection-induced bone loss during hyperglycemia.

In a prior study, we identified genes involved in glucose metabolism and virulence as essential for *S. aureus* survival and disease pathogenesis *in vivo* during osteomyelitis.[2,3,26] To identify genes that contribute to increased pathogenesis of *S. aureus* osteomyelitis during hyperglycemia, we conducted TnSeq, comparing *S. aureus* survival in hyperglycemic mice to euglycemic mice. Similar to our prior TnSeq study, genes involved in purine/pyrimidine and amino acid metabolism were identified as essential for *S. aureus* growth during osteomyelitis in hyperglycemic mice, including *carA*, *carB*, and *aptA*. Both *carA* and *aptA* are important for *S. aureus* survival in nitric oxide stress.[170] Furthermore, *carA* is critical for *S. aureus* extracellular survival in the presence of high H_2O_2.[202] Purine and pyrimidine synthesis enable *S. aureus* to persist in the presence of hydroxyl radicals that oxidize base and ribose moieties of DNA, creating lesions that require repair.[203] The gene *ccpA* was also uniquely essential for *S. aureus* growth during osteomyelitis in hyperglycemic mice, linking the abundance of glucose in tissues with transcriptional control of genes involved in gluconeogenesis, the TCA cycle, and cell adherence and immune evasion.[117,204–206] In the first TnSeq experimental replicate (of two total), *ureB* (which encodes urease B) was also identified as essential for *S. aureus* survival during osteomyelitis infection in hyperglycemic mice. We decided to focus on investigating the role of *ureB* in *S. aureus* survival due to its role in maintaining pH homeostasis and viability under weak acid stress during culture in high glucose.[123] UreB functions by converting urea to ammonia and carbon dioxide, thus consuming protons. We found that UreB was critical for *S. aureus* survival in biofilms and in liquid cultures in high glucose, similarly to prior studies.[123] However, we did not see differences between WT and *ureB* mutant *S. aureus* survival *in vivo* in osteomyelitis during hyperglycemia. The *ureB* mutant may not influence *S. aureus* viability *in vivo* during infection in a hyperglycemic host due to a lack of urea in the bone or other differences in the structure or nutrient content at the site of the infection compared to the *in vitro* conditions.

TnSeq also revealed the importance of *sodA* for *S. aureus* survival during osteomyelitis in hyperglycemic mice. SodA has been implicated in *S. aureus* stress responses during aerobic metabolism and in the presence of ROS produced by innate immune cells.[125,185] Additionally, *sodA* was previously identified as essential for *S. aureus* growth in skin infections in STZ-induced hyperglycemic mice.[108] SodA catalyzes the detoxification of superoxide into hydrogen peroxide, which is further broken down by catalase, and both SOD and catalase activity of bacteria have been correlated to virulence.[125,207–209] Production of superoxide is a known innate immune defense mechanism used to kill intracellular phagocytosed bacteria.[210,211] Previous publications revealed that neutrophils have a decreased capacity for respiratory burst and limited ROS production during hyperglycemic infection.[75,83,89,192] However, oxidative stress from altered metabolism of endothelial cells increases the amount of ROS in tissues of hyperglycemic patients.[165,212,213] Superoxide can also be produced intrinsically by *S. aureus* in response to carbon overflow metabolism. Carbon overflow occurs when *S. aureus* breaks down glucose through glycolysis and results in acetate accumulation.[120] The accumulation of acetate and NADH leads to a bottleneck in the electron transport chain that catalyzes reduction of oxygen, producing ROS.[214] Based on these findings, we hypothesized that a *sodA* mutant would have a defect in survival in high glucose. We observed decreased *S. aureus* growth in glucose-rich media over 5 days in the absence of a functional *sodA* gene.[215] These data are consistent with a model of hyperglycemic skin infection whereby dysfunctional phagocytes were observed to consume less glucose during hyperglycemia, thereby eliminating *S. aureus* competition for glucose and potentiating S. *aureus* virulence.[74] These data suggest that the defect in survival of a *sodA* mutant may be related to intrinsic *S. aureus* ROS production during hyperglycemia.

The *S. aureus* genome encodes two SOD genes, *sodA* and *sodM*.[125,126] The SODs are critical for *S. aureus* survival in the presence of superoxide during distinct phases of growth,

with SodA functions to detoxify ROS during exponential phase, while SodM has a greater role during stationary phase.[126] Both *S. aureus* SODs can utilize manganese as a co-factor, while SodM can also use iron.[184] The distinct characteristics of SodA and SodM may facilitate *S. aureus* survival in the presence of ROS in distinct tissues and/or nutritional microenvironments. Because SodA activity may be compensated by SodM, we decided to interrogate the roles of both genes in osteomyelitis during hyperglycemia. Mutating *sodA* or *sodA* and *sodM* decreases *S. aureus* survival in hyperglycemic infection, while mutating *sodM* does not affect *S. aureus* survival, further supporting the importance of SodA in this model of infection. The greater attenuation of the *sodA sodM* mutant *in vivo* in comparison to mutation of *sodA* alone suggests potentially redundancy of *sodM* in the absence of a functional *sodA*. In comparison, prior studies in euglycemic mice found that both *sodA* and *sodM* are essential for full *S. aureus* virulence following intravenous infection.[216] These data suggest that there could be tissue and microenvironment-specific factors that influence the need for *S. aureus* SODs to support bacterial survival *in vivo*. We did not observe differences in the ability of WT and SOD mutants to survive osteomyelitis in euglycemic vehicle-treated mice. These findings are consistent with a skin abscess model of infection where there was no difference in abscess formation with a *sodA* mutant strain compared to WT in euglycemic mice.[125]

In addition to revealing the mechanisms by which *S. aureus* survives and causes more severe infection during hyperglycemia, we were also interested in identifying host processes that contribute to exacerbated infection. Prior work supports that hyperglycemia influences neutrophil function, and neutrophils influence bone fracture healing.[83,191,192,196] We found that mice with dysfunctional neutrophils had greater *S. aureus* burdens and decreased trabecular bone volume compared to mice with functional neutrophils treated with an isotype control. These findings suggest that modulation of neutrophil function can influence bacterial burdens and trabecular bone homeostasis during osteomyelitis infection.

There are some limitations in this chapter that should be considered. We chose to induce hyperglycemia with STZ to model increased blood glucose while minimizing confounding physiological changes associated with obesity, age, or the need for specialized housing.[35] Limitations of this model include that STZ can be toxic to other organs, and the conclusions may not be generalizable to other models of hyperglycemia.[35,217] To model osteomyelitis, we used an established post-traumatic model, inoculating *S. aureus* directly into the femurs.[3] This model does not effectively reproduce the characteristic clinical progression of contiguous wound dissemination, which is commonly observed with diabetic foot wounds. This work also does not directly address how the host response was compromised during hyperglycemia, although multiple other studies using *S. aureus* infection models have identified changes in the immune response.[6,75,78,84,85] Histologic sections were obtained from hyperglycemic and euglycemic infected femurs but require additional samples and blinded pathology scoring to discern differences in the extent of inflammation. Finally, TnSeq has inherent limitations, as referenced in Chapter II, including the ability of compensatory mutants to rescue the growth of transposon mutants via nutrient sharing or other community interactions.

Future studies should include other models of osteomyelitis, such as foot pad infections, to observe whether osteomyelitis infection dynamics are recapitulated in contiguous wound infection models. Additionally, studies are needed to assess which host processes influence the role of SodA in infection. *S. aureus* glucose transporter mutants can also be used to assess the ability of *S. aureus* to survive in hyperglycemic conditions when it does not have the ability to use exogenous glucose.[218] Measuring changes in metabolites and ROS within the microenvironment of infected femurs in hyperglycemic mice is also an important future direction. Future studies are expanded upon and discussed in Chapter IV.

Taken together, the data in Chapter III reveal that both acute and chronic hyperglycemia increase *S. aureus* infectious burden, dissemination, and bone destruction during osteomyelitis.

We identified 71 genes that are uniquely essential for *S. aureus* growth during osteomyelitis in hyperglycemic mice compared to euglycemic osteomyelitis. Of these genes, *sodA* was further studied due to its role in detoxifying ROS, a biproduct of glucose carbon overflow metabolism. The results of this study highlight a bacterial virulence gene that contributes to exacerbated infection during hyperglycemia and provide a strong rationale for continued investigation into mechanisms of enhanced musculoskeletal disease in the context of hyperglycemia.

Material and Methods

Bacterial strains and culture conditions

Unless otherwise stated, experiments were performed with *S. aureus* USA300 lineage strain AH1263, an erythromycin and tetracycline sensitive derivative of strain LAC, which served as wildtype (WT). Transposon mutants were obtained from BEI Resources and were transduced with phi-85 from JE2 strains into the AH1263 background. Strains *sodA*::tet (*sodA*), *sodM*::erm (*sodM*), and *sodA*::tet *sodM*::erm (*sodA sodM*) in the AH1263 background were created via phi-85-mediated phage transduction of *sodA*::tet and *sodM*::erm from the Newman background.[126,184] The *sodA* complementation construct was created by amplifying *sodA* and its endogenous promoter with primer sequences CTAGCTCTAGATGAGATTTATGCACATTTGGTCA and CTAGCGGTACCTTTATTTTGTTGCATTATATAATTCG. The *sodA* sequence was ligated into pJC1111 and integrated into the chromosome at attachment (*attC*) sites, as previously described.[162] All bacterial cultures were grown overnight in 5 mL TSB at 37°C with shaking at 180 rpm, except as otherwise noted. 10 μg/mL erythromycin, 2 μg/mL tetracycline, or 0.1 mM cadmium chloride were added to cultures with strains possessing antibiotic resistance markers.

Murine model of osteomyelitis during hyperglycemia

All animal experiments were reviewed and approved by the Institutional Animal Care and Use Committee (ACUC) at Vanderbilt University Medical Center and performed in accordance with NIH guidelines, the Animal Welfare Act, and US Federal law. Six - eight week male C57BL/6J mice were obtained from Jackson Laboratories (stock #000664) and intraperitoneally injected daily with 200 µL of 0.1 mM sodium citrate (vehicle) or 40-60 mg/kg streptozotocin (STZ) in 200 µL of 0.1 mM sodium citrate for 5 days to induce hyperglycemia. Acute hyperglycemia infections were performed 10 days after the final intraperitoneal STZ or sodium citrate injection, and chronic hyperglycemia infections were performed 30 days the final intraperitoneal STZ or sodium citrate injection. Blood glucose concentration was quantified from a tail vein bleed immediately prior to inoculation (day 0) and on the day of sacrifice (day 14). STZ-treated mice below the hyperglycemic threshold of 250 mg/dl were removed from the study, except as otherwise noted. Osteomyelitis was induced with ~$1x10^6$ or ~$1x10^5$ CFU in 2 µl via intraosseous injection into the femurs, as previously reported.[3] Competition experiments were conducted by combining standardized inocula of two strains in a 1:1 ratio. Mice were weighed daily and monitored for disease progression. At 4 or 14 days post-infection, mice were sacrificed, and the infected femurs were either homogenized for CFU enumeration or fixed for micro-computed tomography (µCT) (see below). For CFU enumeration, infected femur, contralateral femur, kidneys, liver, and heart were homogenized in Cell Lytic buffer (Sigma) and plated on Tryptic Soy Agar (TSA). Limits of detection based on volume of homogenate plated were 49 CFU per femur, heart, and kidneys and 99 CFU per liver.

Micro-computed tomography analysis of femurs

Infected and contralateral femurs were harvested from mice at day 14 post-infection. Femurs were fixed in 10% neutral buffered formalin for 2 days then moved to 70% ethanol and stored

at 4°C. Fixed femurs were scanned with a μCT50 Scanco instrument (Scanco Medical, Switzerland) and analyzed with μCT Tomography V6.3-4 software (Scanco USA, Inc.). The diaphysis and distal epiphysis of each femur were imaged with 10.0 μm voxel size at 70 kV, 200 μA with an integration time of 350 ms in 10.24 mm view. 1088 slices were obtained to include the diaphysis surrounding the cortical defect formed during inoculation as well as trabecular bone in the distal femur. Three-dimensional reconstructions were analyzed to quantify cortical bone destruction surrounding the inoculation site (mm^3). Trabecular bone volume per total volume (%), trabecular number (1/mm), trabecular thickness (mm), and trabecular spacing (mm) were quantified within the epiphyses, as previously described.[3,175]

Bone histology

After μCT imaging, femurs were decalcified in 20% EDTA for 4 days at 4°C. Decalcified femurs were processed into paraffin, embedded, and sectioned through the infectious nidus and bone marrow cavity at 4 μm thickness with a Leica RM2255 microtome. Sections were stained with hematoxylin and eosin (H&E). A Leica SCN400 Slide Scanner was used to scan stained femur sections at 20X, and images were uploaded to and analyzed within the Digital Slide Archive (Vanderbilt University Medical Center).

Transposon sequencing analysis of experimental osteomyelitis

USA300 LAC transposon library aliquots were obtained and expanded in 10 mL BHI in 50 mL Erlenmeyer flasks loosely covered with foil for 6 hrs at 37°C with shaking at 180 rpm.[170,219] The expanded library was collected by centrifugation, aliquoted for individual experiments, and thawed on ice as needed, as previously described.[219] Briefly, library aliquots were centrifuged at 200 x g for 8 min at 4°C and resuspended in cold, sterile PBS to achieve an inoculum concentration of ~$2.5x10^9$ CFU/ml. 2 μl of inoculum was delivered (final concentration of ~$5x10^6$ CFU) via intraosseous injection into the femurs of C57BL/6J male mice treated with vehicle or STZ, as described above. Mice were sacrificed at day 4 based on

prior studies.[2] Femurs were homogenized in 500 µl of cold, sterile PBS. 150 µl of bone homogenate from two mice were pooled in 4.7 mL BHI in 50 mL Erlenmeyer flasks loosely covered with foil for a 2 hr outgrowth step at 37°C with shaking at 180 rpm. Following outgrowth, host debris was allowed to settle to the bottom of the culture, and the top fraction was transferred to a new conical on ice. The top fraction was pelleted at 8000 x g for 8 min at 4°C, resuspended in an equal volume of 20% glycerol in BHI, and stored at -80°C. In parallel, 2 µl of prepared inoculum was inoculated into 50 mL of BHI in a 250 mL Erlenmeyer flask to serve as an *in vitro* comparator. After 24 hrs of growth at 37°C with shaking at 180 rpm and covered loosely with foil, the cultures were pelleted at 8000 x g for 8 min at 4°C, supernatant was discarded, and samples were stored at -80°C.

Library preparation and analysis of transposon sequencing

Genomic DNA was isolated with a phenol:chloroform:isoamyl alcohol protocol as described previously.[219] The DNA was then sheared to ~350 bp by sonication using a Covaris LE220 instrument. Libraries were prepared for sequencing with the homopolymer tail-mediated ligation PCR technique.[220] Terminal deoxytransferase was used to generate a poly(C)-tailed sequence on the 3' end of the DNA fragments. The transposon junctions were amplified with two rounds of nested PCR and multiplexed with 8 bp indexing primers. The indexed DNA fragments were sequenced on an Illumina Hi-Seq 2500 (Tufts University Core Facility). Reads were trimmed, filtered for quality, and mapped to *S. aureus* FPR3757 accession number NC007793. A Dval score was assigned to each gene based on the number of reads within a given gene in a sample divided by the predicted number of reads for the gene considering its size and total sequencing reads for the given sample. Genes with a Dval between 0.1 and 0.01 were considered compromised in each condition, and genes with a Dval of ≤0.01 were considered essential.

Comparative *S. aureus* growth analysis *in vitro* in different concentrations of glucose

Overnight cultures of WT and mutant strains were washed in PBS and back diluted 1:1000 into 10 mL TSB (250 mg/dl glucose) with and without an additional 500 mg/dl glucose in 50 mL Erlenmeyer flasks. *ureB*::Tn growth curves included TSB (250 mg/dl glucose) with an additional 500 mg/dl glucose with and without the addition of 10 mM urea. For some experiments, TSB was adjusted to a pH of 4.5, 5.5, 6.5, or 7.5 with HCl and NaOH. Cultures were grown at 37°C with shaking at 180 rpm either loosely covered with foil (aerobic) or plugged with a rubber stopper (microaerobic). Viable CFU were measured by serial diluting cultures and plating on TSA at the indicated timepoints. Growth was reported as Log_{10}CFU/mL compared to CFU enumerated at 0 hrs. pH was measured over the course of the experiment with pH test strips (FisherScientific 13-640-516).

Comparative *S. aureus* growth analysis *in vitro* at various pHs for OD600 analysis

Overnight cultures of WT and mutant strains were washed in PBS and back diluted 1:1000 into TSB standardized to various pHs with HCl and NaOH. Cultures were grown in 200 µl volumes in triplicate in 96 well plates. Cultures were grown at 37°C in a BioTek Synergy plate reader with fast shaking. OD600 was measured every 15 min for 24 hrs. Growth was reported as OD600 compared to OD600 enumerated at 0 hrs.

Comparative *S. aureus* growth analysis *in vitro* at various pHs for CFU analysis

Overnight cultures of WT and mutant strains were washed in PBS and back diluted 1:1000 into 10 mL TSB standardized to various pHs with HCl and NaOH in 50 mL Erlenmeyer flasks. Cultures were grown at 37°C with shaking at 180 rpm aerobically, loosely covered with foil. Viable CFU were measured by serial diluting cultures and plating on TSA at the indicated timepoints. Growth was reported as Log_{10}CFU/mL compared to CFU enumerated at 0 hrs. pH was measured at 0 and 5 days with pH test strips (FisherScientific 13-640-516) to ensure maintained pH.

Biofilm assay

Single donor human plasma (Innovative Research) was diluted in 0.05 M carbonate-bicarbonate buffer pH 9.6 to 20% v/v. 96-well plates were coated with solution and incubated at 4°C overnight. Bacterial cultures were grown overnight and standardized to an OD600 of 0.05 in fresh TSB -dextrose with various concentrations of glucose with or without 10 mM urea. Plates were incubated at 37°C, static for various times. Non-adherent cells were removed and wells were washed prior to fixation with methanol. Adherent biomass was stained with crystal violet and eluted in methanol. Cultures were diluted to fall within range of detection and measured with OD590.

Whole bone marrow isolation and macrophage enrichment

Bone marrow was isolated from C57BL/6J 8 to 12 week old male mice by flushing femurs with MEM-α. All experiments were performed with mice of the same age. Cells were centrifuged at 1500 rpm for 5 min and resuspended in ammonium-chloride-potassium buffer for 10 min to lyse red blood cells. PBS was added to deactivate lysis, and cells were centrifuged and resuspended in MEM-α with 1X Penicillin-Streptomycin and 10% FBS (complete media) to be counted. Cells from hyperglycemic mice were immediately plated for gentamicin protection assays, and other cells were frozen in 10% dimethyl sulfoxide (DMSO) in FBS in liquid nitrogen. Frozen cells were thawed rapidly at 37°C and washed in MEM-α to remove DMSO. Fresh and thawed cells were seeded at 8 million cells per 10 cm tissue culture treated dish in complete media with CMG14-12 supernatant at 1:10 vol/vol as a source of M-CSF. Cells were cultured for 4 days before plating at 50,000 cells/well in 96-well plates in complete media with CMG14-12 supernatant containing M-CSF at 1:40 vol/vol to enrich for BMMs.

Gentamicin assay

After 3 days of culture in 96 well plates (see above for bone marrow isolation and BMM enrichment), BMM cell media was switched to complete media with CMG14-12 supernatant

as a source of M-CSF at 1:40 vol/vol or complete media with CMG14-12 supernatant at 1:40 vol/vol with 30 mM (540 mg/dl) glucose.[187,188] Two days later, cells were washed with PBS and unsupplemented serum-free MEM-α was added. *S. aureus* strains were adjusted to a concentration of $5x10^8$ CFU/mL in sterile PBS and added to the BMMs 2 hrs after the media change. BMMs were infected with *S. aureus* at a multiplicity of infection (MOI) of 100. PBS alone was added to control wells as a mock-infection. Plates were centrifuged at 1000 rpm for 1 min to ensure bacteria and BMMs came into contact. Cells were incubated for 1 hr at 37°C for bacterial internalization. Media were removed and cells were washed with PBS before adding MEM-α supplemented 100 μg/mL gentamicin and returning the plate to incubate. After 1 hr, BMMs were lysed with 0.1% Triton-X to serial dilute cultures and enumerate internalized CFU for a 2 hr time point. For a 24 hr time point, cells were switched to MEM-α supplemented 25 μg/mL gentamicin and lysed with Triton-X 22 hrs later to serial dilute and enumerate internalized CFU.

Modulation of neutrophils through anti-Ly6G monoclonal antibody injection

All animal experiments were reviewed and approved by the Institutional ACUC at Vanderbilt University Medical Center and performed in accordance with NIH guidelines, the Animal Welfare Act, and US Federal law. Six - eight week female C57BL/6J mice were obtained from Jackson Laboratories (stock #000664). Osteomyelitis was induced with $1x10^6$ CFU WT *S. aureus* in 2 μl via intraosseous injection into the femurs, as previously reported.[3] Mice were intraperitoneally injected on days -3, 0, 4, 7, and 10 post-infection with 200 μL of isotype control antibody (rat IgG2a clone 2A3) or anti-Ly6G (clone 1A8) monoclonal antibody (BioXcell, West Lebanon, NH) to interrupt neutrophil function. Mice were weighed daily and monitored for disease progression. At various days post-infection, mice were sacrificed, and the infected femurs were either homogenized for CFU enumeration or fixed for micro-computed tomography (μCT) (see below). For CFU enumeration, infected femur was

homogenized in Cell Lytic buffer (Sigma) and plated on TSA. Limits of detection based on volume of homogenate plated were 49 CFU per femur.

Graphical and statistical analysis

Statistical analyses were performed with Prism 9.4.1 (GraphPad Software). Data were checked for normality prior to statistical analysis. In comparisons of two groups, including the comparisons made for CFU burdens and μCT parameters, Mann-Whitney tests were used. To assess the importance of genes for *S. aureus* survival over time *in vitro*, two-way ANOVAs with post hoc Dunnett's multiple comparisons tests were used to compare the influence of the genotype at each time point. Two-way ANOVAs with post hoc Dunnett's multiple comparisons tests were also used to compare the percent weight of animals infected with different *S. aureus* strains (three or more) over 4 or 14 days. Multiple paired t-tests were used to compare the percent weight of animals infected with WT *S. aureus* in two different murine conditions over 4 or 14 days. To measure changes in *S. aureus* survival *in vivo* in experiments with 3 or more bacterial strains, one-way ANOVAs with Kruskal-Wallis and Dunn's multiple comparisons were used due to the non-Gaussian distribution of the data. Changes in *S. aureus* bacterial burden at day 14 in vehicle-treated, STZ-treated not hyperglycemic, and STZ-treated hyperglycemic mice were compared with a one-way ANOVA and Tukey's multiple comparisons test. CFU burdens and neutrophil counts in *in vivo* neutrophil modulation studies with isotype and anti-Ly6G treatment were compared within each time point with multiple Student's t-tests corrected for multiple comparisons.

Coauthor contributions

All experiments were conceptualized and designed by Dr. James Cassat and me. Dr. Nathan Klopfenstein assisted with experimental design for hyperglycemia *in vivo* studies. Dr. Kara Eichelberger assisted with *ureB*::Tn *in vivo* osteomyelitis experiments. Dr. James Cassat

assisted with all other *in vivo* osteomyelitis experiments. Sasi Uppuganti and the Vanderbilt University Institute of Imaging Sciences (VUIIS) assisted with μCT imaging, and Dr. Eric Skaar (Vanderbilt University) provided Newman *sodM*::erm and *sodA*::tet strains. Dr. Anthony Richardson (University of Pittsburg) provided the TnSeq library, and the Tufts University Core Facility – Genomics Core for sequencing the transposon library samples. Dr. Erin Green (Vanderbilt University), Dr. Albert Tai (Tufts University), and Gloria Lam (Tufts University) assisted with the TnSeq data analysis. Dr. Sun Peck and Joshua Johnson performed femur sectioning and histological staining of tissue. I conducted all other experiments.

CHAPTER IV. FUTURE DIRECTIONS

Introduction

This dissertation describes our investigation into the metabolic and virulence mechanisms that contribute to *S. aureus* fitness during osteomyelitis in the presence and absence of the common comorbid metabolic condition of hyperglycemia. In Chapter II, we discuss our identification of a putative nutrient transporter, PheP, as an important determinant for *S. aureus* fitness in both osteomyelitis and intravenous infection in euglycemic conditions. We highlight efforts to understand the primary substrate transported by PheP and the conditions in which this predicted permease is used. In Chapter III, we leveraged a murine model of osteomyelitis with comorbid hyperglycemia. Using this model, we discovered that hyperglycemia exacerbates osteomyelitis disease severity compared to vehicle-treated euglycemic osteomyelitis-infected control mice. Furthermore, we identified virulence factors that contribute to *S. aureus* survival during osteomyelitis infection in a hyperglycemic host. Although these studies revealed new scientific discoveries related to *S. aureus* fitness during osteomyelitis, extensive investigation into the contribution of PheP to *S. aureus* virulence and the host-pathogen interface during hyperglycemia is required to gain a more comprehensive understanding of *S. aureus* virulence during osteomyelitis.

Chapter II remaining questions and future directions

Bacterial transporters are important for survival and can become critical or dispensable based on the nutrient milieu, innate immune cell-derived stress, and other environmental factors. Our research indicates that PheP is important for *S. aureus* survival during both osteomyelitis and disseminated infection in mice. Based on the homology of *pheP* with other amino acid permease genes, it is predicted that PheP is a transmembrane protein involved in

transporting lysine, gamma-aminobutyric acid (GABA), or proline. Further research is required to identify if PheP functions as a transporter as well as the context that this this membrane-spanning protein is used. Areas of future research should include the following: 1) investigate the transcriptome implications of knocking out *S. aureus pheP*, 2) identify the substrate imported or exported by PheP and the metabolic fate of the substrate, 3) investigate redundancy between PheP and other metabolic pathways and regulation of *pheP in vitro*, 4) further test the role of PheP in bacterial intracellular survival, and 5) examine the role of additional virulence factors involved in *S. aureus* survival during osteomyelitis infection.

Investigate the transcriptome implications of knocking out *S. aureus pheP*

Thus far, our efforts to identify the substrate transported by PheP and the nutritional environment that necessitates this transporter have been inconclusive. To comprehensively evaluate the implications of mutating *pheP*, RNA sequencing (RNA-Seq) should be conducted to compare WT and *pheP* mutant *S. aureus* gene regulation in chemically defined media during the lag phase of *pheP* mutant growth (based on findings in **Fig. 7**). By comparing the transcriptome of WT and a *pheP* mutant, we may reveal the downstream changes in metabolism that occur in the absence of the substrate transported by PheP. The transcription of genes involved in transport and biosynthesis of amino acids influenced by PheP can also be quantified with quantitative real-time polymerase chain reaction (RT-qPCR), although this approach requires pre-selection of targeted genes. These studies may reveal a compensatory metabolism pathway that facilitates *pheP* mutant survival *in vitro* but is incapable of functioning within infected tissue.

Identify the substrate imported or exported by PheP and the metabolic fate of the substrate

Based on homology analysis, PheP is predicted to transport phenylalanine, GABA, lysine, or proline. Additionally, Biolog Phenotype MicroArray analysis revealed reduced *pheP*

mutant growth trends in the presence of compounds associated with proline, glutamine, glutamate, and succinate (**Appendix A**). Due to the shared metabolic pathways that many of these amino acids contribute to, identifying the fate of these amino acids may reveal the function of PheP. Growth of WT and *pheP* mutant *S. aureus* in the presence of isotopically labeled metabolites paired with gas-chromatography mass spectrometry (GCMS) could discern which amino acids are imported by PheP. We propose purchasing isotope labeled phenylalanine, proline, lysine, glutamate, glutamine, and succinate and adding each labeled substrate to *S. aureus* growth media, individually. *S. aureus* can then be pelleted, prepared, and processed for GCMS. The fate of each of these substrates may reveal 1) the physiological role of the substrates, 2) the ability of *S. aureus* to run the complete GABA shunt pathway, and 3) differential uptake/incorporation of amino acids between WT and *pheP* mutant *S. aureus*. Additionally, to determine if PheP has a role in importing amino acids, the media composition can be analyzed with mass spectrometry (MS) before and after growth of WT and *pheP* mutant *S. aureus*. Comparing the total media composition between WT and *pheP* growth media could reveal differences in the uptake of nutrients.

Growth analyses in toxic amino acid derivatives can be conducted with WT and *pheP* mutant *S. aureus* as an alternative approach to mapping labeled metabolites onto metabolic networks. Preliminary studies have revealed few differences in growth between WT and *pheP* mutant *S. aureus* in the presence of toxic proline and lysine amino acid analogs (**Fig. 10** and data not shown). However, this approach was successful for identifying GabP as a proline transporter in *Bacillus subtilis*.[221] Additional toxic analogs and concentrations of compounds could further reveal selective inhibition of WT compared to *pheP* mutant *S. aureus.*

Investigate redundancy between PheP and other metabolic pathways and regulation of *pheP in vitro*

Based on predicted homology between PheP and other nutrient transporters/metabolic enzymes, we created a panel of double mutants with *pheP*::kan and transposon mutants *opuD*::Tn, *lysA*::Tn, *putP*::Tn, *gltS*::Tn, SAUSA300_1225::Tn, SAUSA300_1286::Tn, and *codY*::Tn. In unbuffered RPMI at a single time point, there were no significant differences in growth between WT, *pheP*::kan, and any of the *pheP*::kan transposon double mutants (**Fig. 11**). Additional studies are required to investigate the growth of these single, double, and triple mutants in additional media conditions without abundant branched chain amino acids. *pheP* is predicted to be regulated by CodY, which represses genes in the presence of branched chain amino acids. Therefore, we do not anticipate PheP to be essential for *S. aureus* survival in the presence of branched chain amino acids. It is important to further evaluate the ability of *pheP*::kan double and triple mutant strains to grow in the absence of various amino acids.

Further test the role of PheP in bacterial intracellular survival

A prior publication reported that PheP is important for *S. aureus* survival in carbon- and oxygen-limited conditions.[133] However, the implications of these findings for *S. aureus* survival *in vivo* are unknown. While we did not observe differences in intracellular survival between WT and *pheP* mutant *S. aureus*, this work should be repeated in microaerobic or anaerobic conditions to more closely model conditions in prior work. Additionally, it would be beneficial to limit and alter carbon source availability during WT and *pheP* mutant *S. aureus* growth and in gentamicin protection assays in bone marrow-derived macrophages (BMMs). To ensure that gentamicin kills WT and *pheP* mutant *S. aureus* at the same rate, survival curves should also be carried out in various concentrations of gentamicin over time. These studies may reveal a role for PheP in promoting *S. aureus* intracellular invasion or survival in nutrient/oxygen limited conditions.

Examine the role of additional virulence factors in *S. aureus* survival during osteomyelitis infection

While the studies in Chapter II primarily highlight work investigating the role of PheP in *S. aureus* survival, additional virulence factors were also identified as essential for *S. aureus* growth and persistence during osteomyelitis with transposon sequencing (TnSeq). The gene encoding thermonuclease (*nuc*) was an additional gene identified as essential for *S. aureus* survival in an *in vivo*. Nuc is required for neutrophil evasion and has been implicated in biofilm dispersal.[141,222] Models of both pneumonia and peritonitis disease models have previously characterized the role of Nuc as a *S. aureus* virulence factor.[223,224] However, mutation of *nuc* did not influence *S. aureus* survival in osteomyelitis at day 14 post-infection. Interestingly, the mice infected with *nuc* mutant strain of *S. aureus* exhibited greater percent weight increases compared to WT *S. aureus* infected mice. The increased animal weight recovery could be due to differences in bacterial dissemination or changes in infection kinetics, which should be further explored. Future directions should include a time course of infections with WT and *nuc* mutant *S. aureus* to assess infection kinetics and colony forming unit (CFU) analysis at day 14 post-infection with a lower initial inoculum of bacteria ($1x10^5$ CFU). Due to the role of Nuc in promoting *S. aureus* biofilm dispersal, bacteria within the kidneys, liver, and heart should be enumerated to identify changes in dissemination between WT and *nuc* mutant *S. aureus*. The *S. aureus* genome also encodes a second nuclease, *nuc2*.[143] Nuc and Nuc2 have similar biochemical properties, although Nuc is secreted and Nuc2 is an extracellular surface-attached protein.[143] The similar properties of Nuc and Nuc2 may enable Nuc2 to compensate for the loss of *nuc* in the *nuc*::Tn *S. aureus* strain. Future studies could measure the survival of a *nuc*/*nuc2* double mutant *in vivo* during osteomyelitis compared to WT *S. aureus* to identify the role of total thermonuclease activity for *S. aureus* survival.

Chapter III remaining questions and future directions

Individuals with acute and chronic hyperglycemia are at an elevated risk for developing *S. aureus* infections.[167] Furthermore, patients who develop *S. aureus* infections and have comorbid hyperglycemia receive poor prognoses and experience worse infection outcomes.[99] In this work, we observed increases in bacterial survival within bone and greater dissemination to other organs during osteomyelitis in a comorbid hyperglycemic host. We also observed greater infection-induced bone loss in the setting of hyperglycemic osteomyelitis compared to vehicle-treated infected mice. Furthermore, we identified and validated the importance of *S. aureus* superoxide dismutase A (SodA) in promoting bacterial survival *in vitro* in high glucose and *in vivo* in the context of hyperglycemia. Further research is required to uncover the host mechanisms that influence the role of *S. aureus sodA in vivo* during hyperglycemia. Areas of future research should include the following: 1) assess disease pathogenesis during hyperglycemia with additional models of infection, 2) investigate the impact of hyperglycemia on *S. aureus* antibiotic failure and tolerance during osteomyelitis infection, 3) evaluate the role of *S. aureus* glucose metabolism on increased bacterial virulence, 4) identify the mechanism by which of SodA contributes to *S. aureus* survival in high glucose, 5) quantify changes in reactive oxygen species (ROS) during hyperglycemic infection, and 6) investigate metabolite abundance in staphylococcal abscess communities in bone during hyperglycemia.

Assess disease pathogenesis during hyperglycemia with additional models of infection

Chapter III primarily focused on assessing the influence of hyperglycemia on infection dynamics using a post-traumatic murine model of osteomyelitis infection. The post-traumatic osteomyelitis model serves as a paradigm for fracture-related infection and allows us to study the dramatic changes in bone physiology during osteomyelitis. However, this model of infection does not recapitulate the pathophysiology of the most common infections experienced by individuals with chronic hyperglycemia. The direct inoculation of bacteria into the

intermedullary canal of the femur imperfectly models contiguous wound spread that occurs from skin and soft tissue infections to the bone from diabetic ulcers.

Osteomyelitis infections in individuals with chronic hyperglycemia commonly originate from soft tissue infections that spread to the bone.[168] Chronic wounds frequently present on the feet and progress to the bone cortex, followed by the marrow.[168] To most closely model contiguous wound spread to bone, a hind paw model of infection should be used. Prior work highlights the feasibility of studying hind paw infections in NOD mice.[75] However, the influence of streptozotocin (STZ)-induced hyperglycemia on severity of hind paw infection has not been studied. To reveal the extent to which hyperglycemia influences contiguous wound spread to the bone, the *S. aureus* burden in the bone of the infected hind paws can be quantified. Additionally, to identify the contributions of SodA and superoxide dismutase M (SodM) in *S. aureus* contiguous spread, hind paw infections could be infected with WT, *sodA*::tet, *sodM*::erm, *sodA*::tet *sodM*::erm mutant strains. The recovered bacteria can be quantified from both the hind paw soft tissues and the underlying bone to identify if superoxide dismutases (SODs) are important for *S. aureus* survival at the site of infection or for dissemination to the bone. These experiments could reveal genes that drive *S. aureus* pathogenesis and dissemination to the bone from contiguous wound spread during hyperglycemia.

The *S. aureus* strain used to assess the influence of hyperglycemia on infection outcomes was AH1263. It is important to test the fitness of clinical isolates from wounds of diabetes patients using these same models to compare previous findings to clinically relevant strains of *S. aureus*. A clinical analysis of *S. aureus* strains isolated from diabetic foot wounds found variations in copy number and *agr* type between isolates and greater expression of *S. aureus agr*-II gene expression in the presence of co-infecting *Pseudomonas aeruginosa*.[225]

Therefore, expansion of studies to include clinical isolates from diabetes patients is important to assess *S. aureus* strains that most frequently effect individuals with hyperglycemia.

The one model chosen to induce hyperglycemia (STZ treatment) limits the scope in which the conclusions can be drawn from these studies. Limitations of using STZ to induce hyperglycemia include off-target toxicity and an absence of an autoimmune response. Treatment with insulin to reverse STZ-induced hyperglycemia is an important future direction to further validate that conclusions drawn from Chapter III of this work are a result of the hyperglycemia induced by STZ, as opposed to off-target cytotoxicity. Additional murine models can also be used to examine the influence of hyperglycemia on infection severity and fitness of *S. aureus* transposon mutants to discern which conclusions are generalizable across models of type 1 diabetes. For example, nonobese diabetic (NOD) mice are a genetic strain of mice that produce auto-reactive antibodies that target pancreatic islet cells, similarly resulting in beta cell death.[44] Furthermore, rat insulin promoter-diphtheria toxin (RIP-DTR) mice could be used to selectively deplete beta cells via introduction of diphtheria toxin.[43] Type 2 models of diabetes, such as high fat diet fed mice, would provide an obese murine model comparison to assess the extent to which our findings can be extrapolated to other metabolic diseases.[57] More information on murine models of diabetes and their limitations can be found in Chapter I and should be considered as additional models to validate our findings using a murine model of STZ-induced hyperglycemia.

While *S. aureus* is the most frequently isolated bacterium from osteomyelitis during hyperglycemia, upwards of 40% of these infections are polymicrobial.[226] Work in our laboratory and from other groups has revealed interactions among different bacterial species and across kingdoms.[225,227,228] For example, *S. aureus* Agr activation is altered in the presence of other species, such as *Pseudomonas aeruginosa* and *Candida albicans*.[225,229] Therefore, to test the influence of polymicrobial interactions on osteomyelitis infection dynamics during

hyperglycemia, co-infections and co-interactions can be further investigated. Species commonly co-isolated with *S. aureus* from osteomyelitis in diabetes patients include *Streptococcus* species, *Enterobacteriaceae*, *Pseudomoas aeruginosa*, *Prevotella* species, and *Bacteriodes fragilis*.[230] Bone destruction, bacterial survival, and dissemination should be assessed during co-infections with each of these species. Agr is important for increased *S. aureus* virulence during hyperglycemic infection.[74] A *S. aureus* RNAIII Agr fluorescent reporter can be used to measure changes in *S. aureus* quorum sensing and virulence in the presence of additional species *in vitro* and *in vivo* to monitor how *S. aureus* virulence changes in the presence of additional species.

Investigate the impact of hyperglycemia on *S. aureus* antibiotic failure and tolerance during osteomyelitis infection

The formation of abscesses, sequestra, and biofilms can promote antibiotic failure by physically walling off the bacteria and preventing penetration of antibiotics.[14] Intracellular survival of *S. aureus* can also provide reservoirs of bacteria that are protected from antibiotics.[14] Patients with hyperglycemia have an increased risk for developing infections, including infections with multi-drug resistant strains of bacteria.[11,231,232] However, the extent to which antibiotic failure influences treatment recalcitrance and infection persistence during hyperglycemia is unknown. We hypothesize that compromised vasculature, poor wound healing, and increased bacterial biomass during hyperglycemic infection (as described in Chapter I) may impede antibiotic penetrance into the infected tissue, increasing rates of antibiotic failure.[92–94]

Antibiotic tolerance occurs when bacteria can survive in the presence of lethal doses of antibiotics, typically due to altered bacterial growth kinetics.[14] Ongoing work in our laboratory seeks to identify bacterial factors that contribute to antibiotic tolerance, which develops rapidly during osteomyelitis in the setting of delayed treatment with vancomycin. The following

experiments could further reveal the influence of hyperglycemia on the progression of antibiotic tolerance. 1) To assess the time at which antibiotic tolerance is established, a time course of delayed vancomycin treatment administered at 0, 2, 4, 6, 8, and 24 hrs post-infection can be completed for CFU analysis and compared between hyperglycemic and euglycemic mice. 2) To interrogate the ability of vancomycin to reach the site of infection and penetrate staphylococcal abscesses, hyperglycemic and euglycemic mice should be infected with a strain of *S. aureus* with a vancomycin-responsive fluorescent reporter paired with a constitutive fluorescent reporter to normalize to the number of bacteria. Femurs can then be cryosectioned and imaged with confocal fluorescence microscopy to visualize the localization of the bacteria and vancomycin penetration. This study could also reveal antibiotic-protected niches within the bone. 3) To evaluate differences in *S. aureus* intracellular invasion during antibiotic treatment in the presence of high glucose, BMMs should be cultured in various glucose conditions and exposed to gentamicin prior to lysing the host cells and enumerating *S. aureus* CFU. 4) To discern which *S. aureus* genes differentially influence fitness during vancomycin treatment during osteomyelitis in a hyperglycemic host compared to euglycemic mice, TnSeq can be conducted to sequence and compare *S. aureus* transposon mutant fitness. These experiments will collectively reveal the influence of hyperglycemia on *S. aureus* vancomycin tolerance.

Evaluate the role of *S. aureus* glucose metabolism on increased bacterial virulence

In Chapter III, we observed increased *S. aureus* survival and dissemination during osteomyelitis in a hyperglycemic murine host compared to euglycemic infection. However, the mechanism by which *S. aureus* burdens increase during hyperglycemia in osteomyelitis remain unknown. To assess the contribution of *S. aureus* glucose metabolism to the increased bacterial survival during hyperglycemia, glucose transport into *S. aureus* can be prevented. Prior work identified four transporters (GlcA, GlcB, GlcC, and GlcU) used by *S. aureus* to import

glucose.[218] By mutating the *glcA*, *glcB*, *glcC*, and *glcU* genes and repeating osteomyelitis infections in a hyperglycemic host, we could reveal the role of glucose import on *S. aureus* survival and virulence during osteomyelitis. Additional studies with *S. aureus* mutants that are incapable of performing glycolysis could further reveal the contribution of bacterial glucose metabolism to exacerbated osteomyelitis infection severity.

Identify the mechanism by which of SodA contributes to *S. aureus* survival in high glucose

SodA has a known role in detoxifying ROS and was identified as important for *S. aureus* survival in low pH in a prior study by Clements et al.[125] In Chapter III we further revealed the importance of SodA for *S. aureus* survival *in vitro* in high glucose, in acidic pH conditions, and *in vivo* during osteomyelitis in a hyperglycemic host. To build upon the findings in this thesis, a *sodA* fluorescent transcriptional reporter can be used to identify changes in expression of *sodA* in the presence of high glucose concentrations *in vitro* and *in vivo*. Additional studies should also examine the mechanism by which SodA promotes *S. aureus* survival and/or virulence during osteomyelitis. Mutation of *sodA* may render *S. aureus* less fit to survive in the presence of high glucose due to (a) the hyperosmotic media, (b) increased intracellular ROS generation from carbon overflow metabolism, and/or (c) acidifying pH. To test the influence of osmolarity changes without added glucose, WT and *sodA* mutant *S. aureus* can be grown in an equimolar mannitol solution. The intracellular ROS generated by *S. aureus* growth in high glucose can be measured with CellROX, a green fluorescent dye that can be quantified with flow cytometry.[233] The CellROX dye can be normalized to a constitutive fluorescent reporter chromosomally integrated into the *S. aureus* genome to control for differences in bacterial growth. Finally, to assess the influence of pH on *sodA* mutant *S. aureus* growth, WT and *sodA* should be grown in high glucose in a chemostat that is non-permissive for pH deviation. These studies will further reveal the mechanism by which SodA promotes *S. aureus* survival in the condition of elevated glucose.

Quantify changes in ROS during hyperglycemic infection

In addition to further investigating the role of SodA *in vitro*, *in vivo* analysis of ROS production should be assessed and compared between euglycemic and hyperglycemic murine femurs infected with WT and *sodA* mutant *S. aureus*. Quantification of ROS *in vivo* is difficult, as ROS itself is unstable and transient.[234] Lipid peroxidation products and protein carbonyls are more stable artifacts of ROS-induced oxidative damage and can be measured *in situ* with mass spectrometry.[234] F_2-isoprostanes (F_2-isoPs) are common lipid oxidation products that serve as lipid peroxidation biomarkers and have previously been successfully detected with liquid-chromatography mass spectrometry (LC-MS/MS).[235,236] Protein carbonyls are formed from oxidation of specific amino acid residues to carbonyl groups and through reaction of aldehydes with nucleophilic sites on proteins. Similar to lipid peroxidation products, protein carbonyls are best quantified with LC-MS/MS.[237,238] Both lipid peroxidation and protein carbonyl products can also be detected with commercial enzyme-linked immunoassays (ELISAs), although with decreased precision and sensitivity.[235,236,239] By combining optimized bone tissue cryosectioning with liquid extraction surface analysis (microLESA) mass spectrometry, the localization and abundance of oxidative products that accumulate in the presence of ROS in infected hyperglycemic bone tissue could be further clarified.[240]

Investigate metabolite abundance in staphylococcal absence communities in bone

Recent advances by Good et al. dramatically improved the ability to spatially analyze infected murine bone tissue without fixation or decalcification.[240] Matrix-assisted laser desorption/ionization (MALDI) imaging mass spectrometry (IMS) can be used to spatially resolve chemical information in sections of *S. aureus* infected euglycemic and hyperglycemic murine femurs. Preliminary studies in euglycemic mice reveal differentially abundant metabolites in mock and *S. aureus* infected femurs. For example, carnitine was abundant in and around the staphylococcal abscess community with less of the metabolite observed in other

areas of the infected femur or mock-infected bone (**Fig. 41**). *S. aureus* contains a carnitine transporter system, OpuCA, which has been implicated in *S. aureus* osmotic stress tolerance.[241] However, additional studies are required to understand the implications of carnitine abundance in/around the staphylococcal abscess community during euglycemic infection. To identify the influence of carnitine on *S. aureus* survival, growth curves should be conducted with WT and *opuCA* mutant *S. aureus* in hyperosmotic media in the presence and absence of carnitine. Additionally, the influence of carnitine on murine BMM survival and phagocytosis should be explored.

Furthermore, the advanced spatial imaging techniques used to discern abundant metabolites in euglycemic infection can also be applied to hyperglycemic infected tissue. By studying the abundant metabolites and lipids relative to the location of bacteria, we have the opportunity to reveal novel host inflammatory/antimicrobial mechanisms as well as bacterial survival mechanisms during invasive comorbid infection. Due to altered innate immune cell function (described in Chapter I) and enhanced *S. aureus* burden and bone destruction (shown in Chapter III), we hypothesize that lipids and metabolites associated with increased inflammation will localize to the staphylococcal abscess community in mice with comorbid hyperglycemia. To test this hypothesis, hyperglycemic and euglycemic murine femurs should be infected with a constitutively florescent strain of *S. aureus* to localize bacteria. MALDI IMS can be conducted on non-decalcified, unfixed cryosectioned femurs in positive and negative ion mode, revealing the distribution and relative abundance of molecules. Thus far, MALDI IMS has revealed abundant lipids within hyperglycemic vs. euglycemic infected tissue (**Fig. 42**). Future directions include validating the identified lipids and metabolites with homogenization of femur sections followed by LC-MS/MS for fragmentation analysis. MicroLESA can also be used for LC-MS/MS analysis of a defined region of interest to increase the sensitivity and confidence in identifications of less abundant molecules.[242] Additionally,

biologically relevant molecules (i.e. molecules that suggest the formation of protein carbonyls or lipid peroxidation products) should be tested in bacterial growth assays as well as *in vitro* in cell culture assays to identify the influence of these molecules on *S. aureus* virulence, *S. aureus* intracellular survival, *S. aureus* metabolism, and BMM survival.

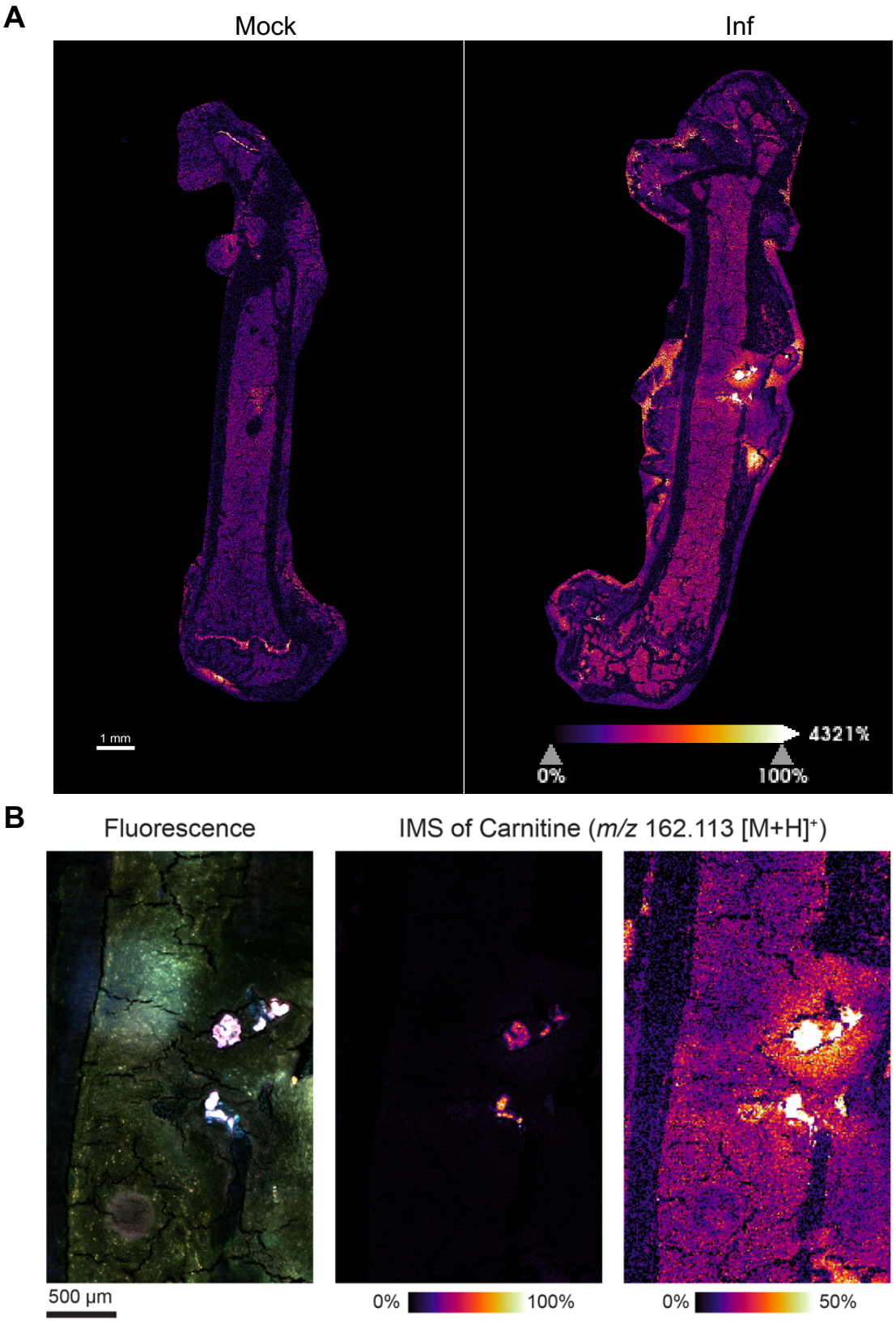
A
Mock
Inf
1 mm
4321%
0%
100%
B
Fluorescence
IMS of Carnitine (m/z 162.113 [M+H]+)
500 µm
0%
100%
0%
50%

Figure 41. Carnitine localizes to the staphylococcal abscess community in *S. aureus* osteomyelitis. Eight-week male mice were infected with either sterile PBS (Mock) or $1x10^6$ CFU of WT *attC*::P*sarA*_mCherry (Inf). Femurs were isolated and flash frozen 14 days post-infection and maintained at -80°C. The samples were embedded in 5% CMC and 10% gelatin and snap frozen. Femurs were cryosectioned at 8 µm thickness with Cryofilm 3C 16UF (SECTION-LAB, Hiroshima, Japan) and mounted on conductive indium tin oxide (ITO)-coated glass slides. α-Cyano-4-hydroxycinnamic acid (CHCA) matrix was sublimed onto samples. (A) 10 µm spatial resolution images were acquired using Bruker timsTOF fleX in positive ion mode. (B) Magnified images of Inf femur were obtained to reveal localization of *S. aureus* (fluorescence) relative to carnitine abundance. Data obtained in collaboration with Christopher Good.

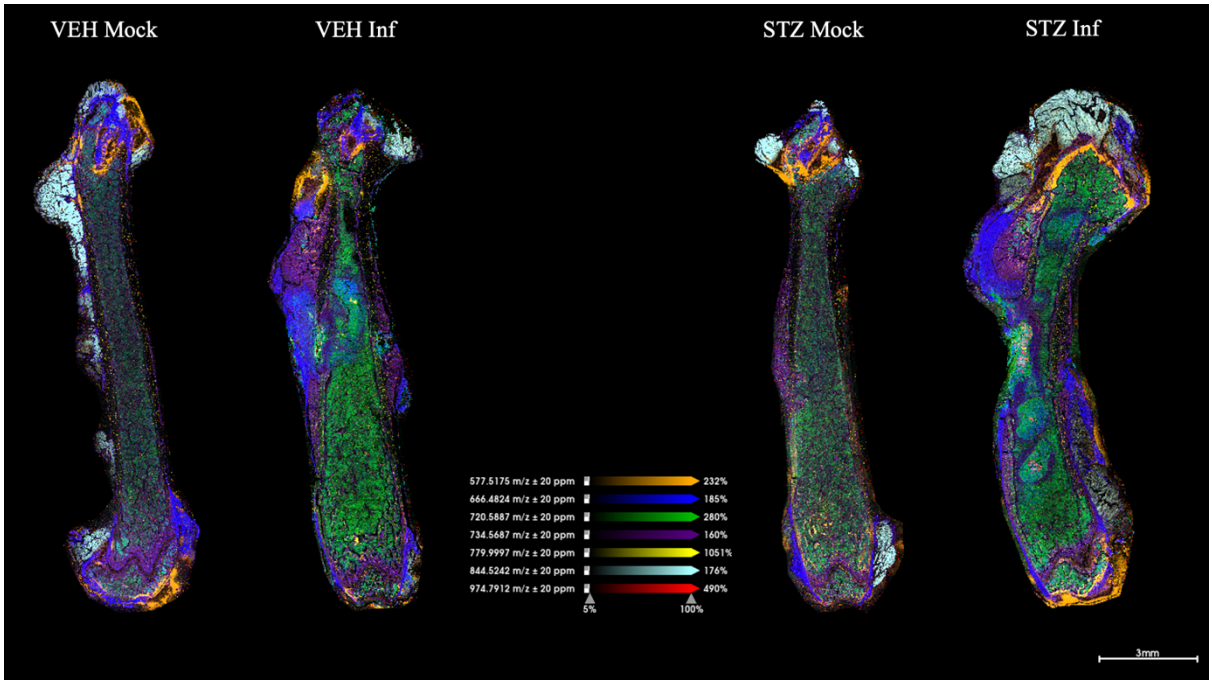

Figure 42. Abundant lipids are detected in distinct bone structures during euglycemia and hyperglycemia in *S. aureus* osteomyelitis. Eight-week old male mice were treated with sodium citrate (VEH) or streptozotocin (STZ) intraperitoneally for 5 days. 10 days after the final injection, mice were infected with either sterile PBS (Mock) or $1x10^6$ CFU of WT *attC*::P*sarA*_mCherry (Inf) 10 days after treatment. Femurs were isolated and flash frozen 14 days post-infection and maintained at -80°C. The samples were embedded in 5% CMC and 10% gelatin and snap frozen. Femurs were cryosectioned at 8 µm thickness with Cryofilm 3C 16UF (SECTION-LAB, Hiroshima, Japan) and mounted on conductive indium tin oxide (ITO)-coated glass slides. 2,5-Dihydroxyacetophenone (DHA) matrix was sublimed onto samples. 10 µm spatial resolution images were acquired using a Bruker timsTOF fleX in positive ion mode. Data obtained in collaboration with Christopher Good.

Concluding remarks

In the work described in this dissertation, we investigated *S. aureus* genes required for survival *in vivo* during invasive infection in euglycemic and hyperglycemic mice. Our findings revealed an important gene with a potential role in *S. aureus* nutrient transport during euglycemic infection. In addition to uncovering changes in bacterial survival and bone homeostasis during infection in a hyperglycemic host, we further revealed genes that contribute to increased *S. aureus* fitness during osteomyelitis in animals with hyperglycemia. This research contributes to an understanding of *S. aureus* adaptations *in vivo* and highlights the importance of further investigation into the intersection of metabolism and virulence during osteomyelitis.

APPENDIX A. PheP Phenotype MicroArray results

Table A1. Biolog assay reveals differences in growth of WT and *pheP S. aureus* in various metabolic conditions at 8 and 24 hrs. Plates 1 and 2 include a single alternative carbon source; plates 3, 6, 7, and 8 include distinct nitrogen sources; plate 4 contains phosphorous and sulfur compounds; plate 5 contains biosynthetic pathway intermediates; and plates 9 and 10 contain altered osmolarity and pH conditions, with all other ingredients necessary for microbial growth included unless otherwise tested. OD590 was recorded for WT and *pheP*::Tn at 0, 8, and 24 hrs in each well and normalized to 0 hrs. *pheP*::Tn growth was normalized to WT from each well. Green indicates greater relative *pheP*::Tn growth, and red indicates greater relative WT growth.

			8 hrs			24 hrs		
Plate	Well	Assay Condition	WT OD590 - t0	*pheP* ::Tn OD590 - t0	(*pheP* -WT)/WT	WT OD590 - t0	*pheP* ::Tn OD590 - t0	(*pheP* -WT)/WT
1	A1	Negative control	0.131	0.109	-0.167938931	0.108	0.095	-0.12037037
1	A10	D-Trehalose	0.64	0.357	-0.4421875	1.197	0.723	-0.395989975
1	A11	D-Mannose	0.679	0.486	-0.284241532	0.955	1.03	0.078534031
1	A12	Dulcitol	0.124	0.144	0.161290323	0.284	0.074	-0.73943662
1	A2	L-arabinose	0.354	0.219	-0.381355932	0.298	0.432	0.44966443
1	A3	N-Acetyl-D-Glucosamine	0.232	0.082	-0.646551724	0.771	0.62	-0.195849546
1	A4	D-Saccharic Acid	0.145	0.087	-0.4	0.411	0.059	-0.856447689
1	A5	Succinic Acid	0.28	0.086	-0.692857143	0.675	0.554	-0.179259259
1	A6	D-Galactose	0.663	0.318	-0.520361991	0.539	0.421	-0.218923933
1	A7	L-Aspartic Acid	0.616	0.176	-0.714285714	0.394	0.238	-0.395939086
1	A8	L-Proline	0.353	0.104	-0.705382436	0.681	0.574	-0.15712188
1	A9	D-Alanine	0.19	0.08	-0.578947368	0.895	0.341	-0.618994413
1	B1	D-Serine	0.058	0.028	-0.517241379	0.116	0.103	-0.112068966
1	B10	Formic Acid	0.327	0.137	-0.581039755	0.844	0.888	0.052132701
1	B11	D-Mannitol	0.688	0.4	-0.418604651	1.158	0.867	-0.251295337
1	B12	L-Glutamic Acid	0.593	0.163	-0.725126476	1.014	0.752	-0.258382643
1	B2	D-Sorbitol	0.386	0.124	-0.678756477	0.37	0.326	-0.118918919
1	B3	Glycerol	0.629	0.391	-0.378378378	1.007	1.075	0.067527309
1	B4	L-Fucose	0.347	0.294	-0.152737752	0.28	0.263	-0.060714286
1	B5	D-Glucuronic Acid	0.198	0.177	-0.106060606	0.183	0.304	0.661202186
1	B6	D-Gluconic Acid	0.642	0.317	-0.50623053	1.157	0.748	-0.353500432
1	B7	D,L-a-Glycerol-Phosphate	0.559	0.107	-0.808586762	0.787	0.625	-0.205844981
1	B8	D-Xylose	0.41	0.202	-0.507317073	0.483	0.55	0.138716356
1	B9	L-Lactic Acid	0.759	0.219	-0.711462451	1.197	1.032	-0.137844612
1	C1	D-Glucose-6-Phosphate	0.828	0.515	-0.378019324	1.063	1.075	0.011288805
1	C10	Maltose	0.708	0.371	-0.475988701	1.363	0.96	-0.295671313
1	C11	D-Melibiose	0.169	0.111	-0.343195266	0.327	0.197	-0.397553517
1	C12	Thymidine	0.453	0.13	-0.713024283	0.852	0.881	0.034037559
1	C2	D-Galactonic Acid-y-Lactone	0.259	0.085	-0.671814672	0.189	0.098	-0.481481481
1	C3	D,L-Malic Acid	0.45	0.128	-0.715555556	0.932	0.884	-0.051502146
1	C4	D-Ribose	0.425	0.198	-0.534117647	0.842	0.56	-0.334916865
1	C5	Tween 20	0.149	0.095	-0.362416107	0.877	0.706	-0.194982896
1	C6	L-Rhamnose	0.36	0.31	-0.138888889	0.302	0.354	0.17218543
1	C7	D-Fructose	0.715	0.482	-0.325874126	1.18	1.151	-0.024576271
1	C8	Acetic Acid	0.747	0.507	-0.321285141	0.903	0.971	0.07530454
1	C9	a-D-Glucose	0.771	0.509	-0.339818418	1.342	1.212	-0.096870343
1	D1	L-Asparagine	0.477	0.121	-0.746331237	0.464	0.636	0.370689655
1	D10	Lactulose	0.222	0.157	-0.292792793	0.633	0.608	-0.039494471
1	D11	Sucrose	0.663	0.409	-0.383107089	1.335	1.228	-0.080149813
1	D12	Uridine	0.703	0.252	-0.641536273	1.08	0.987	-0.086111111
1	D2	D-Aspartic Acid	0.262	0.109	-0.583969466	0.266	0.23	-0.135338346
1	D3	D-Glucosaminic Acid	0.314	0.184	-0.414012739	0.277	0.327	0.180505415
1	D4	1,2-Propanediol	0.168	0.171	0.017857143	0.15	0.277	0.846666667
1	D5	Tween 40	0.129	0.148	0.147286822	0.461	0.55	0.193058568
1	D6	a-Keto-Glucaric Acid	0.583	0.201	-0.655231561	1.242	0.916	-0.262479871
1	D7	a-Keto-Butyric Acid	0.084	0.06	-0.285714286	0.437	0.339	-0.224256293
1	D8	a-Methyl-D-Galactoside	0.23	0.109	-0.526086957	0.171	0.348	1.035087719
1	D9	a-D-Lactose	0.262	0.154	-0.41221374	0.861	0.778	-0.096399535
1	E1	L-gGlutamine	0.482	0.254	-0.473029046	1.195	0.796	-0.333891213
1	E10	Maltotriose	0.733	0.473	-0.354706685	1.189	1.093	-0.080740118
1	E11	2-Deoxy Adenosine	0.15	0.137	-0.086666667	0.362	0.267	-0.262430939
1	E12	Adenosine	0.271	0.143	-0.472324723	0.529	0.895	0.691871456
1	E2	m-Tartaric Acid	0.134	0.089	-0.335820896	0.276	0.206	-0.253623188
1	E3	D-Glucose-1-Phosphate	0.326	0.165	-0.493865031	0.518	0.348	-0.328185328
1	E4	D-Fructose-6-Phosphate	0.872	0.573	-0.342889908	1.168	1.215	0.040239726
1	E5	Tween 80	0.251	0.151	-0.398406375	0.708	0.599	-0.153954802
1	E6	a-Hydroxy Glutaric Acid-y-Lactone	0.143	0.104	-0.272727273	0.159	0.296	0.86163522
1	E7	a-Hydroxy Butyric Acid	0.368	-0.001	-1.002717391	0.729	0.428	-0.412894376
1	E8	a-Methyl-D-Glucoside	0.477	0.221	-0.536687631	1.087	1.136	0.045078197
1	E9	Adonitol	0.259	0.147	-0.432432432	0.378	0.404	0.068783069
1	F1	Glycl-L-Aspartic Acid	0.622	0.137	-0.779742765	1.064	0.883	-0.170112782
1	F10	Glyoxylic Acid	0.312	0.523	0.676282051	0.204	0.359	0.759803922
1	F11	D-Cellobiose	0.457	0.254	-0.444201313	0.438	0.569	0.299086758
1	F12	Inosine	0.883	0.487	-0.448471121	0.986	0.897	-0.090263692
1	F2	Citric Acid	0.149	0.102	-0.315436242	0.221	0.266	0.20361991
1	F3	myo-Inositol	0.249	0.242	-0.02811245	0.319	0.359	0.12539185
1	F4	D-Threonine	0.292	0.039	-0.866438356	0.347	0.181	-0.478386167
1	F5	Fumaric Acid	0.368	0.15	-0.592391304	0.906	0.839	-0.073951435
1	F6	Bromo Succinic Acid	0.299	0.111	-0.628762542	0.658	0.226	-0.656534954
1	F7	Propionic Acid	0.257	0.108	-0.579766537	0.272	0.229	-0.158088235
1	F8	Mucic Acid	0.214	0.235	0.098130841	0.184	0.211	0.14673913
1	F9	Glycolic Acid	0.19	0.01	-0.947368421	0.49	0.189	-0.614285714
1	G1	Glycyl-L-Glutamic Acid	0.726	0.162	-0.776859504	1.269	0.958	-0.245074862
1	G10	Methyl Pyruvate	0.52	0.195	-0.625	0.945	0.934	-0.011640212
1	G11	D-Malic Acid	0.097	0.095	-0.020618557	0.339	0.261	-0.230088496
1	G12	L-Malic Acid	0.498	0.294	-0.409638554	0.911	0.913	0.00219539
1	G2	Tricarballylic Acid	0.168	0.101	-0.398809524	0.186	0.133	-0.284946237
1	G3	L-Serine	0.248	0.144	-0.419354839	0.513	0.415	-0.191033138
1	G4	L-Threonine	0.646	0.386	-0.40247678	0.947	0.918	-0.03062302
1	G5	L-Alanine	0.247	0.124	-0.497975709	0.734	0.424	-0.422343324
1	G6	L-Alanyl-Glycine	0.48	0.115	-0.760416667	1.068	1.004	-0.059925094
1	G7	Acetoacetic Acid	0.933	0.455	-0.512325831	0.917	0.754	-0.177753544
1	G8	N-Acetyl-B-D-Mannosamine	0.596	0.212	-0.644295302	0.96	1.185	0.234375
1	G9	Mono Methyl Succinate	0.423	0.092	-0.78250591	0.573	0.558	-0.02617801
1	H1	Glycyl-L-Proline	0.169	0.112	-0.337278107	0.402	0.797	0.982587065
1	H10	D-Galacturonic Acid	0.392	0.356	-0.091836735	0.321	0.555	0.728971963
1	H11	Phenylethyl-amine	0.228	0.195	-0.144736842	0.357	0.371	0.039215686
1	H12	2-Aminoethanol	0.181	0.024	-0.867403315	0.129	0.03	-0.76744186
1	H2	p-Hydroxy Phenyl Acetic Acid	0.173	0.132	-0.23699422	0.147	0.165	0.12244898
1	H3	m-Hydroxy Phenyl Acetic Acid	0.182	0.071	-0.60989011	0.418	0.089	-0.78708134
1	H4	Tyramine	0.09	0.121	0.344444444	0.036	0.13	2.611111111
1	H5	D-Psicose	0.753	0.527	-0.300132802	0.777	0.855	0.1003861
1	H6	L-Lyxose	0.347	0.181	-0.478386167	0.655	0.333	-0.491603053
1	H7	Glucuronamide	0.312	0.431	0.381410256	0.511	0.407	-0.203522505
1	H8	Pyruvic Acid	0.852	0.275	-0.677230047	1.133	0.968	-0.145631068
1	H9	L-Galacturonic Acid	0.352	0.221	-0.372159091	0.4	0.433	0.0825

			8 hrs			24 hrs		
Plate	Well	Assay Condition	WT OD590 - t0	*pheP* ::Tn OD590 - t0	(*pheP* -WT)/WT	WT OD590 - t0	*pheP* ::Tn OD590 - t0	(*pheP* -WT)/WT
2	A1	Negative control	0.324	0.121	-0.62654321	0.324	0.285	-0.12037037
2	A10	Laminarin	0.214	0.156	-0.271028037	0.221	0.107	-0.515837104
2	A11	Mannan	0.19	0.185	-0.026315789	0.131	0.226	0.72519084
2	A12	Pectin	0.758	0.443	-0.415567282	0.926	0.916	-0.010799136
2	A2	Chondroitin Sulfate C	0.445	0.16	-0.640449438	0.392	0.147	-0.625
2	A3	a-Cyclodextrin	0.047	0.097	1.063829787	0.07	0.092	0.314285714
2	A4	B-Cyclodextrin	0.168	0.09	-0.464285714	0.116	0.079	-0.318965517
2	A5	y-Cyclodextrin	0.164	0.11	-0.329268293	0.107	0.052	-0.514018692
2	A6	Dextrin	0.457	0.253	-0.446389497	0.546	0.395	-0.276556777
2	A7	Gelatin	0.154	0.146	-0.051948052	0.136	0.102	-0.25
2	A8	Glycogen	0.196	0.132	-0.326530612	0.187	0.11	-0.411764706
2	A9	Inulin	0.369	0.259	-0.298102981	0.372	0.245	-0.341397849
2	B1	N-Acetyl-D-Glactosamine	0.244	0.187	-0.233606557	0.273	0.258	-0.054945055
2	B10	i-Erythritol	0.264	0.186	-0.295454545	0.252	0.143	-0.432539683
2	B11	D-Fucose	0.584	0.401	-0.313356164	0.48	0.338	-0.295833333
2	B12	3-0-B-D-Galactopyranosyl-D-Arabinose	0.082	0.089	0.085365854	0.096	0.085	-0.114583333
2	B2	N-Acetyl-Neuraminic Acid	0.224	0.248	0.107142857	0.507	0.324	-0.360946746
2	B3	B-D-Allose	0.156	0.148	-0.051282051	0.267	0.201	-0.247191011
2	B4	Amygdalin	0.2	0.194	-0.03	0.258	0.131	-0.492248062
2	B5	D-Arabinose	0.305	0.287	-0.059016393	0.383	0.464	0.211488251
2	B6	D-Arabitol	0.251	0.185	-0.262948207	0.367	0.227	-0.38147139
2	B7	L-Arabitol	0.165	0.184	0.115151515	0.382	0.162	-0.57591623
2	B8	Arbutin	0.266	0.196	-0.263157895	0.366	0.275	-0.24863388
2	B9	2-Deoxy-D-Ribose	0.225	0.219	-0.026666667	0.4	0.376	-0.06
2	C1	Gentiobiose	0.361	0.284	-0.213296399	0.522	0.416	-0.203065134
2	C10	a-Methyl-D-Mannoside	0.285	0.185	-0.350877193	0.269	0.219	-0.185873606
2	C11	B-Methyl-D-Xyloside	0.33	0.185	-0.439393939	0.235	0.222	-0.055319149
2	C12	Palatinose	0.6	0.345	-0.425	0.776	0.616	-0.206185567
2	C2	L-Glucose	0.353	0.335	-0.050991501	0.498	0.367	-0.263052209
2	C3	Lactitol	0.266	0.133	-0.5	0.36	0.157	-0.563888889
2	C4	D-Melexitose	0.336	0.219	-0.348214286	0.601	0.414	-0.311148087
2	C5	Maltitol	0.372	0.185	-0.502688172	1.025	0.594	-0.420487805
2	C6	a-Methyl-D-Glucoside	0.207	0.148	-0.285024155	0.259	0.238	-0.081081081
2	C7	B-Methyl-D-Galactoside	0.147	0.168	0.142857143	0.258	0.169	-0.34496124
2	C8	3-Methyl Glucose	0.574	0.277	-0.517421603	0.585	0.288	-0.507692308
2	C9	B-Methyl-D-Glucuronic Acid	0.256	0.221	-0.13671875	0.361	0.364	0.008310249
2	D1	D-Raffinose	0.308	0.2	-0.350649351	0.342	0.277	-0.19005848
2	D10	y-Amino Butyric Acid	0.241	0.215	-0.107883817	0.365	0.217	-0.405479452
2	D11	gamma-Amino Valeric Acid	0.235	0.219	-0.068085106	0.289	0.203	-0.297577855
2	D12	Butyric Acid	0.193	0.204	0.056994819	0.5	0.235	-0.53
2	D2	Salicin	0.203	0.116	-0.428571429	0.337	0.22	-0.347181009
2	D3	Sedoheptulosan	0.199	0.183	-0.08040201	0.326	0.264	-0.190184049
2	D4	L-Sorbose	0.314	0.127	-0.595541401	0.339	0.325	-0.041297935
2	D5	Stachyose	0.235	0.193	-0.178723404	0.341	0.276	-0.190615836
2	D6	D-Tagatose	0.512	0.393	-0.232421875	0.52	0.505	-0.028846154
2	D7	Turanose	0.499	0.198	-0.603206413	1.171	0.983	-0.160546541
2	D8	Xylitol	0.195	0.157	-0.194871795	0.277	0.311	0.122743682
2	D9	N-Ascetyl-D-Glucosaminitol	0.307	0.149	-0.51465798	0.433	0.377	-0.129330254
2	E1	Capric Acid	-0.081	-0.066	-0.185185185	0.005	-0.073	-15.6
2	E10	a-Keto-Valeric Acid	0.366	0.173	-0.527322404	0.939	0.614	-0.346112886
2	E11	Itaconic Acid	0.073	0.058	-0.205479452	0.104	0.067	-0.355769231
2	E12	5-Keto-D-Gluconic Acid	0.609	-0.095	-1.155993432	0.558	0.14	-0.749103943
2	E2	Caproic Acid	0.334	0.195	-0.416167665	0.601	0.462	-0.231281198
2	E3	Citraconic Acid	0.238	0.2	-0.159663866	0.359	0.162	-0.548746518
2	E4	Citramalic Acid	0.286	0.215	-0.248251748	0.363	0.229	-0.369146006
2	E5	D-Glucosamine	0.377	0.17	-0.549071618	1.429	0.582	-0.592722183
2	E6	2-Hydroxy Benzoic Acid	0.1	0.054	-0.46	0.297	0.178	-0.400673401
2	E7	4-Hydroxy Benzoic Acid	0.16	0.112	-0.3	0.276	0.18	-0.347826087
2	E8	B-Hydroxy Butryric Acid	0.216	0.154	-0.287037037	0.328	0.149	-0.545731707
2	E9	Glycolic Acid	0.198	0.152	-0.232323232	0.279	0.287	0.028673835
2	F1	D-Lactic Acid Methyl Ester	0.479	0.226	-0.528183716	0.725	0.79	0.089655172
2	F10	Sauccinamic Acid	0.325	0.214	-0.341538462	0.335	0.29	-0.134328358
2	F11	D-Tartaric Acid	0.186	0.205	0.102150538	0.21	0.278	0.323809524
2	F12	L-Tartaric Acid	0.213	0.218	0.023474178	0.372	0.161	-0.567204301
2	F2	Malonic Acid	0.272	0.22	-0.191176471	0.388	0.297	-0.234536082
2	F3	Melibionic Acid	0.36	0.213	-0.408333333	0.458	0.391	-0.14628821
2	F4	Oxalic Acid	0.356	0.311	-0.126404494	0.441	0.366	-0.170068027
2	F5	Oxalomalic Acid	0.514	0.244	-0.525291829	0.9	0.689	-0.234444444
2	F6	Quinic Acid	0.23	0.187	-0.186956522	0.307	0.386	0.25732899
2	F7	D-Ribono-1,4-Lactone	0.178	0.081	-0.54494382	0.215	0.221	0.027906977
2	F8	Sebacic Acid	0.216	0.097	-0.550925926	0.235	0.124	-0.472340426
2	F9	Sorbic Acid	0.132	0.139	0.053030303	0.492	0.435	-0.115853659
2	G1	Acetamide	0.261	0.184	-0.295019157	0.248	0.257	0.036290323
2	G10	L-Leucine	0.24	0.269	0.120833333	0.308	0.274	-0.11038961
2	G11	L-Lysine	0.266	0.21	-0.210526316	0.465	0.478	0.027956989
2	G12	L-Methionine	0.366	0.177	-0.516393443	0.613	0.223	-0.636215334
2	G2	L-Alaninamide	0.242	0.195	-0.194214876	0.449	0.25	-0.443207127
2	G3	N-Acetyl-L-Glutamic Acid	0.202	0.224	0.108910891	0.237	0.214	-0.097046414
2	G4	L-Arginine	0.429	0.196	-0.543123543	1.095	0.922	-0.157990868
2	G5	Glycine	0.401	0.19	-0.526184539	0.907	0.659	-0.273428886
2	G6	L-Histidine	0.308	0.194	-0.37012987	1.187	0.827	-0.303285594
2	G7	L-Homoserine	0.262	0.207	-0.209923664	0.409	0.464	0.134474328
2	G8	Hydroxy-L Proline	0.47	0.098	-0.791489362	0.623	0.511	-0.179775281
2	G9	L-Isoleucine	0.154	0.11	-0.285714286	0.424	0.304	-0.283018868
2	H1	L-Ornithine	0.649	0.232	-0.642526965	1.036	0.957	-0.076254826
2	H10	2,3-Butanediol	0.28	0.223	-0.203571429	0.536	0.238	-0.555970149
2	H11	2,3-Butanedione	0.155	0.145	-0.064516129	0.514	0.472	-0.081712062
2	H12	3-Hydroxy-2-Butanone	0.308	0.186	-0.396103896	0.316	0.192	-0.392405063
2	H2	L-Phenylalanine	0.283	0.207	-0.268551237	0.254	0.278	0.094488189
2	H3	L-Pyroglutamic Acid	0.289	0.208	-0.280276817	0.32	0.225	-0.296875
2	H4	L-Valanine	0.227	0.216	-0.04845815	0.236	0.188	-0.203389831
2	H5	D,L-Carnitine	0.243	0.22	-0.094650206	0.246	0.199	-0.191056911
2	H6	Sec-Butylamine	0.322	0.244	-0.242236025	0.685	0.542	-0.208759124
2	H7	D,L-Octopamine	0.27	0.228	-0.155555556	0.295	0.208	-0.294915254
2	H8	Putrescine	0.226	0.181	-0.199115044	0.289	0.296	0.024221453
2	H9	Dihydroxy acetone	0.24	0.242	0.008333333	0.401	0.341	-0.149625935

			8 hrs			24 hrs		
Plate	Well	Assay Condition	WT OD590 - t0	*pheP*::Tn OD590 - t0	(*pheP*-WT)/WT	WT OD590 - t0	*pheP*::Tn OD590 - t0	(*pheP*-WT)/WT
3	A1	Negative control	0.132	0.174	0.318181818	0.598	0.565	-0.055183946
3	A10	L-Aspartic Acid	0.135	0.136	0.007407407	0.8	0.618	-0.2275
3	A11	L-Cysteine	0.231	0.218	-0.056277056	0.384	0.402	0.046875
3	A12	L-Glutamic Acid	0.132	0.139	0.053030303	0.416	0.399	-0.040865385
3	A2	Ammonia	0.166	0.16	-0.036144578	0.676	0.636	-0.059171598
3	A3	Nitrite	0.121	0.118	-0.024793388	0.278	0.258	-0.071942446
3	A4	Nitrate	0.12	0.105	-0.125	0.234	0.178	-0.239316239
3	A5	Urea	0.141	0.125	-0.113475177	0.234	0.318	0.358974359
3	A6	Biuret	0.138	0.128	-0.072463768	0.143	0.131	-0.083916084
3	A7	L-Alanine	0.094	0.115	0.223404255	0.146	0.089	-0.390410959
3	A8	L-Arginine	0.104	0.137	0.317307692	0.25	0.28	0.12
3	A9	L-Asparagine	0.138	0.137	-0.007246377	0.527	0.536	0.017077799
3	B1	L-Glutamine	0.167	0.17	0.017964072	0.765	0.835	0.091503268
3	B10	L-Serine	0.086	0.105	0.220930233	0.37	0.222	-0.4
3	B11	L-Threonine	0.323	0.185	-0.427244582	0.754	0.725	-0.038461538
3	B12	L-Tryptophan	0.188	0.165	-0.122340426	0.347	0.43	0.239193084
3	B2	Glycine	0.223	0.221	-0.00896861	1.015	0.64	-0.369458128
3	B3	L-Histidine	0.08	0.154	0.925	0.447	0.582	0.302013423
3	B4	L-Isoleucine	0.115	0.113	-0.017391304	0.469	0.5	0.066098081
3	B5	L-Leucine	0.215	0.131	-0.390697674	0.324	0.251	-0.225308642
3	B6	L-Lysine	0.149	0.125	-0.161073826	0.288	0.274	-0.048611111
3	B7	L-Methionine	0.127	0.122	-0.039370079	0.301	0.259	-0.139534884
3	B8	L-Phenylalanine	0.135	0.153	0.133333333	0.546	0.451	-0.173992674
3	B9	L-Proline	0.131	0.132	0.007633588	0.425	0.369	-0.131764706
3	C1	L-Tyrosine	-0.017	0.054	-4.176470588	0.382	0.345	-0.096858639
3	C10	L-Citrulline	0.152	0.147	-0.032894737	0.435	0.392	-0.098850575
3	C11	L-Homoserine	0.151	0.158	0.046357616	0.671	0.643	-0.041728763
3	C12	L-Ornitine	0.145	0.139	-0.04137931	0.349	0.293	-0.160458453
3	C2	L-Valine	0.156	0.17	0.08974359	0.64	0.757	0.1828125
3	C3	D-Alanine	0.18	0.166	-0.077777778	0.466	0.557	0.19527897
3	C4	D-Asparagine	0.175	0.154	-0.12	0.489	0.28	-0.427402863
3	C5	D-Aspartic Acid	0.149	0.139	-0.067114094	0.302	0.339	0.122516556
3	C6	D-Glutamic Acid	0.199	0.146	-0.266331658	0.446	0.341	-0.235426009
3	C7	D-Lysine	0.148	0.139	-0.060810811	0.534	0.395	-0.260299625
3	C8	D-Serine	0.128	0.137	0.0703125	0.461	0.491	0.065075922
3	C9	D-Valine	0.156	0.153	-0.019230769	0.407	0.604	0.484029484
3	D1	N-Acetyl-L-Glutamic Acid	0.166	0.197	0.186746988	0.522	0.416	-0.203065134
3	D10	Ethaylenediamine	0.131	0.16	0.221374046	0.61	0.537	-0.119672131
3	D11	Putrescine	0.147	0.153	0.040816327	0.577	0.39	-0.324090121
3	D12	Agmatine	0.157	0.138	-0.121019108	0.469	0.318	-0.32196162
3	D2	N-Phthaloyl-L-Glutamic Acid	0.158	0.15	-0.050632911	0.619	0.689	0.113085622
3	D3	L-Pyroglutamic Acid	0.168	0.154	-0.083333333	0.544	0.441	-0.189338235
3	D4	Hydroxylamine	0.21	0.157	-0.252380952	0.59	0.375	-0.36440678
3	D5	Mehylamine	0.18	0.186	0.033333333	0.474	0.542	0.143459916
3	D6	N-Amylamine	0.196	0.184	-0.06122449	0.433	0.502	0.159353349
3	D7	N-Butylamine	0.218	0.192	-0.119266055	0.403	0.471	0.168734491
3	D8	Ethylamine	0.219	0.174	-0.205479452	0.73	0.452	-0.380821918
3	D9	Ethanolamine	0.187	0.146	-0.219251337	0.587	0.362	-0.38330494
3	E1	Histamine	0.188	0.177	-0.058510638	0.286	0.296	0.034965035
3	E10	D-Mannosamine	0.191	0.171	-0.104712042	0.848	0.843	-0.005896226
3	E11	N-Acetyl-D-Glucosamine	0.166	0.169	0.018072289	0.551	0.463	-0.159709619
3	E12	N-Aceytl-D-Galactosamine	0.156	0.153	-0.019230769	0.347	0.314	-0.095100865
3	E2	B-Phenylethyl-amine	0.21	0.17	-0.19047619	0.523	0.478	-0.086042065
3	E3	Tyramine	0.203	0.181	-0.108374384	0.648	0.587	-0.094135802
3	E4	Acetamide	0.19	0.184	-0.031578947	0.703	0.503	-0.284495021
3	E5	Formamide	0.183	0.183	0	0.802	0.686	-0.144638404
3	E6	Glucuronamide	0.206	0.184	-0.106796117	0.94	1.015	0.079787234
3	E7	D,L-Lactamide	0.184	0.164	-0.108695652	0.751	0.765	0.018641811
3	E8	D-Glucosamine	0.216	0.16	-0.259259259	0.697	0.683	-0.020086083
3	E9	D-Galactosamine	0.168	0.143	-0.148809524	0.556	0.665	0.196043165
3	F1	N-Acetyl-D-Mannosamine	0.021	0.191	8.095238095	0.259	0.368	0.420849421
3	F10	Uracil	0.063	-0.015	-1.238095238	0.434	0.306	-0.294930876
3	F11	Uridine	0.212	0.109	-0.485849057	0.342	0.245	-0.283625731
3	F12	Inosine	0.146	0.159	0.089041096	0.329	0.344	0.045592705
3	F2	Adenine	0.156	0.148	-0.051282051	0.297	0.236	-0.205387205
3	F3	Adenosine	0.168	0.16	-0.047619048	0.373	0.358	-0.040214477
3	F4	Cytidine	0.182	0.171	-0.06043956	0.583	0.543	-0.068610635
3	F5	Cytosine	0.159	0.168	0.056603774	0.355	0.558	0.571830986
3	F6	Guanine	0.523	0.271	-0.481835564	0.586	0.261	-0.554607509
3	F7	Guanosine	0.227	0.179	-0.211453744	0.371	0.457	0.23180593
3	F8	Thymine	0.159	0.162	0.018867925	0.518	0.42	-0.189189189
3	F9	Thymidine	0.065	0.056	-0.138461538	0.43	0.384	-0.106976744
3	G1	Xanthine	0.109	0.154	0.412844037	0.369	0.396	0.073170732
3	G10	D,L-a-Amino-Caprylic Acid	0.249	0.249	-1.11468E-16	0.892	0.8	-0.103139013
3	G11	gamma-Amino Valeric Acid	0.175	0.148	-0.154285714	0.49	0.325	-0.336734694
3	G12	a-Amino-N-Valeric Acid	0.179	0.145	-0.189944134	0.338	0.303	-0.103550296
3	G2	Xanthosine	0.069	0.064	-0.072463768	0.262	0.308	0.175572519
3	G3	Uric Acid	0.168	0.228	0.357142857	0.456	0.384	-0.157894737
3	G4	Alloxan	0.21	0.197	-0.061904762	0.33	0.347	0.051515152
3	G5	Allantoin	0.208	0.175	-0.158653846	0.448	0.638	0.424107143
3	G6	Parabanic Acid	0.155	0.253	0.632258065	0.599	0.682	0.138564274
3	G7	D,L-a-Amino-N-Butyric Acid	0.163	0.163	3.40559E-16	0.552	0.671	0.21557971
3	G8	y-Amino-N-Butyric Acid	0.174	0.171	-0.017241379	0.461	0.47	0.019522777
3	G9	e-Amino-N-Caproic Acid	0.145	0.172	0.186206897	0.44	0.464	0.054545455
3	H1	Ala-Asp	0.14	0.134	-0.042857143	0.875	0.496	-0.433142857
3	H10	Gly-Glu	0.338	0.2	-0.408284024	1.242	0.906	-0.270531401
3	H11	Gly-Met	0.232	0.127	-0.452586207	1.149	0.448	-0.610095735
3	H12	Met-Ala	0.15	0.125	-0.166666667	0.527	0.107	-0.796963947
3	H2	Ala-Gln	0.206	0.123	-0.402912621	0.773	0.303	-0.608020699
3	H3	Ala-Glu	0.15	0.132	-0.12	0.994	0.598	-0.398390342
3	H4	Ala-Gly	0.243	0.155	-0.362139918	0.871	0.893	0.025258324
3	H5	Ala-His	0.14	0.127	-0.092857143	0.367	0.233	-0.365122616
3	H6	Ala-Leu	0.176	0.132	-0.25	0.548	0.143	-0.739051095
3	H7	Ala-Thr	0.239	0.155	-0.351464435	0.807	0.712	-0.11771995
3	H8	Gly-Asn	0.305	0.155	-0.491803279	0.963	0.903	-0.062305296
3	H9	Gly-Gln	0.367	0.162	-0.558583106	0.848	0.876	0.033018868

			8 hrs			24 hrs		
Plate	Well	Assay Condition	WT OD590 - t0	*pheP* ::Tn OD590 - t0	(*pheP* -WT)/WT	WT OD590 - t0	*pheP* ::Tn OD590 - t0	(*pheP* -WT)/WT
4	A1	Negative control	0.197	0.124	-0.370558376	0.265	0.151	-0.430188679
4	A10	Adenosine-5'-monophosphate	0.237	0.126	-0.46835443	0.524	0.441	-0.158396947
4	A11	Adenosine-2',3'-cyclic monophosphate	0.179	0.119	-0.335195531	0.471	0.431	-0.08492569
4	A12	Adenosine-3'-.5'-cyclic monophosphate	0.154	0.15	-0.025974026	0.189	0.15	-0.206349206
4	A2	Phosphate	0.24	0.148	-0.383333333	0.499	0.317	-0.364729459
4	A3	Pyrophosphate	0.273	0.239	-0.124542125	1.072	0.747	-0.303171642
4	A4	Trimeta Phosphate	0.159	0.139	-0.125786164	0.478	0.296	-0.380753138
4	A5	Tripoly Phosphate	0.172	0.12	-0.302325581	0.545	0.357	-0.344954128
4	A6	Triethyl Phosphate	0.038	-0.024	-1.631578947	0.218	-0.055	-1.252293578
4	A7	Hypophosphite	0.242	0.092	-0.619834711	0.224	0.083	-0.629464286
4	A8	Adenosine-2'-monophosphate	0.174	0.094	-0.459770115	0.349	0.248	-0.289398281
4	A9	Adenosine-3'-monophosphate	0.199	0.132	-0.336683417	0.355	0.292	-0.177464789
4	B1	Thiophosphate	0.257	0.131	-0.490272374	0.908	0.767	-0.155286344
4	B10	Guanosine-5'-monophosphate	0.171	0.147	-0.140350877	0.47	0.455	-0.031914894
4	B11	Guanosine-2',3'-cyclic monophosphate	0.172	0.15	-0.127906977	0.599	0.318	-0.469115192
4	B12	Guanosine-3',5'-cyclic monophosphate	0.234	0.116	-0.504273504	0.333	0.164	-0.507507508
4	B2	Dithiosphosphate	0.255	0.154	-0.396078431	1.245	1.01	-0.18875502
4	B3	D,L-a-Glycerol Phosphate	0.209	0.146	-0.301435407	0.748	0.48	-0.35828877
4	B4	B-Glycerol Phosphate	0.251	0.144	-0.426294821	0.631	0.56	-0.11251981
4	B5	Carbamyl Phosphate	0.198	0.141	-0.287878788	0.929	0.415	-0.5532831
4	B6	D-2-Phospho-Glyceric Acid	0.199	0.122	-0.386934673	1.062	0.287	-0.729755179
4	B7	D-3-Phospho-Glyceric Acid	0.164	0.143	-0.12804878	0.889	0.367	-0.587176603
4	B8	Guanosine-2'-monophosphate	0.264	0.133	-0.496212121	0.643	0.284	-0.558320373
4	B9	Guanosine-3'-monophosphate	0.167	0.144	-0.137724551	0.689	0.381	-0.447024673
4	C1	Phosphoenol Pyruvate	0.206	0.161	-0.218446602	1.11	0.548	-0.506306306
4	C10	Cytidine-5'-monophosphate	0.38	0.29	-0.236842105	0.845	0.628	-0.256804734
4	C11	Cytidine-2',3' cyclic monophosphate	0.174	0.164	-0.057471264	0.544	0.376	-0.308823529
4	C12	Cytidine-3',5'-cyclic monophosphate	0.168	0.137	-0.18452381	0.474	0.248	-0.476793249
4	C2	Phospho-Glycolic Acid	0.24	0.241	0.004166667	1.052	0.796	-0.243346008
4	C3	D-Glucose-1-Phosphate	0.346	0.22	-0.36416185	0.912	0.756	-0.171052632
4	C4	D-Glucose-6-Phosphate	0.445	0.166	-0.626966292	1.141	0.556	-0.512708151
4	C5	2-Deoxy-D-Glucose-6-Phosphate	0.407	0.145	-0.643734644	0.303	0.194	-0.359735974
4	C6	D-Glucosamine-6-Phosphate	0.338	0.136	-0.597633136	0.932	0.142	-0.847639485
4	C7	6-Phospho-Gluconic Acid	0.341	0.143	-0.580645161	0.919	0.502	-0.453754081
4	C8	Cytidine-2-monophosphate	0.412	0.157	-0.618932039	0.973	0.768	-0.210688592
4	C9	Cytidine-3-monophosphate	0.369	0.143	-0.612466125	0.419	0.302	-0.279236277
4	D1	D-Mannose-1-Phosphate	0.274	0.165	-0.397810219	0.662	0.779	0.17673716
4	D10	Uridine-5'-monophosphate	0.362	0.342	-0.055248619	0.963	0.746	-0.225337487
4	D11	Uridine-2'3'-cyclic monophosphate	0.296	0.189	-0.361486486	0.815	0.627	-0.230674847
4	D12	Uridine-3',5'-cyclic monophosphate	0.216	0.146	-0.324074074	0.334	0.191	-0.428143713
4	D2	D-Mannose-6-Phosphate	0.293	0.239	-0.184300341	0.955	0.857	-0.102617801
4	D3	Cysteamine-S-Phosphate	0.45	0.342	-0.24	1.103	1.136	0.029918404
4	D4	Phospho-L-Arginine	0.394	0.311	-0.210659898	1.131	0.805	-0.288240495
4	D5	O-Phospho-D-Serine	0.383	0.154	-0.597911227	1.053	0.488	-0.536562203
4	D6	O-Phospho-L-Serine	0.374	0.135	-0.639037433	0.976	0.631	-0.353483607
4	D7	O-Phospho-L-Threonine	0.376	0.143	-0.619680851	0.779	0.48	-0.383825417
4	D8	Uridine-2'-monophosphate	0.327	0.25	-0.235474006	0.974	0.495	-0.491786448
4	D9	Uridine-3'-monophosphate	0.401	0.323	-0.194513716	0.966	0.827	-0.14389234
4	E1	O-Phospho-D-Tyrosine	0.291	0.167	-0.426116838	0.556	0.505	-0.091726619
4	E10	Thymidine-5'-monophosphate	0.293	0.338	0.153583618	0.226	0.472	1.088495575
4	E11	Inositol Hexaphosphate	0.196	0.176	-0.102040816	0.856	0.531	-0.379672897
4	E12	Thymidine 3'5'-cyclic monophosphate	0.176	0.134	-0.238636364	0.521	0.49	-0.05950096
4	E2	O-Phospho-L-Tyrosine	0.379	0.293	-0.226912929	0.877	0.822	-0.062713797
4	E3	Phosphocreatine	0.386	0.32	-0.170984456	1.071	0.799	-0.253968254
4	E4	Phosphoryl Choline	0.44	0.316	-0.281818182	0.81	0.406	-0.498765432
4	E5	O-Phosphoryl-Ethanolamine	0.494	0.337	-0.317813765	0.853	0.498	-0.416178195
4	E6	Phospho Acetic Acid	0.41	0.325	-0.207317073	0.52	0.204	-0.607692308
4	E7	2-Aminoethyl Phosphonic Acid	0.471	0.337	-0.284501062	0.518	0.237	-0.542471042
4	E8	Methylene Disphosphonic Acid	0.355	0.357	0.005633803	0.645	0.315	-0.511627907
4	E9	Thymidine-3'-monophosphate	0.391	0.336	-0.140664962	0.724	0.734	0.013812155
4	F1	Negative control	0.269	0.165	-0.3866171	0.869	0.45	-0.482163406
4	F10	L-Cysteic Acid	0.372	0.322	-0.134408602	0.469	0.408	-0.130063966
4	F11	Cysteamine-S-Phosphate	0.204	0.213	0.044117647	0.871	1.221	0.401836969
4	F12	L-Cysteine Sulfinic Acid	0.185	0.155	-0.162162162	0.884	0.548	-0.380090498
4	F2	Sulfate	0.361	0.275	-0.238227147	0.668	0.826	0.236526946
4	F3	Thiosulfate	0.426	0.315	-0.26056338	1.278	0.521	-0.592331768
4	F4	Tetrathionate	0.413	0.34	-0.176755448	0.967	0.994	0.027921406
4	F5	Thiophosphate	0.438	0.343	-0.216894977	1.33	0.955	-0.281954887
4	F6	Dithiophosphate	0.368	0.332	-0.097826087	1.186	1.002	-0.155143339
4	F7	L-Cysteine	0.368	0.353	-0.04076087	1.247	0.881	-0.293504411
4	F8	D-Cysteine	0.408	0.343	-0.159313725	1.043	0.98	-0.060402685
4	F9	L-Cysteinyl-Glycine	0.547	0.348	-0.363802559	1.2	0.978	-0.185
4	G1	N-Acetyl-L-Cysteine	-0.153	-0.068	-0.555555556	0.034	0.536	14.76470588
4	G10	N-Acetyl-D,L-Methionine	0.238	0.234	-0.016806723	0.878	0.718	-0.182232346
4	G11	L-Methionine Sulfoxide	0.254	0.174	-0.31496063	0.787	0.823	0.045743329
4	G12	L-Methionine Sulfone	0.234	0.156	-0.333333333	0.513	0.516	0.005847953
4	G2	S-Methyl-L-Cysteine	0.371	0.248	-0.331536388	0.982	1.008	0.026476578
4	G3	Cystathionine	0.356	0.304	-0.146067416	1.034	1.03	-0.003868472
4	G4	Lanthionine	0.359	0.292	-0.186629526	0.996	0.752	-0.24497992
4	G5	Glutathione	0.934	0.283	-0.697002141	0.893	0.729	-0.183650616
4	G6	D,L-Ethionine	0.311	0.24	-0.22829582	0.779	0.816	0.047496791
4	G7	L-Methionine	0.425	0.243	-0.428235294	0.867	0.751	-0.133794694
4	G8	D-Methionine	-0.327	0.257	-1.785932722	-0.008	0.591	-74.875
4	G9	Glycyl-L-Methionine	0.373	0.229	-0.386058981	1.038	0.798	-0.231213873
4	H1	L-Djenkolic Acid	0.264	0.169	-0.359848485	0.796	0.907	0.139447236
4	H10	2-Hydroxyethane Sulfonic Acid	0.233	0.173	-0.25751073	0.834	0.451	-0.459232614
4	H11	Methane Sulfonic Acid	0.213	0.175	-0.178403756	0.909	0.587	-0.354235424
4	H12	Tetramethylene Sulfone	0.183	0.148	-0.191256831	0.897	0.51	-0.431438127
4	H2	Thiourea	0.277	0.186	-0.328519856	1.097	0.786	-0.283500456
4	H3	1-Thio-B-D-Glucose	0.314	0.19	-0.394904459	0.97	0.535	-0.448453608
4	H4	D,L-Lipoamide	0.218	0.176	-0.19266055	1.139	0.906	-0.204565408
4	H5	Taurocholic Acid	0.267	0.159	-0.404494382	0.604	0.371	-0.385761589
4	H6	Taurine	0.238	0.176	-0.260504202	0.817	0.653	-0.200734394
4	H7	Hypotaurine	0.228	0.188	-0.175438596	0.999	0.843	-0.156156156
4	H8	P-Amino Benzene Sulfonic Acid	0.198	0.174	-0.121212121	0.89	0.758	-0.148314607
4	H9	Butane Sulfonic Acid	0.229	0.187	-0.183406114	0.797	0.767	-0.037641154

			8 hrs			24 hrs		
Plate	Well	Assay Condition	WT OD590 - t0	*pheP* ::Tn OD590 - t0	(*pheP* -WT)/WT	WT OD590 - t0	*pheP* ::Tn OD590 - t0	(*pheP* -WT)/WT
5	A1	Negative control	0.095	0.132	0.389473684	0.064	0.002	-0.96875
5	A10	Adenine	0.093	0.086	-0.075268817	0.053	0.01	-0.811320755
5	A11	Adenosine	0.091	0.08	-0.120879121	0.051	0.011	-0.784313725
5	A12	2'-Deoxy Adenosine	0.067	0.045	-0.328358209	0.022	0.012	-0.454545455
5	A2	Positive control	0.152	0.095	-0.375	0.088	0.009	-0.897727273
5	A3	L-Alanine	0.163	0.1	-0.386503067	0.062	0.008	-0.870967742
5	A4	L-Arginine	0.114	0.089	-0.219298246	0.04	0.014	-0.65
5	A5	L-Asparagine	0.094	0.069	-0.265957447	0.021	0.026	0.238095238
5	A6	L-Aspartic Acid	0.074	0.049	-0.337837838	0.018	0.006	-0.666666667
5	A7	L-Cysteine	0.087	0.051	-0.413793103	0.026	0.013	-0.5
5	A8	L-Glutamic Acid	0.106	0.066	-0.377358491	0.03	0.036	0.2
5	A9	Adenosin-3',5'-cyclic monophosphate	0.096	0.081	-0.15625	0.026	0.009	-0.653846154
5	B1	L-Glutamine	0.138	0.081	-0.413043478	0.082	0.007	-0.914634146
5	B10	Guanine	0.245	0.287	0.171428571	0.058	0.031	-0.465517241
5	B11	Guanosine	0.219	0.211	-0.03652968	0.07	0.056	-0.2
5	B12	2'-Deoxy Guanosine	0.137	0.081	-0.408759124	0.057	0.041	-0.280701754
5	B2	Glycine	0.187	0.201	0.07486631	0.061	0.012	-0.803278689
5	B3	L-Histidine	0.229	0.235	0.026200873	0.098	0.018	-0.816326531
5	B4	L-Isoleucine	0.121	0.096	-0.20661157	0.063	0.012	-0.80952381
5	B5	L-Leucine	0.094	0.085	-0.095744681	0.054	0.022	-0.592592593
5	B6	L-Lysine	0.112	0.078	-0.303571429	0.05	0.041	-0.18
5	B7	L-Methionine	0.131	0.086	-0.34351145	0.068	0.06	-0.117647059
5	B8	L-Phenylalanine	0.115	0.082	-0.286956522	0.066	0.024	-0.636363636
5	B9	Guanosine-3'5'-cyclic monophosphate	0.109	0.151	0.385321101	0.068	0.01	-0.852941176
5	C1	L-Proline	0.11	0.082	-0.254545455	0.079	0.021	-0.734177215
5	C10	Hypoxanthine	0.335	0.291	-0.131343284	0.373	0.109	-0.707774799
5	C11	Inosine	0.326	0.275	-0.156441718	0.144	0.022	-0.847222222
5	C12	2'-Deoxy Inosine	0.154	0.075	-0.512987013	0.068	0.065	-0.044117647
5	C2	L-Serine	0.329	0.293	-0.109422492	0.311	0.007	-0.977491961
5	C3	L-Threonine	0.328	0.326	-0.006097561	0.352	0.025	-0.928977273
5	C4	L-Tryptophan	0.308	0.243	-0.211038961	0.101	0.021	-0.792079208
5	C5	L-Tyrosine	0.286	0.36	0.258741259	0.06	0.025	-0.583333333
5	C6	L-Valine	0.11	0.226	1.054545455	0.074	0.044	-0.405405405
5	C7	L-Isoleucine + L-Valine	0.128	0.241	0.8828125	0.068	0.022	-0.676470588
5	C8	trans-4-Hydroxy L-Proline	0.331	0.327	-0.012084592	0.067	0.046	-0.313432836
5	C9	(5) 4-Amino Imidazole-4(5)-Carboxamide	0.406	0.379	-0.066502463	0.354	0.124	-0.649717514
5	D1	L-Ornithine	0.11	0.119	0.081818182	0.098	0.046	-0.530612245
5	D10	Cytosine	0.363	0.263	-0.275482094	0.345	0.037	-0.892753623
5	D11	Cytidine	0.282	0.291	0.031914894	0.13	0.038	-0.707692308
5	D12	2'-Deoxy Cytidine	0.154	0.072	-0.532467532	0.072	0.084	0.166666667
5	D2	L-Citrulline	0.306	0.323	0.055555556	0.363	0.067	-0.815426997
5	D3	Chorismic Acid	0.326	0.315	-0.033742331	0.28	0.026	-0.907142857
5	D4	(-)Shikimic Acid	0.29	0.344	0.186206897	0.322	0.061	-0.810559006
5	D5	L-Homoserine Lactone	0.285	0.318	0.115789474	0.308	0.052	-0.831168831
5	D6	D-Alanine	0.365	0.364	-0.002739726	0.194	0.034	-0.824742268
5	D7	D-Aspartic Acid	0.368	0.325	-0.116847826	0.212	0.093	-0.561320755
5	D8	D-Glutamic Acid	0.316	0.263	-0.167721519	0.335	0.033	-0.901492537
5	D9	D,L-a,e-Diaminopimelic Acid	0.334	0.347	0.038922156	0.339	0.041	-0.879056047
5	E1	Putrescine	0.141	0.139	-0.014184397	0.095	0.06	-0.368421053
5	E10	Uracil	0.347	0.352	0.014409222	0.322	0.068	-0.788819876
5	E11	Uridine	0.349	0.282	-0.191977077	0.15	0.05	-0.666666667
5	E12	2'-Deoxy Uridine	0.117	0.084	-0.282051282	0.07	0.074	0.057142857
5	E2	Spermidine	0.38	0.266	-0.3	0.332	0.007	-0.978915663
5	E3	Spermine	0.339	0.359	0.05899705	0.382	0.108	-0.717277487
5	E4	Pyridoxine	0.346	0.323	-0.066473988	0.355	0.065	-0.816901408
5	E5	Pyridoxal	0.378	0.258	-0.317460317	0.361	0.055	-0.847645429
5	E6	Pyridoxamine	0.381	0.3	-0.212598425	0.35	0.07	-0.8
5	E7	B-Alanine	0.321	0.323	0.00623053	0.334	0.026	-0.922155689
5	E8	D-Pantothenic Acid	0.319	0.298	-0.065830721	0.363	0.043	-0.8815427
5	E9	Orotic Acid	0.313	0.306	-0.022364217	0.34	0.037	-0.891176471
5	F1	Quinolinic Acid	0.153	0.118	-0.22875817	0.106	0.066	-0.377358491
5	F10	Thymine	0.302	0.288	-0.046357616	0.299	0.142	-0.525083612
5	F11	Glutatione (reduced form)	0.321	0.258	-0.196261682	0.136	0.279	1.051470588
5	F12	Thymidine	0.126	0.077	-0.388888889	0.066	0.072	0.090909091
5	F2	Nicotinic Acid	0.359	0.327	-0.08913649	0.347	0.076	-0.780979827
5	F3	Nicotinamide	0.382	0.339	-0.112565445	0.349	0.027	-0.922636103
5	F4	B-Nicotinamide Adenine Dinucleotide	0.406	0.214	-0.472906404	0.376	0.093	-0.752659574
5	F5	gamma-Amino-Levulinic Acid	0.322	0.309	-0.040372671	0.365	0.057	-0.843835616
5	F6	Hematin	0.346	0.335	-0.031791908	0.334	0.046	-0.862275449
5	F7	Deferoxamine Mesylate	0.232	0.363	0.564655172	0.326	0.163	-0.5
5	F8	D-(+)-Glucose	0.293	0.356	0.215017065	0.376	0.038	-0.89893617
5	F9	N-Acetyl D-Glucosamine	0.291	0.308	0.058419244	0.381	0.163	-0.572178478
5	G1	Oxaloacetic Acid	0.132	0.085	-0.356060606	0.104	0.087	-0.163461538
5	G10	Pyrrolo-Quinoline Quinone	0.395	0.276	-0.301265823	0.319	0.229	-0.282131661
5	G11	Menadione	0.316	0.272	-0.139240506	0.066	0.195	1.954545455
5	G12	myo-Inositol	0.121	0.09	-0.256198347	0.085	0.082	-0.035294118
5	G2	D-Biotin	0.235	0.296	0.259574468	0.139	0.054	-0.611510791
5	G3	Cyano-Cobalamine	0.307	0.306	-0.003257329	0.285	0.197	-0.30877193
5	G4	p-Amino -Benzoic Acid	0.301	0.289	-0.03986711	0.365	0.068	-0.81369863
5	G5	Folic Acid	0.379	0.325	-0.142480211	0.362	0.018	-0.950276243
5	G6	Inosine + Thiamine	0.342	0.336	-0.01754386	0.386	0.024	-0.937823834
5	G7	Thiamine	0.332	0.327	-0.015060241	0.295	0.206	-0.301694915
5	G8	Thiamine Pyrophosphate	0.26	0.29	0.115384615	0.319	0.251	-0.213166144
5	G9	Riboflavin	0.315	0.358	0.136507937	0.334	0.246	-0.263473054
5	H1	Butyric Acid	0.133	0.079	-0.406015038	0.102	0.083	-0.18627451
5	H10	Tween 40	0.148	0.089	-0.398648649	0.075	0.095	0.266666667
5	H11	Tween 60	0.149	0.088	-0.409395973	0.094	0.098	0.042553191
5	H12	Tween 80	0.1	0.055	-0.45	0.11	0.067	-0.390909091
5	H2	D,L-a-Hydroxy-Butyric Acid	0.171	0.113	-0.339181287	0.123	0.106	-0.138211382
5	H3	a-Keto-Butyric Acid	0.152	0.119	-0.217105263	0.125	0.108	-0.136
5	H4	Caprylic Acid	0.145	0.122	-0.15862069	0.12	0.103	-0.141666667
5	H5	D,L-a-Lipoic Acid (oxidized form)	0.169	0.138	-0.183431953	0.142	0.12	-0.154929577
5	H6	D,L-Mevalonic Acid	0.138	0.107	-0.224637681	0.12	0.106	-0.116666667
5	H7	D,L-Carnitine	0.156	0.116	-0.256410256	0.138	0.119	-0.137681159
5	H8	Chioline	0.151	0.11	-0.271523179	0.124	0.108	-0.129032258
5	H9	Tween 20	0.14	0.097	-0.307142857	0.099	0.13	0.313131313

			8 hrs			24 hrs		
Plate	Well	Assay Condition	WT OD590 - t0	*pheP* ::Tn OD590 - t0	(*pheP* -WT)/WT	WT OD590 - t0	*pheP* ::Tn OD590 - t0	(*pheP* -WT)/WT
6	A1	Negative control	0.116	0.067	-0.422413793	0.279	0.288	0.032258065
6	A10	Ala-Lys	0.084	0.039	-0.535714286	0.353	0.126	-0.64305949
6	A11	Ala-Phe	0.051	0.089	0.745098039	0.298	0.522	0.751677852
6	A12	Ala-Pro	0.066	0.042	-0.363636364	0.14	0.125	-0.107142857
6	A2	Positive control: L-Glutamine	0.153	0.07	-0.54248366	0.983	0.801	-0.185147508
6	A3	Ala-Ala	0.106	0.036	-0.660377358	0.37	0.348	-0.059459459
6	A4	Ala-Arg	0.119	0.032	-0.731092437	0.339	0.065	-0.808259587
6	A5	Ala-Asn	0.126	0.04	-0.682539683	0.429	0.236	-0.44988345
6	A6	Ala-Glu	0.147	0.053	-0.639455782	0.62	0.48	-0.225806452
6	A7	Ala-Gly	0.28	0.065	-0.767857143	0.93	0.645	-0.306451613
6	A8	Ala-His	0.073	0.033	-0.547945205	0.319	0.218	-0.31661442
6	A9	Ala-Leu	0.055	0.035	-0.363636364	0.276	0.16	-0.420289855
6	B1	Ala-Ser	0.114	0.028	-0.754385965	0.172	0.065	-0.622093023
6	B10	Arg-Ile	0.055	0.037	-0.327272727	0.301	0.335	0.112956811
6	B11	Areg-Leu	0.055	0.038	-0.309090909	0.512	0.227	-0.556640625
6	B12	Asp-Lys	0.107	0.076	-0.289719626	0.219	0.236	0.077625571
6	B2	Ala-Thr	0.263	0.054	-0.794676806	0.647	0.732	0.13137558
6	B3	Ala-Trp	0.122	0.053	-0.56557377	0.294	0.323	0.098639456
6	B4	Ala-Tyr	0.11	0.033	-0.7	0.238	0.251	0.054621849
6	B5	Arg-Ala	0.112	0.044	-0.607142857	0.337	0.207	-0.385756677
6	B6	Arg-Arg	0.123	0.045	-0.634146341	0.23	0.167	-0.273913043
6	B7	Arg-Asp	0.115	0.064	-0.443478261	0.942	0.804	-0.146496815
6	B8	Arg-Gln	0.078	0.053	-0.320512821	0.881	0.589	-0.331441544
6	B9	Arg-Glu	0.089	0.068	-0.235955056	0.887	0.696	-0.215332582
6	C1	Arg-Met	0.114	0.033	-0.710526316	0.381	0.112	-0.706036745
6	C10	Asp-Glu	0.082	0.068	-0.170731707	0.535	0.36	-0.327102804
6	C11	Asp-leu	0.187	0.035	-0.812834225	0.861	0.334	-0.612078978
6	C12	Asp-Lys	0.148	0.076	-0.486486486	0.346	0.261	-0.24566474
6	C2	Arg-Phe	0.156	0.085	-0.455128205	0.584	0.557	-0.046232877
6	C3	Arg-Ser	0.155	0.049	-0.683870968	0.486	0.205	-0.5781893
6	C4	Arg-Trp	0.137	0.065	-0.525547445	0.26	0.229	-0.119230769
6	C5	Arg-Tyr	0.148	0.047	-0.682432432	0.453	0.549	0.21192053
6	C6	Arg-Val	0.139	0.041	-0.705035971	0.613	0.369	-0.398042414
6	C7	Asn-Glu	0.149	0.065	-0.563758389	0.716	0.667	-0.068435754
6	C8	Asn-Val	0.086	0.041	-0.523255814	0.629	0.235	-0.626391097
6	C9	Asp-Asp	0.125	0.08	-0.36	0.773	0.726	-0.06080207
6	D1	Asp-Phe	0.159	0.105	-0.339622642	0.43	0.522	0.213953488
6	D10	Glu-Ser	0.104	0.093	-0.105769231	0.975	0.323	-0.668717949
6	D11	Glu-Trp	0.095	0.057	-0.4	0.554	0.677	0.222021661
6	D12	Glu-Tyr	0.203	0.09	-0.556650246	0.522	0.626	0.199233716
6	D2	Asp-Trp	0.159	0.066	-0.58490566	0.561	0.429	-0.235294118
6	D3	Asp-Val	0.209	0.033	-0.842105263	0.925	0.549	-0.406486486
6	D4	Cys-Gly	0.188	0.041	-0.781914894	0.54	0.46	-0.148148148
6	D5	Gln-Gln	0.135	0.043	-0.681481481	0.33	0.198	-0.4
6	D6	Gln-Gly	0.43	0.049	-0.886046512	0.852	0.709	-0.167840376
6	D7	Glu-Asp	0.079	0.074	-0.063291139	0.854	0.738	-0.135831382
6	D8	Glu-Glu	0.152	0.083	-0.453947368	0.894	0.772	-0.136465324
6	D9	Glu-Gly	0.393	0.108	-0.72519084	0.841	1.009	0.199762188
6	E1	Glu-Val	0.165	0.08	-0.515151515	0.416	0.271	-0.348557692
6	E10	Gly-Phe	0.18	0.156	-0.133333333	0.873	0.521	-0.403207331
6	E11	Gly-Pro	0.183	0.08	-0.56284153	0.635	0.751	0.182677165
6	E12	Gly-Ser	0.252	0.081	-0.678571429	0.54	0.561	0.038888889
6	E2	Gly-Ala	0.284	0.07	-0.753521127	0.632	0.607	-0.039556962
6	E3	Gly-Arg	0.385	0.094	-0.755844156	0.865	0.61	-0.294797688
6	E4	Gly-Cys	0.149	0.066	-0.55704698	0.326	0.349	0.070552147
6	E5	Gly-Gly	0.289	0.096	-0.667820069	0.807	0.676	-0.162329616
6	E6	Gly-His	0.286	0.09	-0.685314685	0.605	0.485	-0.198347107
6	E7	Gly-Leu	0.345	0.041	-0.88115942	0.97	0.459	-0.526804124
6	E8	Gly-Lys	0.233	0.107	-0.540772532	0.856	0.595	-0.304906542
6	E9	Gly-Met	0.186	0.054	-0.709677419	0.961	0.706	-0.265348595
6	F1	Gly-Thr	0.303	0.091	-0.699669967	0.494	0.406	-0.178137652
6	F10	His-Pro	0.059	0.032	-0.457627119	0.21	0.204	-0.028571429
6	F11	His-Ser	0.151	0.014	-0.907284768	0.238	0.046	-0.806722689
6	F12	His-Trp	0.091	0.062	-0.318681319	0.157	0.231	0.47133758
6	F2	Gly-Trp	0.28	0.088	-0.685714286	0.525	0.479	-0.087619048
6	F3	Gly-Tyr	0.185	0.105	-0.432432432	0.449	0.456	0.0155902
6	F4	Gly-Val	0.359	0.073	-0.796657382	0.859	0.664	-0.227008149
6	F5	His-Asp	0.17	0.051	-0.7	0.784	0.468	-0.403061224
6	F6	His-Gly	0.221	0.049	-0.778280543	0.746	0.525	-0.296246649
6	F7	His-Leu	0.117	0.036	-0.692307692	0.575	0.293	-0.490434783
6	F8	His-Lys	0.063	0.061	-0.031746032	0.206	0.261	0.266990291
6	F9	His-Met	0.144	0.042	-0.708333333	0.505	0.272	-0.461386139
6	G1	His-Tyr	0.124	0.086	-0.306451613	0.225	0.257	0.142222222
6	G10	Ile-Phe	0.047	0.057	0.212765957	0.117	0.195	0.666666667
6	G11	Ile-Pro	0.075	0.058	-0.226666667	0.332	0.198	-0.403614458
6	G12	Ile-Ser	0.058	0.032	-0.448275862	0.56	0.026	-0.953571429
6	G2	His-Val	0.146	0.049	-0.664383562	0.411	0.199	-0.515815085
6	G3	Ile-Ala	0.145	0.066	-0.544827586	0.352	0.117	-0.667613636
6	G4	Ile-Arg	0.124	0.057	-0.540322581	0.32	0.198	-0.38125
6	G5	Ile-Gln	0.133	0.056	-0.578947368	0.588	0.21	-0.642857143
6	G6	Ile-Gly	0.354	0.056	-0.84180791	0.92	0.688	-0.252173913
6	G7	Ile-His	0.143	0.048	-0.664335664	0.298	0.329	0.104026846
6	G8	Ile-Ile	0.049	0.048	-0.020408163	0.165	0.184	0.115151515
6	G9	Ile-Met	0.043	0.039	-0.093023256	0.184	0.16	-0.130434783
6	H1	Ile-Trp	0.137	0.042	-0.693430657	0.19	0.246	0.294736842
6	H10	Leu-Leu	0.046	0.047	0.02173913	0.294	0.186	-0.367346939
6	H11	Leu-Met	0.058	0.045	-0.224137931	0.447	0.149	-0.666666667
6	H12	Leu-Phe	0.075	0.116	0.546666667	0.256	0.562	1.1953125
6	H2	Ile-Tyr	0.227	0.052	-0.77092511	0.282	0.203	-0.280141844
6	H3	Ile-Val	0.133	0.054	-0.593984962	0.227	0.194	-0.145374449
6	H4	Leu-Ala	0.144	0.042	-0.708333333	0.516	0.131	-0.746124031
6	H5	Leu-Arg	0.047	0.053	0.127659574	0.343	0.109	-0.682215743
6	H6	Leu-Asp	0.171	0.057	-0.666666667	0.812	0.297	-0.634236453
6	H7	Leu-Glu	0.154	0.05	-0.675324675	0.553	0.481	-0.130198915
6	H8	Leu-Gly	0.291	0.063	-0.783505155	0.635	0.5	-0.212598425
6	H9	Leu-Ile	0.137	0.047	-0.656934307	0.266	0.285	0.071428571

			8 hrs			24 hrs		
Plate	Well	Assay Condition	WT OD590 - t0	*pheP*::Tn OD590 - t0	(*pheP*-WT)/WT	WT OD590 - t0	*pheP*::Tn OD590 - t0	(*pheP*-WT)/WT
7	A1	Negative control	0.189	0.115	-0.391534392	0.414	0.367	-0.11352657
7	A10	Lys-Leu	0.147	0.07	-0.523809524	0.437	0.172	-0.606407323
7	A11	Lys-Lys	0.184	0.108	-0.413043478	0.483	0.348	-0.279503106
7	A12	Lys-Phe	0.189	0.106	-0.439153439	0.393	0.371	-0.055979644
7	A2	Postiive control: L-Glutamine	0.183	0.12	-0.344262295	0.814	0.888	0.090909091
7	A3	Leu-Ser	0.132	0.05	-0.621212121	0.418	0.077	-0.815789474
7	A4	Leu-Trp	0.137	0.082	-0.401459854	0.34	0.302	-0.111764706
7	A5	Leu-Val	0.158	0.077	-0.512658228	0.483	0.29	-0.399585921
7	A6	Leu-Ala	0.297	0.088	-0.703703704	0.321	0.142	-0.557632399
7	A7	Lys-Arg	0.169	0.08	-0.526627219	0.34	0.219	-0.355882353
7	A8	Lys-Glu	0.15	0.092	-0.386666667	0.788	0.544	-0.30964467
7	A9	Lys-Ile	-0.334	0.074	-1.221556886	-0.062	0.188	-4.032258065
7	B1	Lys-Pro	0.181	0.087	-0.519337017	0.21	0.169	-0.195238095
7	B10	Met-Glu	0.193	0.08	-0.585492228	0.835	0.422	-0.494610778
7	B11	Met-Gly	0.245	0.079	-0.67755102	1.163	0.502	-0.568357696
7	B12	Met-His	0.163	0.068	-0.582822086	0.463	0.226	-0.51187905
7	B2	Lys-Ser	0.124	0.075	-0.39516129	0.354	0.143	-0.596045198
7	B3	Lys-Thr	0.245	0.084	-0.657142857	0.748	0.623	-0.167112299
7	B4	Lys-Trp	0.159	0.091	-0.427672956	0.267	0.267	0
7	B5	Lys-Tyr	0.174	0.086	-0.505747126	0.334	0.423	0.266467066
7	B6	Lys-Val	0.172	0.084	-0.511627907	0.4	0.291	-0.2725
7	B7	Met-Arg	0.157	0.076	-0.515923567	0.573	0.298	-0.479930192
7	B8	Met-Asp	0.178	0.078	-0.561797753	0.573	0.218	-0.619546248
7	B9	Met-Gln	0.164	0.084	-0.487804878	0.799	0.21	-0.737171464
7	C1	Met-Ile	0.236	0.07	-0.703389831	0.448	0.101	-0.774553571
7	C10	Phe-Gly	0.296	0.217	-0.266891892	0.974	0.912	-0.063655031
7	C11	Phe-Lie	0.163	0.128	-0.214723926	0.242	0.305	0.260330579
7	C12	Phe-Phe	0.171	0.12	-0.298245614	0.412	0.43	0.04368932
7	C2	Met-Leu	0.199	0.074	-0.628140704	0.627	0.182	-0.709728868
7	C3	Met-Lys	0.174	0.074	-0.574712644	0.425	0.144	-0.661176471
7	C4	Met-Met	0.114	0.043	-0.622807018	0.338	0.179	-0.470414201
7	C5	Met-Phe	0.178	0.124	-0.303370787	0.58	0.52	-0.103448276
7	C6	Met-Pro	0.179	0.077	-0.569832402	0.358	0.277	-0.226256983
7	C7	Met-Trp	0.177	0.085	-0.519774011	0.556	0.446	-0.197841727
7	C8	Met-Val	0.173	0.082	-0.526011561	0.419	0.249	-0.405727924
7	C9	Phe-Ala	0.188	0.13	-0.308510638	0.411	0.345	-0.160583942
7	D1	Phe-Pro	0.163	0.134	-0.17791411	0.306	0.316	0.032679739
7	D10	Pro-Phe	0.425	0.392	-0.077647059	0.899	0.94	0.045606229
7	D11	Pro-Pro	0.211	0.135	-0.360189573	0.257	0.479	0.86381323
7	D12	Pro-Tyr	0.177	0.127	-0.282485876	0.498	0.427	-0.142570281
7	D2	Phe-Ser	0.115	0.102	-0.113043478	0.162	0.217	0.339506173
7	D3	Phe-Trp	0.192	0.172	-0.104166667	0.77	0.836	0.085714286
7	D4	Pro-Ala	0.188	0.071	-0.622340426	0.401	0.14	-0.650872818
7	D5	Pro-Asp	0.175	0.117	-0.331428571	0.399	0.4	0.002506266
7	D6	Pro-Gln	0.222	0.109	-0.509009009	1.008	0.916	-0.091269841
7	D7	Pro-Gly	0.196	0.157	-0.198979592	0.824	0.784	-0.048543689
7	D8	Pro-Hyp	0.188	0.124	-0.340425532	0.428	0.306	-0.285046729
7	D9	Pro-Leu	0.19	0.092	-0.515789474	0.606	0.354	-0.415841584
7	E1	Ser-Ala	0.153	0.079	-0.483660131	0.265	0.097	-0.633962264
7	E10	Ser-Val	0.202	0.095	-0.52970297	0.494	0.162	-0.672064777
7	E11	Thr-Ala	0.284	0.109	-0.616197183	0.349	0.707	1.025787966
7	E12	Thr-Arg	0.167	0.122	-0.269461078	0.253	0.511	1.019762846
7	E2	Ser-Gly	0.213	0.082	-0.615023474	0.707	0.69	-0.024045262
7	E3	Ser-His	0.142	0.076	-0.464788732	0.607	0.209	-0.65568369
7	E4	Ser-Leu	0.166	0.081	-0.512048193	0.316	0.165	-0.477848101
7	E5	Ser-Met	0.189	0.081	-0.571428571	0.662	0.219	-0.66918429
7	E6	Ser-Phe	0.167	0.12	-0.281437126	0.369	0.382	0.035230352
7	E7	Ser-Pro	0.179	0.088	-0.508379888	0.807	0.32	-0.603469641
7	E8	Ser-Ser	0.145	0.081	-0.44137931	0.196	0.137	-0.301020408
7	E9	Ser-Tyr	0.169	0.087	-0.485207101	0.335	0.273	-0.185074627
7	F1	Thr-Glu	0.327	0.131	-0.599388379	0.805	0.385	-0.52173913
7	F10	Trp-Gly	0.259	0.103	-0.602316602	0.627	0.354	-0.435406699
7	F11	Trp-Leu	0.187	0.107	-0.427807487	0.318	0.191	-0.399371069
7	F12	Trp-Lys	0.183	0.125	-0.316939891	0.275	0.447	0.625454545
7	F2	Thr-Gly	0.313	0.11	-0.6485623	0.796	0.737	-0.074120603
7	F3	Thr-Leu	0.268	0.073	-0.72761194	0.66	0.628	-0.048484848
7	F4	Thr-Met	0.246	0.07	-0.715447154	0.734	0.646	-0.119891008
7	F5	Thr-Pro	0.251	0.104	-0.585657371	0.78	0.824	0.056410256
7	F6	Trp-Ala	0.205	0.079	-0.614634146	0.268	0.221	-0.175373134
7	F7	Trp-Arg	0.233	0.094	-0.596566524	0.359	0.22	-0.38718663
7	F8	Trp-Asp	0.17	0.083	-0.511764706	0.285	0.416	0.459649123
7	F9	Trp-Glu	0.236	0.103	-0.563559322	0.585	0.657	0.123076923
7	G1	Trp-Phe	0.18	0.139	-0.227777778	0.284	0.313	0.102112676
7	G10	Tyr-Leu	0.197	0.106	-0.461928934	0.397	0.417	0.050377834
7	G11	Tyr-Lys	0.2	0.096	-0.52	0.386	0.359	-0.069948187
7	G12	Tyr-Phe	0.306	0.339	0.107843137	0.548	0.8	0.459854015
7	G2	Trp-Ser	0.185	0.088	-0.524324324	0.307	0.187	-0.390879479
7	G3	Trp-Trp	0.152	0.111	-0.269736842	0.186	0.178	-0.043010753
7	G4	Trp-Tyr	0.178	0.092	-0.483146067	0.268	0.147	-0.451492537
7	G5	Tyr-Ala	0.206	0.086	-0.582524272	0.41	0.324	-0.209756098
7	G6	Tyr-Gln	0.159	0.083	-0.477987421	0.78	0.64	-0.179487179
7	G7	Tyr-Glu	0.224	0.092	-0.589285714	0.718	0.596	-0.169916435
7	G8	Try-Gly	0.234	0.096	-0.58974359	0.527	0.28	-0.468690702
7	G9	Tyr-His	0.237	0.094	-0.603375527	0.309	0.175	-0.433656958
7	H1	Tyr-Trp	0.176	0.081	-0.539772727	0.565	0.381	-0.325663717
7	H10	Val-Tyr	0.185	0.111	-0.4	0.354	0.33	-0.06779661
7	H11	Val-Val	0.18	0.105	-0.416666667	0.605	0.327	-0.459504132
7	H12	y-Glu-Gly	0.124	0.133	0.072580645	0.233	0.281	0.206008584
7	H2	Tyr-Tyr	0.173	0.096	-0.445086705	0.206	0.173	-0.160194175
7	H3	Val-Arg	0.182	0.095	-0.478021978	0.462	0.286	-0.380952381
7	H4	Val-Asn	0.146	0.089	-0.390410959	0.669	0.625	-0.065769806
7	H5	Val-Asp	0.196	0.096	-0.510204082	0.822	0.566	-0.311435523
7	H6	Val-Gly	0.297	0.095	-0.68013468	0.847	0.399	-0.52892562
7	H7	Val-His	0.191	0.084	-0.560209424	0.664	0.383	-0.423192771
7	H8	Val-Ile	0.204	0.099	-0.514705882	0.592	0.181	-0.694256757
7	H9	Val-Leu	0.228	0.137	-0.399122807	0.444	0.397	-0.105855856

			8 hrs			24 hrs		
Plate	Well	Assay Condition	WT OD590 - t0	*pheP* ::Tn OD590 - t0	(*pheP* -WT)/WT	WT OD590 - t0	*pheP* ::Tn OD590 - t0	(*pheP* -WT)/WT
8	A1	Negative Control	0.173	0.139	-0.196531792	0.145	0.51	2.517241379
8	A10	asp-gly	0.441	0.118	-0.732426304	0.309	0.845	1.734627832
8	A11	glu-ala	0.179	0.076	-0.575418994	0.154	0.633	3.11038961
8	A12	gly-asn	0.434	0.121	-0.721198157	0.264	0.859	2.253787879
8	A2	Positive control: L-Glutamine	0.192	0.129	-0.328125	0.347	0.403	0.161383285
8	A3	Ala-Asp	0.145	0.089	-0.386206897	0.295	0.486	0.647457627
8	A4	Ala-Gln	0.174	0.076	-0.563218391	0.415	0.271	-0.346987952
8	A5	Ala-Ile	0.152	0.072	-0.526315789	0.112	0.197	0.758928571
8	A6	Ala-Met	0.166	0.067	-0.596385542	0.193	0.093	-0.518134715
8	A7	Ala-Val	0.17	0.071	-0.582352941	0.288	0.108	-0.625
8	A8	Asp-Ala	0.172	0.075	-0.563953488	0.56	0.382	-0.317857143
8	A9	asp-gln	0.155	0.076	-0.509677419	0.416	0.591	0.420673077
8	B1	gly-asp	0.261	0.133	-0.490421456	0.249	0.572	1.297188755
8	B10	leu-pro	0.163	0.078	-0.521472393	0.334	0.354	0.05988024
8	B11	leu-tyr	0.169	0.072	-0.573964497	0.162	0.268	0.654320988
8	B12	lys-asp	0.175	0.093	-0.468571429	0.195	0.653	2.348717949
8	B2	gly-ile	0.218	0.081	-0.628440367	0.336	0.476	0.416666667
8	B3	his-ala	0.152	0.078	-0.486842105	0.203	0.214	0.054187192
8	B4	his-glu	0.165	0.088	-0.466666667	0.564	0.585	0.037234043
8	B5	his-his	0.182	0.077	-0.576923077	0.523	0.296	-0.434034417
8	B6	ile-asn	0.173	0.075	-0.566473988	0.811	0.229	-0.717632552
8	B7	ile-leu	0.151	0.062	-0.589403974	0.166	0.197	0.186746988
8	B8	leu-asn	0.164	0.074	-0.548780488	0.659	0.13	-0.802731411
8	B9	leu-his	0.159	0.073	-0.540880503	0.648	0.274	-0.577160494
8	C1	lys-gly	0.252	0.104	-0.587301587	0.253	0.616	1.434782609
8	C10	phe-val	0.149	0.129	-0.134228188	0.338	0.432	0.278106509
8	C11	pro-arg	0.177	0.128	-0.276836158	0.2	0.319	0.595
8	C12	pro-asn	0.237	0.125	-0.47257384	0.222	0.702	2.162162162
8	C2	lys-met	0.179	0.084	-0.530726257	0.141	0.132	-0.063829787
8	C3	met-thr	0.235	0.088	-0.625531915	0.351	0.549	0.564102564
8	C4	met-tyr	0.17	0.08	-0.529411765	0.224	0.146	-0.348214286
8	C5	phe-asp	0.154	0.137	-0.11038961	0.649	0.795	0.224961479
8	C6	phe-glu	0.165	0.138	-0.163636364	0.618	0.785	0.270226537
8	C7	gln-glu	0.123	0.039	-0.682926829	0.48	0.371	-0.227083333
8	C8	phe-met	0.162	0.128	-0.209876543	0.366	0.641	0.75136612
8	C9	phe-tyr	0.225	0.145	-0.355555556	0.2	0.363	0.815
8	D1	pro-glu	0.157	0.117	-0.25477707	0.184	0.277	0.505434783
8	D10	ser-glu	0.188	0.101	-0.462765957	0.509	0.428	-0.15913556
8	D11	thr-asp	0.409	0.143	-0.650366748	0.402	0.832	1.069651741
8	D12	thr-gln	0.297	0.116	-0.609427609	0.196	0.801	3.086734694
8	D2	pro-ile	0.153	0.095	-0.379084967	0.211	0.191	-0.09478673
8	D3	pro-lys	0.181	0.132	-0.270718232	0.208	0.45	1.163461538
8	D4	pro-ser	0.196	0.114	-0.418367347	0.533	0.573	0.075046904
8	D5	pro-trp	0.19	0.109	-0.426315789	0.477	0.457	-0.041928721
8	D6	pro-val	0.165	0.107	-0.351515152	0.241	0.464	0.925311203
8	D7	ser-asn	0.142	0.082	-0.422535211	0.472	0.148	-0.686440678
8	D8	ser-asp	0.148	0.08	-0.459459459	0.552	0.48	-0.130434783
8	D9	ser-gln	0.216	0.083	-0.615740741	0.155	0.199	0.283870968
8	E1	thr-phe	0.244	0.212	-0.131147541	0.277	0.518	0.870036101
8	E10	val-met	0.166	0.117	-0.295180723	0.201	0.332	0.651741294
8	E11	val-phe	0.182	0.142	-0.21978022	0.296	0.613	1.070945946
8	E12	val-pro	0.17	0.069	-0.594117647	0.19	0.414	1.178947368
8	E2	thr-ser	0.253	0.118	-0.533596838	0.467	0.661	0.415417559
8	E3	trp-val	0.167	0.084	-0.497005988	0.114	0.165	0.447368421
8	E4	tyr-ile	0.186	0.089	-0.521505376	0.156	0.3	0.923076923
8	E5	tyr-val	0.164	0.085	-0.481707317	0.239	0.301	0.259414226
8	E6	val-ala	0.201	0.085	-0.577114428	0.416	0.242	-0.418269231
8	E7	val-gln	0.183	0.075	-0.590163934	0.225	0.264	0.173333333
8	E8	val-glu	0.181	0.085	-0.53038674	0.681	0.547	-0.196769457
8	E9	val-lys	0.181	0.112	-0.38121547	0.318	0.473	0.487421384
8	F1	val-ser	0.193	0.082	-0.575129534	0.206	0.18	-0.126213592
8	F10	D-leu-D-leu	0.194	0.12	-0.381443299	0.208	0.359	0.725961538
8	F11	D-leu-gly	0.207	0.141	-0.31884058	0.316	0.622	0.96835443
8	F12	D-leu-tyr	0.197	0.137	-0.304568528	0.227	0.386	0.700440529
8	F2	B-ala-ala	0.245	0.128	-0.47755102	0.218	0.43	0.972477064
8	F3	B-ala-gly	0.182	0.134	-0.263736264	0.18	0.465	1.583333333
8	F4	B-ala-his	0.172	0.149	-0.13372093	0.229	0.355	0.550218341
8	F5	met-B-his	0.181	0.088	-0.513812155	0.271	0.335	0.236162362
8	F6	B-ala-phe	0.184	0.137	-0.255434783	0.295	0.287	-0.027118644
8	F7	D-ala-D-ala	0.173	0.127	-0.265895954	0.256	0.346	0.3515625
8	F8	D-ala-gly	0.206	0.153	-0.257281553	0.465	0.624	0.341935484
8	F9	D-ala-leu	0.177	0.101	-0.429378531	0.294	0.219	-0.255102041
8	G1	y-Glu-gly	0.181	0.137	-0.243093923	0.107	0.375	2.504672897
8	G10	phe-B-ala	0.187	0.167	-0.106951872	0.307	0.553	0.801302932
8	G11	ala-ala-ala	0.178	0.1	-0.438202247	0.203	0.209	0.02955665
8	G12	D-ala-gly-gly	0.282	0.148	-0.475177305	0.243	0.507	1.086419753
8	G2	y-D-glu-gly	0.214	0.135	-0.369158879	0.307	0.377	0.228013029
8	G3	gly-D-ala	0.195	0.151	-0.225641026	0.402	0.324	-0.194029851
8	G4	gly-D-asp	0.646	0.145	-0.775541796	0.34	0.376	0.105882353
8	G5	gly-D-ser	0.203	0.132	-0.349753695	0.288	0.303	0.052083333
8	G6	gly-D-thr	0.207	0.135	-0.347826087	0.255	0.379	0.48627451
8	G7	gly-D-val	-0.418	0.126	-1.301435407	-0.254	0.398	-2.566929134
8	G8	leu-B-ala	0.218	0.108	-0.504587156	0.262	0.346	0.320610687
8	G9	leu-D-leu	0.19	0.135	-0.289473684	0.374	0.32	-0.144385027
8	H1	gly-gly-ala	0.353	0.115	-0.674220963	0.162	0.462	1.851851852
8	H10	leu-leu-leu	0.136	0.084	-0.382352941	0.316	0.183	-0.420886076
8	H11	phe-gly-gly	0.251	0.209	-0.167330677	0.347	0.625	0.801152738
8	H12	tyr-gly-gly	0.068	0.098	0.441176471	0.104	0.285	1.740384615
8	H2	gly-gly-D-leu	0.182	0.141	-0.225274725	0.223	0.576	1.582959641
8	H3	gly-gly-gly	0.316	0.142	-0.550632911	0.37	0.517	0.397297297
8	H4	gly-gly-Ile	0.25	0.102	-0.592	0.318	0.566	0.779874214
8	H5	gly-gly-leu	0.33	0.113	-0.657575758	0.697	0.755	0.083213773
8	H6	gly-gly-phe	0.308	0.209	-0.321428571	0.378	0.666	0.761904762
8	H7	val-tyr-val	0.181	0.097	-0.464088398	0.203	0.196	-0.034482759
8	H8	gly-phe-phe	0.187	0.187	0	0.309	0.544	0.760517799
8	H9	leu-gly-gly	0.323	0.094	-0.708978328	0.782	0.402	-0.485933504

			8 hrs			24 hrs		
Plate	Well	Assay Condition	WT OD590 - t0	*pheP* ::Tn OD590 - t0	(*pheP* -WT)/WT	WT OD590 - t0	*pheP* ::Tn OD590 - t0	(*pheP* -WT)/WT
9	A1	NaCl 1%	1.126	1.151	0.022202487	1.971	1.901	-0.035514967
9	A10	NaCl 8%	0.599	0.33	-0.449081803	1.76	1.558	-0.114772727
9	A11	NaCl 9%	0.567	0.161	-0.716049383	1.716	1.24	-0.277389277
9	A12	NaCl 10%	0.46	-0.154	-1.334782609	1.471	0.965	-0.343983685
9	A2	NaCl 2%	1.164	1.05	-0.097938144	1.967	1.937	-0.015251652
9	A3	NaCl 3%	1.042	1.012	-0.028790787	1.651	1.869	0.132041187
9	A4	NaCl 4%	1.253	0.895	-0.285714286	1.977	1.712	-0.134041477
9	A5	NaCl 5%	0.875	1.085	0.24	1.652	1.987	0.202784504
9	A6	NaCl 5.5%	0.952	0.853	-0.103991597	2.158	1.843	-0.145968489
9	A7	NaCl 6%	0.738	0.329	-0.554200542	1.757	1.541	-0.122936824
9	A8	NaCl 6.5%	0.981	0.573	-0.415902141	2.1	1.523	-0.274761905
9	A9	NaCl 7%	0.79	0.471	-0.403797468	1.948	1.65	-0.152977413
9	B1	NaCl 6%	0.772	0.598	-0.225388601	1.816	1.678	-0.075991189
9	B10	NaCl 6% + Creatine	0.909	0.36	-0.603960396	2.027	1.384	-0.317217563
9	B11	NaCl 6% + Creatinine	0.936	0.375	-0.599358974	2.047	1.552	-0.241817294
9	B12	NaCl 6% + L-Carnitine	0.723	0.577	-0.201936376	1.66	1.628	-0.019277108
9	B2	NaCl 6% + Betaine	0.821	0.6	-0.269183922	1.92	1.716	-0.10625
9	B3	NaCl 6% + N-N Dimethyl Glycine	0.768	0.629	-0.180989583	1.879	1.727	-0.080894093
9	B4	NaCl 6% + Sarcosine	0.795	0.496	-0.376100629	1.818	1.529	-0.158965897
9	B5	NaCl 6% Dimethyl sulphonyl propionate	0.511	0.015	-0.970645793	1.825	0.708	-0.612054795
9	B6	NaCl 6% + MOPS	0.809	0.587	-0.274412855	1.862	1.812	-0.026852846
9	B7	NaCl 6% + Ectione	0.893	0.526	-0.410974244	1.907	1.869	-0.019926586
9	B8	NaCl 6% + Choline	0.948	0.292	-0.691983122	2.148	1.765	-0.1783054
9	B9	NaCl 6% + Phosphoryl Choline	0.711	0.379	-0.466947961	1.889	1.633	-0.13552144
9	C1	NaCl 6% + KCl	0.96	0.755	-0.213541667	1.774	1.809	0.019729425
9	C10	NaCl 6% + Trimethylamine	0.811	0.568	-0.299630086	1.914	1.759	-0.080982236
9	C11	NaCl 6% + Ostopine	0.926	0.935	0.009719222	1.783	2.082	0.167694896
9	C12	NaCl 6% + Trigonelline	0.889	0.836	-0.059617548	1.9	1.777	-0.064736842
9	C2	NaCl 6% + L-Proline	0.81	0.662	-0.182716049	1.928	1.866	-0.032157676
9	C3	NaCl 6% + N-Acetyl L-Glutamine	0.797	0.615	-0.228356336	1.939	1.603	-0.173285199
9	C4	NaCl 6% + Glutamic Acid	0.835	0.567	-0.320958084	1.97	1.731	-0.121319797
9	C5	NaCl 6% + y-Amino-N-Butyric Acid	0.583	0.505	-0.133790738	1.869	1.809	-0.032102729
9	C6	NaCl 6% + Glutatione	1.07	0.793	-0.258878505	2.094	1.891	-0.096943649
9	C7	NaCl 6% + Glycerol	0.688	0.61	-0.113372093	1.985	1.836	-0.075062972
9	C8	NaCl 6% + Trehalose	0.887	0.67	-0.24464487	1.746	1.774	0.016036655
9	C9	NaCl 6% + Trimethylamine-N-oxide	0.742	0.652	-0.121293801	1.936	1.752	-0.095041322
9	D1	Potassium chloride 3%	1.186	1.13	-0.047217538	2.057	2.142	0.041322314
9	D10	Ethylene glycol 10%	0.955	1.101	0.152879581	1.974	2.244	0.136778116
9	D11	Ethylene glycol 20%	0.963	0.926	-0.038421599	1.875	2.224	0.186133333
9	D12	Ethylene glycol 15%	0.877	1.022	0.165336374	1.611	2.114	0.31222843
9	D2	Potassium chloride 4%	1.152	1.054	-0.085069444	2.507	2.468	-0.015556442
9	D3	Potassium chloride 5%	1.188	1.043	-0.122053872	2.399	2.378	-0.008753647
9	D4	Potassium chloride 6%	1.084	1.19	0.097785978	2.351	2.225	-0.053594215
9	D5	Sodium sulfate 2%	1.157	0.917	-0.207433016	2.322	2.114	-0.08957795
9	D6	Sodium sulfate 3%	1.111	1.085	-0.02340234	2.122	2.202	0.037700283
9	D7	Sodium sulfate 4%	1.178	1.247	0.058573854	1.905	2.157	0.132283465
9	D8	Sodium sulfate 5%	1.36	1.33	-0.022058824	2.218	2.139	-0.035617674
9	D9	Ethylene glycol 5%	1.199	1.082	-0.097581318	2.274	2.259	-0.006596306
9	E1	Sodium formate 1%	1.262	1.138	-0.098256735	2.184	2.037	-0.067307692
9	E10	Urea 5%	1.341	1.096	-0.182699478	2.428	2.276	-0.062602965
9	E11	Urea 6%	1.33	1.018	-0.234586466	2.348	2.258	-0.038330494
9	E12	Urea 7%	1.215	0.678	-0.441975309	1.932	1.483	-0.232401656
9	E2	Sodium formate 2%	1.221	1.046	-0.143325143	2.057	1.875	-0.088478367
9	E3	Sodium formate 3%	1.202	1.121	-0.067387687	2.018	1.994	-0.011892963
9	E4	Sodium formate 4%	1.225	0.805	-0.342857143	2.252	2.121	-0.058170515
9	E5	Sodium formate 5%	0.798	0.493	-0.382205514	2.019	2.183	0.081228331
9	E6	Sodium formate 6%	0.427	0.227	-0.468384075	1.698	1.985	0.169022379
9	E7	Urea 2%	1.271	1.094	-0.139260425	2.343	2.267	-0.032437047
9	E8	Urea 3%	1.295	1.029	-0.205405405	2.394	2.26	-0.055973266
9	E9	Urea 4%	1.202	0.88	-0.267886855	2.256	2.069	-0.082890071
9	F1	Sodium Lactate 1%	1.268	0.984	-0.223974763	2.294	2.012	-0.122929381
9	F10	Sodium Lactate 10%	0.199	0.061	-0.693467337	0.153	0.101	-0.339869281
9	F11	Sodium Lactate 11%	0.065	0.078	0.2	0.11	0.111	0.009090909
9	F12	Sodium Lactate 12%	0.046	0.08	0.739130435	0.079	0.107	0.35443038
9	F2	Sodium Lactate 2%	0.873	0.571	-0.345933562	2.156	2.181	0.011595547
9	F3	Sodium Lactate 3%	0.086	0.089	0.034883721	1.536	0.383	-0.750651042
9	F4	Sodium Lactate 4%	0.169	0.073	-0.568047337	0.246	0.129	-0.475609756
9	F5	Sodium Lactate 5%	0.074	0.068	-0.081081081	0.127	0.113	-0.11023622
9	F6	Sodium Lactate 6%	0.076	0.08	0.052631579	0.129	0.123	-0.046511628
9	F7	Sodium Lactate 7%	0.078	0.377	3.833333333	0.131	0.504	2.847328244
9	F8	Sodium Lactate 8%	0.068	0.193	1.838235294	0.138	0.283	1.050724638
9	F9	Sodium Lactate 9%	0.039	0.08	1.051282051	0.093	0.122	0.311827957
9	G1	Sodium Phosphate pH 7 20mM	1.446	1.328	-0.081604426	2.305	2.048	-0.111496746
9	G10	Ammonium Sulfate pH 8 20mM	0.865	0.925	0.069364162	1.702	1.895	0.113396005
9	G11	Ammonium Sulfate pH 8 50mM	1.064	0.256	-0.759398496	2.015	0.895	-0.555831266
9	G12	Ammonium Sulfate pH 8 100mM	0.982	1.013	0.031568228	1.437	1.654	0.151009047
9	G2	Sodium Phosphate pH 7 50mM	1.364	1.426	0.045454545	2.308	2.348	0.017331023
9	G3	Sodium Phosphate pH 7 100mM	1.693	1.424	-0.158889545	2.442	2.417	-0.01023751
9	G4	Sodium Phosphate pH 7 200mM	1.599	1.703	0.06504065	2.187	2.396	0.095564701
9	G5	Sodium Benzoate pH 5.2 20mM	0.89	0.594	-0.33258427	1.661	1.306	-0.213726671
9	G6	Sodium Benzoate pH 5.2 50mM	0.156	0.048	-0.692307692	0.571	0.149	-0.739054291
9	G7	Sodium Benzoate pH 5.2 100mM	0.241	0.088	-0.634854772	0.27	0.123	-0.544444444
9	G8	Sodium Benzoate pH 5.2 200mM	0.101	0.088	-0.128712871	0.125	0.097	-0.224
9	G9	Ammonium Sulfate pH 8 10mM	1.003	1.042	0.03888335	1.861	2.09	0.123052123
9	H1	Sodium Nitrate 10mM	1.313	1.163	-0.114242193	1.639	1.626	-0.007931666
9	H10	Sodium Nitrite 60mM	0.549	0.346	-0.369763206	0.846	0.4	-0.527186761
9	H11	Sodium Nitrite 80mM	0.345	0.307	-0.110144928	0.564	0.319	-0.434397163
9	H12	Sodium Nitrite 100mM	0.587	0.292	-0.502555366	0.776	0.569	-0.266752577
9	H2	Sodium Nitrate 20mM	1.354	1.244	-0.081240768	1.669	1.341	-0.196524865
9	H3	Sodium Nitrate 40mM	1.393	1.316	-0.055276382	1.457	1.844	0.265614276
9	H4	Sodium Nitrate 60mM	1.245	1.384	0.111646586	1.409	1.776	0.260468417
9	H5	Sodium Nitrate 80mM	1.334	1.149	-0.13868066	1.299	1.37	0.054657429
9	H6	Sodium Nitrate 100mM	1.391	1.297	-0.067577283	1.858	1.399	-0.247039828
9	H7	Sodium Nitrite 10mM	1.125	1.04	-0.075555556	1.904	1.978	0.038865546
9	H8	Sodium Nitrite 20mM	0.945	0.826	-0.125925926	1.435	1.25	-0.128919861
9	H9	Sodium Nitrite 40mM	0.603	0.524	-0.131011609	0.692	0.66	-0.046242775

			8 hrs			24 hrs		
Plate	Well	Assay Condition	WT OD590 - t0	*pheP* ::Tn OD590 - t0	(*pheP* -WT)/WT	WT OD590 - t0	*pheP* ::Tn OD590 - t0	(*pheP* -WT)/WT
10	A1	pH 3.5	0.153	0.01	-0.934640523	0.028	0.001	-0.964285714
10	A10	pH 9	1.697	1.515	-0.107248085	2.15	1.977	-0.080465116
10	A11	pH 9.5	1.625	1.514	-0.068307692	1.967	2.108	0.071682766
10	A12	pH 10	1.749	1.4	-0.199542596	1.903	1.973	0.036784025
10	A2	pH 4	0.187	0.054	-0.711229947	0.066	0.008	-0.878787879
10	A3	pH 4.5	0.177	0.082	-0.536723164	0.057	0.029	-0.49122807
10	A4	pH 5	0.593	0.355	-0.401349073	0.98	0.678	-0.308163265
10	A5	pH 5.5	1.008	0.83	-0.176587302	1.463	1.589	0.086124402
10	A6	pH 6	1.215	1.087	-0.105349794	1.899	1.889	-0.005265929
10	A7	pH 7	1.438	1.353	-0.059109875	2.063	2.122	0.028599127
10	A8	pH 8	1.538	1.428	-0.071521456	2.179	2.096	-0.038090867
10	A9	pH 8.5	1.682	1.443	-0.142092747	2.12	2.098	-0.010377358
10	B1	pH 4.5	0.143	0.061	-0.573426573	0.034	0.014	-0.588235294
10	B10	pH 4.5 + L-Isoleucine	0.102	0.32	2.137254902	-0.067	0.08	-2.194029851
10	B11	pH 4.5 + L-Leucine	0.256	0.244	-0.046875	0.009	0.025	1.777777778
10	B12	pH 4.5 + L-Lysine	0.146	0.072	-0.506849315	-0.003	0.065	-22.66666667
10	B2	pH 4.5 + L-Alanine	0.136	0.025	-0.816176471	-0.033	-0.049	0.484848485
10	B3	pH 4.5 + L-Arginine	0.191	0.177	-0.073298429	0.04	-0.051	-2.275
10	B4	pH 4.5 + L-Asparagine	0.223	0.254	0.139013453	0.14	0.131	-0.064285714
10	B5	pH 4.5 + L-Aspartic Acid	0.193	0.236	0.222797927	0.128	0.079	-0.3828125
10	B6	pH 4.5 + L-Glutamic Acid	0.275	0.197	-0.283636364	0.103	0.072	-0.300970874
10	B7	pH 4.5 + L-Glutamine	0.334	0.294	-0.119760479	0.117	0.138	0.179487179
10	B8	pH 4.5 + L-Glycine	0.265	0.304	0.147169811	0.168	0.142	-0.154761905
10	B9	pH 4.5 + L-Histidine	0.277	0.293	0.057761733	0.182	0.108	-0.406593407
10	C1	pH 4.5 + L-Methionine	0.22	0.049	-0.777272727	0.046	0.024	-0.47826087
10	C10	pH 4.5 + L-Ornithine	0.344	0.278	-0.191860465	0.127	0.128	0.007874016
10	C11	pH 4.5 + L-Homoarginine	0.184	0.204	0.108695652	-0.022	-0.032	0.454545455
10	C12	pH 4.5 + L-Homoserine	0.236	0.127	-0.461864407	0.039	0.098	1.512820513
10	C2	pH 4.5 + L-Phenylalanine	0.241	0.262	0.087136929	0.102	0.002	-0.980392157
10	C3	pH 4.5 + L-Proline	0.3	0.3	0	0.251	0.226	-0.099601594
10	C4	pH 4.5 + L-Serine	0.261	0.306	0.172413793	0.267	0.145	-0.456928839
10	C5	pH 4.5 + L-Threonine	0.34	0.275	-0.191176471	0.111	0.256	1.306306306
10	C6	pH 4.5 + L-Tryptophan	0.273	0.284	0.04029304	0.104	0.176	0.692307692
10	C7	pH 4.5 + L-Citrulline	0.543	0.28	-0.484346225	0.283	0.201	-0.28975265
10	C8	pH 4.5 + L-Valine	0.348	0.329	-0.054597701	0.197	0.199	0.010152284
10	C9	pH 4.5 + Hydroxy-L-Proline	0.295	0.117	-0.603389831	0.175	0.035	-0.8
10	D1	pH 4.5 + Anthranillic Acid	0.027	0.053	0.962962963	-0.119	0.03	-1.25210084
10	D10	pH 4.5 + D,L-Diamino-Pimelic Acid	0.303	0.291	-0.03960396	0.09	0.129	0.433333333
10	D11	pH 4.5 + Trimethylamine-N-oxide	0.252	0.256	0.015873016	0.083	0.087	0.048192771
10	D12	pH 4.5 + Urea	0.061	-0.028	-1.459016393	-0.133	0.972	-8.308270677
10	D2	pH 4.5 + L-Norleucine	0.224	0.088	-0.607142857	0.131	-0.038	-1.290076336
10	D3	pH 4.5 + L-Norvaline	0.284	0.235	-0.172535211	0.233	0.285	0.223175966
10	D4	pH 4.5 + a-Amino-N-Butyric Acid	0.254	0.278	0.094488189	0.257	0.217	-0.155642023
10	D5	pH 4.5 + p-Amino-Benzoic Acid	0.291	0.246	-0.154639175	0.238	0.23	-0.033613445
10	D6	pH 4.5 + L-Cysteic Acid	0.307	0.271	-0.117263844	0.177	0.239	0.350282486
10	D7	pH 4.5 + L-Lysine	0.205	0.365	0.780487805	0.217	0.202	-0.069124424
10	D8	pH 4.5 + 5-Hydroxy Lysine	0.306	0.178	-0.418300654	0.183	0.162	-0.114754098
10	D9	pH 4.5 + 5-Hydroxy Tryptophan	0.286	0.245	-0.143356643	0.211	0.208	-0.014218009
10	E1	pH 9.5	1.457	1.363	-0.064516129	2.006	1.722	-0.141575274
10	E10	pH 9.5 + L-Isoleucine	1.87	1.486	-0.205347594	1.718	1.778	0.034924331
10	E11	pH 9.5 + L-Leucine	1.621	1.501	-0.074028378	1.677	1.568	-0.064997018
10	E12	pH 9.5 + L-Lysine	1.62	1.442	-0.109876543	1.48	1.659	0.120945946
10	E2	pH 9.5 + L-Alanine	1.74	1.663	-0.044252874	1.968	1.81	-0.080284553
10	E3	pH 9.5 + L-Arginine	1.799	1.716	-0.046136743	2.048	2.33	0.137695313
10	E4	pH 9.5 + L-Asparagine	1.68	1.598	-0.048809524	1.96	2.033	0.037244898
10	E5	pH 9.5 + L-Aspartic Acid	1.712	1.568	-0.08411215	2.143	2.066	-0.035930938
10	E6	pH 9.5 + L-Glutamic Acid	1.75	1.852	0.058285714	1.984	2.301	0.159778226
10	E7	pH 9.5 + L-Glutamine	1.857	1.88	0.012385568	2.033	2.244	0.103787506
10	E8	pH 9.5 + L-Glycine	1.732	1.848	0.066974596	2.017	2.268	0.124442241
10	E9	pH 9.5 + L-Histidine	1.591	1.57	-0.013199246	1.618	1.792	0.107540173
10	F1	pH 9.5 + L-Methionine	1.631	0.852	-0.477621091	1.743	1.187	-0.318990247
10	F10	pH 9.5 + L-Ornithine	1.261	0.873	-0.307692308	1.524	1.059	-0.30511811
10	F11	pH 9.5 + L-Homoarginine	1.719	1.487	-0.134962187	2.121	1.79	-0.156058463
10	F12	pH 9.5 + L-Homoserine	1.625	1.568	-0.035076923	1.594	1.775	0.113550816
10	F2	pH 9.5 + L-Phenylalanine	1.589	1.596	0.004405286	1.574	1.73	0.099110546
10	F3	pH 9.5 + L-Proline	1.707	1.576	-0.076742824	2.167	2.195	0.012921089
10	F4	pH 9.5 + L-Serine	1.803	1.715	-0.048807543	2.134	2.11	-0.011246485
10	F5	pH 9.5 + L-Threonine	1.737	1.64	-0.055843408	1.914	2.129	0.112330199
10	F6	pH 9.5 + L-Tryptophan	1.631	1.448	-0.112201104	2.021	2.006	-0.007422068
10	F7	pH 9.5 + L-Citrulline	1.885	2.029	0.076392573	2.349	2.613	0.11238825
10	F8	pH 9.5 + L-Valine	1.777	1.759	-0.010129432	2.148	1.998	-0.069832402
10	F9	pH 9.5 + Hydroxy-L-Proline	1.725	1.635	-0.052173913	1.996	2.097	0.050601202
10	G1	pH 9.5 + Anthranillic Acid	1.637	1.628	-0.005497862	1.712	1.78	0.039719626
10	G10	pH 9.5 + Creatine	1.609	1.546	-0.039154755	2.069	2.198	0.062348961
10	G11	pH 9.5 + Trimethylamine-N-oxide	0.181	1.255	5.933701657	0.672	1.862	1.770833333
10	G12	pH 9.5 + Urea	1.509	1.051	-0.30351226	1.946	1.633	-0.160842754
10	G2	pH 9.5 + L-Norleucine	1.621	1.698	0.047501542	1.546	1.871	0.210219922
10	G3	pH 9.5 + L-Norvaline	1.844	1.705	-0.07537961	2.086	1.91	-0.084372004
10	G4	pH 9.5 + Agmatine	0.481	0.411	-0.145530146	0.489	0.45	-0.079754601
10	G5	pH 9.5 + Cadaverine	0.582	0.421	-0.276632302	0.641	0.449	-0.299531981
10	G6	pH 9.5 + Putrescine	0.398	0.53	0.331658291	1.904	2.103	0.104516807
10	G7	pH 9.5 + Histamine	0.553	0.586	0.059674503	1.306	1.437	0.100306279
10	G8	pH 9.5 + Phenylethylamine	0.641	0.564	-0.120124805	0.418	0.369	-0.11722488
10	G9	pH 9.5 + Tyramine	0.501	0.761	0.518962076	0.397	0.641	0.614609572
10	H1	X-Caprylate	0.889	1.037	0.16647919	0.609	0.684	0.123152709
10	H10	X-a-D-Mannoside	1.413	1.302	-0.078556263	1.641	1.616	-0.015234613
10	H11	X-PO4	1.382	1.214	-0.121562952	1.066	0.815	-0.235459662
10	H12	X-SO4	1.456	1.342	-0.078296703	1.864	1.749	-0.061695279
10	H2	X-a-D-Glucoside	1.415	1.221	-0.137102473	1.228	1.233	0.004071661
10	H3	X-B-D-Glucoside	1.36	1.244	-0.085294118	1.811	1.738	-0.040309221
10	H4	X-a-D-Galactoside	1.67	1.492	-0.106586826	2.142	1.802	-0.158730159
10	H5	X-B-D-Galactoside	1.566	1.394	-0.109833972	1.661	1.619	-0.025285972
10	H6	X-a-D-Glucuronide	1.545	1.327	-0.141100324	2.076	1.911	-0.079479769
10	H7	X-B-D-Glucuronide	1.404	1.249	-0.11039886	1.905	1.851	-0.028346457
10	H8	X-B-D-Glucosaminide	1.551	1.197	-0.228239845	1.833	1.797	-0.019639935
10	H9	X-B-D-Galactosaminide	1.443	1.253	-0.131670132	1.783	1.886	0.057767807

APPENDIX B. Hyperglycemia transposon sequencing results

Table B1. *S. aureus* genes identified as essential for bacterial survival during osteomyelitis in hyperglycemic mice (Dval<0.01) by TnSeq analysis. *In vitro* condition n = 2 and vehicle and STZ conditions n = 6. Red indicates Dval<0.01, yellow indicates Dval<0.1.

USA 300 Locus	USA 300 Annotation	Avg *In vitro* Dval	Avg Vehicle Dval	Avg STZ Dval	Dval ratio STZ/Vehicle	Compromised in vitro?	Compromised in Vehicle?
SAUSA300_2214	FmhB protein	0.020991915	0.094326519	0.00025935	0.002749488	X	X
SAUSA300_1887	geranylgeranylglyceryl phosphate synthase family protein, PcrB	0.070869336	0.046393414	0.001800544	0.038810333	X	X
SAUSA300_1682	catabolite control protein A	0.069810323	0.070937935	0.00025935	0.003656007	X	X
SAUSA300_0625	teichoic acid ABC transporter protein	0.029919695	0.031364059	0.00025935	0.008269007	X	X
SAUSA300_0751	tRNA-Arg	1.889152853	1.851989131	0.00025935	0.000140038		
SAUSA300_0348	twin-arginine translocation protein, TatA/E family	0.16848963	0.049664834	0.00025935	0.005221997		X
SAUSA300_1914	GntR family regulatory protein	0.330968221	0.192469964	0.00025935	0.001347481		
SAUSA300_1823	tRNA-Ser	0.060184268	0.024885775	0.002757285	0.110797648	X	X
SAUSA300_1406	phiSLT ORF 104b-like protein	0.74744902	0.068407846	0.003325035	0.048606041		X
SAUSA300_1825	tRNA-Ser	0.048246778	0.028714742	0.003813889	0.132819877	X	X
SAUSA300_1629	threonyl-tRNA synthetase	0.075079895	0.082220633	0.007987498	0.097147126	X	X
SAUSA300_1726	crcB family protein	0.154933519	0.488635818	0.009247294	0.018924716		
SAUSA300_1614	glutamate-1-semialdehyde-2,1-aminomutase	0.085759764	0.260423627	0.00409181	0.015712131	X	
SAUSA300_1513	superoxide dismutase (Mn/Fe family)	0.120544879	0.260160466	0.00025935	0.000996883		
SAUSA300_1593	protein-export membrane protein SecF	0.022864608	0.015902672	0.00045796	0.028797671	X	X
SAUSA300_0763	carboxylesterase	0.010841799	0.023273827	0.005022352	0.215793983	X	X
SAUSA300_1591	adenine phosphoribosyltransferase	0.252611739	0.662257121	0.00025935	0.000391615		
SAUSA300_1095	carbamoyl-phosphate synthase, small subunit	0.037906039	0.094168636	0.00025935	0.002754098	X	X
SAUSA300_0996	dihydrolipoamide dehydrogenase	0.023146317	0.04582584	0.00025935	0.005659462	X	X
SAUSA300_2606	imidazole glycerol phosphate synthase subunit hisF	0.775787559	1.135878683	0.00025935	0.000228325		
SAUSA300_2219	molybdenum cofactor biosynthesis protein A	0.452548966	0.592059977	0.00025935	0.000438046		
SAUSA300_1182	pyruvate ferredoxin oxidoreductase, alpha subunit	0.025617394	0.027474566	0.000492468	0.017924514	X	X
SAUSA300_1195	tRNA delta(2)-isopentenylpyrophosphate transferase	0.085444189	0.075367971	0.000915064	0.012141287	X	X
SAUSA300_2292	isopentenyl-diphosphate delta-isomerase	0.021328702	0.02884698	0.001878126	0.065106502	X	X
SAUSA300_1112	protein phosphatase 2C domain protein	0.254133761	0.083398413	0.002027568	0.024311835		X
SAUSA300_1096	carbamoyl-phosphate synthase, large subunit	0.030947419	0.108403898	0.00258671	0.023861783	X	
SAUSA300_0945	isochorismate synthase family protein	0.089671405	0.094674924	0.008190423	0.086511005	X	X
SAUSA300_0235	L-lactate dehydrogenase	0.150432582	0.074266515	0.009058892	0.12197815		X
SAUSA300_0454	recombination protein RecR	0.095745825	0.558699253	0.00025935	0.000464203	X	
SAUSA300_1039	ribonuclease HIII	0.136490304	0.487391617	0.00025935	0.000532118		
SAUSA300_1468	DNA repair protein RecN	0.034929421	0.082606821	0.001238931	0.014997929	X	X
SAUSA300_1251	DNA topoisomerase IV, subunit A	0.091358919	0.094223246	0.003733489	0.039623862	X	X
SAUSA300_1656	universal stress protein family	0.05378754	0.366091114	0.007202291	0.019673494	X	
SAUSA300_0006	DNA gyrase, A subunit	0.029066593	0.024980373	0.007379942	0.29542963	X	X
SAUSA300_1420	conserved hypothetical phage protein	0.4880503	0.128728995	0.00025935	0.002014695		
SAUSA300_0792	conserved hypothetical protein	1.541986809	6.170506545	0.00025935	4.20305E-05		
SAUSA300_0933	conserved hypothetical protein	0.025345578	5.464665996	0.00025935	4.74594E-05	X	
SAUSA300_1794	conserved hypothetical protein	0.087631903	3.072085103	0.00025935	8.44214E-05	X	
SAUSA300_1552	conserved hypothetical protein	0.156728111	1.541411799	0.00025935	0.000168255		
SAUSA300_0931	conserved hypothetical protein	2.127720434	1.236444995	0.00025935	0.000209754		
SAUSA300_1797	conserved hypothetical protein	0.515071025	0.989799861	0.00025935	0.000262022		
SAUSA300_0957	conserved hypothetical protein	0.108430987	0.974442154	0.00025935	0.000266152		
SAUSA300_1175	conserved hypothetical protein	0.034303278	0.831389257	0.00025935	0.000311947	X	
SAUSA300_1012	conserved hypothetical protein	0.507879292	0.744755314	0.00025935	0.000348235		
SAUSA300_1040	conserved hypothetical protein	0.468988469	0.575949279	0.00025935	0.000450299		
SAUSA300_1721	conserved hypothetical protein	0.357157659	0.445423396	0.00025935	0.000582254		
SAUSA300_1215	conserved hypothetical protein	1.421378703	0.345528858	0.00025935	0.000750587		
SAUSA300_0937	conserved hypothetical protein	0.093906093	0.317384979	0.00025935	0.000817145	X	
SAUSA300_1572	conserved hypothetical protein	0.082547995	0.302665078	0.00025935	0.000856887	X	
SAUSA300_0847	conserved hypothetical protein	0.029609372	0.262979047	0.00025935	0.000986199	X	
SAUSA300_0997	conserved hypothetical protein	0.216547238	0.21016794	0.00025935	0.001234011		
SAUSA300_1010	conserved hypothetical protein	0.764604237	0.204717532	0.00025935	0.001266866		
SAUSA300_1084	conserved hypothetical protein	1.26286161	0.161939258	0.00025935	0.001601524		
SAUSA300_2132	conserved hypothetical protein	0.148202578	0.117905356	0.00025935	0.002199642		
SAUSA300_1204	conserved hypothetical protein	0.422677465	0.111673209	0.00025935	0.002322398		
SAUSA300_0906	conserved hypothetical protein	0.070339456	0.033978822	0.00025935	0.007632684	X	X
SAUSA300_2547	conserved hypothetical protein	0.095537371	0.028611597	0.00025935	0.009064493	X	X
SAUSA300_0857	conserved hypothetical protein	0.091275779	0.02129396	0.00025935	0.012179492	X	X
SAUSA300_1935	phi77 ORF029-like protein	0.109362926	0.691880947	0.00025935	0.000374847		
SAUSA300_1429	phiSLT ORF53-like protein	0.397280812	0.737758677	0.00025935	0.000351537		
SAUSA300_1411	phiSLT ORF66-like protein	0.357076945	1.630466604	0.00025935	0.000159065		
SAUSA300_0663	putative lipoprotein	0.127588782	0.542002141	0.00025935	0.000478503		
SAUSA300_1492	putative lipoprotein	0.034035853	0.016867858	0.00025935	0.015375374	X	X
SAUSA300_0035	truncated hypothetical protein	0.660124585	1.710639102	0.00025935	0.00015161		
SAUSA300_2143	conserved hypothetical protein	0.505895254	0.887672785	0.000579076	0.000652353		
SAUSA300_1414	phiSLT ORF 78B-like protein	0.241319969	0.228570322	0.001695388	0.007417358		
SAUSA300_1757	serine protease SplB	0.611947673	0.29361746	0.002147651	0.007314453		
SAUSA300_0026	conserved hypothetical protein OrfX	0.180468185	0.532053966	0.005190957	0.009756448		
SAUSA300_1924	holin	1.013877153	0.961253799	0.006689285	0.006958916		
SAUSA300_0920	conserved hypothetical protein	0.88238289	0.264643647	0.008888675	0.033587336		
SAUSA300_1342	conserved hypothetical protein	0.331375464	0.711509767	0.009564624	0.013442717		

Table B2. *S. aureus* transposon mutants with compromised fitness during osteomyelitis (Dval<0.1) in hyperglycemic mice but not *in vitro* or in euglycemic infection, as identified by TnSeq analysis. *In vitro* condition n = 2 and vehicle and STZ conditions n = 6. Yellow indicates Dval<0.1.

USA 300 Locus	USA 300 Annotation	Avg *In vitro* Dval	Avg Vehicle Dval	Avg STZ Dval	Dval ratio STZ/Vehicle
SAUSA300_0308	ABC transporter, permease protein	0.490129267	0.616006153	0.04638433	0.075298485
SAUSA300_1345	asparaginyl-tRNA synthetase	0.28993173	0.384617317	0.089353624	0.232318256
SAUSA300_0513	glutamyl-tRNA synthetase	0.228018682	0.345086043	0.07992978	0.231622754
SAUSA300_2033	K+-transporting ATPase, B subunit	0.659266028	0.858809426	0.095885776	0.111649655
SAUSA300_0988	potassium uptake protein	0.237775911	0.111706618	0.057297718	0.512930385
SAUSA300_1170	transcriptional regulator, GntR family	0.142635526	0.165520727	0.025030655	0.151223692
SAUSA300_0447	tRNA-Ser	0.20266131	0.159350456	0.017772006	0.1115278
SAUSA300_1866	two-component sensor histidine kinase	0.332279995	0.136079582	0.052853823	0.388403769
SAUSA300_0577	putative transcriptional regulator	0.420486787	0.335787199	0.057317191	0.170694986
SAUSA300_2563	putative transcriptional regulator	0.383700014	0.527249454	0.061897954	0.117397853
SAUSA300_0195	RpiR family transcriptional regulator	0.54536562	0.546072748	0.063949659	0.117108314
SAUSA300_1455	transcriptional regulator, AraC family	0.196767634	0.658233132	0.011568928	0.01757573
SAUSA300_1007	inositol monophosphatase family protein	0.593825633	0.462676534	0.048941843	0.105779824
SAUSA300_1512	penicillin-binding protein 3	0.171050585	0.215631267	0.084985941	0.394126242
SAUSA300_1055	fibrinogen-binding protein	0.179843532	0.394810617	0.08113842	0.205512254
SAUSA300_0116	iron compound ABC transporter, permease protein SirB	0.64608191	0.345858849	0.088075879	0.254658452
SAUSA300_0344	putative lipoprotein	0.872103781	0.198330697	0.012148062	0.061251548
SAUSA300_0999	spermidine/putrescine ABC transporter, ATP-binding protein	0.141300437	0.241180257	0.071312061	0.295679514
SAUSA300_1001	spermidine/putrescine ABC transporter, permease protein	0.29457968	0.563537419	0.068006349	0.12067761
SAUSA300_1002	spermidine/putrescine ABC transporter, spermidine/putrescine-binding protein	0.470846857	0.116560701	0.078960879	0.677422818
SAUSA300_1299	putative tellurite resistance protein	0.54102266	0.419832776	0.034791561	0.082870046
SAUSA300_2485	methylated DNA-protein cysteine methyltransferase	0.176764323	0.791211693	0.062870275	0.07946075
SAUSA300_1605	rod shape-determining protein MreC	0.202646722	0.28830262	0.043707016	0.151601175
SAUSA300_1305	2-oxoglutarate dehydrogenase, E2 component, dihydrolipoamide succinyltransferase	0.679241823	0.319254525	0.07389339	0.231456045
SAUSA300_1564	acetyl-CoA carboxylase, biotin carboxyl carrier protein	0.667675803	0.543935123	0.069754138	0.128239812
SAUSA300_1313	carboxyl-terminal protease	0.242227458	1.072594694	0.036930222	0.034430733
SAUSA300_0838	D-alanine-activating enzyme/D-alanine-D-alanyl, dltD protein	0.17974059	0.251368359	0.0793988	0.315866325
SAUSA300_0697	exsB protein	0.112322392	0.142136076	0.040576882	0.285479118
SAUSA300_2225	molybdenum cofactor biosynthesis protein C	0.375367234	0.965802373	0.056287487	0.058280544
SAUSA300_0825	oxidoreductase, 2-nitropropane dioxygenase family	0.659249281	0.159186387	0.054550817	0.342685185
SAUSA300_0970	phosphoribosylformylglycinamidine synthase I	0.376887983	1.460463933	0.08585366	0.058785197
SAUSA300_1491	proline dipeptidase	0.354546449	0.266255534	0.057604766	0.216351432
SAUSA300_1315	PTS system, glucose-specific IIA component	0.249049869	1.066831826	0.010480373	0.009823829
SAUSA300_1139	succinyl-CoA synthetase, alpha subunit	0.262959204	5.560403062	0.042623393	0.007665522
SAUSA300_0665	acetyltransferase, GNAT family	1.520691788	1.170260557	0.015634564	0.0133599
SAUSA300_0441	acetyltransferase, GNAT family	0.482284534	0.120050847	0.099452841	0.828422646
SAUSA300_1428	conserved hypothetical phage protein	0.48799898	0.101006121	0.068385681	0.677044911
SAUSA300_1853	conserved hypothetical protein	0.942138437	0.851636431	0.010672903	0.01253223
SAUSA300_1325	conserved hypothetical protein	0.134563734	0.122955109	0.012574423	0.102268404
SAUSA300_2529	conserved hypothetical protein	0.612560461	0.694862082	0.013381314	0.019257511
SAUSA300_0465	conserved hypothetical protein	0.604635956	1.972033824	0.016821858	0.008530208
SAUSA300_0243	conserved hypothetical protein	0.969005409	0.181318046	0.028888277	0.159323782
SAUSA300_1053	conserved hypothetical protein	0.197818757	0.148849753	0.0366234	0.246042731
SAUSA300_1692	conserved hypothetical protein	0.275412435	1.359637166	0.037299294	0.02743327
SAUSA300_0463	conserved hypothetical protein	0.270556045	1.057420462	0.039995047	0.037823221
SAUSA300_1203	conserved hypothetical protein	0.531534288	0.776550662	0.048808058	0.062852381
SAUSA300_1706	conserved hypothetical protein	0.444288959	0.406692208	0.068359788	0.168087283
SAUSA300_1041	conserved hypothetical protein	0.18760876	0.817839638	0.076825237	0.093936798
SAUSA300_0655	conserved hypothetical protein	0.531852992	0.280626734	0.078598402	0.280081661
SAUSA300_1100	conserved hypothetical protein	0.581057373	0.301069795	0.079501488	0.264063314
SAUSA300_1277	conserved hypothetical protein	0.881983734	0.32147742	0.091989402	0.286145763
SAUSA300_0831	conserved hypothetical protein	0.294392218	0.31983834	0.092847751	0.290295877
SAUSA300_0011	conserved hypothetical protein	0.378838704	0.271835843	0.093822136	0.345142622
SAUSA300_1937	phi77 ORF045-like protein	1.694587616	1.207502983	0.043863462	0.036325759
SAUSA300_1405	phiSLT ORF 101-like protein, terminase, small subunit	0.526834837	0.15704799	0.092398826	0.588347714
SAUSA300_1399	phiSLT ORF110-like protein	0.763083833	0.101516588	0.055925305	0.550898196
SAUSA300_1395	phiSLT ORF116b-like protein	0.584689284	1.364661215	0.08633539	0.063265072
SAUSA300_1376	putative lipoprotein	0.662293021	0.510554721	0.014378699	0.028162896
SAUSA300_0913	putative membrane protein	0.449496615	0.540341288	0.081939014	0.151643074
SAUSA300_0316	ROK family protein	0.817666261	0.589156867	0.069467005	0.117909183
SAUSA300_0658	transcriptional regulator, LysR family	0.160756131	0.430252834	0.082636901	0.192065907

REFERENCES

1. Butrico CE, Cassat JE. Quorum sensing and toxin production in *Staphylococcus aureus* osteomyelitis: pathogenesis and paradox. *Toxins (Basel)*. 2020;12(8). doi:10.3390/TOXINS12080516

2. Wilde AD, Snyder DJ, Putnam NE, Valentino MD, Hammer ND, Longeran ZR, et al. Bacterial hypoxic responses revealed as critical determinants of the host-pathogen outcome by TnSeq analysis of *Staphylococcus aureus* invasive infection. *PLoS Pathog*. 2015;11(12). doi:10.1371/journal.ppat.1005341

3. Cassat JE, Hammer ND, Campbell JP, Benson MA, Perrien DS, Mrak LN, et al. A secreted bacterial protease tailors the *Staphylococcus aureus* virulence repertoire to modulate bone remodeling during osteomyelitis. *Cell Host Microbe*. 2013;13(6):759-772. doi:10.1016/j.chom.2013.05.003

4. Brandt SL, Putnam NE, Cassat JE, Serezani CH. Innate immunity to *Staphylococcus aureus*: evolving paradigms in soft tissue and invasive infections. *J Immunol*. 2018;200(12):3871-3880. doi:10.4049/jimmunol.1701574

5. Kavanagh N, Ryan EJ, Widaa A, Sexton G, Fennell J, O'Rourke S, et al. Staphylococcal osteomyelitis: disease progression, treatment challenges, and future directions. *Clin Microbiol Rev*. 2018;31(2). doi:10.1128/CMR.00084-17

6. Farnsworth CW, Shehatou CT, Maynard R, Nishitani K, Kates SL, Zuscik MJ, et al. A humoral immune defect distinguishes the response to *Staphylococcus aureus* infections in mice with obesity and type 2 diabetes from that in mice with type 1 diabetes. *Infect Immun*. 2015;83(6):2264-2274. doi:10.1128/IAI.03074-14

7. Giai Via A, Mccarthy MB, Francke M, Oliva F, Mazzocca AD, Maffulli N. Hyperglycemia induces osteogenic differentiation of bone marrow derived stem cells: an *in vitro* study. *J Transl Sci*. 2020;7:1-8. doi: 10.15761/JTS.1000417

8. Catalfamo DL, Britten TM, Storch DI, Calderon NL, Sorenson HL, Wallet SM. Hyperglycemia induced and intrinsic alterations in type 2 diabetes-derived osteoclast function. *Oral Dis*. 2013;19(3):303-312. doi:10.1111/odi.12002

9. Jafar N, Edriss H, Nugent K. The effect of short-term hyperglycemia on the innate immune system. *Am J M Sc*. 2016;351(2):201-211. doi:10.1016/j.amjms.2015.11.011

10. Khan RMM, Chua ZJY, Tan JC, Yang Y, Liao Z, Zhao Y. From pre-diabetes to diabetes: diagnosis, treatments, and translational research. *Medicina*. 2019;55(9):546. doi:10.3390/MEDICINA55090546

11. Gedela V, Gosala SL. Diabetes a risk for antimicrobial resistance? *Int J Basic Clin Pharmacol*. 2017;6(12):2811-2814. doi:10.18203/2319-2003.IJBCP20175103

12. Lew DP, Waldvogel FA. Osteomyelitis. *Lancet*. 2004;364(9431):369-79. doi:10.1016/S0140-6736(04)16727-5

13. Olson ME, Horswill AR. *Staphylococcus aureus* osteomyelitis: bad to the bone. *Cell Host Microbe*. 2013;13(6):629. doi:10.1016/J.CHOM.2013.05.015

14. Cassat JE, Gimza BD. Mechanisms of antibiotic failure during *Staphylococcus aureus* osteomyelitis. *Front Immunol.* 2021;12:638085. doi:10.3389/fimmu.2021.638085

15. Belthur MV, Birchansky SB, Verugo AA, Mason EO Jr., Hulten KG, Kaplan SL, Smith EO, Phillips WA WJ. Pathologic fractures in children with acute *Staphylococcus aureus* osteomyelitis. *J Bone Joint Surg Am*. 2012;94(1):34-42. doi:10.2106/JBS.J.01915

16. Garcia Del Pozo E, Collazos J, Carton JA, Camporro D, Asensi V. Factors predictive of relapse in adult bacterial osteomyelitis of long bones. *BMC Infect Dis*. 2018;18(1):1-11. doi:10.1186/S12879-018-3550-6

17. Urish KL, Cassat JE. *Staphylococcus aureus* osteomyelitis: Bone, bugs, and surgery. *Infect Immun*. 2020;88(7). doi:10.1128/IAI.00932-19

18. Spagnolo N, Greco F, Rossi A, Ciolli L, Teti A, Posteraro P. Chronic staphylococcal osteomyelitis: a new experimental rat model. *Infect Immun*. 1993;61(12):5225-5230. doi: 10.1128/iai.61.12.5225-5230.1993

19. Power ME, Olson ME, Domingue PAG, Costerton JW. A rat model of *Staphylococcus aureus* chronic osteomyelitis that provides a suitable system for studying the human infection. *J Med Microbiol*. 1990;33(3):189-198. doi:10.1099/00222615-33-3-189

20. Alderson M, Speers D, Emslie K, Nade S. Acute haematogenous osteomyelitis and septic arthritis--a single disease. An hypothesis based upon the presence of transphyseal blood vessels. *J Bone Joint Surg Br*. 1986;68(2):268-274. doi: 10.1302/0301-620X.68B2.3958014

21. Harik NS, Smeltzer MS. Management of acute hematogenous osteomyelitis in children. *Expert Rev Anti Infect Ther*. 2010;8(2):175-181. doi:10.1586/eri.09.130

22. Hatzenbuehler J, Pulling TJ. Diagnosis and management of osteomyelitis. *Am Fam Physician*. 2011.1;84(9). doi:10.2165/00019053-199916060-00003

23. Hannan C, Attinger C. Special considerations in the management of osteomyelitis defects (diabetes, the ischemic or dysvascular bed, and irradiation). *Semin Plast Surg*. 2009;23(2):132-140. doi:10.1055/s-0029-1214165

24. de Mesy Bentley KL, Trombetta R, Nishitani K, Bello-Irizarry SN, Ninomiya M, Zhang L, et al. Evidence of *Staphylococcus aureus* deformation, proliferation, and migration in canaliculi of live cortical bone in murine models of osteomyelitis. *J Bone Miner Res*. 2017;32(5):985-990. doi:10.1002/jbmr.3055

25. Roux A, Todd DA, Velázquez J v, Cech NB, Sonenshein AL. CodY-mediated regulation of the *Staphylococcus aureus* Agr system integrates nutritional and population density signals. 2014. 196(6):1184-96. doi:10.1128/JB.00128-13

26. Potter AD, Butrico CE, Ford CA, Curry JM, Trenary IA, Tummarakota SS, et al. Host nutrient milieu drives an essential role for aspartate biosynthesis during invasive *Staphylococcus aureus* infection. *PNAS*. 2020;117(22):12394-12401. doi:10.1073/pnas.1922211117

27. Cheng AG, Kim HK, Burts ML, Krausz T, Schneewind O, Missiakas DM. Genetic requirements for *Staphylococcus aureus* abscess formation and persistence in host tissues. *FASEB J*. 2009;23(10):3393-3404. doi:10.1096/fj.09-135467

28. Mouri Mi, Badireddy M. Hyperglycemia. StatPearls website. https://www.ncbi.nlm.nih.gov/books/NBK430900/. Accessed February 17, 2023.

29. Centers for Disease Control and Prevention. National Diabetes Statistics Report website. https://www.cdc.gov/diabetes/data/statistics-report/index.html. Accessed February 17, 2023.

30. O'Neal KS, Johnson JL, Panak RL. Recognizing and appropriately treating latent autoimmune diabetes in adults. *Diabetes Spectr*. 2016;29(4):249. doi:10.2337/DS15-0047

31. Giwa AM, Ahmed R, Omidian Z, Majety N, Karakus KE, Omer SM, et al. Current understandings of the pathogenesis of type 1 diabetes: genetics to environment. *World J Diabetes*. 2020;11(1):13. doi:10.4239/WJD.V11.I1.13

32. Centers for Disease Control and Prevention. What is diabetes? https://www.cdc.gov/diabetes/basics/diabetes.html. Accessed February 12, 2023.

33. Kolb H, Martin S. Environmental/lifestyle factors in the pathogenesis and prevention of type 2 diabetes. *BMC Med*. 2017;15(1). doi:10.1186/S12916-017-0901-X

34. Burekovic A, Dizdarevic-Bostandzic A, Godinjak A. Poorly regulated blood glucose in diabetic patients-predictor of acute infections. *Med Arch*. 2014;68(3):163-166. doi:10.5455/medarh.2014.68.163-166

35. King AJF. The use of animal models in diabetes research. *Br J Pharmacol*. 2012;166(3):877. doi:10.1111/J.1476-5381.2012.01911.X

36. Bansal R, Ahmad N, Kidwai JR. Alloxan-glucose interaction: effect on incorporation of 14C-leucine into pancreatic islets of rat. *Acta Diabetol Lat*. 1980;17(2):135-143. doi:10.1007/BF02580995

37. Sandler S, Swenne I. Streptozotocin, but not alloxan, induces DNA repair synthesis in mouse pancreatic islets *in vitro*. *Diabetologia*. 1983;25(5):444-447. doi:10.1007/BF00282526

38. Szkudelski T. The mechanism of alloxan and streptozotocin action in B cells of the rat pancreas. *Physiol Res*. 2021;50:536-546.

39. Dekel Y, Glucksam Y, Elron-Gross I, Margalit R. Insights into modeling streptozotocin-induced diabetes in ICR mice. *Lab Anim*. 2009;38(2):55-60. doi:10.1038/LABAN0209-55

40. Like AA, Rossini AA. Streptozotocin-induced pancreatic insulitis: new model of diabetes mellitus. *Science*. 1976;193(4251):415-417. doi:10.1126/SCIENCE.180605

41. Xu B, Allard C, Alvarez-Mercado AI, Fuselier T, Kim JH, Coons LA, et al. Estrogens promote misfolded proinsulin degradation to protect insulin production and delay diabetes. *Cell Rep*. 2018;24(1):181-196. doi:10.1016/j.celrep.2018.06.019

42. Kim B, Kim YY, Nguyen PTT, Nam H, Suh JG. Sex differences in glucose metabolism of streptozotocin-induced diabetes inbred mice (C57BL/6J). *Appl Biol Chem*. 2020;63(1):1-8. doi:10.1186/S13765-020-00547-5

43. Thorel F, Nepote V, Avril I, Kohno K, Desgraz R, Chera S, Herrera PL. Conversion of adult pancreatic alpha-cells to beta-cells after extreme beta cell loss. *Nature*. 2010;464(7292):1149-1154. doi:10.1038/nature08894.

44. Hanafusa T, Miyagawa J ichiro, Nakajima H, Tomita K, Kuwajima M, Matsuzawa Y, Tarui S. The NOD mouse. *Diabetes Res Clin Pract*. 1994;24. doi:10.1016/0168-8227(94)90267-4

45. Melanitou E, Devendra D, Liu E, Miao D, Eisenbarth GS. Early and quantal (by litter) expression of insulin autoantibodies in the nonobese diabetic mice predict early diabetes onset. *J Immunol*. 2004;173(11):6603-6610. doi:10.4049/JIMMUNOL.173.11.6603

46. Pozzilli P, Signore A, Williams AJK, Beales PE. NOD mouse colonies around the world--recent facts and figures. *Immunol Today*. 1993;14(5):193-196. doi:10.1016/0167-5699(93)90160-M

47. Chen D, Thayer TC, Wen L, Wong FS. Mouse models of autoimmune diabetes: the nonobese diabetic (NOD) mouse. *Methods Mol Biol*. 2020;2128:87. doi:10.1007/978-1-0716-0385-7_6

48. Yoshioka M, Kayo T, Ikeda T, Koizumi A. A novel locus, Mody4, distal to D7Mit189 on chromosome 7 determines early-onset NIDDM in nonobese C57BL/6 (Akita) mutant mice. *Diabetes*. 1997;46(5):887-894. doi:10.2337/DIAB.46.5.887

49. Mathews CE, Langley SH, Leiter EH. New mouse model to study islet transplantation in insulin-dependent diabetes mellitus. *Transplantation*. 2002;73(8):1333-1336. doi:10.1097/00007890-200204270-00024

50. Yang XQ, Wang YY, Chen AF. Increased superoxide contributes to enhancement of vascular contraction in Ins2(Akita) diabetic mice, an autosomal dominant mutant model. *Clin Exp Pharmacol Physiol*. 2008;35(9):1097-1103. doi:10.1111/J.1440-1681.2007.04756.X

51. Schmidt RE, Green KG, Snipes LL, Feng D. Neuritic Dystrophy and neuronopathy in Akita (Ins2Akita) diabetic mouse sympathetic ganglia. *Exp Neurol*. 2009;216(1):207. doi:10.1016/J.EXPNEUROL.2008.11.019

52. Hu P, McKenzie JA, Buettmann EG, Migotsky N, Gardner MJ, Silva MJ. Type 1 diabetic Akita mice have low bone mass and impaired fracture healing. *Bone*. 2021;147. doi:10.1016/J.BONE.2021.115906

53. Jordan GW, Cohen SH. Encephalomyocarditis virus-induced diabetes mellitus in mice: model of viral pathogenesis. *Rev Infect Dis*. 1987;9(5):917-924. doi:10.1093/CLINIDS/9.5.917

54. Gamble DR, Taylor KW. Diabetes in mice after Coxsackie B 4 virus infection. *Br Med J*. 1973;3(5870):25. doi:10.1136/BMJ.3.5870.25

55. Craighead JE, McLane MF. Diabetes mellitus: induction in mice by encephalomyocarditis virus. *Science.* 1968;162(3856):913-914. doi:10.1126/SCIENCE.162.3856.913

56. Sevilla N, Homann D, Herrath M von, Rodriguez F, Harkins S, Whitton JL, Oldstone MB. Virus-induced diabetes in a transgenic model: role of cross-reacting viruses and quantitation of effector T cells needed to cause disease. *J Virol*. 2000;74(7):3284. doi:10.1128/JVI.74.7.3284-3292.2000

57. Surwit RS, Kuhn CM, Cochrane C, McCubbin JA, Feinglos MN. Diet-induced type II diabetes in C57BL/6J mice. *Diabetes*. 1988;37(9):1163-1167. doi:10.2337/DIAB.37.9.1163

58. Winzell MS, Ahrén B. The high-fat diet-fed mouse: a model for studying mechanisms and treatment of impaired glucose tolerance and type 2 diabetes. *Diabetes*. 2004;53. doi:10.2337/DIABETES.53.SUPPL_3.S215

59. Zhang Y, Proenca R, Maffei M, Barone M, Leopold L, Friedman JM. Positional cloning of the mouse obese gene and its human homologue. *Nature.* 1994;372(6505):425-432. doi:10.1038/372425a0

60. Lindström P. The physiology of obese-hyperglycemic mice [ob/ob mice]. *ScientificWorldJournal*. 2007;7:666-685. doi:10.1100/tsw.2007.117

61. Chen H, Charlat O, Tartaglia LA, Woolf EA, Weng X, Ellis SJ, et al. Evidence that the diabetes gene encodes the leptin receptor: identification of a mutation in the leptin receptor gene in db/db mice. *Cell*. 1996;84(3):491-495. doi:10.1016/S0092-8674(00)81294-5

62. Buchanan J, Mazumder PK, Hu P, Chakrabarti G, Roberts MW, Yun UJ, et al. Reduced cardiac efficiency and altered substrate metabolism precedes the onset of hyperglycemia and contractile dysfunction in two mouse models of insulin resistance and obesity. *Endocrinology*. 2005;146(12):5341-5349. doi:10.1210/EN.2005-0938

63. Singh H, Miyamoto S, Darshi M, Torralba MG, Kwon K, Sharma K, Pieper R. Gut microbial changes in diabetic db/db mice and recovery of microbial diversity upon pirfenidone treatment. *Microorganisms*. 2020;8(9):1347. doi:10.3390/MICROORGANISMS8091347

64. Kluth O, Mirhashemi F, Scherneck S, Kaiser D, Kluge R, Neschen S, H-G Joost, Schurmann A. Dissociation of lipotoxicity and glucotoxicity in a mouse model of obesity associated diabetes: role of forkhead box O1 (FOXO1) in glucose-induced beta cell failure. *Diabetologia*. 2011;54(3):605-616. doi:10.1007/S00125-010-1973-8

65. Kim JH, Saxton AM. The TALLYHO mouse as a model of human type 2 diabetes. *Methods Mol Biol*. 2012;933:75-87. doi:10.1007/978-1-62703-068-7_6

66. Nakamura N. Reduced aldehyde dehydrogenase activity and arginine vasopressin receptor 2 expression in the kidneys of male TALLYHO/JngJ mice of prediabetic age. *Endocrine*. 2011;40(3):379-385. doi:10.1007/S12020-011-9528-4

67. Okazaki M, Saito Y, Udaka Y, Maruyama M, Murakami H, Ota S, Kikuchi T, Oguchi K. Diabetic nephropathy in KK and KK-Ay mice. *Exp Anim*. 2002;51(2):191-196. doi:10.1538/EXPANIM.51.191

68. Kottaisamy CPD, Raj DS, Kumar VP, Sankaran U. Experimental animal models for diabetes and its related complications—a review. *Lab Anim Res*. 2021;37(1). doi:10.1186/S42826-021-00101-4

69. Chang JH, Gurley SB. Assessment of diabetic nephropathy in the Akita mouse. *Methods Mol Biol*. 2012;933:17-29. doi:10.1007/978-1-62703-068-7_2

70. Martins T, Castro-Ribeiro C, Lemos S, Ferreira T, Nascimento-Goncalves E, Rosa E, et al. Murine Models of Obesity. *Obesities.* 2022;2(2):127-147. doi:10.3390/OBESITIES2020012

71. Denvir J, Boskovic G, Fan J, Primerano DA, Parkman JK, Kim JH. Whole genome sequence analysis of the TALLYHO/Jng mouse. *BMC Genomics*. 2016;17(1):1-15. doi:10.1186/S12864-016-3245-6

72. Kim JH, Saxton AM. The TALLYHO mouse as a model of human type 2 diabetes. *Methods Mol Biol*. 2012;933:75-87. doi:10.1007/978-1-62703-068-7_6

73. Brandt SL, Wang S, Dejani NN, Klopfenstein N, Winfree S, Filgueiras L, et al. Excessive localized leukotriene B4 levels dictate poor skin host defense in diabetic mice. *JCI Insight*. 2018;3(17). doi:10.1172/JCI.INSIGHT.120220

74. Thurlow LR, Stephens AC, Hurley KE, Richardson AR. Lack of nutritional immunity in diabetic skin infections promotes *Staphylococcus aureus* virulence. *Sci Adv*. 2020;6(46). doi:10.1126/SCIADV.ABC5569

75. Rich J, Lee JC. The pathogenesis of *Staphylococcus aureus* infection in the diabetic NOD mouse. *Diabetes*. 2005;54(10):2904-2910. doi:10.2337/DIABETES.54.10.2904

76. Cheng AG, DeDent AC, Schneewind O, Missiakas D. A play in four acts: *Staphylococcus aureus* abscess formation. *Trends Microbiol*. 2011;19(5):225-232. doi:10.1016/j.tim.2011.01.007

77. Cho JS, Guo Y, Ramos RI, Hebroni F, Plaisier SB, Xuan C, et al. Neutrophil-derived IL-1β is sufficient for abscess formation in immunity against *Staphylococcus aureus* in mice. *PLoS Pathog*. 2012;8(11):e1003047. doi:10.1371/journal.ppat.1003047

78. Brandt SL, Serezani CH. Too much of a good thing: how modulating LTB 4 actions restore host defense in homeostasis or disease. 2017;33:37-43. doi:10.1016/j.smim.2017.08.006

79. Kobayashi SD, Malachowa N, DeLeo FR. Pathogenesis of *Staphylococcus aureus* abscesses. *Am J Pathol*. 2015;185(6):1518-1527. doi:10.1016/j.ajpath.2014.11.030

80. Feuerstein R, Seidl M, Prinz M, Henneke P. MyD88 in macrophages is critical for abscess resolution in staphylococcal skin infection. *J Immunol*. 2015;194(6):2735-2745. doi:10.4049/JIMMUNOL.1402566

81. Filgueiras LR, Brandt SL, Wang S, Wang Z, Morris DL, Evans-Molina C, et al. Leukotriene B4-mediated sterile inflammation promotes susceptibility to sepsis in a mouse model of type 1 diabetes. *Sci Signal*. 2015;8(361). doi:10.1126/scisignal.2005568

82. Hanses F, Park S, Rich J, Lee JC. Reduced neutrophil apoptosis in diabetic mice during staphylococcal infection leads to prolonged Tnfα production and reduced neutrophil clearance. *PLoS One*. 2011;6(8):e23633. doi:10.1371/journal.pone.0023633

83. Wong SL, Demers M, Martinod K, Gallant M, Wang Y, Goldfine AB, et al. Diabetes primes neutrophils to undergo NETosis, which impairs wound healing. *Nat Med*. 2015;21(7):815-819. doi:10.1038/nm.3887

84. Dejani NN, Brandt SL, Pineros A, Glosson-Byers NL, Wang S, Son YM, et al. Topical prostaglandin E analog restores defective dendritic cell-mediated Th17 host defense against methicillin-resistant *Staphylococcus aureus* in the skin of diabetic mice. *Diabetes*. 2016;65(12):3718-3729. doi:10.2337/DB16-0565

85. Ribeiro Filgueiras L, Brandt SL, Raquel de Oliveira Ramalho T, Jancar S, Henrique Serezani C. Imbalance between HDAC and HAT activities drives aberrant STAT1/MyD88 expression in macrophages from type 1 diabetic mice. *J Diabetes Complications*. 2017;31(2):334-339. doi:10.1016/j.jdiacomp.2016.08.001

86. Wierusz-Wysocka B, Wysocki H, Wykrętowicz A, Klimas R. The influence of increasing glucose concentrations on selected functions of polymorphonuclear neutrophils. *Acta Diabetol Lat*. 1988;25(4):283-288. doi:10.1007/BF02581126

87. Perner A, Nielsen SE, Rask-Madsen J. High glucose impairs superoxide production from isolated blood neutrophils. *Intensive Care Med*. 2003;29(4):642-645. doi:10.1007/S00134-002-1628-4

88. Kjersem H, Hilsted J, Madsbad S, Wandall JH, Johansen KS, Borregaard N. Polymorphonuclear leucocyte dysfunction during short term metabolic changes from normo- to hyperglycemia in type 1 (insulin dependent) diabetic patients. *Infection*. 1988;16(4):215-221. doi:10.1007/BF01650754

89. Marhoffer W, Stein M, Maeser E, Federlin K. Impairment of polymorphonuclear leukocyte function and metabolic control of diabetes. *Diabetes Care*. 1992;15(2):256-260. doi:10.2337/diacare.15.2.256

90. Lovati AB, Drago L, Monti L, et al. Diabetic mouse model of orthopaedic implant-related *Staphylococcus aureus* infection. *PLoS One*. 2013;8(6):e67628. doi:10.1371/journal.pone.0067628

91. Buse JB, Wexler DJ, Tsapas A, Rossing P, Mingrone G, Mathieu C, et al. 2019 update to: management of hyperglycemia in type 2 diabetes, 2018. A consensus report by the American Diabetes Association (ADA) and the European Association for the Study of Diabetes (EASD). *Diabetes Care*. 2020;43(2):487-493. doi:10.2337/DCI19-0066

92. Rajab B, Alamrim A, Alamri A. Prognosis of chronic complications of diabetes mellitus (DM) after multiple events of diabetic ketoacidosis (DKA). *IJMDC.* 2019;3(5):474-479. doi:10.24911/IJMDC.51-1546551993

93. Mooradian AD. Central nervous system complications of diabetes mellitus — a perspective from the blood–brain barrier. *Brain Res Rev*. 1997;23(3):210-218. doi:10.1016/S0165-0173(97)00003-9

94. Rask-Madsen C, King GL. Vascular complications of diabetes: mechanisms of injury and protective factors. *Cell Metab*. 2013;17(1):20. doi:10.1016/J.CMET.2012.11.012

95. Li T, Li Z, Huang L, Tang J, Ding Z, Zeng Z, Liu Y, Liu J. Cigarette smoking and peripheral vascular disease are associated with increasing risk of ESKAPE pathogen infection in diabetic foot ulcers. *Diabetes Metab Syndr Obes*. 2022;15:3271-3283. doi:10.2147/DMSO.S383701

96. English P, Williams G. Hyperglycaemic crises and lactic acidosis in diabetes mellitus. *Postgrad Med J*. 2004;80(943):253-261. doi:10.1136/PGMJ.2002.004291

97. Hoffman WH, Cudrici CD, Zafranskaia E, Rus H. Complement activation in diabetic ketoacidosis brains. *Exp Mol Pathol*. 2006;80(3):283-288. doi:10.1016/J.YEXMP.2005.12.007

98. Vincent AM, Callaghan BC, Smith AL, Feldman EL. Diabetic neuropathy: cellular mechanisms as therapeutic targets. *Nat Rev Neurol*. 2011;7(10):573-583. doi:10.1038/NRNEUROL.2011.137

99. Noor S, Zubair M, Ahmad J. Diabetic foot ulcer—A review on pathophysiology, classification and microbial etiology. *Diabetes Metab Syndr*. 2015;9(3):192-199. doi:10.1016/J.DSX.2015.04.007

100. Loureiro MB, Ururahy MAG, Freire-Neto FP, Oliveira GHM, Duarte VM, Luchessi AD, et al. Low bone mineral density is associated to poor glycemic control and increased OPG expression in children and adolescents with type 1 diabetes. *Diabetes Res Clin Pract*. 2014;103(3):452-457. doi:10.1016/J.DIABRES.2013.12.018

101. de Oliveira GJPL, Basso TLD, Fontanari LA, Faloni AP de S, Marcantonio É, Orrico SRP. Glycemic control protects against trabecular bone microarchitectural damage in a juvenile male rat model of streptozotocin-induced diabetes. *Endocr Res*. 2017;42(3):171-179. doi:10.1080/07435800.2017.1292521

102. Erdal N, Gürgül S, Demirel C, Yildiz A. The effect of insulin therapy on biomechanical deterioration of bone in streptozotocin (STZ)-induced type 1 diabetes mellitus in rats. *Diabetes Res Clin Pract*. 2012;97(3):461-467. doi:10.1016/J.DIABRES.2012.03.005

103. Motyl K, McCabe LR. Streptozotocin, type I diabetes severity and bone. *Biol Proced Online*. 2009;11(1):296. doi:10.1007/S12575-009-9000-5

104. Balci Yuce H, Karatas O, Aydemir Turkal H, Gorgun EP, Ocakli S, Benli I, Cayli S. The effect of melatonin on bone loss, diabetic control, and apoptosis in rats with diabetes with ligature-induced periodontitis. *J Periodontol*. 2016;87(4):e35-e43. doi:10.1902/JOP.2015.150315

105. Iitsuka N, Hie M, Tsukamoto I. Zinc supplementation inhibits the increase in osteoclastogenesis and decrease in osteoblastogenesis in streptozotocin-induced diabetic rats. *Eur J Pharmacol*. 2013;714(1-3):41-47. doi:10.1016/J.EJPHAR.2013.05.020

106. Ma R, Wang L, Zhao B, et al. Diabetes perturbs bone microarchitecture and bone strength through regulation of Sema3A/IGF-1/β-Catenin in rats. *Cell Physiol Biochem*. 2017;41(1):55-66. doi:10.1159/000455936

107. Bischoff M, Wonnenberg B, Nippe N, Nyffenegger-Jann N, Voss M, Beisswenger C, et al. CcpA affects infectivity of *Staphylococcus aureus* in a hyperglycemic environment. *Front Cell Infect Microbiol*. 2017;7:172. doi:10.3389/fcimb.2017.00172

108. Jacquet R, LaBauve AE, Akoolo L, Patel S, Alqarzaee AA, Fok Lung TW, et al. Dual gene expression analysis identifies factors associated with *Staphylococcus aureus* virulence in diabetic mice. *Infect Immun*. 2019;87(5). doi:10.1128/IAI.00163-19

109. Sotto A, Lina G, Richard JL, Combescure C, Bourg G, Vidal L, et al. Virulence potential of *Staphylococcus aureus* strains isolated from diabetic foot ulcers. *Diabetes Care*. 2008;31(12):2318-2324. doi:10.2337/DC08-1010

110. Lowy FD. Medical progress: *Staphylococcus aureus* infections. *NEJM*. 1998;339(8):520-532. doi:10.1056/NEJM199808203390806

111. Kong C, Neoh HM, Nathan S. Targeting *Staphylococcus aureus* toxins: a potential form of anti-virulence therapy. *Toxins (Basel)*. 2016;8(3). doi:10.3390/toxins8030072

112. Brandis G, Cao S, Huseby DL, Hughes D. Having your cake and eating it - *Staphylococcus aureus* small colony variants can evolve faster growth rate without losing their antibiotic resistance. *Microbial Cell*. 2017;4(8):275-277. doi:10.15698/mic2017.08.587

113. Jenul C, Horswill AR. Regulation of *Staphylococcus aureus* virulence. *Microbiol Spectr*. 2019;7(2). doi:10.1128/microbiolspec.GPP3-0031-2018

114. Majerczyk CD, Sadykov MR, Luong TT, Lee C, Somerville GA, Sonenshein AL. *Staphylococcus aureus* CodY negatively regulates virulence gene expression. *J Bacteriol*. 2008;190(7):2257-2265. doi:10.1128/JB.01545-07

115. Pohl K, Francois P, Stenz L, Schlink F, Geiger T, Herbert S, et al. CodY in *Staphylococcus aureus*: a regulatory link between metabolism and virulence gene expression. *J Bacteriol*. 2009;191(9):2953-2963. doi:10.1128/JB.01492-08

116. Majerczyk CD, Dunman PM, Luong TT, Lee CY, Sadykov MR, Somerville GA, et al. Direct targets of CodY in *Staphylococcus aureus*. *J Bacteriol*. 2010;192(11):2861-2877. doi:10.1128/JB.00220-10

117. Seidl K, Stucki M, Ruegg M, Goerke C, Wolz C, Harris L, et al. *Staphylococcus aureus* CcpA affects virulence determinant production and antibiotic resistance. *Antimicrob Agents Chemother*. 2006;50(4):1183-1194. doi:10.1128/AAC.50.4.1183-1194.2006

118. Esen E, Long F. Aerobic glycolysis in osteoblasts. *Curr Osteoporos Rep*. 2014;12(4):433-438. doi:10.1007/s11914-014-0235-y

119. Kim JM, Jeong D, Kang HK, Jung SY, Kang SS, Min BM. Osteoclast precursors display dynamic metabolic shifts toward accelerated glucose metabolism at an early stage of RANKL-stimulated osteoclast differentiation. *Cell Physiol Biochem*. 2007;20(6):935-946. doi: 10.1159/000110454

120. Thomas VC, Sadykov MR, Chaudhari SS, Jones J, Endres JL, Widhelm TJ, et al. A central role for carbon-overflow pathways in the modulation of bacterial cell death. *PLoS Pathog*. 2014;10(6):1004205. doi:10.1371/JOURNAL.PPAT.1004205

121. Zhou C, Fey PD. The acid response network of *Staphylococcus aureus*. *Curr Opin Microbiol*. 2020;55:67. doi:10.1016/J.MIB.2020.03.006

122. Yang -j, Dunman PM, Projan SJ, Bayles KW. Characterization of the *Staphylococcus aureus* CidR regulon: elucidation of a novel role for acetoin metabolism in cell death and lysis. *Mol Microbiol*. 2006;60(2):458-468. doi:10.1111/J.1365-2958.2006.05105.X

123. Zhou C, Bhinderwala F, Lehman MK, Thomas VC, Chaudhari SS, Yamada KJ, et al. Urease is an essential component of the acid response network of *Staphylococcus aureus* and is required for a persistent murine kidney infection. *PLoS Pathog*. 2019;15(1). doi:10.1371/JOURNAL.PPAT.1007538

124. Thurlow LR, Joshi GS, Clark JR, Spontak JS, Neely CJ, Maile R, Richardson AR. Functional modularity of the arginine catabolic mobile element contributes to the success of USA300 methicillin-resistant *Staphylococcus aureus*. *Cell Host Microbe*. 2013;13(1):100. doi:10.1016/J.CHOM.2012.11.012

125. Clements MO, Watson SP, Foster SJ. Characterization of the major superoxide dismutase of *Staphylococcus aureus* and its role in starvation survival, stress resistance, and pathogenicity. *J Bacteriol*. 1999;181(13):3898-3903.

126. Wright M, Hart ME. Identification and characterization of a second superoxide dismutase gene (*sodM*) from *Staphylococcus aureus*. *J Bacteriol*. 2001;183(11):3399-3407. doi:10.1128/JB.183.11.3399-3407.2001

127. Turner KH, Wessel AK, Palmer GC, Murray JL, Whiteley M. Essential genome of *Pseudomonas aeruginosa* in cystic fibrosis sputum. *PNAS.* 2015;112(13):4110-4115. doi:10.1073/PNAS.1419677112

128. Shan Y, Lazinski D, Rowe S, Camilli A, Lewis K. Genetic basis of persister tolerance to aminoglycosides in *Escherichia coli*. *mBio*. 2015;6(2). doi:10.1128/MBIO.00078-15

129. Roux D, Danilchanka O, Guillard T, Cattoir V, Aschard H, Fu Y, et al. Fitness cost of antibiotic susceptibility during bacterial infection. *Sci Transl Med*. 2015;7(297). doi:10.1126/SCITRANSLMED.AAB1621

130. Bachman MA, Breen P, Deornellas V, Mu Q, Zhao L, Wu W, et al. Genome-wide identification of *Klebsiella pneumoniae* fitness genes during lung infection. *mBio*. 2015;6(3). doi:10.1128/MBIO.00775-15

131. Barquist L, Boinett CJ, Cain AK. Approaches to querying bacterial genomes with transposon-insertion sequencing. *RNA Biol*. 2013;10(7):1161-1169. doi:10.4161/RNA.24765

132. van Opijnen T, Camilli A. Transposon insertion sequencing: a new tool for systems-level analysis of microorganisms. *Nat Rev Microbiol.* 2013;11(7):435-442. doi:10.1038/nrmicro3033

133. Horsburgh MJ, Wiltshire MD, Crossley H, Ingham E, Foster SJ. PheP, a putative amino acid permease of *Staphylococcus aureus*, contributes to survival *in vivo* and during starvation. *Infect Immun*. 2004;72(5):3073-3076. doi:10.1128/IAI.72.5.3073-3076.2004

134. Taylor D, Holland KT. Amino acid requirements for the growth and production of some exocellular products of *Staphylococcus aureus*. *J Appl Bacteriol*. 1989;66(4):319-329. doi:10.1111/J.1365-2672.1989.TB02485.X

135. Jack DL, Paulsen IT, Saier J. The amino acid/polyamine/organocation (APC) superfamily of transporters specific for amino acids, polyamines and organocations. *Microbiology (Reading)*. 2000;146 (Pt 8)(8):1797-1814. doi:10.1099/00221287-146-8-1797

136. Kim GL, Hooven TA, Norambuena J, Li B, Boyd JM, Yang JH, Parker D. Growth and stress tolerance comprise independent metabolic strategies critical for *Staphylococcus aureus* infection. *mBio*. 2021;12(3). doi:10.1128/MBIO.00814-21

137. Vitko NP, Richardson AR. Laboratory maintenance of methicillin-resistant *Staphylococcus aureus* (MRSA). *Curr Protoc Microbiol*. 2013; 9(9C.2). doi:10.1002/9780471729259.MC09C02S28

138. Shea A, Wolcott M, Daefler S, Rozak DA. Biolog phenotype microarrays. *Methods Mol Biol*. 2012;881:331-373. doi:10.1007/978-1-61779-827-6_12

139. Lucas AL, Manna AC. Phenotypic characterization of *sarR* mutant in *Staphylococcus aureus*. *Microb Pathog*. 2013;57:52-61. doi:10.1016/j.micpath.2012.11.008

140. Mike LA, Choby JE, Brinkman PR, Olive LQ, Butter BF, Ivan SJ, et al. Two-component system cross-regulation integrates *Bacillus anthracis* response to heme and cell envelope stress. *PLoS Pathog*. 2014;10(3). doi:10.1371/journal.ppat.1004044

141. Mann EE, Rice KC, Boles BR, Endres JL, Ranjit D, Chandramohan L, Tsang LH. Modulation of eDNA release and degradation sffects *Staphylococcus aureus* biofilm maturation. *PLoS One*. 2009;4(6). doi:10.1371/journal.pone.0005822

142. Cheng AG, McAdow M, Kim HK, Bae T, Missiakas DM, Schneewind O. Contribution of coagulases towards *Staphylococcus aureus* disease and protective immunity. *PLoS Pathog*. 2010;6(8):e1001036. doi:10.1371/journal.ppat.1001036

143. Kiedrowski MR, Crosby HA, Hernandez FJ, Malone CL, McNamara JO, Horswill AR. *Staphylococcus aureus* Nuc2 Is a functional, surface-attached extracellular nuclease. *PLoS One*. 2014;9(4):95574. doi:10.1371/journal.pone.0095574

144. Price-Whelan A, Poon CK, Benson MA, Eidem TT, Roux CM, Boyd JM et al. Transcriptional profiling of *Staphylococcus aureus* during growth in 2 M NaCl leads to clarification of physiological roles for Kdp and Ktr K+ uptake systems. *mBio*. 2013;4(4). doi:10.1128/MBIO.00407-13

145. Girish TS, Gopal B. Crystal structure of *Staphylococcus aureus* metallopeptidase (Sapep) reveals large domain motions between the manganese-bound and apo-states. *J Biol Chem*. 2010;285(38):29406. doi:10.1074/JBC.M110.147579

146. Rong M, Zheng X, Ye M, Bai J, Xie X, Jin Y, He X. Phenotypic plasticity of *Staphylococcus aureus* in liquid medium containing vancomycin. *Front Microbiol*. 2019;10. doi:10.3389/FMICB.2019.00809

147. Joshi GS, Spontak JS, Klapper DG, Richardson AR. ACME encoded *speG* abrogates the unique hypersensitivity of *Staphylococcus aureus* to exogenous polyamines. *Mol Microbiol*. 2011;82(1):9. doi:10.1111/J.1365-2958.2011.07809.X

148. Kim JK, Kim YS, Lee HM, Jin HS, Neupane C, Kim S, et al. GABAergic signaling linked to autophagy enhances host protection against intracellular bacterial infections. *Nat Commun*. 2018;9(1). doi:10.1038/S41467-018-06487-5

149. Dagorn A, Chapalain A, Mijouin L, Hillion M, Duclairoir-Poc C, Chevalier S, et al. Effect of GABA, a bacterial metabolite, on *Pseudomonas fluorescens* surface properties and cytotoxicity. *Int J Mol Sci*. 2013;14(6):12186. doi:10.3390/IJMS140612186

150. Dagorn A, Hillion M, Chapalain A, Lesouhaitier O, Poc CD, Vieilard J, et al. Gamma-aminobutyric acid acts as a specific virulence regulator in *Pseudomonas aeruginosa*. *Microbiology (Reading)*. 2013;159(Pt 2):339-351. doi:10.1099/MIC.0.061267-0

151. Schwan WR. Proline transport and growth changes in proline transport mutants of *Staphylococcus aureus*. *Microorganisms*. 2022;10(10). doi:10.3390/MICROORGANISMS10101888

152. Halsey CR, Lei S, Wax JK, Lehman MK, Nuxoll AS, Steinke L, et al. Amino acid catabolism in *Staphylococcus aureus* and the function of carbon catabolite repression. *mBio*. 2017;8(1). doi:10.1128/MBIO.01434-16

153. Zeden MS, Kviatkovski I, Schuster CF, Thomas VC, Fey PD, Gründling A. Identification of the main glutamine and glutamate transporters in *Staphylococcus aureus* and their impact on c-di-AMP production. *Mol Microbiol*. 2020;113(6):1085. doi:10.1111/MMI.14479

154. Alreshidi M, Dunstan H, Roberts T, Bardakci F, Badraoui R, Adnan M, et al. Changes in amino acid metabolism of *Staphylococcus aureus* following growth to the stationary phase under adjusted growth conditions. *Microorganisms*. 2022;10(8). doi:10.3390/MICROORGANISMS10081503

155. Zhao Y, Han Y, Sun Y, Wei Z, Chen J, Niu X, et al. Comprehensive succinylome profiling reveals the pivotal role of lysine succinylation in energy metabolism and quorum sensing of *Staphylococcus epidermidis*. *Front Microbiol*. 2021;11:3556. doi:10.3389/FMICB.2020.632367

156. Yao X, Lu CD. Functional characterization of the *potRABCD* operon for spermine and spermidine uptake and regulation in *Staphylococcus aureus*. *Curr Microbiol*. 2014;69(1):75-81. doi:10.1007/S00284-014-0556-1

157. Rhee HJ, Kim EJ, Lee JK. Physiological polyamines: simple primordial stress molecules. *J Cell Mol Med*. 2007;11(4):685-703. doi:10.1111/J.1582-4934.2007.00077.X

158. Corrigan RM, Campeotto I, Jeganathan T, Roelofs KG, Lee VT, Gründling A. Systematic identification of conserved bacterial c-di-AMP receptor proteins. *Proc Natl Acad Sci U S A*. 2013;110(22):9084-9089. doi:10.1073/PNAS.1300595110

159. Gries CM, Bose JL, Nuxoll AS, Fey PD, Bayles KW. The Ktr potassium transport system in *Staphylococcus aureus* and its role in cell physiology, antimicrobial resistance, and pathogenesis. *Mol Microbiol*. 2013;89(4):760. doi:10.1111/MMI.12312

160. Ranjit DK, Endres JL, Bayles KW. *Staphylococcus aureus* CidA and LrgA proteins exhibit holin-like properties. *J Bacteriol*. 2011;193(10):2468-2476. doi:10.1128/JB.01545-10

161. Bae T, Schneewind O. Allelic replacement in *Staphylococcus aureus* with inducible counter-selection. *Plasmid*. 2006;55(1):58-63. doi:10.1016/J.PLASMID.2005.05.005

162. Fey PD, Endres JL, Yajjala VK, Widhelm TJ, Boissy RJ, Bose JL, Bayles KW. A genetic resource for rapid and comprehensive phenotype screening of nonessential *Staphylococcus aureus* genes. *mBio*. 2013;4(1). doi:10.1128/MBIO.00537-12

163. Spahich NA, Vitko NP, Thurlow LR, Temple B, Richardson AR. *Staphylococcus aureus* lactate- and malate-quinone oxidoreductases contribute to nitric oxide resistance and virulence. *Mol Microbiol*. 2016;100(5):759-773. doi:10.1111/mmi.13347

164. Brandt SL, Klopfenstein N, Wang S, Winfree S, McCarthy BP, Territo PR, et al. Macrophage-derived LTB4 promotes abscess formation and clearance of *Staphylococcus aureus* skin infection in mice. *PLoS Pathog*. 2018;14(8). doi:10.1371/journal.ppat.1007244

165. Giacco F, Brownlee M. Oxidative stress and diabetic complications. *Circ Res*. 2010;107(9):1058. doi:10.1161/CIRCRESAHA.110.223545

166. Liemburg-Apers DC, Willems PHGM, Koopman WJH, Grefte S. Interactions between mitochondrial reactive oxygen species and cellular glucose metabolism. *Arch Toxicol*. 2015;89(8):1209. doi:10.1007/S00204-015-1520-Y

167. Muller LMAJ, Gorter KJ, Hak E, Goudzwaard WL, Schellevis FG, Hoepelman AIM, Rutten GEHM. Increased risk of common infections in patients with type 1 and type 2 diabetes mellitus. *Clion Infect Dis.* 2005:41(3):281-288. doi: 10.1086/431587

168. Giurato L, Meloni M, Izzo V, Uccioli L. Osteomyelitis in diabetic foot: a comprehensive overview. *World J Diabetes*. 2017;8(4):135. doi:10.4239/WJD.V8.I4.135

169. Vitko NP, Spahich NA, Richardson AR. Glycolytic dependency of high-level nitric oxide resistance and virulence in *Staphylococcus aureus*. *mBio*. 2015;6(2). doi:10.1128/mBio.00045-15

170. Grosser MR, Paluscio E, Thurlow LR, Dillon MM, Cooper VS, Kawula TH, Richardson AR. Genetic requirements for *Staphylococcus aureus* nitric oxide resistance and virulence. *PLoS Pathog*. 2018;14(3):e1006907. doi:10.1371/JOURNAL.PPAT.1006907

171. Arora S, Kumar Ojha S, Vohora D. Characterisation of Streptozotocin Induced Diabetes Mellitus in Swiss Albino Mice. *Glob J Pharmacol*. 2009;3(2):81-84. Corpus ID: 14245020

172. Rossini AA, Williams RM, Appel MC, Like AA, Joslin EP. Sex differences in the multiple-dose streptozotocin model of diabetes. *Endocrinology*. 1978;103(4). doi: 10.1210/endo-103-4-1518

173. Leiter EH. Multiple low-dose streptozotocin-induced hyperglycemia and insulitis in C57BL mice: influence of inbred background, sex, and thymus (diabetes/inbred mice/nude mice). *PNAS*. 1982;79(2):630-634. doi: 10.10/pnas.79.2.630

174. Klopfenstein N, Brandt SL, Castellanos S, Gunzer M, Blackman A, Serezani CH. SOCS-1 inhibition of type I interferon restrains *Staphylococcus aureus* skin host defense. *PLoS Pathog*. 2021;17(3):e1009387. doi:10.1371/JOURNAL.PPAT.1009387

175. Putnam NE, Fulbright LE, Curry JM, Ford CA, Petronglo JR, Hendrix AS, Cassat JE. MyD88 and IL-1R signaling drive antimicrobial immunity and osteoclast-driven bone loss during *Staphylococcus aureus* osteomyelitis. *PLoS Pathog*. 2019;15(4). doi:10.1371/journal.ppat.1007744

176. Napoli N, Chandran M, Pierroz DD, Abrahamsen B, Schwartz AV, Ferrari SL. Mechanisms of diabetes mellitus-induced bone fragility. *Nat Rev Endocrinol*. 2017;13(4):208-219. doi:10.1038/nrendo.2016.153

177. Jiao H, Xiao E, Graves DT. Diabetes and its effect on bone and fracture healing. *Curr Osteoporos Rep*. 2015;13(5):327-335. doi:10.1007/s11914-015-0286-8

178. Luo Z, Chen M, Chen T, She P, Wu Y. Lactic acid produced by glycolysis contributed to *Staphylococcus aureus* aggregation induced by glucose. *Curr Microbiol*. 2019;76(5). doi:10.1007/S00284-019-01666-Z

179. Gaupp R, Schlag S, Liebeke M, Lalk M, Götz F. Advantage of upregulation of succinate dehydrogenase in *Staphylococcus aureus* biofilms. *J Bacteriol*. 2010;192(9):2385-2394. doi:10.1128/JB.01472-09

180. Lindgren JK, Thomas VC, Olson ME, Chaudhari SS, Nuxoll AS, Schaeffer CR, et al. Arginine deiminase in *Staphylococcus epidermidis* functions to augment biofilm maturation through pH homeostasis. *J Bacteriol*. 2014;196(12):2277-2289. doi:10.1128/JB.00051-14

181. Cosgrove K, Coutts G, Jonsson IM, Tarkowski A, Kokai-Kun JF, Mond JJ, Foster SJ. Catalase (KatA) and alkyl hydroperoxide reductase (AhpC) have compensatory roles in peroxide stress resistance and are required for survival, persistence, and nasal colonization in *Staphylococcus aureus*. *J Bacteriol*. 2007;189(3):1025-1035. doi:10.1128/JB.01524-06

182. Attia AS, Cassat JE, Aranmolate SO, Zimmerman LJ, Boyd KL, Skaar EP. Analysis of the *Staphylococcus aureus* abscess proteome identifies antimicrobial host proteins and bacterial stress responses at the host-pathogen interface. *Pathog Dis*. 2013;69(1):36-48. doi:10.1111/2049-632X.12063

183. Ballal A, Manna AC. Regulation of superoxide dismutase (*sod*) genes by *sarA* in *Staphylococcus aureus*. *J Bacteriol*. 2009;191(10):3301-3310. doi:10.1128/JB.01496-08

184. Garcia YM, Barwinska-Sendra A, Tarrant E, Skaar EP, Waldron KJ, Kehl-Fie TE. A superoxide dismutase capable of functioning with iron or manganese promotes the resistance of *Staphylococcus aureus* to calprotectin and nutritional immunity. *PLoS Pathog*. 2017;13(1). doi:10.1371/JOURNAL.PPAT.1006125

185. Karavolos MH, Horsburgh M, Ingham E, Foster SJ. Role and regulation of the superoxide dismutases of *Staphylococcus aureus*. *Microbiol.* 2003;149(10):2749-2758. doi:10.1099/mic.0.26353-0

186. Kubica M, Guzik K, Koziel J, Zarebski M, Richter W, Gajkowska B, et al. A potential new pathway for *Staphylococcus aureus* dissemination: the silent survival of *S. aureus*

phagocytosed by human monocyte-derived macrophages. *PLoS One*. 2008;3(1):e1409. doi:10.1371/JOURNAL.PONE.0001409

187. Lian D, Zhu L, Yu Y, Zhang X, Lin Y, Liu J, et al. Kakonein restores hyperglycemia-induced macrophage digestion dysfunction through regulation of cathepsin B-dependent NLRP3 inflammasome activation. *J Leukoc Biol*. 2022;112(1):143-155. doi:10.1002/JLB.3MA0821-418R

188. Dai J, Jiang C, Chen H, Chai Y. Rapamycin attenuates high glucose-induced inflammation through modulation of mTOR/NF-κB pathways in macrophages. *Front Pharmacol*. 2019;10:1292. doi:10.3389/FPHAR.2019.01292

189. Guerra FE, Borgogna TR, Patel DM, Sward EW, Voyich JM, et al. Epic immune battles of history: neutrophils vs. *Staphylococcus aureus*. *Front Cell Infect Microbiol.* 2017;7. doi:10.3389/fcimb.2017.00286

190. Gresham HD, Lowrance JH, Caver TE, Wilson BS, Cheung AL, Lindberg FP. Survival of *Staphylococcus aureus* inside neutrophils contributes to infection. *Journal Immunol*. 2000;164(7):3713-3722. doi:10.4049/jimmunol.164.7.3713

191. Sadzeviciene R, Zekonis J, Zekonis G, Paipaliene P. Oxidative function of neutrophils in periodontitis patients with type 1 diabetes mellitus. *Medicina.* 2006;42(6):479-483. PMID: 16816542

192. Marhoffer W, Stein M, Schleinkofer L, Federlin K. Evidence of *ex vivo* and *in vitro* impaired neutrophil oxidative burst and phagocytic capacity in type 1 diabetes mellitus. *Diabetes Res Clin Pract*. 1993;19(3):183-188. doi:10.1016/0168-8227(93)90112-I

193. Daley JM, Thomay AA, Connolly MD, Reichner JS, Albina JE. Use of Ly6G-specific monoclonal antibody to deplete neutrophils in mice. *J Leukoc Biol*. 2007;83(1):64-70. doi:10.1189/jlb.0407247

194. Faget J, Boivin G, Ancey PB, Gkasti A, Mussard J, Engblom C, et al. Efficient and specific Ly6G + cell depletion: a change in the current practices toward more relevant functional analyses of neutrophils. 2018;18. doi:10.1101/498881

195. Wang JX, Bair AM, King SL, Shnayder R, Huang YF, Shieh CC, et al. Ly6G ligation blocks recruitment of neutrophils via a β2-integrin-dependent mechanism. *Blood*. 2012;120(7):1489-1498. doi:10.1182/blood-2012-01-404046

196. Bastian OW, Koenderman L, Alblas J, Leenen LPH, Blokhuis TJ. Neutrophils contribute to fracture healing by synthesizing fibronectin+ extracellular matrix rapidly after injury. *Clin Immunol*. 2016;164:78-84. doi:10.1016/j.clim.2016.02.001

197. Forsblom E, Ruotsalainen E, Järvinen A. Prognostic impact of hyperglycemia at onset of methicillin-sensitive *Staphylococcus aureus* bacteraemia. *Eur J Clin Microbiol Infect Dis*. 2017;36(8):1405-1413. doi:10.1007/s10096-017-2946-3

198. Bader MS. Hyperglycemia and mortality in elderly patients with *Staphylococcus aureus* bacteremia. *South Med J*. 2007;100(3):252-256. doi:10.1097/01.SMJ.0000257383.66288.68

199. Tuchscherr L, Korpos È, van de Vyver H, Findeisen C, Kherkheulidze S, Siegmund A, et al. *Staphylococcus aureus* requires less virulence to establish an infection in diabetic hosts. *Int J Med Microbiol*. 2018;308(7):761-769. doi:10.1016/j.ijmm.2018.05.004

200. Farnsworth CW, Schott EM, Benvie AM, Zukoski J, Kates SL, Schwarz EM, et al. Obesity/type 2 diabetes increases inflammation, periosteal reactive bone formation, and osteolysis during *Staphylococcus aureus* implant-associated bone infection. *J Orthop Res*. 2018;36(6):1614-1623. doi:10.1002/jor.23831

201. Farnsworth CW, Schott EM, Jensen SE, Zukoski J, Benvie AM, Refaai MA, et al. Adaptive upregulation of clumping factor A (ClfA) by *Staphylococcus aureus* in the obese, type 2 diabetic host mediates increased virulence. *Infect Immun*. 2017;85(6). doi:10.1128/IAI.01005-16

202. Buvelot H, Roth M, Jaquet V, Lozkhin A, Renzoni A, Bonetti EJ, et al. Hydrogen peroxide affects growth of *S. aureus* through downregulation of genes involved in pyrimidine biosynthesis. *Front Immunol*. 2021;12:1-13. doi:10.3389/fimmu.2021.673985

203. Imlay JA. The molecular mechanisms and physiological consequences of oxidative stress: lessons from a model bacterium. *Nat Rev Microbiol*. 2013;11(7):443. doi:10.1038/NRMICRO3032

204. Nuxoll AS, Halouska SM, Sadykov MR, Hanke ML, Bayles KW, Kielian T, et al. CcpA regulates arginine biosynthesis in *Staphylococcus aureus* through repression of proline catabolism. *PLoS Pathog*. 2012;8(11):e1003033. doi:10.1371/journal.ppat.1003033

205. Seidl K, Müller S, François P, Kriebitzsch C, Schrenzel J, Engelmann S, et al. Effect of a glucose impulse on the CcpA regulon in *Staphylococcus aureus*. *BMC Microbiol*. 2009;9(95). doi:10.1186/1471-2180-9-95

206. Richardson AR, Somerville GA, Sonenshein AL. Regulating the intersection of metabolism and pathogenesis in gram-positive bacteria. *Microbiol Spectr*. 2015;3(3). doi:10.1128/microbiolspec.MBP-0004-2014

207. Tally FP, Goldin BR, Jacobus NV, Gorbach SL. Superoxide dismutase in anaerobic bacteria of clinical significance. *Infect Immun*. 1977;16(1):20-25. doi: 10.1128/iai.1.20-25.1977

208. Mandell GL. Catalase, superoxide dismutase, and virulence of *Staphylococcus aureus*. *In vitro* and *in vivo* studies with emphasis on staphylococcal – leukocyte interaction. *J Clin Invest*. 1975;55(3):561-566. doi: 10.1172/JCI107963

209. Farrant JL, Sansone A, Canvin JR, Pallen MJ, Langford PR, Wallis TS, et al. Bacterial copper- and zinc-cofactored superoxide dismutase contributes to the pathogenesis of systemic salmonellosis. *Mol Microbiol*. 1997;25(4):785-796. doi:10.1046/J.1365-2958.1997.5151877.X

210. Ganz T. Oxygen-independent microbicidal mechanisms of phagocytes. *Proc Assoc Am Physicians*. 1999;111(5):390-395. doi:10.1111/PAA.1999.111.5.390

211. Segal AW. The electron transport chain of the microbicidal oxidase of phagocytic cells and its involvement in the molecular pathology of chronic granulomatous disease. *J Clin Investig.* 1989;83(6):1785. doi:10.1172/JCI114083

212. Yan LJ. Pathogenesis of chronic hyperglycemia: from reductive stress to oxidative stress. *J Diabetes Res*. 2014;2014. doi:10.1155/2014/137919

213. Volpe CMO, Villar-Delfino PH, dos Anjos PMF, Nogueira-Machado JA. Cellular death, reactive oxygen species (ROS) and diabetic complications. *Cell Death Dis.* 2018;9(2):1-9. doi:10.1038/s41419-017-0135-z

214. Lemire J, Alhasawi A, Appanna VP, Tharmalingam S, Appanna VD. Metabolic defence against oxidative stress: the road less travelled so far. *J Appl Microbiol*. 2017;123(4):798-809. doi:10.1111/JAM.13509

215. Thomas VC, Chaudhari SS, Jones J, Zimmerman MC, Bayles KW. Electron paramagnetic resonance (EPR) spectroscopy to detect reactive oxygen species in *Staphylococcus aureus*. *Bio Protoc*. 2015;5(17). doi: 10.21769/bioprotoc.1586

216. Kehl-Fie TE, Chitayat S, Hood MI, Damo S, Restrepo N, Garcia C, et al. Nutrient metal sequestration by calprotectin inhibits bacterial superoxide defense, enhancing neutrophil killing of *Staphylococcus aureus*. *Cell Host Microbe*. 2011;10(2):158-164. doi:10.1016/j.chom.2011.07.004

217. Lee JH, Yang SH, Oh JM, Lee MG. Pharmacokinetics of drugs in rats with diabetes mellitus induced by alloxan or streptozocin: comparison with those in patients with type I diabetes mellitus. *J Pharm Pharmacol*. 2010;62(1):1-23. doi:10.1211/JPP.62.01.0001

218. Vitko NP, Grosser MR, Khatri D, Lance TR, Richardson AR. Expanded glucose import capability affords *Staphylococcus aureus* optimized glycolytic flux during infection. *mBio*. 2016;7(3). doi:10.1128/mBio.00296-16

219. Peek CT, Ibberson CB, Cassat JE. Identification of virulence determinants during host-pathogen interaction using Tn-Seq technology. *Methods Mol Bio*. 2020;2069:155-175. doi:10.1007/978-1-4939-9849-4_12

220. Lazinski DW, Camilli A. Homopolymer tail-mediated ligation PCR: a streamlined and highly efficient method for DNA cloning and library construction. *Biotechniques*. 2013;54(1):25-34. doi:10.2144/000113981

221. Zaprasis A, Hoffmann T, Stannek L, Gunka K, Commichau FM, Bremer E. The γ-aminobutyrate permease GabP serves as the third proline transporter of *Bacillus subtilis*. *J Bacteriol*. 2014;196(3):515-526. doi:10.1128/JB.01128-13

222. Kiedrowski MR, Kavanaugh JS, Malone CL, Mootz JM, Voyich JM, Smeltzer MS, et al. Nuclease modulates biofilm formation in community-associated methicillin-resistant *Staphylococcus aureus*. *PLoS One*. 2011;6(11). doi:10.1371/JOURNAL.PONE.0026714

223. Olson ME, Nygaard TK, Ackermann L, Watkins RL, Zurek OW, Pallister KB, et al. *Staphylococcus aureus* nuclease is an SaeRS-dependent virulence factor. *Infect Immun*. 2013;81(4):1316-1324. doi:10.1128/IAI.01242-12

224. Berends ETM, Horswill AR, Haste NM, Monestier M, Nizet V, von Köckritz-Blickwede M. Nuclease expression by *Staphylococcus aureus* facilitates escape from neutrophil extracellular traps. *J Innate Immun*. 2010;2(6):576-586. doi:10.1159/000319909

225. Matias C, Serrano I, Van-Harten S, Mottola C, Mendes JJ, Tavares L, Oliveira M. Polymicrobial interactions influence the *agr* copy number in *Staphylococcus aureus* isolates from diabetic foot ulcers. *Anton Leeuw Int J G*. 2018;111(11):2225-2232. doi:10.1007/s10482-018-1103-z

226. Kremers HM, Nwojo ME, Ransom JE, Wood-Wentz CM, Joseph Melton L, Huddleston PM. Trends in the epidemiology of osteomyelitis a population-based study, 1969 to 2009. *J Bone Joint Surg Am*. 2014;97(10):837-845. doi:10.2106/JBJS.N.01350

227. Nair N, Biswas R, Götz F, Biswas L. Impact of *Staphylococcus aureus* on pathogenesis in polymicrobial infections. *Infect Immun*. 2014;82(6):2162-2169. doi:10.1128/IAI.00059-14

228. Todd OA, Peters BM. *Candida albicans* and *Staphylococcus aureus* pathogenicity and polymicrobial interactions: lessons beyond Koch's postulates. *J Fungi*. 2019;5(3). doi:10.3390/jof5030081

229. Todd OA, Fidel PL, Harro JM, Hilliard JJ, Tkaczyk C, Sellman BR, et al. *Candida albicans* augments *Staphylococcus aureus* virulence by engaging the staphylococcal *agr* quorum sensing system. *mBio*. 2019;10(3). doi:10.1128/MBIO.00910-19

230. Citron DM, Goldstein EJC, Merriam CV, Lipsky BA, Abramson MA. Bacteriology of moderate-to-severe diabetic foot infections and *in vitro* activity of antimicrobial agents. *J Clin Microbiol*. 2007;45(9):2819. doi:10.1128/JCM.00551-07

231. Yan X, Song J fang, Zhang L, Li X. Analysis of risk factors for multidrug-resistant organisms in diabetic foot infection. *BMC Endocr Disord*. 2022;22(1):1-7. doi:10.1186/S12902-022-00957-0

232. Carrillo-Larco RM, Anza-Ramírez C, Saal-Zapata G, Villarreal-Zegarra D, Zafra-Tanaka JH, Ugarte-Gil C, Bernabe-Ortiz A. Type 2 diabetes mellitus and antibiotic-resistant infections: a systematic review and meta-analysis. *J Epidemiol Community Health*. 2022;76(1):75-84. doi:10.1136/JECH-2020-216029

233. McBee ME, Chionh YH, Sharaf ML, Ho P, Cai MWL, Dedon PC. Production of superoxide in bacteria is stress- and cell state-dependent: a gating-optimized flow cytometry method that minimizes ROS measurement artifacts with fluorescent dyes. *Front Microbiol*. 2017;8:459. doi:10.3389/FMICB.2017.00459

234. Murphy MP, Bayir H, Belousov V, Chang CJ, Davies KJA, Davies MJ, et al. Guidelines for measuring reactive oxygen species and oxidative damage in cells and *in vivo*. *Nat Metab.* 2022;4(6):651-662. doi:10.1038/s42255-022-00591-z

235. Soffler C, Campbell VL, Hassel DM. Measurement of urinary F2-isoprostanes as markers of *in vivo* lipid peroxidation: A comparison of enzyme immunoassays with gas chromatography-mass spectrometry in domestic animal species. *J Vet Diagn Invest*. 2010;22(2):200-209. doi:10.1177/104063871002200205

236. Il'yasova D, Morrow JD, Ivanova A, Wagenknecht LE. Epidemiological marker for oxidant status: comparison of the ELISA and the gas chromatography/mass spectrometry assay for urine 2,3-dinor-5,6-dihydro-15-F2t-isoprostane. *Ann Epidemiol*. 2004;14(10):793-797. doi:10.1016/J.ANNEPIDEM.2004.03.003

237. Hawkins CL, Davies MJ. Detection, identification, and quantification of oxidative protein modifications. *J Biol Chem*. 2019;294(51):19683. doi:10.1074/JBC.REV119.006217

238. Rabbani N, Thornalley PJ. Reading patterns of proteome damage by glycation, oxidation and nitration: quantitation by stable isotopic dilution analysis LC-MS/MS. *Essays Biochem*. 2020;64(1):169-183. doi:10.1042/EBC20190047

239. Winterbourn CC, Buss IH. Protein carbonyl measurement by enzyme-linked immunosorbent assay. *Methods Enzymol*. 1999;300:106-111. doi:10.1016/S0076-6879(99)00118-4

240. Good CJ, Neumann EK, Butrico CE, Cassat JE, Caprioli RM, Spraggins JM. High spatial resolution MALDI imaging mass spectrometry of fresh-frozen bone. *Anal Chem*. 2022;94(7):3165-3172. doi:10.1021/ACS.ANALCHEM.1C04604

241. Schuster CF, Bellows LE, Tosi T, Campeotto I, Corrigan RM, Freemont P, Grundling A. The second messenger c-di-AMP inhibits the osmolyte uptake system OpuC in *Staphylococcus aureus*. *Sci Signal*. 2016;9(441):ra81. doi:10.1126/SCISIGNAL.AAF7279

242. Ryan DJ, Patterson NH, Putnam NE, Wilde AD, Weiss A, Perry WJ, et al. MicroLESA: integrating autofluorescence microscopy, *in situ* micro-digestions, and liquid extraction surface analysis for high spatial resolution targeted proteomic studies. *Anal Chem*. 2019;91(12):7578-7585. doi:10.1021/acs.analchem.8b05889